T H E U N I V E R S I T Y O F M I C H I G A N

COLLEGE OF ENGINEERING
Department of Civil Engineering

Technical Report

DYNAMIC PRESSURE DISTRIBUTION AT THE BASE OF A RIGID FOOTING SUBJECTED TO VIBRATORY LOADS

Y. S. Chae

ORA Project 05366

under contract with:

WATERWAYS EXPERIMENT STATION
U.S. ARMY CORPS OF ENGINEERS
CONTRACT NO. DA-22-079-ENG-340
VICKSBURG, MISSISSIPPI

administered through:

OFFICE OF RESEARCH ADMINISTRATION ANN ARBOR

May 1964

This report was also a dissertation submitted in partial fulfillment of the requirements for the degree of Doctor of Philosophy in The University of Michigan, 1964.

FOREWORD

The investigation covered in the dissertation by Mr. Y. S. Chae includes a study of the pressure distribution beneath a rigid footing which is undergoing steady-state oscillation. The primary objectives of this study were to evaluate the changes in phase relation and magnitude of the pressures at different points beneath this footing at the zone of contact and to establish experimentally values for the displacement functions.

The test results were obtained using a footing one foot in diameter resting at the surface of a bed of Ottawa sand compacted to its maximum density. Consequently, the results indicated herein have direct quantitative value for similar footings on sand. However, it is felt that the experimental values of the displacement function can be used with the theory for at least modest extrapolations in footing sizes.

The experimentally determined displacement functions are comparable to those determined theoretically for footings beneath which the pressure distribution is assumed to remain constant regardless of frequency of oscillation. However, as shown in the text, important differences exist in the phase relationship between the pressures at different points along the surface of this footing. These frequency-dependent phase relationships between pressures on the footing should be of extreme importance in evaluating the distribution of pressures, or soil structure interaction pressures, obtained for different rates of loading.

After obtaining these displacement functions experimentally, it is possible to evaluate the behavior of this footing when subjected to impulsive loadings. This may be done by superposition of a series of sinusoidal loadings to develop an equivalent pulse loading. In the next phase of the project it is anticipated that impulsive loadings will be applied to the footing and compared to the theoretically predicted responses.

It should be noted that this investigation has been restricted to dynamic behavior of a footing-soil system which is essentially elastic and does not cause significant penetration of the footing. However, it is believed that by approaching this problem step by step, beginning with small magnitude displacements, the procedure may gradually be extended for study of the footing-soil behavior in the range of inelastic action with permanent deformations included.

F. E. Richart, Jr.

J. R. Hall, Jr.

TABLE OF CONTENTS

TABLE OF CONTENTS (Continued)

TABLE OF CONTENTS (Concluded)

LIST OF TABLES

LIST OF FIGURES

LIST OF FIGURES (Continued)

LIST OF FIGURES (Continued)

LIST OF SYMBOLS

A^*_{max}, A_{max}	amplitude of oscillation (maximum)
$A(1)_{max}$	dimensionless amplitude factor corresponding to amplitude produced by a rotating mass oscillator
$A(2)_{max}$	dimensionless amplitude factor corresponding to amplitude produced by a constant force oscillator
$A'(2)_{max}$	"unit" amplitude factor
$\overline{A}$	area of foundation base
a	strain gage resistance ratio
a_o	dimensionless frequency factor, or velocity ratio
B	least width of footing
b	mass ratio for vertical oscillation
C_1,C_2	capacitance in bridge circuit
c	coefficient of viscous damping
c_c	critical damping
c_m	coefficient used by Pauw
D_r	relative density
E	modulus of linear deformation
e	base of natural logarithms, 2.7182...
e	void ratio
e_f	circuit efficiency
e_{max}	void ratio in loosest state
e_{min}	void ratio in densest state

F_1 and F_2	dimensionless frequency functions (from f_1, f_2, and a_o)
$F_1 \ldots F_6$	force on each ring
$\overline{F}$	amplitude of force on ring
F_T	total force on bottom plate
f	frequency of excitation
f	displacement function
f_o	resonant frequency for forced vibration
f_1 and f_2	displacement functions
f_n	natural frequency of free vibration
f_{nr}	reduced natural frequency
G	shear modulus of elasticity
G_s	specific gravity of solid particles
g	acceleration due to gravity
I	current in circuit
I_{max}	maximum current capacity
i	$\sqrt{-1}$
K	strain gage factor
K	spring constant
K'	dynamic spring constant of subgrade = $K/\overline{A}$
K_v	coefficient defined by Eq. (41)
L	power transmitted to soil
ℓ	arm of rotation for two eccentric mass oscillator

M_s	apparent mass of soil
m_b	total mass of bottom plate (footing)
m_e	unbalanced rotating mass
m_o	total static mass of oscillator plus footing
m_t	total mass of upper plate (footing) plus any static weight
$m_1 \ldots m_5$	mass of each of the outer ring
m_6	mass of center ring
N_1	displacement magnification factor
n	total number of ring
P	vertical force applied at the base of footing
P_1	amplitude of vertical force P
Q	periodic force applied
Q_1	amplitude of periodic force
R_g	gage resistance measured at each arm of Wheatstone bridge
$R_1 \ldots R_6$	reaction under each ring
R_T	total reaction under footing
R_v	coefficient defined by Eq. (40)
R_{vc}	coefficient defined by Eq. (45)
r	distance from the source of vibration
r_o	radius of footing
S	factor which is a function of Poisson's ratio
S_r	resistive sensitivity

S_s	maximum strain gage sensitivity
t	time
V	supply voltage applied to Wheatstone bridge
V'	output voltage from bridge
v	velocity of elastic wave
v_c	velocity of compression wave
v_R	velocity of Rayleigh wave
v_s	velocity of shear wave
W	weight of block supported by weightless spring
W_o	total static weight of the oscillator plus footing
W_s	weight of "in-phase" soil
W_v	weight of vibrator
w	water content
X	amplitude of vibration (displacement)
X_{max}	maximum displacement
x	displacement
$\dot{x}$	velocity
$\ddot{x}$	acceleration
x_s	static displacement
α	sloping angle of stress distribution cone
γ	unit weight of soil (bulk density)
γ_s	unit weight of solid particles

γ_w	unit weight of water
γ_d	unit dry weight of soil (dry density)
η	dimensionless, time independent function
λ	wavelength
λ	Lame's constant
μ	Poisson's ratio of elastic body or soil
$\overline{\mu}$	a constant to show proportionality between the shear and Rayleigh wave velocities
ν	damping factor = c/c_c
ρ	mass density of soil
$\phi_{Q\text{-}R_T}$	phase shift between input force and soil reaction
$\phi_{Q\text{-}x}$	phase shift between input force and displacement
$\phi_{Q\text{-}\ddot{x}}$	phase shift between input force and acceleration
$\phi_{\ddot{x}\text{-}F_6}$	phase shift between acceleration and force on the center ring
$\phi_{F_j\text{-}F_6}$	phase shift between the force on one of the outer rings and that on the center ring
$\phi_{F_j\text{-}x}$	phase shift between a ring force and displacement
$\phi_{F_T\text{-}x}$	phase shift between the total force on footing and displacement
$\phi_{R_T\text{-}x}$	phase shift between the total reaction and displacement
ω	angular frequency
ω_n	natural angular frequency

ABSTRACT

This thesis is an experimental study of the behavior of footing-soil systems subjected to vibratory loads. The base of the footing consisted of six independent concentric circular rings connected through load cells to a rigid mass. The footing, resting on the surface of a sand bed, was set into steady state vibration by an electromagnetic oscillator.

From measurements of the periodic variations of loads on each ring, the inertia force of the mass, and the input force, it was possible to obtain information on the changes in distribution of dynamic pressure amplitude, the phase relations for the six segments of the footing base, and data needed to establish empirical values for the displacement functions associated with the theoretical approach.

The experimental results were analyzed and compared with the theoretical work, which regarded the system to be an idealized circular mass resting on the surface of a homogeneous, isotropic, semi-infinite elastic body.

It was found that the dynamic pressure was functions of the intensity of applied load, mass ratio (a dimensionless quantity defining a footing-soil system), and the frequency of oscillation. Under a constant total soil reaction the dynamic pressure appeared to shift towards the edge with increasing frequency, changing the shape of distribution from a parabolic type to that corresponding to a rigid base. Under a given frequency the effect of an increased intensity of the applied load was to shift the dynamic pressure towards the center portion of the footing. The effect of mass ratio was found to be dependent upon the frequency of oscillation.

Empirical values obtained for the displacement functions also indicated that the dynamic pressure did not maintain the same shape of distribution curve, but changed with the frequency of oscillation.

Finally, it was established experimentally that the displacement, the dynamic soil pressure, and their phase relations could be defined by the dimensionless displacement functions.

CHAPTER I

INTRODUCTION

The function of a structural foundation is to transmit the imposed loads to the ground on which it is placed. In designing such a foundation to carry a static load it is essential to ensure that the ground is capable of carrying the load without the risk of shear failure and that the amount of displacement under the loading should not exceed a specified value.

Such a problem of the bearing capacity of soils becomes just as important, if not more so, for a foundation carrying dynamic or vibratory loads. With increasing use of industrial machines, blasting operations in construction, and the installation of new defense facilities such as missile launching pads and radar towers, the study of structure-foundation systems under dynamic loads has become increasingly important and essential in recent years.

In analyzing the problem of statically loaded footings resting on soil the most critical quantities to be considered are the unit pressure under the footing and the shearing resistance of the supporting soil. In the dynamically loaded systems, however, there is an additional factor which cannot be overlooked—the natural frequency of the system. Resonance will occur when the operational speed of a machine happens to coincide with the natural frequency of the foundation-soil system, and

at this resonance the amplitude of motion is greatly amplified, which may lead to structural damage.

The first approximation used in the study of a foundation-soil system was to consider the system as being a single mass supported by a weightless spring. Using a suitable coefficient of subgrade reaction for the spring constant, and neglecting the mass of the supporting soil, the natural frequency of the system was computed. The results of such an analysis, however, disagreed with the experimental results for the simple reason that the supporting soil did not behave as a weightless spring.

This led to the second approximation, which considered the inclusion of an "in-phase" soil, that is, that portion of the "foundation soil vibrating with the oscillator." Thus, the oscillating mass was composed of the oscillator and its foundation plus the mass of the "in-phase" soil. The past researchers starting with Hertwig, et al., at DEGEBO (Deutchen Forschungsgesellschaft für Bodenmechanik) (9)* found, however, that the mass of the "in-phase" soil varied with different surface loading conditions such as the magnitude of the applied force and the area of loading, and was frequency dependent. This method is still in practice, nevertheless, and attempts have been made by a number of researchers to determine the exact mass of the "in-phase" soil in various ways, but very little success has been reported.

---

*Numbers in parentheses refer to references listed at the end of the text.

A purely analytical solution to this problem was first developed by Reissner (16) in 1936. He presented a solution for the system in which the oscillator rested on a semi-infinite, homogeneous, isotropic, elastic body (elastic half-space) in terms of two displacement functions defined in Chapter II. His solution was limited to the case of the vertical excitation of an oscillator on a circular base, assuming a uniform contact pressure between the oscillator and the elastic body. Reissner's theory has since been extended: Sung (20) and Quinlan (15) treated the problem for various types of contact pressure distribution; Arnold et al., (1) considered the cases for different modes of oscillation; recently, Hsieh (10) has transformed the basic equations in the Reissner-Sung theory into those equations comparable to the conventional one-degree-of-freedom system with viscous damping.

Richart (17), (18) put these analytical solutions into a very practical and important use for civil engineers. He demonstrated that the theoretical solutions could be used to determine the dynamic characteristics of a foundation-soil system under vibratory loads, if the following quantities are known: the static weight of the oscillator, the radius of the loading area, the dynamic force applied, Poisson's ratio, density, and shear modulus of the foundation material, and the pressure distribution.

Of these quantities affecting the dynamic characteristics of an oscillator-foundation system, all but the Poisson's ratio and shear modulus of the material, and the pressure distribution are known or can

easily be measured. The elastic constants such as the shear modulus and the Poisson's ratio may be determined from measured elastic wave velocities. There have been numerous studies in the past, both theoretically and experimentally, on the measurement of elastic wave velocities and on the factors affecting them. Some of the most recent studies have been made by Hardin (8), and Hall (6), who evaluated the effects of confining pressure, void ratio, amplitude, and other parameters on wave velocities in granular materials.

Purpose and Scope of the Present Research

The primary objective of the present research was to evaluate experimentally the pressure distribution at the base of a footing subjected to vibratory loads. The pressure distribution is dependent upon the frequency of oscillation and the characteristics of the oscillator-soil system; the effects of these factors on the pressure distribution were to be studied. The experimental results obtained were to be used to check part of the theory of vibrations based on a semi-infinite elastic solids.

In the present research the dynamic load employed was limited to that of steady state vibration (constant force oscillator) in the vertical mode only. The foundation soil was an Ottawa sand compacted to maximum density. The cases for other types of dynamic loads such as impact, different modes of oscillation or for different soil types and conditions are left for future research.

The present research, therefore, includes the following investigations:

1. Resonant Frequency and Maximum Amplitude
   a. Effect of mass ratio.
   b. Effect of input force.
2. Pressure Distribution
   a. Effect of mass ratio.
   b. Effect of input force.
   c. Effect of frequency.
3. Determination of Displacement Functions

   Experimental results obtained were to be used to determine the displacement functions through a computer program. The displacement functions are defined by Eq. (18) in Chapter II.

For the present research the mass ratio was varied from 5.8 to 24.9, the magnitude of the input force ranged from 9.0 to 22.5 lb vector, and the range of oscillating frequency was from 50 to 1000 cps.

CHAPTER II

ANALYTICAL BACKGROUND AND REVIEW OF PREVIOUS WORK

When a rigid body is subjected to vibratory loads six types of displacement can be produced according to the six degrees of freedom in such a body in space. There can be three types of translational displacement in the direction of three axes in the body, and three types of rotational motion about the three axes. Due to the complexities of the problem involved the majority of theoretical and experimental studies in the past have been confined to the simplest form of motion in the vertical direction.

In this chapter a review of both theoretical and experimental studies made in the past is presented. The first part of this chapter deals mainly with the theoretical development of the theory of vibrations based on a semi-infinite elastic body. In the second half is presented a short review of selected literature which is closely related to the subject but has not been reviewed in the first part.

Basic Concepts on One-Degree-of-Freedom Vibrations

For the reason that the terms and equations corresponding to the basic theories for one-degree-of-freedom vibration are applied or compared in the study of the dynamic characteristics of foundation-soil systems, a brief review of theory is made for the cases of one-degree-of-

freedom free and forced vibrations with or without damping.

FREE VIBRATIONS WITHOUT DAMPING

The behavior of a single mass resting on a weightless linear spring and subjected to a single impulse, as shown in Fig. 1, may be described as:

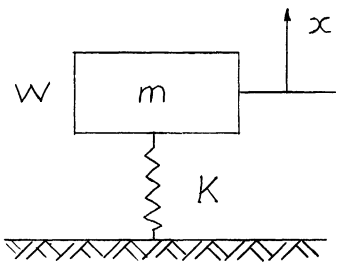

$$m\ddot{x} + Kx = 0 \qquad (1)$$

where

m = mass of the block
x = displacement
K = spring constant
$\ddot{x}$ = acceleration

Fig. 1. A mass supported by weightless spring.

The natural frequency of such a system is given by:

$$f_n = \frac{1}{2\pi}\sqrt{\frac{K}{m}} = \frac{1}{2\pi}\sqrt{\frac{K \cdot g}{W}} \qquad (2)$$

where

f_n = natural frequency of the system

W = weight of the block

g = gravitational acceleration.

FORCED VIBRATION WITH VISCOUS DAMPING

Constant Amplitude of Force Oscillation

In free vibration the oscillation is damped because of energy dis-

sipated by friction. Oscillatory motion can be maintained, however, at constant amplitude by the application of an external periodic force as defined by $Q = Q_1 \sin \omega t$, where Q_1 is constant force, ω is angular frequency and t is time.

Assuming viscous damping, the equation of motion of the spring-mass system shown in Fig. 2 becomes:

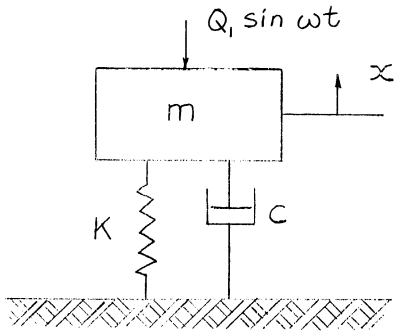

$$m\ddot{x} + c\dot{x} + Kx = Q_1 \sin \omega t \qquad (3)$$

where

$\dot{x}$ = velocity
c = coefficient of viscous damping

Fig. 2. Forced vibration with viscous damping.

The displacement of the mass under the steady state oscillation is expressed by

$$x = X \sin (\omega t - \phi_{Q-x}) \qquad (4)$$

in which X is the amplitude of steady oscillation and ϕ_{Q-X} the phase shift between the exciting force and the resulting motion of the mass. From Eq. (4)

$$\dot{x} = X\omega \cos (\omega t - \phi_{Q-x})$$

$$\ddot{x} = -X\omega^2 \sin (\omega t - \phi_{Q-x}) = -x\omega^2$$

For the condition of $\Sigma F = 0$, the following vector diagrams may be drawn:

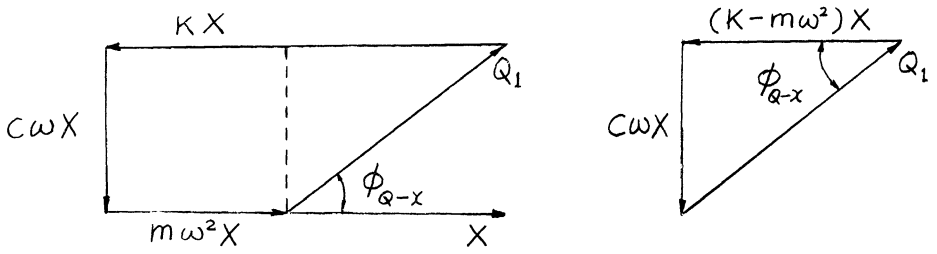

Fig. 3. Vector diagrams for forced vibration with viscous damping.

From Fig. 3 expressions for X and ϕ_{Q-X} may be obtained as

$$X = \frac{Q_1}{\sqrt{(K - m\omega^2)^2 + (c\omega)^2}} \tag{5}$$

$$\phi_{Q-x} = \tan^{-1} \frac{c\omega}{K - m\omega^2} \tag{6}$$

Equations (5) and (6) may be reduced to

$$X = \frac{Q_1 / K}{\sqrt{\left(1 - \frac{m\omega^2}{K}\right)^2 + \left(\frac{c\omega}{K}\right)^2}} \tag{5'}$$

$$\phi_{Q-x} = \tan^{-1} \frac{c\omega/K}{1 - \frac{m\omega^2}{K}} \tag{6'}$$

Using the following quantities:

$\omega_n = \sqrt{K/m}$ = natural circular frequency of undamped oscillation

$\nu = c/c_c$ = damping factor

$c_c = 2m\omega_n = 2\sqrt{Km}$ = critical damping coefficient

$X_s = Q_1/K$ = static displacement under force Q_1.

Equations (5') and (6') may further be reduced to

$$\frac{X}{X_S} = N_1 = \frac{1}{\sqrt{\left[1-\left(\frac{\omega}{\omega_n}\right)^2\right]^2 + \left(2\nu\frac{\omega}{\omega_n}\right)^2}} \tag{7}$$

$$\phi_{Q\text{-}x} = \tan^{-1}\frac{2\nu\frac{\omega}{\omega_n}}{1-\left(\frac{\omega}{\omega_n}\right)^2} \tag{8}$$

The term N_1, called the magnification factor, represents the factor by which the static displacement under force Q_1 must be multiplied to determine the amplitude X. The amplitude at $\phi_{Q\text{-}X} = 90°$ may be expressed by

$$X = \frac{Q_1}{c\,\omega_n} = \frac{X_S}{2\nu} \tag{9}$$

at which the frequency is close to the resonant frequency for small ν.

In Fig. 4 are drawn the curves showing the relations between the amplitude and the frequency ratio. Fig. 5 shows how the phase angle shifts with the frequency ratio under different damping factors. It is clear from Eqs. (7) and (8), and these figures that N_1 and $\phi_{Q\text{-}X}$ are functions only of the frequency ratio ω/ω_n and the damping factor ν. At $\omega/\omega_n = 1$, that is, at resonance under undamped condition, N_1 becomes infinite and $\phi_{Q\text{-}X}$ indeterminate. It should also be noted that under constant force type oscillation the maximum amplitude magnification occurs at the value of ω/ω_n less than 1.0. For small values of damping the amplitude peaks occur at the frequency ratio very close to 1.0, but as the damping factor becomes larger the frequency ratio for the maximum amplitude occurs farther away from the frequency ratio of 1.0.

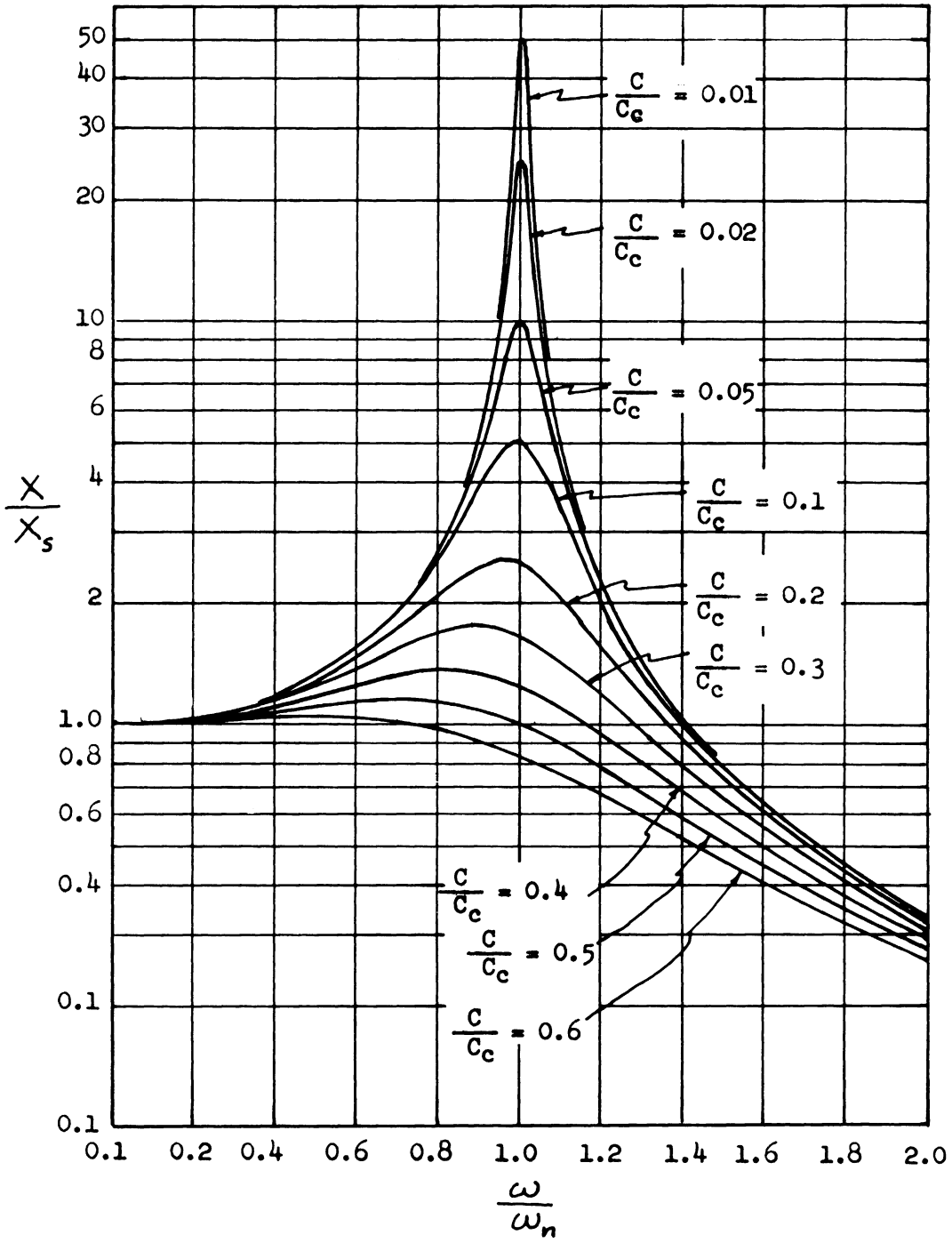

Fig. 4. Amplitude-frequency curves for viscous damped constant force vibration.

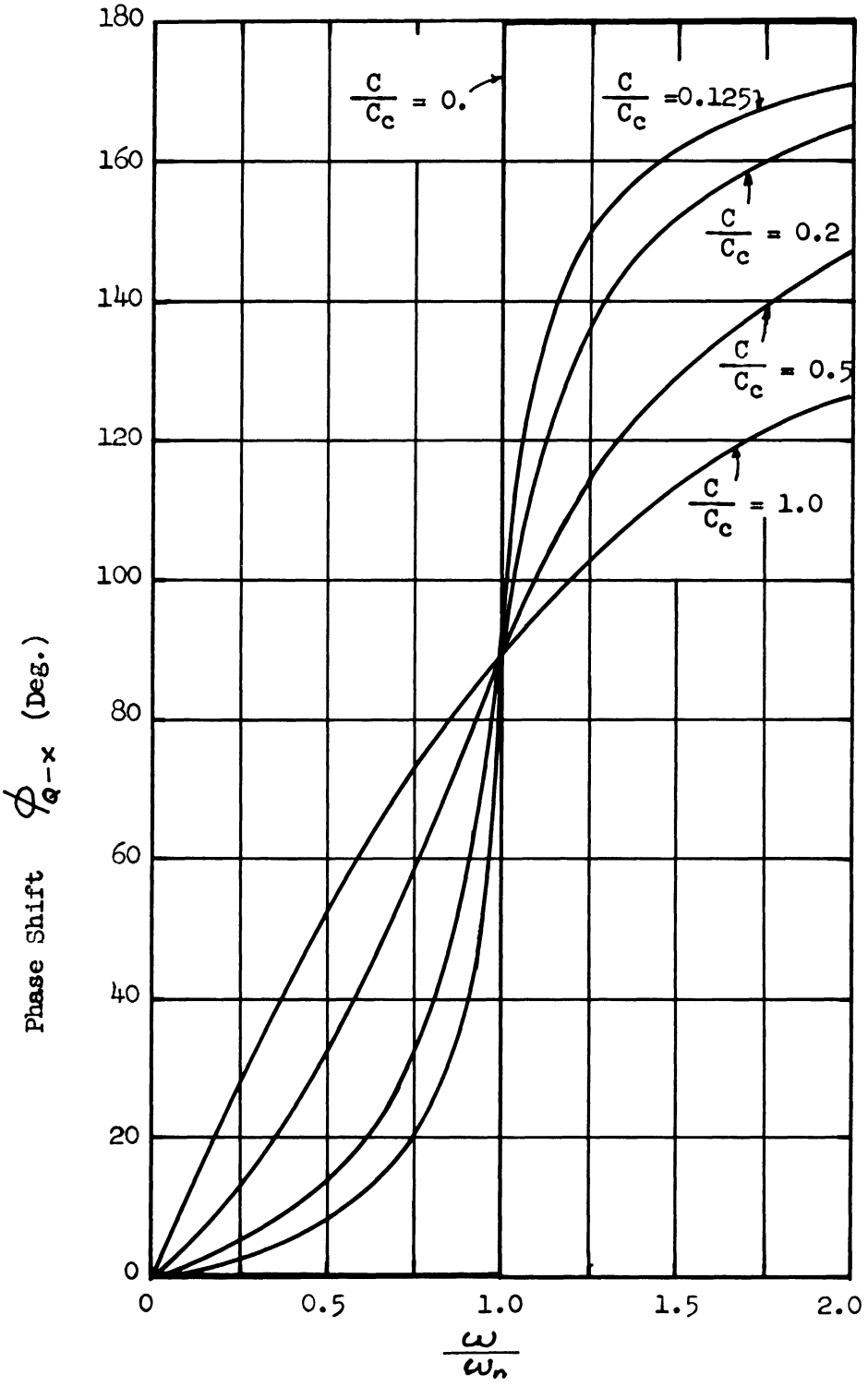

Fig. 5. Phase shift-frequency curves for viscous damped constant force vibration.

Rotating Mass Type Oscillator

The exciting force can also be generated by rotating unbalanced weights. They are rotated in opposite directions so that the forces are applied only in vertical direction. The magnitude of the force is dependent upon both the eccentricity and frequency of excitation as

$$Q_1 = 2 m_e \ell \omega^2 \sin \omega t \tag{10}$$

in which m_e is the mass of the eccentric weights and ℓ is the arm of rotation. Using the value of Q_1 as defined by Eq. (10), the expression for the displacement X and the phase shift ϕ_{Q-X} may be obtained as

$$\frac{X}{\frac{2 m_e \ell}{m_o}} = \frac{\left(\frac{\omega}{\omega_n}\right)^2}{\sqrt{\left[1-\left(\frac{\omega}{\omega_n}\right)^2\right]^2 + \left[2\nu \frac{\omega}{\omega_n}\right]^2}}$$

$$= N_1 \cdot \left(\frac{\omega}{\omega_n}\right)^2 \tag{11}$$

and

$$\phi_{Q-X} = \tan^{-1} \frac{2\nu\left(\frac{\omega}{\omega_n}\right)}{1-\left(\frac{\omega}{\omega_n}\right)^2} \tag{12}$$

By the use of these equations curves showing the relations among the amplitude, phase shift and the frequency ratio may be drawn. Under rotating mass type oscillation the maximum amplitude magnification occurs at the value of ω/ω_n greater than 1.0. With increasing damping factor the frequency ratio for the maximum amplitude shifts farther away from $\omega/\omega_n = 1.0$.

Theory of Vibrations Based On A Semi-Infinite Elastic Body

ELASTIC WAVES IN IDEAL ELASTIC BODY

When a disturbance is caused in an infinite, elastic, isotropic, homogeneous body such a disturbance may be propagated in the form of body waves. The body wave is composed of two distinctly different waves: one is the wave of volume change, designated as the compression wave, longitudinal wave or P-wave; the other is the wave of distortion at constant volume, designated as a shear wave, transverse wave or S-wave. In the propagation of compression waves the direction of motion of particles is along the direction of propagation, and in the shear waves the direction is perpendicular to the direction of propagation. The amplitude of the propagated wave decreases with the distance from the source approximately inversely proportional to the distance (that is, $1/r$). In a semi-infinite, elastic, isotropic, homogeneous body, a third type of wave appears because of the free surface. After Rayleigh, who investigated the behavior of this surface wave in a semi-infinite elastic medium, this type of wave is called a Rayleigh wave or R-wave. Lamb (12) carried out a comprehensive study of the behavior of Rayleigh waves and presented a solution for a semi-infinite elastic body subjected to an impulsive load applied at the surface. The amplitude of the propagated Rayleigh wave diminishes according to the law of annular divergence (that is, $1/\sqrt{r}$).

The velocity of the shear wave is given by

$$v_s = \sqrt{\frac{G}{\rho}} = \sqrt{\frac{G \cdot g}{\gamma}} \tag{13}$$

in which G is the shear modulus of elasticity, ρ is the mass density, and γ is the unit weight of the elastic material. The velocities of the compression and Rayleigh waves are dependent upon Poisson's ratio and are related to the shear wave velocities. The compression wave velocity for the condition of confined compression is expressed by

$$v_c = \sqrt{\frac{\lambda + 2G}{\rho}} \tag{14}$$

in which λ is a Lame's constant. For the condition of unconfined compression the velocity may be expressed by

$$v_c = \sqrt{\frac{E}{\rho}} \tag{15}$$

in which E is the modulus of elasticity. The velocity of Rayleigh wave is related to the shear wave velocity in the form of

$$v_R = \bar{\mu}\, v_s \tag{16}$$

where $\bar{\mu}$ is a function of Poisson's ratio and varies between 0.875 and 0.955 for the corresponding Poisson's ratio of zero to 0.5.

THEORY OF THE RESPONSE OF RIGID FOOTINGS UNDER VERTICAL OSCILLATION IN A SEMI-INFINITE ELASTIC BODY

An accurate solution of the problem of vertical vibrations of a footing resting on soil can be made on the consideration of a mathematical model as shown in Fig. 6, in which a solid rests on the surface of a semi-infinite, isotropic, homogeneous, elastic body (an elastic half-space). To date no exact solution of the problem has been found, but several researchers have presented the approximate solutions.

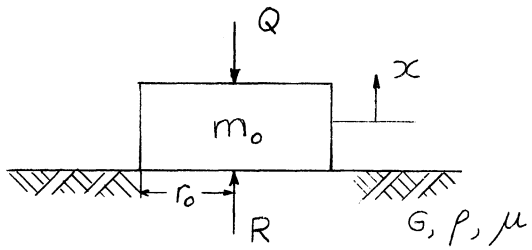

Fig. 6. A mathematical model of footing-soil system.

Lamb (12) was the first one to study the propagation of waves in elastic solids and derived the solution for the dynamic displacement caused by a vertical harmonic force applied at a point on the surface of a semi-infinite elastic body. Reissner (16) considered the vertical motion of a rigid mass of circular base resting on a semi-infinite elastic medium when subjected to a periodic vertical force, and obtained, by integration of the effects of the periodic vertical point load over the circular area, an approximate solution under the assumption of uniform pressure distribution between the circular base and the elastic body. Reissner's work was extended later by Sung (20) to cover the systems under uniform, parabolic and rigid base types of pressure distributions

over the circular area. More recently, Lysmer and Richart (13) extended Sung's work to include the cases of oscillations in high frequency ranges, and pulses of arbitrary shape. In the analysis given below the work by Lysmer and Richart is generally followed.

In analyzing the footing-soil system, such as shown in Fig. 6, it is necessary to make several simplifying assumptions as to the geometry and the physical properties of the footing and the supporting soil as the exact solution is not possible. It is assumed that the soil can be represented as a semi-infinite body and it is homogeneous, isotropic and perfectly elastic; that the footing is axial-symmetric and absolutely rigid, thus producing uniform displacement under the footing; there are no shear stresses acting on the plane of contact between the footing and the soil. The periodic force is assumed to act vertically through the center of gravity of the footing.

For vertical forced vibrations induced by a periodic force Q(t), the equation of motion of the footing may be expressed as

$$m_o \ddot{x} = R - Q \tag{17}$$

or

$$m_o \ddot{x} = R_1 e^{i\omega t} - Q_1 e^{i(\omega t + \phi_{Q-R})} \tag{17'}$$

where

m_o = mass of footing

x = displacement of footing

Q = periodic force having amplitude of Q_1

ω = angular frequency of exciting force

R = soil reaction having amplitude of R_1

$\phi_{Q\text{-}R}$ = phase shift between the exciting force and reaction

$i = \sqrt{-1}$

e = 2.71828...

It should be noted in Eq. (17) that the displacement and soil reaction are regarded as positive when they are acting upward.

In order to solve the above equation, it is necessary to determine the dependence of the soil reaction upon the displacement, the characteristics of the footing and the soil. It was assumed that there was a linear relation between the soil reaction and the displacement of the foundation. Thus, the relation between these two quantities are determined in terms of the modulus of elasticity or shear modulus.

As a result of mathematical computations (16), (20), which are omitted here, Reissner-Sung showed that the vertical displacement may be expressed as

$$\chi = \frac{R}{G r_o} (f_1 + i f_2) \tag{18}$$

or

$$X = \frac{R_1}{G r_o} (f_1 + i f_2)\, e^{i\omega t} \tag{18'}$$

in which G is the shear modulus of the soil; r_o is the radius of the footing; f_1 and f_2 are time-independent, dimensionless functions, designated as the displacement functions. It can be seen from the definition of the

function that f is dependent only upon the boundary conditions and the properties of the soil. Therefore, the displacement function f can at most be a function of the variables which define the footing-soil model— r_o, ω, G, ρ (the mass density of soil), and μ (Poisson's ratio of soil).

Combining the first four variables to introduce a dimensionless quantity denoting the frequency factor of the system,

$$a_o = \omega r_o \sqrt{\frac{\rho}{G}} \tag{19}$$

it can now be said that the displacement function is only dependent upon the frequency ratio, assuming the Poisson's ratio is constant for a soil.

Since the shear wave velocity in the soil is $v_s = \sqrt{G/\rho}$ [Eq. (13)], and

$$v_s = f \lambda \tag{20}$$

in which f is the frequency of oscillation and λ the wavelength, a_o can be rewritten to another form as

$$a_o = \frac{\omega r_o}{v_s} = 2\pi \frac{r_o}{\lambda} \tag{21}$$

or

$$\frac{r_o}{\lambda} = \frac{a_o}{2\pi} \tag{21'}$$

This indicates that the size of the footing may be represented in terms of the wavelength of the shear waves in the soil through the frequency factor.

Another dimensionless quantity, designated as the mass ratio of the system b, is derived from the mass and radius of the footing m_o, r_o, and the mass density of the soil ρ as:

$$b = \frac{m_o}{\rho r_o^3} \tag{22}$$

The quantity b can be interpreted as the ratio of the static mass of the oscillator to that of a cylinder of elastic soil having a radius r_o and a height r_o/π.

The reaction R is related to Q_1 in the form

$$R = Q_1 \eta e^{i\omega t} \tag{23}$$

in which η is a dimensionless and time-independent function. From Eqs. (17), (18), and (23)

$$\eta = \frac{1}{1 + b a_o^2 (f_1 + i f_2)} \tag{24}$$

substituting this back into Eqs. (18) and (23) one gets

$$R = \frac{Q_1 e^{i\omega t}}{1 + b a_o^2 (f_1 + i f_2)} \tag{25}$$

and

$$\chi = \frac{Q_1}{G r_o} \frac{(f_1 + i f_2) e^{i\omega t}}{1 + b a_o^2 (f_1 + i f_2)} \tag{26}$$

It follows that for a weightless footing, that is, $m_o = b = 0$, Eq. (26) is reduced to

$$x = \frac{Q_1}{G r_o} (f_1 + i f_2) e^{i\omega t} \tag{27}$$

The displacement function can be determined, therefore, from the solution of the special case of a weightless footing subjected to a periodic loading Q_1.

Substituting the value of X determined by Eq. (18') into Eq. (17') and separating them into the real and imaginary part, the following relationships are obtained:

$$\phi_{Q-R} = \tan^{-1} \frac{b a_o^2 f_2}{1 + b a_o^2 f_1} \tag{28}$$

$$R_1 = \frac{Q_1}{\sqrt{(1 + b a_o^2 f_1)^2 + (b a_o^2 f_2)^2}} \tag{29}$$

The expression thus found for R_1 is then substituted back into the right hand side of Eq. (18') and neglecting the imaginary part, the following expression for the displacement (amplitude) X is obtained:

$$X = \frac{Q_1}{G r_o} \sqrt{\frac{f_1^2 + f_2^2}{(1 + b a_o^2 f_1)^2 + (b a_o^2 f_2)^2}} \tag{30}$$

The phase shift between the soil reaction and the displacement may be expressed as

$$\phi_{R-X} = \tan^{-1} \frac{-f_2}{f_1} \tag{31}$$

and the phase shift between the input force and the displacement equals

$$\phi_{Q-x} = \phi_{Q-R} + \phi_{R-x} \tag{32}$$

Thus, from Eqs. (28) and (31)

$$\phi_{Q-x} = \tan^{-1} \frac{-f_2}{f_1 + b a_o^2 (f_1^2 + f_2^2)} \tag{33}$$

The time average of the power transmitted from the footing into the soil can be calculated by integrating the product of Q and $\dot{x}$ as

$$L = \frac{Q_1^2}{2 r_o^2 \sqrt{\rho G}} \frac{a_o f_2}{(1 + b a_o^2 f_1)^2 + (b a_o^2 f_2)^2} \tag{34}$$

The above derivations indicate that if the function f can be determined, the displacement, soil reaction, the phase relations, and the power input may be computed by these equations. It should be pointed out here that the function f is dependent only on two variables, and thus the function can be determined experimentally.

DETERMINATION OF THE DISPLACEMENT FUNCTION

The theoretical evaluation of the displacement function was first made by Reissner (16) assuming uniform contact pressure distribution. His work was extended by Sung (20) who analyzed for uniform, parabolic and rigid base type pressure distribution. The results of his computation are reproduced in Tables I and II, and in Fig. 7 for graphical representation. These charts clearly demonstrate the effect of the type

TABLE I

POWER SERIES REPRESENTATION OF THE FUNCTION $-f_1$ (Sung)

Rigid Base	$\mu = 0$	$-f_1 = 0.250000 - 0.109375\, a_o^2 + 0.010905\, a_o^4 - \ldots + \ldots$
	$\mu = 1/4$	$-f_1 = 0.187500 - 0.070313\, a_o^2 + 0.006131\, a_o^4 - \ldots + \ldots$
	$\mu = 1/3$	$-f_1 = 0.166667 - 0.060764\, a_o^2 + 0.005085\, a_o^4 - \ldots + \ldots$
	$\mu = 1/2$	$-f_1 = 0.125000 - 0.046875\, a_o^2 + 0.003581\, a_o^4 - \ldots + \ldots$
Uniform	$\mu = 0$	$-f_1 = 0.318310 - 0.092841\, a_o^2 + 0.007405\, a_o^4 - \ldots + \ldots$
	$\mu = 1/4$	$-f_1 = 0.238733 - 0.059683\, a_o^2 + 0.004163\, a_o^4 - \ldots + \ldots$
	$\mu = 1/3$	$-f_1 = 0.212207 - 0.051578\, a_o^2 + 0.003453\, a_o^4 - \ldots + \ldots$
	$\mu = 1/2$	$-f_1 = 0.159155 - 0.039789\, a_o^2 + 0.002432\, a_o^4 - \ldots + \ldots$
Parabolic	$\mu = 0$	$-f_1 = 0.424414 - 0.074272\, a_o^2 + 0.004232\, a_o^4 - \ldots + \ldots$
	$\mu = 1/4$	$-f_1 = 0.318310 - 0.047747\, a_o^2 + 0.002379\, a_o^4 - \ldots + \ldots$
	$\mu = 1/3$	$-f_1 = 0.282942 - 0.041262\, a_o^2 + 0.001973\, a_o^4 - \ldots + \ldots$
	$\mu = 1/2$	$-f_1 = 0.212207 - 0.031831\, a_o^2 + 0.001389\, a_o^4 - \ldots + \ldots$

TABLE II

POWER SERIES REPRESENTATION OF THE FUNCTION f_2 (Sung)

Rigid Base	$\mu = 0$	$f_2 = 0.214474\, a_o - 0.039416\, a_o^3 + 0.002444\, a_o^5 - \ldots + \ldots$
	$\mu = 1/4$	$f_2 = 0.148594\, a_o - 0.023677\, a_o^3 + 0.001294\, a_o^5 - \ldots + \ldots$
	$\mu = 1/3$	$f_2 = 0.130630\, a_o - 0.020048\, a_o^3 + 0.001052\, a_o^5 - \ldots + \ldots$
	$\mu = 1/2$	$f_2 = 0.104547\, a_o - 0.014717\, a_o^3 + 0.000717\, a_o^5 - \ldots + \ldots$
Uniform	$\mu = 0$	$f_2 = 0.214474\, a_o - 0.029561\, a_o^3 + 0.001528\, a_o^5 - \ldots + \ldots$
	$\mu = 1/4$	$f_2 = 0.148594\, a_o - 0.017757\, a_o^3 + 0.000808\, a_o^5 - \ldots + \ldots$
	$\mu = 1/3$	$f_2 = 0.130630\, a_o - 0.015037\, a_o^3 + 0.000658\, a_o^5 - \ldots + \ldots$
	$\mu = 1/2$	$f_2 = 0.104547\, a_o - 0.011038\, a_o^3 + 0.000444\, a_o^5 - \ldots + \ldots$
Parabolic	$\mu = 0$	$f_2 = 0.214474\, a_o - 0.019708\, a_o^3 + 0.000764\, a_o^5 - \ldots + \ldots$
	$\mu = 1/4$	$f_2 = 0.148594\, a_o - 0.011837\, a_o^3 + 0.000405\, a_o^5 - \ldots + \ldots$
	$\mu = 1/3$	$f_2 = 0.130630\, a_o - 0.010024\, a_o^3 + 0.000328\, a_o^5 - \ldots + \ldots$
	$\mu = 1/2$	$f_2 = 0.104547\, a_o - 0.007358\, a_o^3 + 0.000222\, a_o^5 - \ldots + \ldots$

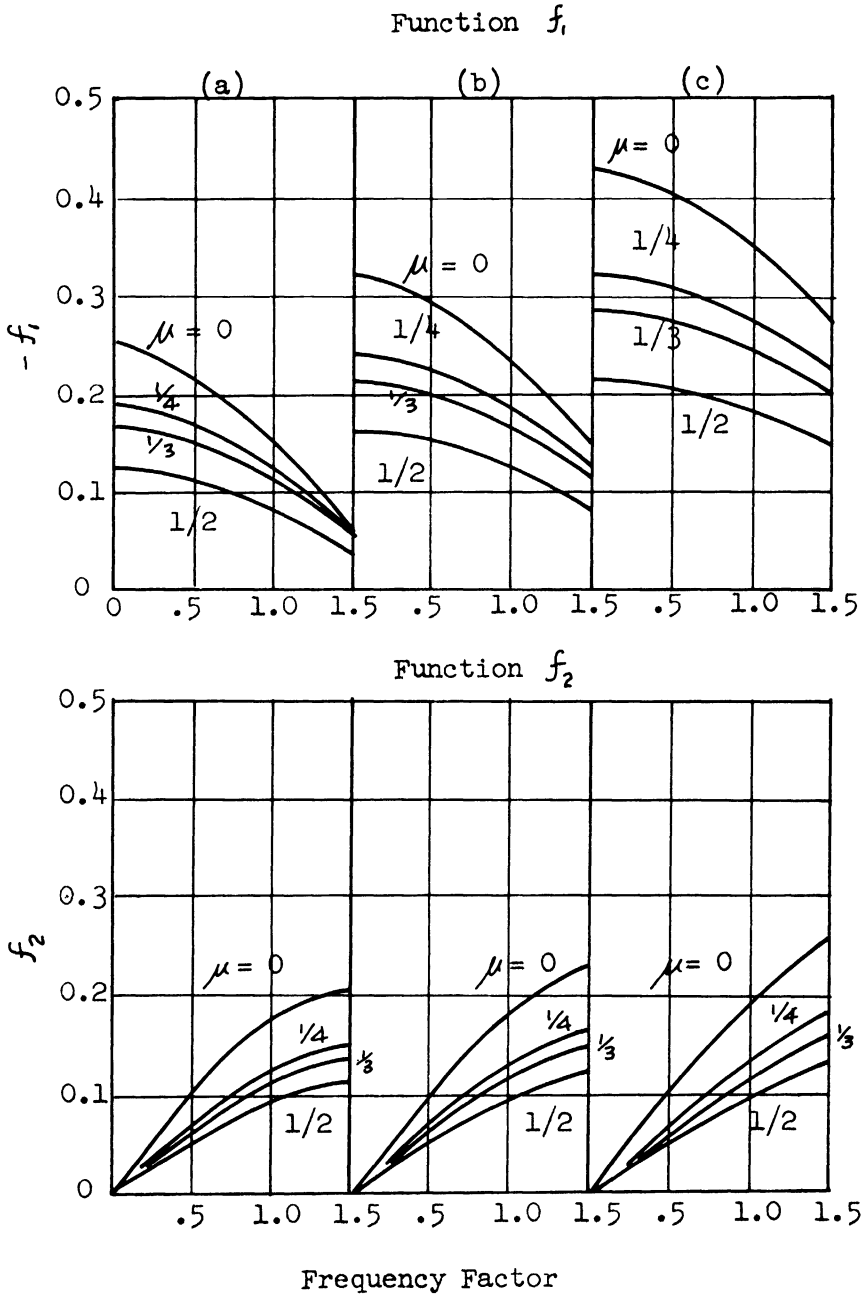

Fig. 7. Graphical representation of the displacement function for the three types of pressure distribution (Sung).

of pressure distribution on the function f and consequently, on the dynamic behavior of a footing-soil system. These charts also indicate how the function varies with Poisson's ratio of soil. It should be pointed out that Sung, in his analysis, assumed the type of pressure distribution to be the same for all frequencies. He also limited the analysis to the region $0 < a_o < 1.5$, and accordingly, used only the first three terms of power series shown in Tables I and II, for he considered that within this region the displacement function could be represented sufficiently by taking the first three terms. Should more of the higher order terms be taken, the result would be smaller than his results.

Recently Lysmer and Richart (13) extended Sung's work from a different approach to include the higher order terms in the computation and to treat the systems in higher frequency range ($a_o > 1.5$). They also considered the case of arbitrary pulses. Their analysis was based on the assumption of uniform displacement under the footing. In Fig. 8 is shown the results of their computation in a graphical form. The curves shown in this figure represent the variation of f_1 and f_2 with frequency factor a_o. It is noted in this chart that the f_1 and f_2 values obtained by Lysmer and Richart check well with the solution obtained by Sung for rigid base type pressure distribution for small values of frequency factor a_o. It has been shown from the theoretical analysis that the imaginary component of the function f_2 has an asymptote expressed by $S/\pi \cdot a_o$ where $S = [(1-2\mu)/2(1-\mu)]^{1/2}$. Thus for $\mu = 1/3$ the asymptote is expressed as being $1/2\pi \cdot a_o$. It can also be noted that for large values

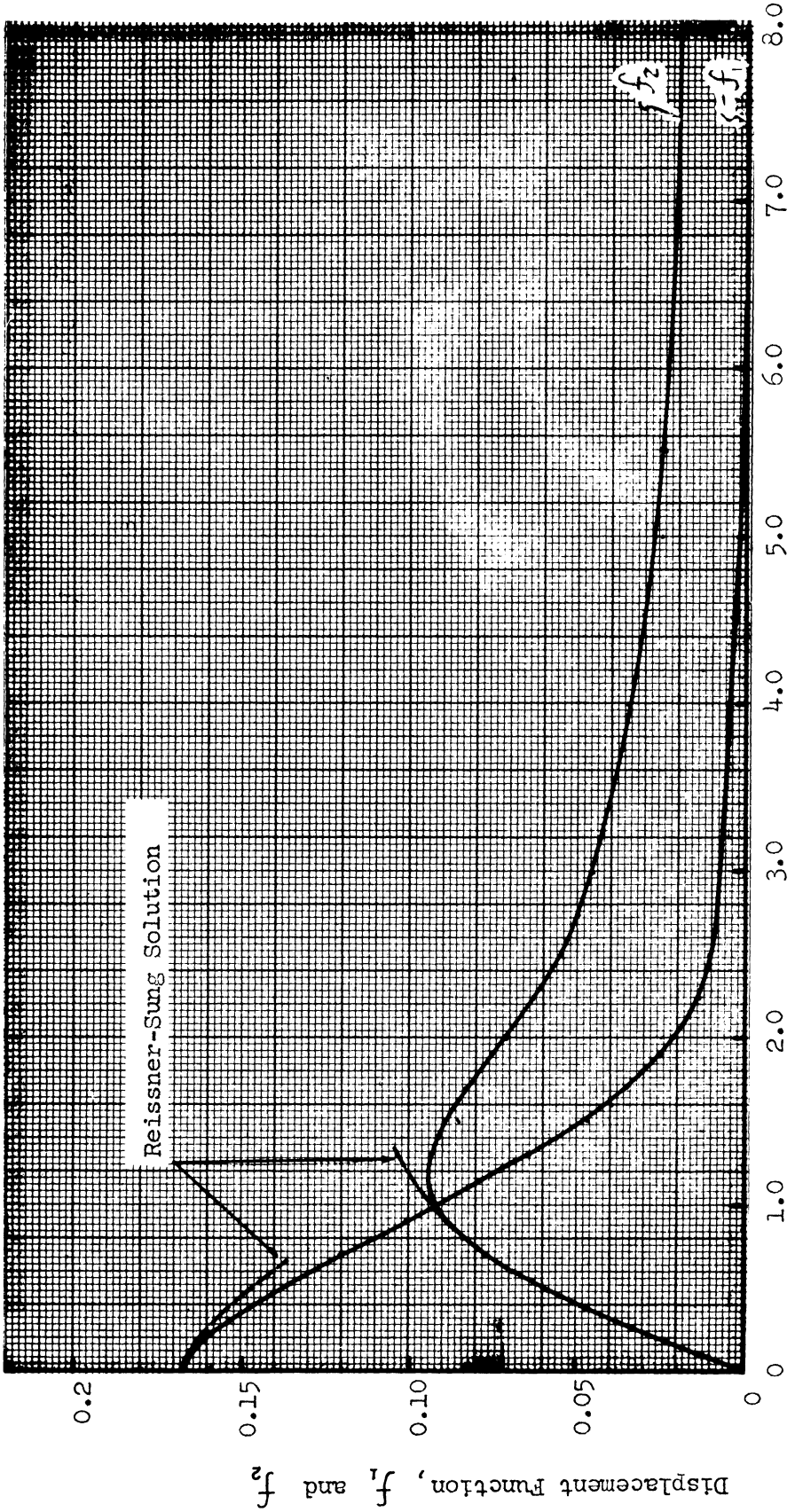

Fig. 8. Theoretical displacement functions for rigid base pressure distribution and for Poisson's ratio of 1/3 (Lysmer and Richart).

of a_o the real part of the function f has no importance.

Based on the computed f values a theoretical curve is drawn, Fig. 9, to show the phase relation between the soil reaction and the displacement for rigid base type pressure and for Poisson's ratio of 1/3. The phase shift between R_T and X is independent of the mass ratio and depends only on the frequency. The phase angle approaches 90 degrees with increasing frequency factor.

RESONANT FREQUENCY AND MAXIMUM AMPLITUDE OF THE SYSTEM

A theoretical solution for the natural frequency and the maximum amplitude can be obtained from the relations existing among the elastic characteristics of the subsoil, the frequency factor and the mass ratio of the system. From Eq. (30) is obtained a relation

$$\frac{X G r_o}{Q_1} = \left[\frac{f_1^2 + f_2^2}{(1 + b a_o^2 f_1)^2 + (b a_o^2 f_2)^2} \right]^{\frac{1}{2}} \qquad (35)$$

The left side of this equation is a dimensionless quantity and indicates the amplitude of oscillation since G, r_o, Q_1 are constant for a particular system. This dimensionless quantity has been called the "dimensionless amplitude factor" by Richart (17). Curves showing the relations between the amplitude factor and the frequency factor for different values of the mass ratio b are drawn (after Richart) in Fig. 10. The curves are similar in appearance to those obtained for damped forced vibration as shown in Fig. 4. The resonant frequency for a particular system (mass ratio) can

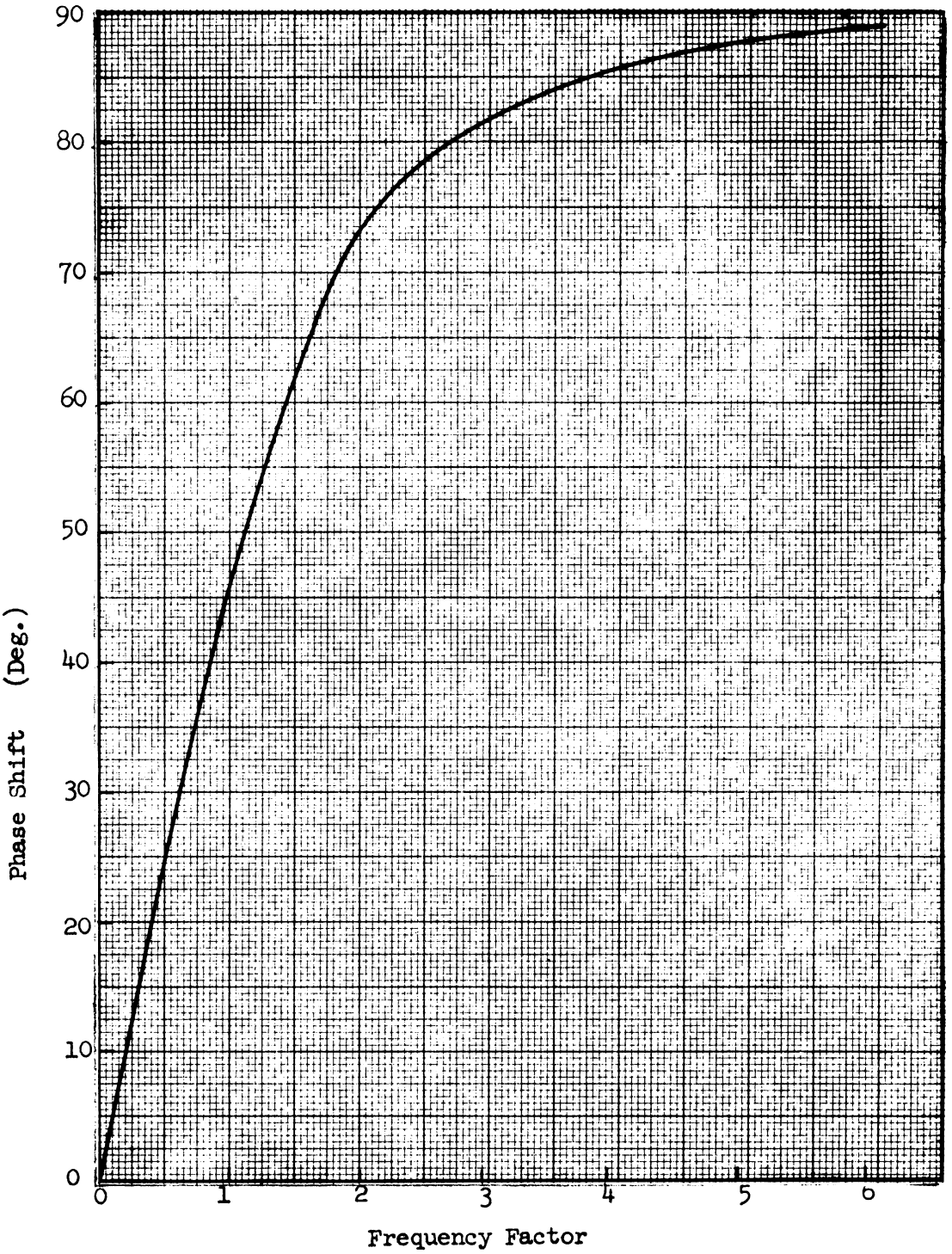

Fig. 9. Theoretical curve showing phase shift between the reaction and displacement vs. frequency factor for rigid base pressure distribution.

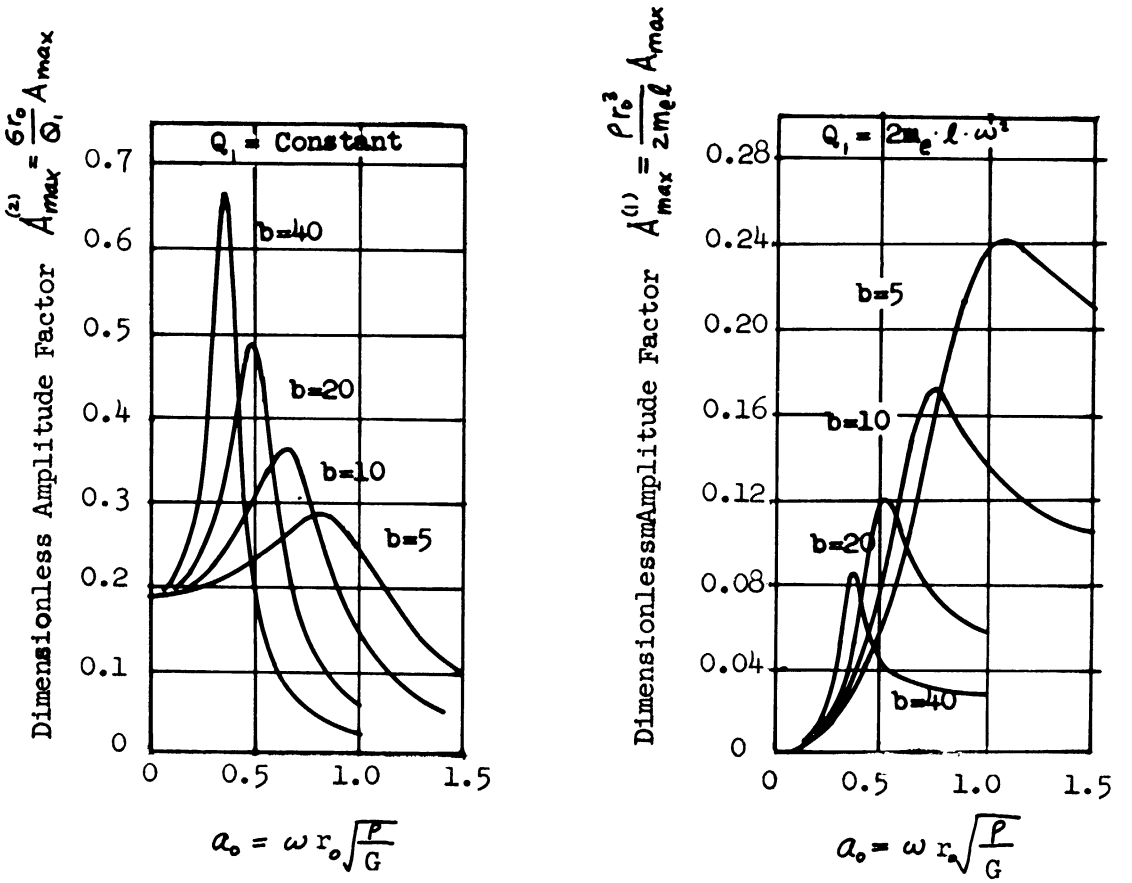

(a) For Costant Amplitude of Force Oscillation

(b) For Rotating-Mass Type Oscillator

Fig. 10. Dimensionless amplitude factor vs. frequency factor for rigid base oscillator (Richart).

be determined from the value of a_o corresponding to the peak amplitude for a specified system. In the same way, the maximum amplitude for a system can be obtained from the peak value of the amplitude factor. In this manner Richart, using the computations made by Sung, has prepared Fig. 11 for the case of rigid base type pressure distribution at the base of a circular footing.

Charts presented in Fig. 11 have a very important and practical use. The resonant frequency and the maximum amplitude for any oscillator-soil system may be determined by the use of these charts. In order to use these charts, however, data for the unit weight, Poisson's ratio and shear modulus of soil, the weight and size of the oscillator base, and the magnitude of exciting force should be known. Of all these quantities, the shear modulus and Poisson's ratio are believed to be difficult to measure, requiring a separate dynamic test, if not intelligently approximated.

It may be observed from these charts that the effects of the mass ratio on both the resonant frequency and the maximum amplitude are very profound. It should be pointed out here, however, that the shear modulus of the subsoil is not constant, but varies with the confining pressure and thus with the mass ratio.

DAMPING IN AN IDEALIZED ELASTIC SOIL

In deriving the initial equation of motion for an oscillator-soil system [Eq. (17)] the term for the damping in soil was not taken into

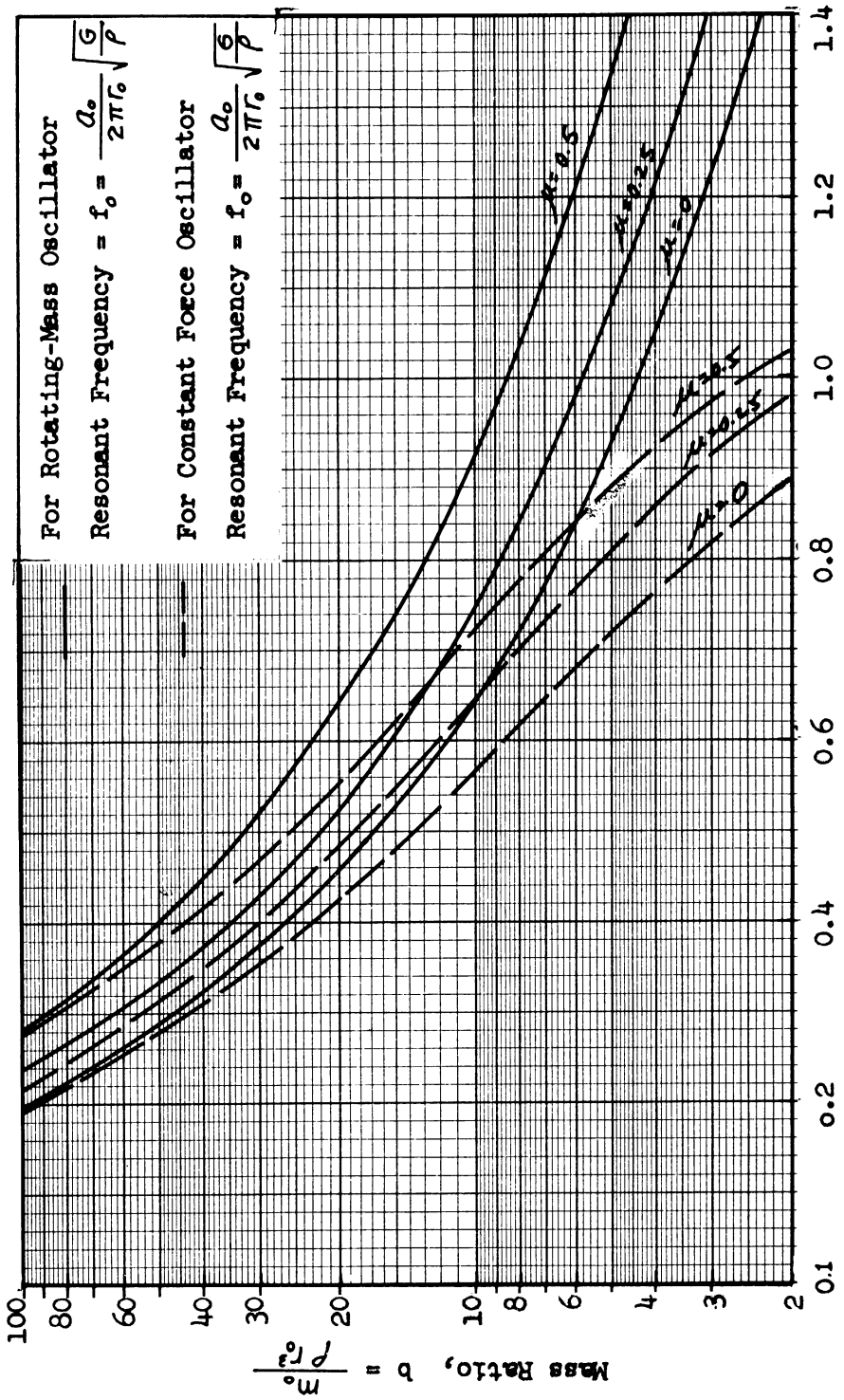

Fig. 11(a). Frequency factor vs. mass ratio for rigid base type pressure distribution (Richart).

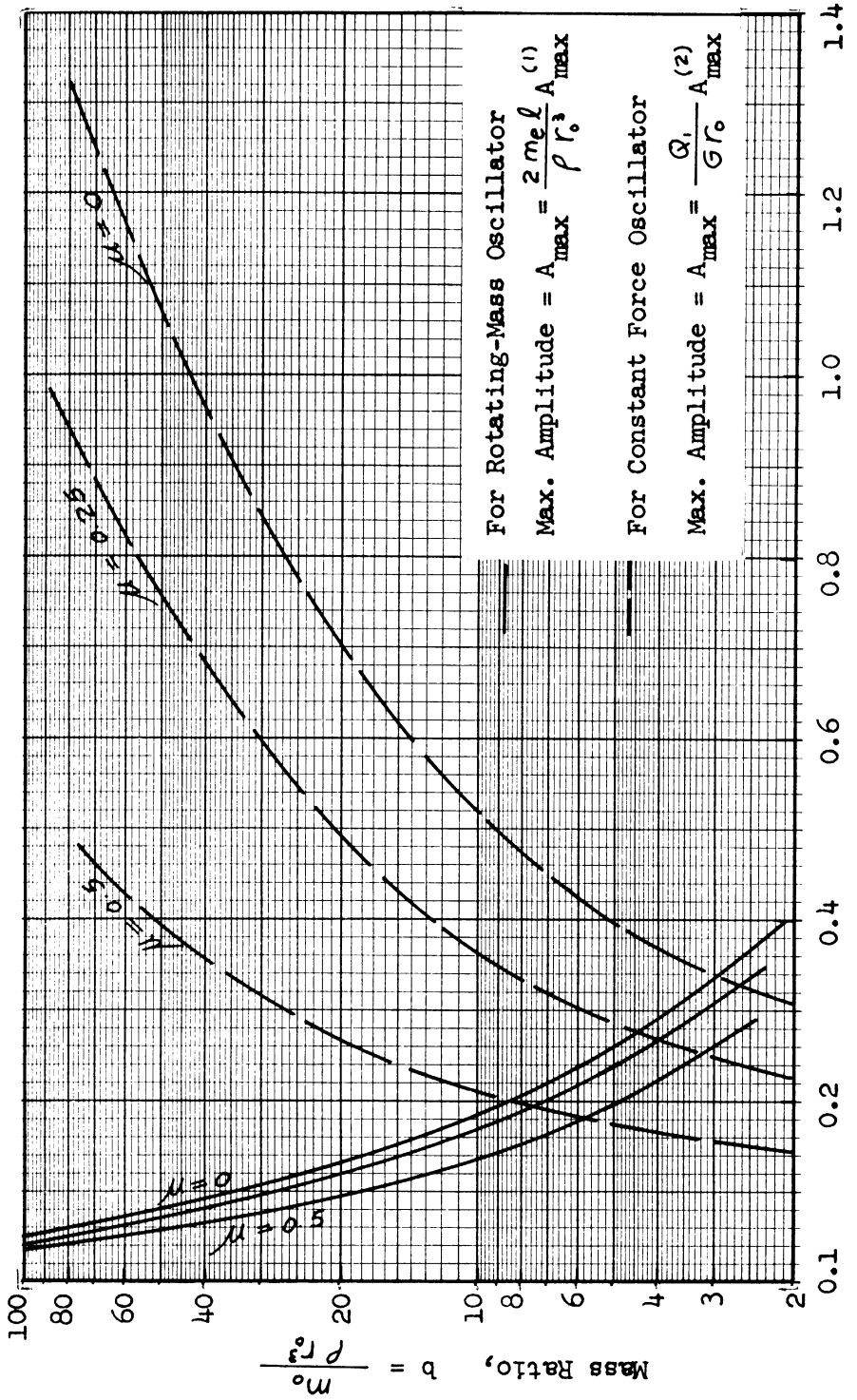

Fig. 11(b). Dimensionless amplitude factor vs. mass ratio for rigid base type pressure distribution (Richart).

consideration. The results of the theoretical analysis, as shown in Fig. 10, indicates that the amplitude of vibration never reaches infinity with changing frequency as is the case in an ideally elastic system with one degree of freedom. This means that even an idealized elastic soil has a damping effect on the amplitude of foundation vibrations. This is due to the dispersion of energy by the propagation of elastic waves, since the assumption of an ideal elastic body precludes energy losses by internal damping within the medium. This dispersion type of damping or geometrical damping in a semi-infinite elastic body has been clearly illustrated by Hsieh (10), who has transformed the fundamental equations in the Reissner-Sung theory into a form comparable to that developed for the conventional one-degree-of-freedom system with viscous damping. The following derivations are from Hsieh's study condensed by Hall and Richart (7).

The vertical displacement x of a weightless rigid circular disk resting on a semi-infinite elastic body, and subjected to a vertical periodic force $P = P_1 e^{i\omega t}$ has been given previously in Eq. (27) as

$$x = \frac{P_1}{G r_o} (f_1 + i f_2) e^{i\omega t} \qquad (27')$$

Taking the derivative of Eq. (27') with respect to time gives

$$\dot{x} = \frac{P_1 \omega}{G r_o} (i f_1 - f_2) e^{i\omega t} \qquad (36)$$

Combining these two equations, is obtained

$$f_1 \omega x - f_2 \dot{x} = \frac{P_1 \omega}{G r_o}(f_1^2+f_2^2)\, e^{i\omega t} = \frac{P\omega}{G r_o}(f_1^2+f_2^2) \qquad (37)$$

or

$$P = \frac{-G r_o}{\omega}\left(\frac{f_2}{f_1^2+f_2^2}\right)\dot{x} + G r_o\left(\frac{f_1}{f_1^2+f_2^2}\right)x \qquad (37')$$

Equation (37') indicates that the force transmitted to the elastic body is a function not only of the displacement of the plate, but also is a function of its velocity. By using the notations a_o and

$$F_1 = \frac{-f_1}{f_1^2+f_2^2} \qquad (38)$$

$$F_2 = \frac{f_2}{a_o(f_1^2+f_2^2)} \qquad (38')$$

Eq. (37') becomes

$$P = -\sqrt{G\rho}\; r_o^2 F_2 \dot{x} - G r_o F_1 x \qquad (39)$$

The values of F_1 and F_2 may be calculated for any values of Poisson's ratio using the computed values of f_1 and f_2.

Equation (39) may further be simplified by substituting

$$R_v = \sqrt{G\rho}\; r_o^2 F_2 \qquad (40)$$

and

$$K_v = G r_o F_1 \tag{41}$$

to give

$$P = -R_v \dot{x} - K_v x \tag{42}$$

If a cylindrical mass of radius r_o and weight W_o is placed on the weightless rigid disk and subjected to a vertical exciting force Q the equation of motion becomes

$$m_o \ddot{x} = P + Q \tag{43}$$

substituting Eq. (42) to Eq. (43)

$$m_o \ddot{x} + R_v \dot{x} + K_v x = Q \tag{44}$$

Equation (44) is identical to the equation for the one-degree-of-freedom forced vibration with viscous damping as was shown in Eq. (3), except that both R_v and K_v are dependent upon the frequency factor a_o.

Hall and Richart have shown that the magnitude of dispersion damping can be evaluated in terms comparable to conventional damping criteria if critical damping is specified, from $c_c = 2\sqrt{Km}$, as

$$R_{vc} = 2\sqrt{K_v m_o} \tag{45}$$

Then the damping ratio can be determined from

$$\frac{R_v}{R_{vc}} = \frac{\sqrt{G\rho}\, r_o^2 F_2}{2\sqrt{G r_o m_o F_1}} \tag{46}$$

By substituting the mass ratio of system $b = m_o/\rho r_o^3$, Eq. (46) can further be simplified to

$$\frac{R_v}{R_{vc}} = \frac{F_2}{2\sqrt{b F_1}} \tag{47}$$

Thus the dispersion type of damping in the system is a function directly of the mass ratio, and thus can be estimated for a particular system with the value of a_o at the maximum amplitude, which may be determined from the curves given in Fig. 11.

Brief Review of Previous Work on the Study of Oscillator-Soil Systems

The first five works to be reviewed are based on the theory of vibrations other than that of a semi-infinite elastic body. They are more or less arranged in a chronological order.

HERTWIG, FRÜH, AND LORENZ (DEGEBO) (1933)

DEGEBO (German Research Society for Soil Mechanics) (9) is generally credited to be the first organization to conduct extensive experiments in the field to determine the dynamic characteristics of vibrator-soil systems. Using a centrifugal force type (two mass) oscillator, various tests were conducted in the hope of finding practically usable relations between the properties of soil and the dynamic characteristics of the

vibrator-soil system. Variation of the natural frequencies with the different types of soil were investigated and thought at first that such frequencies were independent of the test system employed.

Finding that the experimental results obtained did not agree with the theoretically predicted values [Eq. (2)], Hertwig, et al., introduced a correction factor which involved the "in-phase" soil, that is, the weight of the subsoil oscillating with the vibrator. Thus, as shown in Fig. 12, the oscillating mass was considered to be composed of the mass of the oscillator plus the mass of the "in-phase" soil. The standard natural frequency equation [Eq. (2)] was transformed to read as

$$f_n = \frac{1}{2\pi}\sqrt{\frac{K'\bar{A}g}{W_s + W_v}} \qquad (48)$$

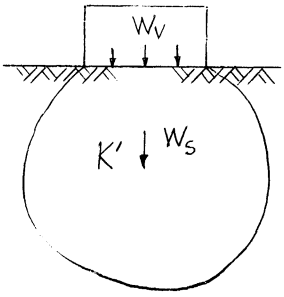

Fig. 12. "In-phase" soil under the oscillator.

where

$K' = K/\bar{A}$ = coefficient of subgrade reaction
$\bar{A}$ = contact area between vibrator and soil
W_S = weight of "in-phase" soil
W_V = weight of vibrator

The determination of the exact mass of the "in-phase" soil was rather difficult, however, since they found that the mass varied with the loasing condition and with the exciting frequency. This method of analysis is, therefore, at best very crude and is limited in its application.

Nevertheless, this method of analysis has been employed by a number of researchers since, and several methods of approach have been proposed.

CROCKETT AND HAMMOND (1948)

Crockett and Hammond (3) conceived the concept of "a bulb of pressure" in the soil below the footing oscillating with the vibrator. Although there was no experimental evidence that the "bulb of pressure" represented the equivalent weight of the "in-phase" soil, they found that the idea appeared to give reasonably accurate results in practice. Notwithstanding the fact that whether the "bulb of pressure" actually is the mass of the soil oscillating with the vibrator, it must be realized that the mass of an "in-phase" soil is a function not only of the weight of the oscillator but also of the exciting frequency and the magnitude of the input force, and consequently, the determination of the exact mass of the bulb of pressure for different variables should be rather difficult.

Crockett and Hammond also maintained that soil has a peculiar "self" frequency depending on its physical properties. A certain soil can have a range of resonant frequency, but it has no such frequency by itself alone. Whenever the resonant frequency of a particular soil is mentioned it is the resonant frequency of the oscillator-soil system, and thus the characteristics of the whole system should be mentioned.

PAUW (1953)

A more rational method of analysis based on the "in-phase" mass concept was made by Pauw (14). Having noted that the zone which vibrates

under the influence of the periodic impulses is not sharply defined and depends on the physical properties of the subgrade, Pauw proposed an analysis of the problem based on an analogy whereby both the equivalent spring factors and the apparent mass of soil vibrating with the foundation may be determined in a rational manner. His "soil-spring" analogy is based on the assumption that the modulus of elasticity is proportional to the effective depth for cohesionless soils, and constant for cohesive soils, and that the stress distribution beneath the plate has a form of truncated pyramid having uniform stress distribution over any section parallel to the contact surface.

Based on the above assumptions and using the concept of static stress-displacement he derived the equations to express the equivalent soil spring constants for horizontal and vertical contact surfaces. Equations for the "apparent" soil mass factors were developed by equating the kinetic energy of an equivalent concentrated mass to the total kinetic energy in the effective zone as follows:

$$M_s = \frac{\rho B^3}{g \alpha} \cdot C_m \qquad (49)$$

where

M_s = apparent soil mass

ρ = soil density

B = least dimension of the footing

g = gravitationsl acceleration

α = angle of sloping planes of effective zone (truncated pyramid)

c_m = factor defined by a equation

Pauw presented the results of his work in the form of charts for the determination of the apparent soil mass and the equivalent spring constants. With these values so obtained, the natural frequency of a vibrator-soil system may be determined by the standard equation [Eq. (48)].

Pauw noted that his methods for computing the apparent mass is limited to cohesionless soils, and cannot be applied to cohesive soils.

EASTWOOD (1953)

Eastwood (4) conducted an experimental investigation to determine the factors affecting the natural frequency of vibrator-soil systems and to study the effects of vibrations on the bearing properties of foundations on sand. A box of sand measuring 4 ft on three sides was used as he found the size of the box was large enough to avoid any interference with the modes of vibrations of the footings used. Varying the size, shape, and weight of footings, the natural frequencies of various footing-soil systems were determined by picking up signals, which were produced by a single impulse with a hammer.

He found that at low loads the frequencies were almost independent of the footing size for a given load intensity, but for high loads they were almost inversely proportional to the size of the footing as shown

in Fig. 13. In this respect he stated that the conclusion of DEGEBO that the resonant frequency increases with the size of the footing was shown to be fallacious.

From the experiments he also observed that it was impossible to estimate the effective mass of soil which acted with the vibration ("in-phase" mass) as the mass appeared to vary with the test conditions. For in-undated foundations he noted that the natural frequencies were again almost independent of the footing shape at low load, but the frequencies were only a little over half those on the dry sand. At high load intensities the frequency was again roughly inversely proportional to the footing width. His observation, that the natural frequency was constant regardless of the thickness of the supporting sand, is hard to understand as the author admitted of being unable to explain why that should be so. According to a later study by Warburton (22), the thickness of layer beneath the footing is a definite factor affecting the response of the footing in oscillation up to the depth having the six plate diameters.

TSCHEBOTARIOFF (1953)

A statistical approach based on the past performance records of machine-foundations was made by Tschebotarioff (21). He noted that the results of the past investigations on the study of the soil characteristics which influence the natural frequency of machine-foundation showed a wide variance with each investigator and apparent contradictions against each other. He observed that the difficulties in deter-

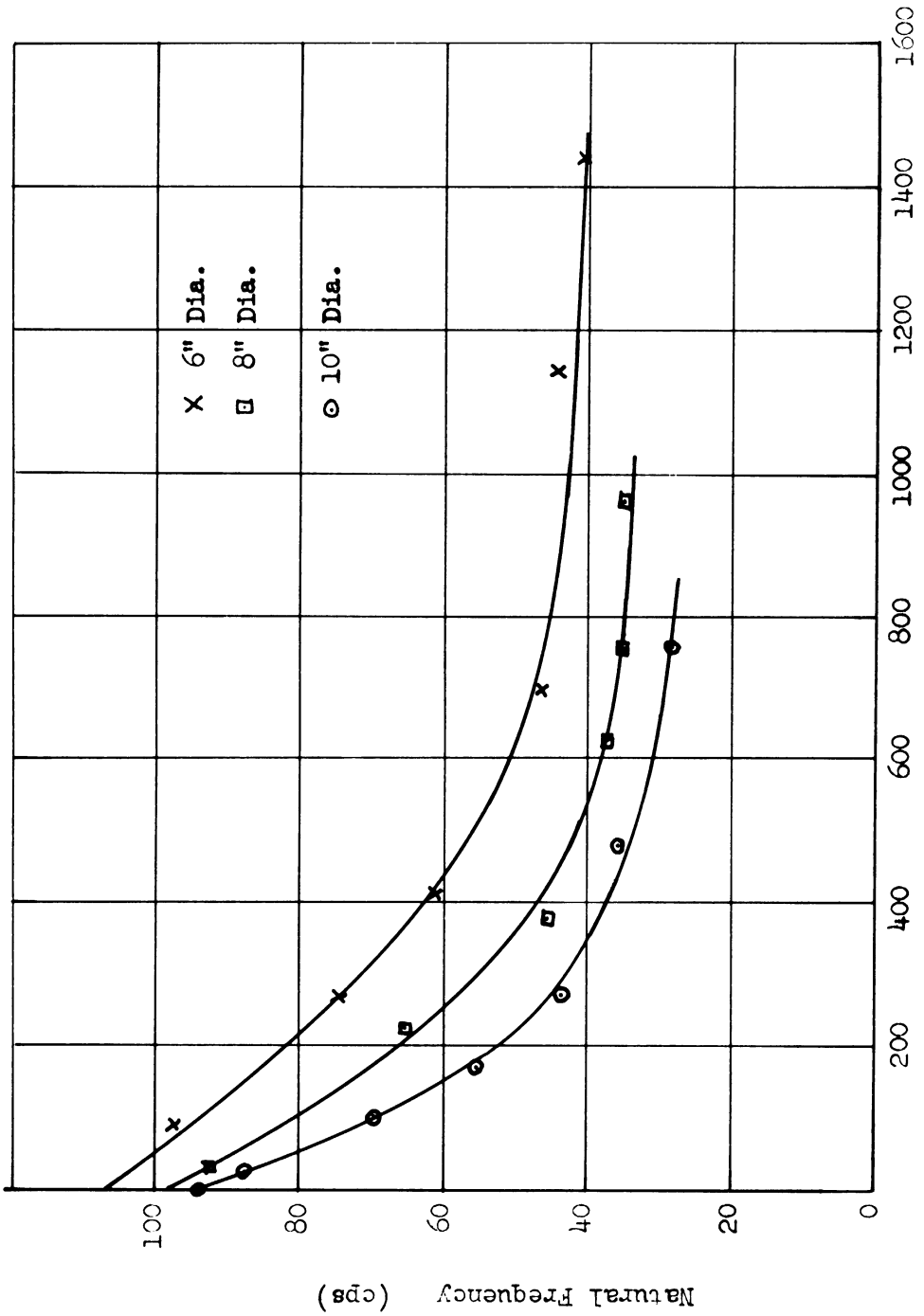

Fig. 13. Natural frequencies of circular footings on dry sand (Eastwood).

mining the natural frequency of one particular soil resulted from the variation of dynamic soil modulus values which were dependent upon the characteristics of the vibrating soil or the oscillator itself.

From the available records from the past by DEGEBO, VIOS (Russia), the U. S. Coast and Geodetic Survey on earthquakes in California, and Princeton University, he attempted to analyze the problem by what he termed a "reduced" natural frequency, by modifying the conventional formula [Eq. (48)] to read:

$$f_n = \sqrt{\frac{\bar{A}}{W_v}} \cdot \frac{1}{2\pi} \sqrt{\frac{K' g}{\left(1 + \frac{W_s}{W_v}\right)}} \tag{50}$$

or

$$f_{nr} = \sqrt{p} \cdot f_n \tag{51}$$

where

$p = W_V/\bar{A}$ = average unit pressure on the ground

f_{nr} = "reduced natural frequency"

The "reduced" natural frequency is the natural frequency at an average unit pressure on the ground equal to unity. Plotting of the reduced natural frequency for the aforementioned data and some more data that became available later showed a definite pattern for a given type of soil. This implied that the value of the dynamic modulus of soil reaction K' in the formulas [Eqs. (48) or (50)] changed with the size of the loading area, and the ratio of W_S/W_V either remained constant or

varied only slightly. Figure 14 has been reproduced to show the relations between the loaded area and the reduced natural frequency.

In the following are reviewed the theoretical and experimental investigations based on the theory of vibrations for a semi-infinite elastic body.

QUINLAN (1953)

Quinlan (15), independent of Sung, analyzed the problem based on the work by Reissner. He obtained the theoretical solutions for the cases of circular and the long rectangular vibrator under various assumptions as to contact pressure distribution. His final results yielded similar solutions to those by Sung.

ARNOLD, BYCROFT, AND WARBURTON (1955)

Arnold, Bycroft, and Warburton (1) considered theoretically the forced vibration of a rigid body resting on a homogeneous elastic medium of infinite surface area and constant depth which may be finite or infinite. Four different modes of vibration for a body with a circular base were investigated: (a) vertical translation, (b) horizontal translation, (c) torsion, and (d) rocking.

For the experiment they used foam rubber to investigate the amplitude-frequency responses under vertical and rotational excitations produced by an electromagnetic oscillator. They obtained close agreement between the theoretical and experimental results for the vertical translational modes, but for the rotational modes the experimental values were smaller

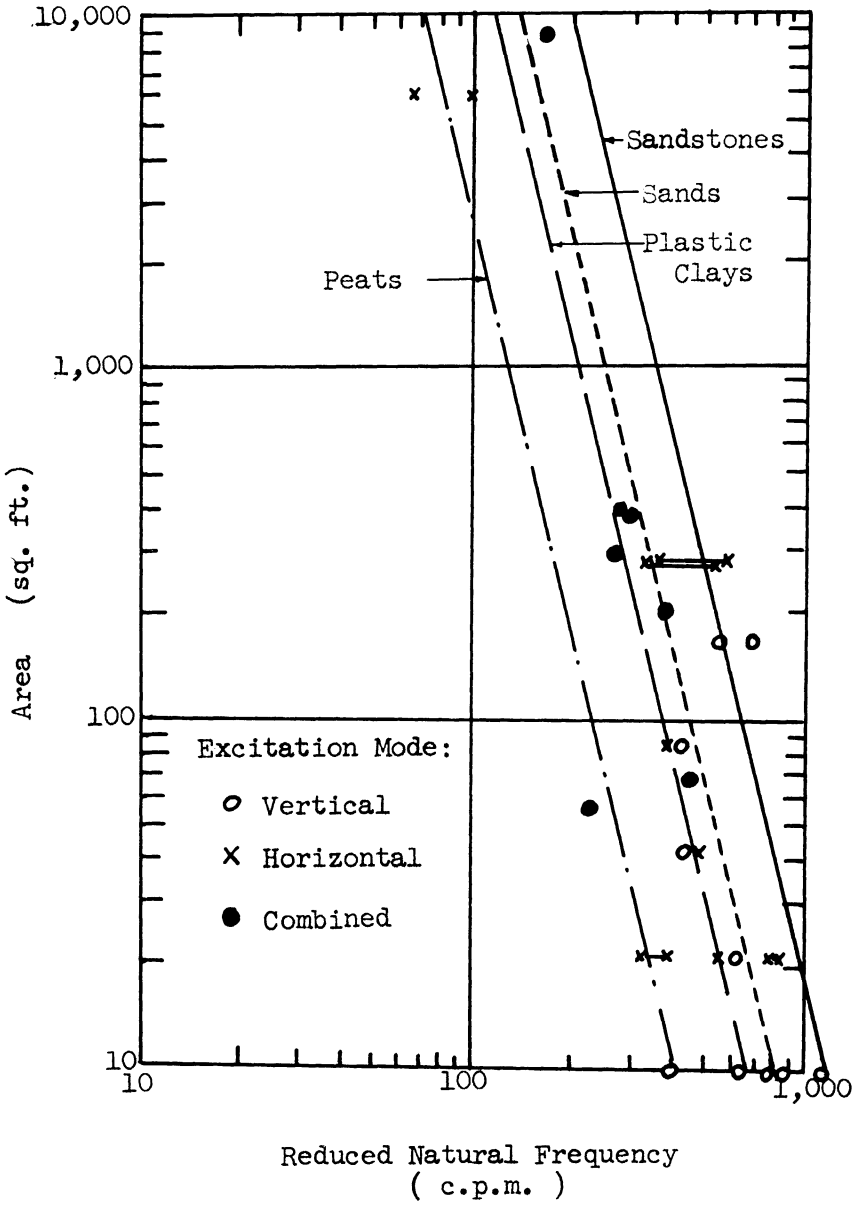

Fig. 14. Reduced natural frequency vs. foundation area (Tschebotarioff).

than the theoretical values, especially at frequencies close to resonance. They felt that this was due to the experimental damping effect, which should be more predominant with the rotational modes.

WARBURTON (1957)

Warburton (22) extended the work (1) to include the case of a surface layer of a soil underlain by a perfectly rigid base for vertical modes of excitations, and compared them with the experimental results given previously by Arnold, Bycroft and himself. He produced the charts showing the relationship between the mass ratio and frequency factor for different depth of stratum factors. He found that there was good agreement between the theoretical and experimental values of the resonant frequency. Any discrepancies between them were attributed to the assumed stress distribution between the mass and the stratum, and the neglected damping in the analysis. The presence of underlying rigid layer led to higher resonant frequencies, especially so at thin layers and high mass ratio values. He also observed that for the soil tested (sandy soil) the natural frequency was independent of the thickness of the stratum if it exceeded six times the diameter of the footings. It was also found that the amplitude of vibration on a layered system was much greater than that on a semi-infinite medium.

RICHART (1953)

Richart's contributions to the development of the theory and the use of it have previously been reviewed. In this section his proposal for

the use of an "effective radius" in relation to the pressure distribution is reviewed.

Sung's investigations clearly indicated that the dynamic characteristics of a vibrator-soil system depend upon the pressure distribution at the base of the footing. From a consideration of the radius of the loaded area Richart (18) proposed to use an "effective" radius of footing for each pressure distribution corresponding to an equivalent uniformly distributed load. The method of determining the equivalent uniformly distributed pressures is illustrated in Fig. 15. These charts show that three types of pressure distribution, uniform, parabolic and rigid base, can be represented by a statically equivalent ring loading ($Q_1 e^{i\omega t}/\pi r_o$) which acts along the circumference of a ring through the centroid of each pressure distribution curve. From this, the radii for equivalent uniformly distributed pressure can be determined. This radius, which yields the same results as those by using the actual radius of loading area with the actual pressure distribution, is termed the "effective" radius. This concept of an "effective" radius shows that as long as the effective radius remains constant, the dynamic characteristics of the systems would be independent of base plate radius or the type of pressure distribution.

JONES (1958)

Jones (11) employed two different methods to measure the dynamic properties in situ: one by the phase velocity of the surface vibrations

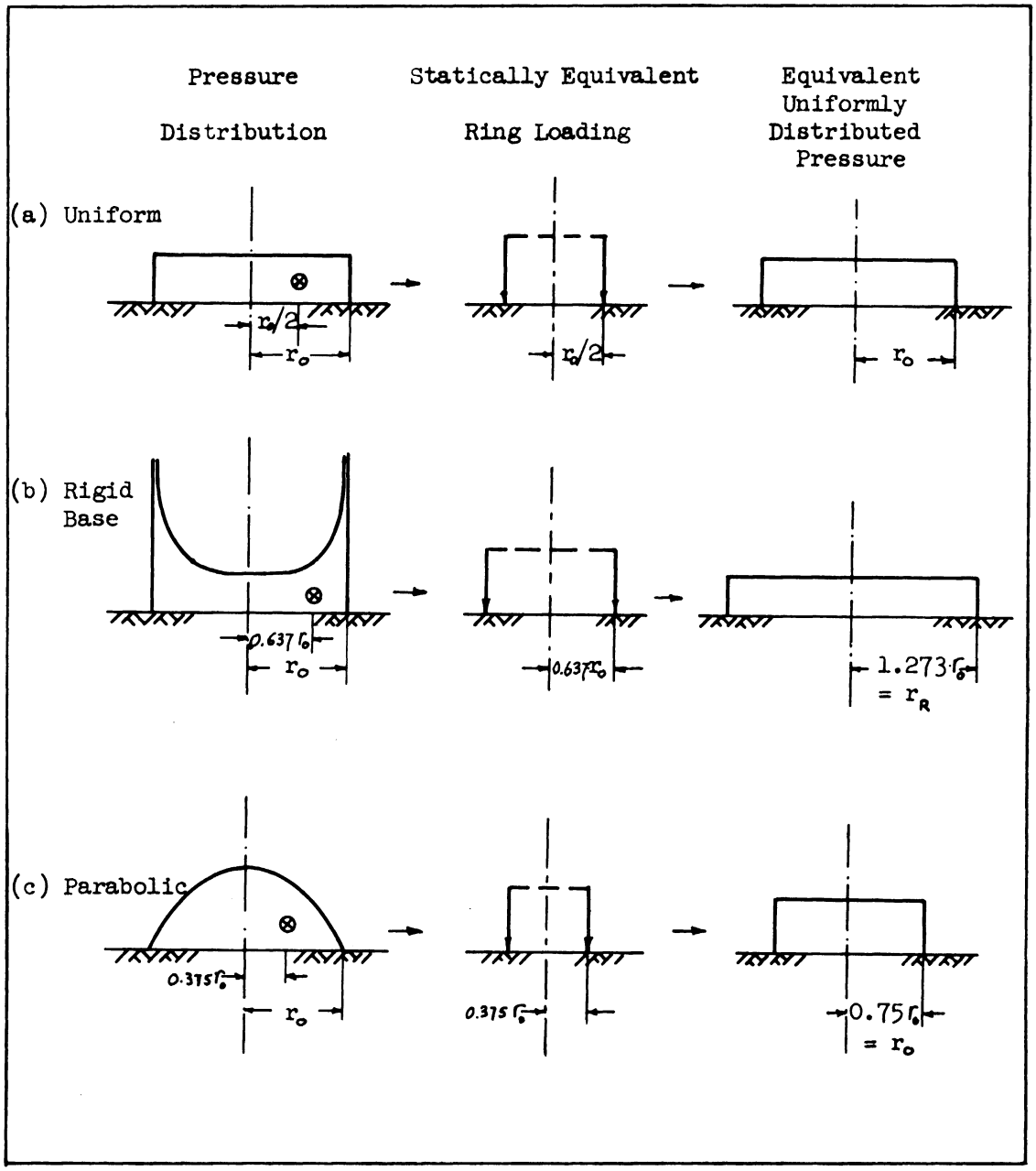

Fig. 15. Method of determining the equivalent uniformly distributed pressures (Richart).

and the other by the resonant frequency of oscillator-soil systems.

For the first part of his experiment he used an electromagnetic vibrator driven by a variable frequency oscillator and power amplifier. The vibrations were produced within the frequency range of 35 to 400 cps. A seismic pickup was moved away from the vibrator at several points where the vibrations were in phase with those at the vibrator. From the distance measured between the points (wavelength) and the exciting frequency the phase velocity was obtained. Measurements were made at distances up to 40 to 80 ft from the vibrator.

Conducting the tests on a silty clay soil underlain by a stratum of gravel he found that the phase velocity decreased with increasing frequency, but approached an approximately constant magnitude at frequencies greater than 150 cps. Correlating this constant magnitude of the phase velocity to the C.B.R. value, he observed there was an empirical relation between the two. The dynamic shear moduli computed from the test results were found to be in agreement with those determined by other techniques.

For the second part of the experiment the same electromagnetic vibrator was used. The vibrator was placed on a leveled ground of sandy clay soil and was loaded with different weights before being driven at resonance. The current in the magnet (driver coil) was varied from 0.5 to 2 amperes. The plates of different sizes (4 to 12 in. diameter) were used. From the values of resonant frequencies the dynamic shear moduli were computed by the theory of vibrations based on an elastic half-space.

In comparing the results for the shear moduli with those obtained by the phase velocity he noted that the results would agree much better if one type of pressure distribution was assumed over the other. Since there was no way of knowing the exact type of stress distribution he concluded that for these particular sites the best choice would be that of midway between uniform and rigid base type pressure distributions.

It was observed also that the resonant frequency decreased with the increasing force of vibration as others had previously noted. He found that the change was greater with the softer soil, and also depended upon the mass of the footing, in that the drop in the natural frequency was greater with the lighter footing at the same input force as shown in the table below:

TABLE III

CHANGE IN NATURAL FREQUENCY DUE TO CHANGE IN CURRENT (FORCE)

Weight, lb	Drop in f_o
75.5	72.5-69.2
118	52.5-50.4
161	43.7-42.8

To see the effects of the mass and diameter of the plate the total weight of the plate was varied from 50 to 340 lb at site C (wet surface and soft), and from 70 to 266 lb at site D (dry and soft), and the size of the plate was varied from 4 to 12 in. in diameter. The results obtained for the plate of 12 in. diameter are summarized in Table IV.

TABLE IV

SUMMARY OF TEST RESULTS

b	f_o at 0.5^{amp} (cps)	f_o at 1.5^{amp} (cps)	G/uniform (psi)	G/rigid base (psi)
4	110	104	2,390	2,270
8	83.5	79	2,450	2,180
12	72.5	71	2,680	2,260
16	64	62.5	2,690	2,280
20	56.5	58	2,640	2,220
24	50	49	2,430	2,000

The results for the natural frequencies have been plotted (by the writer) as shown in Fig. 16. It can clearly be seen from Fig. 16 or from Table IV that the resonant frequency decreased with increasing mass ratio. The values of the shear modulus (G) obtained, assuming uniform or rigid type pressure distribution, were mutually consistent and gave average values of 2,550 and 2,240 psi respectively. He observed, however, that the shear moduli increased with increasing mass ratio for smaller plates, and attributed this fact to local compaction of soil during the experiment. It must be realized, however, that in a later investigation Hardin and Richart (8) recorded that the shear wave velocity, from which the shear modulus is computed, increased with the 1/4 to 1/2 power of confining pressure which, of course, is directly proportional to the weight of footing.

It has been previously stated that the determination of the shear modulus and Poisson's ratio of soils and the knowledge of elastic wave dissipations are essential in the evaluation of the dynamic characteris-

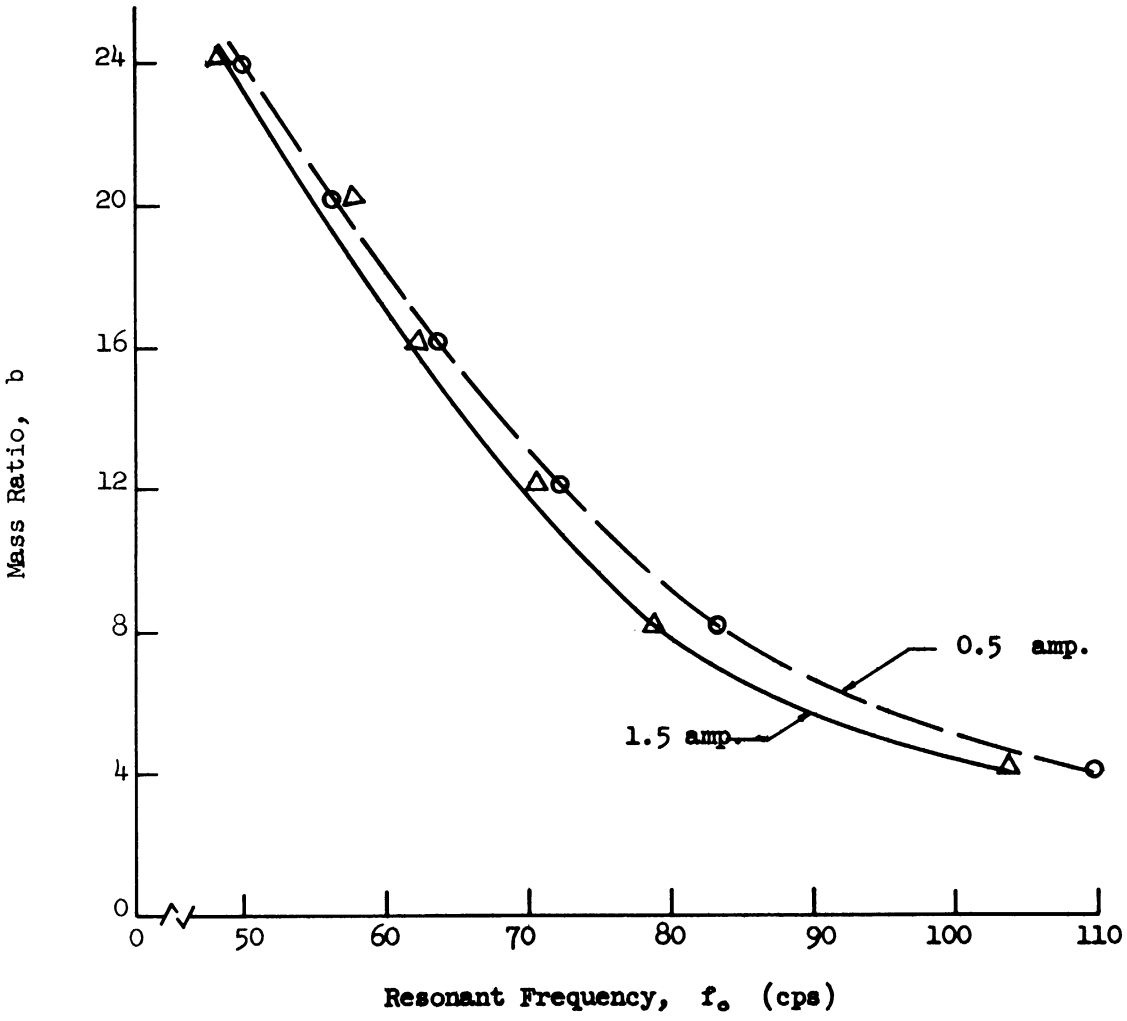

Fig. 16. Resonant frequency vs. mass ratio for different input force (Jones).

tics of foundation-soil systems. These elastic constants of a soil may be obtained from the measurement of shear wave velocities. There have been numerous investigations, both theoretical and experimental, conducted on these subjects in the past. In the following are reviewed only two reports of the work that have been carried out recently.

HARDIN AND RICHART (1963)

Using the resonant column method an extensive series of laboratory tests were conducted to evaluate the compressive and shear wave velocities in specimens of Ottawa sand, crushed quartz sand, and crushed quartz silt. In one type of equipment used the specimen was free at both ends so that at its lowest mode the wavelength was equal to twice the length of the specimen. In the other type of equipment used the specimen was fixed at one end and free at the other. This fixed-free type equipment was developed by Hall (6).

The tests were conducted to observe the effects of the confining pressure, the moisture content, void ratio, and the grain characteristics of the materials. The test results showed that for confining pressure between 2,000 and 8,000 psf, the shear wave velocities varied with approximately the 1/4 power of confining pressure for dry, saturated, and drained sands. For lower pressures, they varied with powers between the 1/2 and 1/4 powers depending on the grain shape and the moisture content. On the shear wave velocity in fine grained materials, the effect of time, and the degree of consolidation appeared to be significant,

aside from the effect of confining pressure. (A more extensive study on the wave propagation in fine-grained materials is being conducted at present in the Soil Dynamics Laboratory at The University of Michigan.) They also found that for dry sand the shear wave velocity decreased linearly with increasing void ratio under a specified confining pressure, and was independent of grain size, gradation, and relative density.

HALL (1962)

The main emphasis placed by Hall (6) in the study of wave propagations was in the evaluation of the effect of vibration amplitude on the wave velocities and damping in granular soils. Utilizing the resonant column method with the "fixed-free" apparatus described previously, the tests were conducted on Ottawa sand, glass beads, and a silt-sized crushed quartz. Vibration amplitudes employed were much larger than those used by Hardin.

The test results showed that both the compressive and shear wave velocities decreased with increasing amplitude of vibration. This decrease, it was observed, might be as much as 10 to 15% as the double amplitude was increased from 1×10^{-5} to 2.5×10^{-3} radians in torsion or from 2×10^{-6} to 1×10^{-3} in. in the longitudinal tests. This amount of change was comparable to that produced by changes in void ratio from the maximum to minimum value.

Using the same apparatus described above, he evaluated (7) the effects of confining pressure, amplitude of vibration, degree of satura-

tion, and the grain characteristics of materials on the internal damping in granular soils. Measurements for damping were made by recording the decay curve of vibration. His findings showed that for dry Ottawa sand the logarithmic decrement varied with approximately the 1/4 power of amplitude, but for saturated sand the variation was much less than for the dry condition. As to the effect of confining pressure on sand, it was observed that the damping appeared to decrease with an increase in confining pressure.

WATERWAYS EXPERIMENT STATION, CORPS OF ENGINEERS (1963)

Any theory, in order to be valid, must be supported by experimental or field test data. During the period of 1960 through 1962 an extensive series of tests were conducted by the Waterways Experiment Station (WES), and the test results, without analyses, have since been reported (23).

The writer has had an opportunity of analyzing the obtained data based on the concept of a foundation-soil system as being a mass resting on a semi-infinite elastic body.

The tests were conducted on a selected site at the WES area (silty clay), and on another site at Eglin Air Force Base, Florida (sand). Four reinforced concrete circular bases were built at both sites (designated as bases 1, 2, 3, and 4) having diameters of 62.0, 87.6, 107.6, and 124.0 in. respectively. Bases 2, 3, and 4 are multiples of base 1 in regard to contact area. In addition, base 5 (same area and weight as base 3) was used at the Eglin site for surcharge effect, and base 16 (16 ft in

diameter) was constructed at the WES site. The vibrator (two-rotating-mass type) was approximately 53 in. long, 48 in. wide, and 24 in. deep, and weighed 5,600 lb. The eccentric masses weighed 339 lb each, and the eccentricity was varied from 0.105 to 0.418 in. This means that the input force could be varied from 365 to 52,070 lb in the vertical mode of vibration, depending on the frequency of operation employed.

The tests consisted of applying sinusoidal forces and moments to the bases in the vertical, torsional, and rocking modes of oscillation. The variables considered were the static weight, the size of bases, and the frequency (constant area tests, equal weight tests, equal static pressure tests, etc.). The elastic moduli of the soils at the sites were determined by surface seismic methods.

The test results for the displacement and phase shift were obtained for each setting of base-soil system. For the vertical mode of vibration alone, data were obtained for 63 tests at the WES site, and for 39 tests at the Eglin site.

All the test results have been tabulated and summarized. An analysis of the test results for the case of vertical oscillation is presented in Figs. 17 and 18. In the analyses the resonant frequency was determined by the "tangent" method, that is to say, by drawing a line tangent to the displacement-frequency curve through the origin and reading the frequency at the contact point. The amplitude ratio shown as ordinate in the graph is the ratio of the measured maximum amplitude to that computed using the curves prepared by Richart, Fig. 11, assuming a

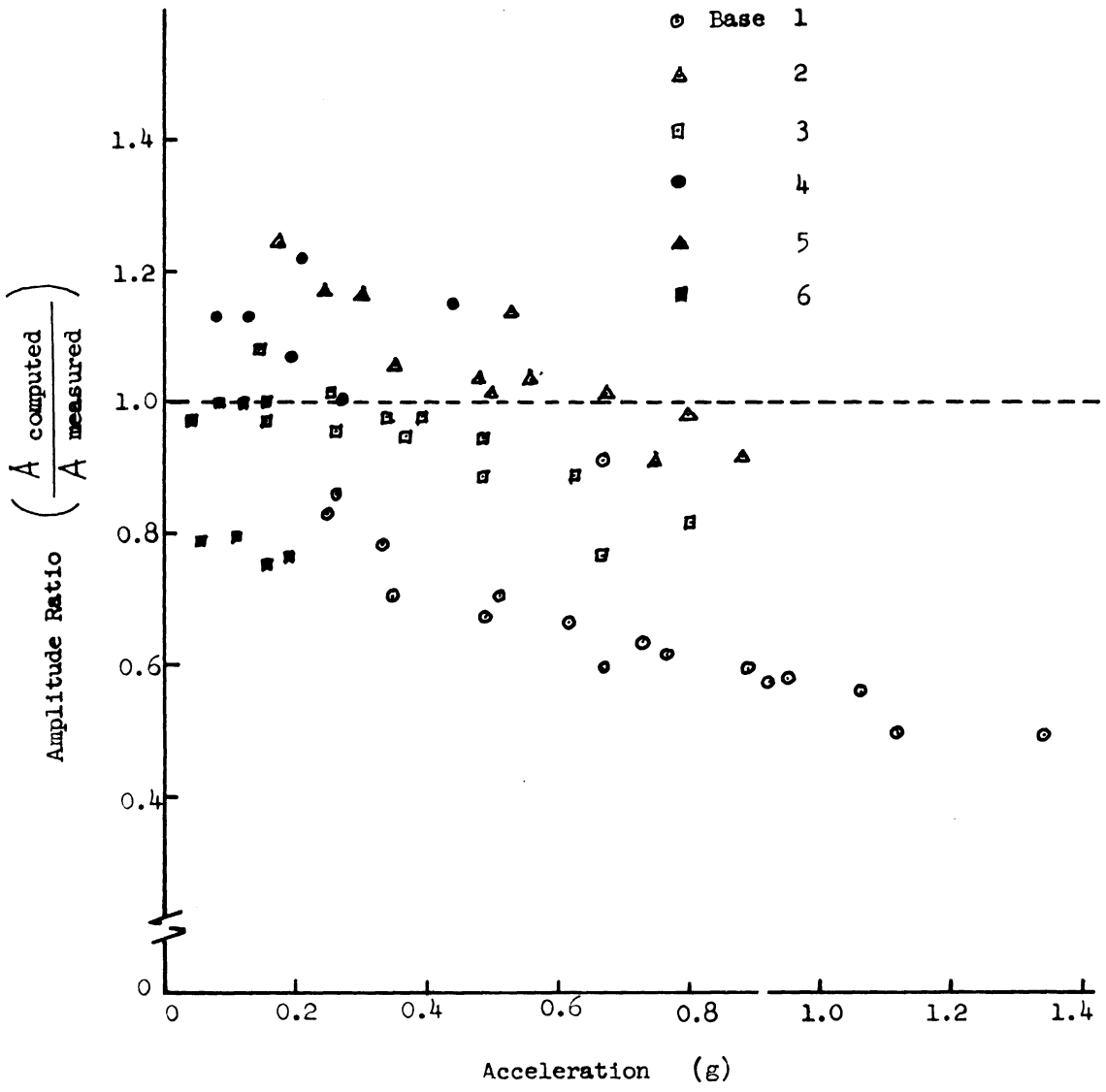

Fig. 17. Comparison of test results for maximum amplitude with the theoretical values (Waterways Experiment Station).

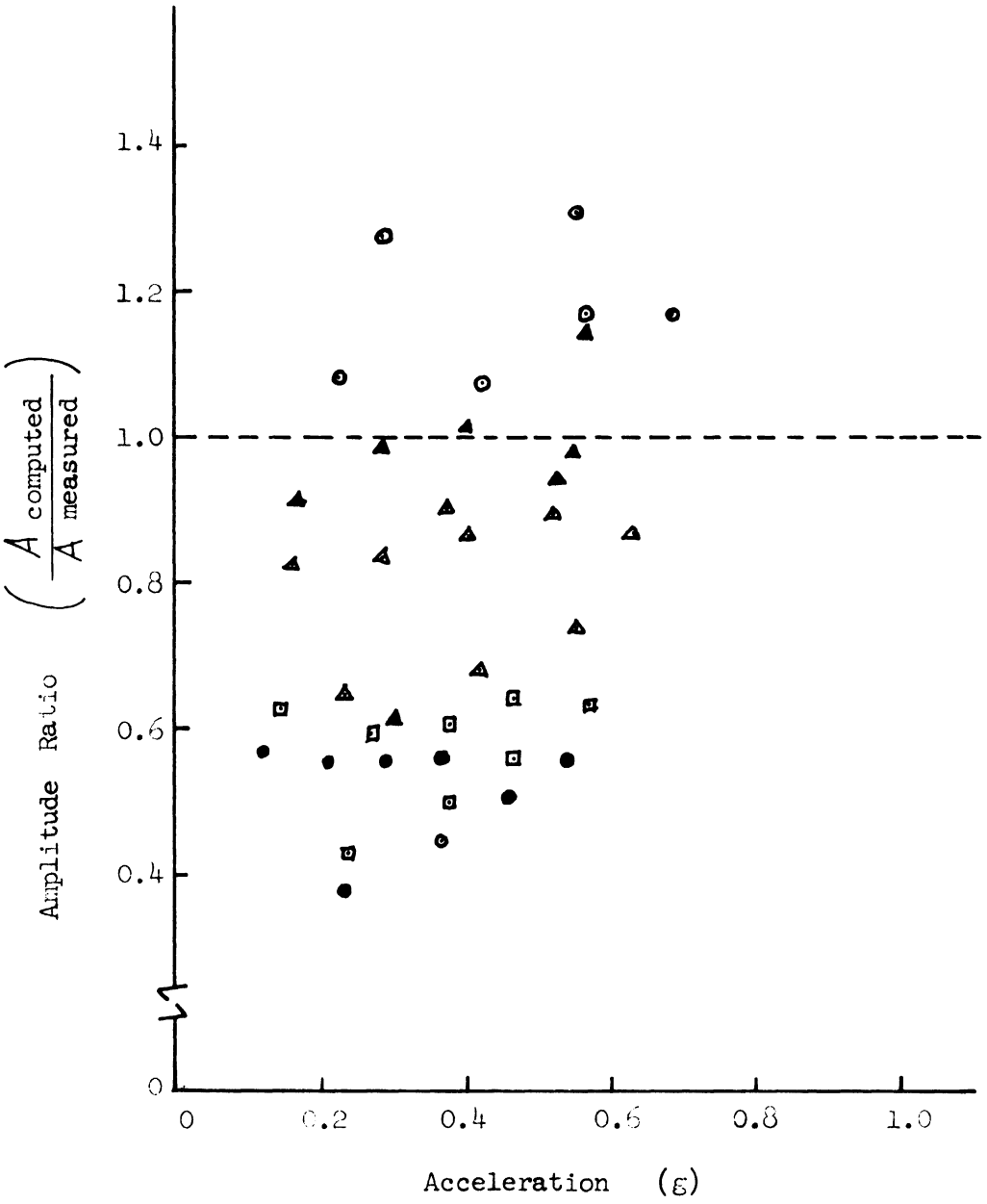

Fig. 18. Comparison of test results for maximum amplitude with the theoretical values (Waterways Experiment Station—Eglin Air Force Base).

rigid base type pressure distribution. The elastic constants of the materials used in the computation were those determined from their seismic tests. Figures 17 and 18 show that agreement between the theoretically computed values and those obtained by the field tests is rather good, considering the difficulties in measuring some of the quantities, such as phase shift, in the field and in the evaluation of the elastic constants of the soil.

In Table V below are summarized some of the typical test results. The test results shown are for the vertical mode tests at the WES site, conducted for an equal eccentricity (ℓ = 0.105 in.). In the equal weight tests each base had the same static weight of 30,970 lb, and in the equal static pressure tests each base, regardless of the size, was loaded to provide a static pressure of 4.25 psi. Thus, tests were performed in which (a) a constant weight was maintained, and contact area and pressure varied; and (b) a constant contact pressure was maintained, and the weight and contact area varied.

From the analyses of the tests in vertical modes at the WES site, such as shown in Table V, the following conclusions have been tentatively drawn by the writer:

1. For an equal size of footings both the resonant frequency and the maximum amplitude decreases with the greater mass ratio, that is more static weight. This checks with the "semi-infinite elastic body" theory.

TABLE V

SUMMARY OF TEST RESULTS
(Waterways Experiment Station)

Base	Test No.	Mass Ratio	Resonant Frequency (cps)	Maximum Amplitude ($\times 10^{-4}$ in.)
		Equivalent Weight Tests		
1	28	15.3	15.0	107
2	7	5.4	17.4	45
3	6	2.3	17.8	37
4	13	1.9	17.0	27
		Equal Static Pressure Tests		
1	1	6.3	19.6	155
2	11	4.5	18.4	51
3	2	3.6	18.0	37
4	5	3.2	15.8	22
		Equal Radius Tests		
1	20	15.3	14.5	110
1	28	15.3	15.0	107
1	8	12.7	15.4	126
1	12	12.7	15.1	140
1	1	6.3	19.6	155

Vertical mode of vibration; eccentricity ℓ = 0.107 in.

2. If the mass ratio is the same the resonant frequency decreases with increasing eccentricity, that is, greater input force. (Note that the input force is also dependent upon the frequency.)

3. For an equal static pressure the resonant frequency and the maximum amplitude decreases as the mass ratio decreases, that is, with larger footings. This may be explained by the "elastic half-space" theory that a_o/r_o in the frequency equation and $A_{max}^{(1)}/r_o^3$ in the amplitude equation become smaller with the greater mass ratio, that is larger r.

4. For an equal weight the resonant frequency appears to increase with decreasing mass ratio. The maximum amplitude decreases definitely with smaller values of the mass ratio for the same reason given in 3.

CHAPTER III

THEORY FOR THE EXPERIMENTAL DETERMINATION OF PRESSURE DISTRIBUTION

General

DESCRIPTION OF TEST SYSTEMS

There are seven test systems employed in the present research as described in the following table:

TABLE VI

DESCRIPTION OF TEST SYSTEMS

Test System No.	Weight of Footing (lb)	Mass Ratio
1	80.0	5.83
2	120.0	8.74
3	171.1	12.47
4	217.6	15.85
5	257.1	18.73
6	302.3	22.02
7	342.3	24.94

Frequency Range = 50-1,000 cps
Range of Input Force (constant amplitude) = 9.0-22.5 lb vector
Radius of Footing = 0.5 ft (constant)

STATIC CONTACT PRESSURE DISTRIBUTION UNDER A RIGID FOOTING

The normal stress (the soil reaction) developed at the surface of contact between a footing and the supporting soil is termed contact pressure. It is known that the static contact pressure at the base of a

perfectly rigid footing resting on a semi-infinite elastic body increases from the center toward the rim of the base where it reaches an infinite value as shown in Fig. 19(a) in order to produce a uniform settlement. Since the pressure along the edges cannot exceed a certain finite value (bearing capacity) at which the material passes from elastic to plastic state, the pressure in a real soil is shifted, as the load is increased, toward the center until the distribution becomes uniform at the instant when the material fails by general shear failure. If a footing rests on a dry cohesionless sand, the pressure under any load increases from zero at the edges toward the center where it reaches a maximum value as shown in Fig. 19(b).

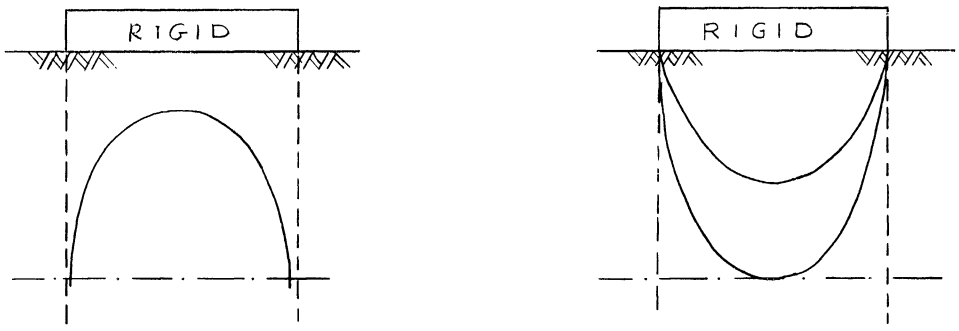

(a) Real, Elastic Material (b) Cohesionless Sand

Fig. 19. Contact pressure distribution under a rigid footing.

It has been stated previously that the pressure distribution varies between that of a rigid base and that of a parabolic type with the varying applied force. This leads to say that the repeated application of a static force (stress or strain history)—which is essentially a dynamic

load--causes a change in the pressure distribution. A change in the pressure distribution also occurs when the footing rests on a real soil whose properties differ from those of the "idealized" soil, which was the basis of the analytical solutions.

The Footing-Soil System in the Present Investigation

FORCE-REACTION-PHASE RELATIONS IN RING SYSTEM

The simplest possible system for the determination of pressure distribution is a circular footing of radius r_o resting on the surface of a subsoil. Since the actual pressure distribution under a rigid footing is not uniform, but varies both in phase and magnitude with the distance r from the center, the footing should be replaced by some sort of ring system as shown in Fig. 20. In the ring system the pressure distribution under each narrow ring is not uniform, but by taking an average pressure it may be assumed that the average pressure is acting at the center of the ring.

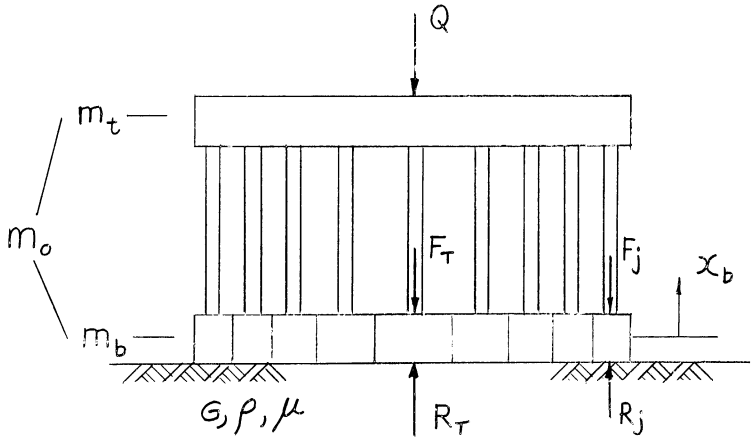

Fig. 20. Footing composed of concentric rings used in present research.

The footing employed in the present research is similar in structure to the one used by Faber (5) who investigated the static pressure distribution under a footing, and consists of two plates: the upper plate is of one solid piece and any static weight used can rigidly be bolted to the plate (mass = m_t); the lower plate is formed by six concentric rings (mass = m_b) of an equal area except the center one, and each ring is connected to the upper plate by means of load cells on which force measurements are made.

The equation of motion for the footing is, from Eq. (17)

$$m_o \ddot{x} + Q = R_T \tag{17}$$

in which R_T is the total reaction pressure under the footing. For the ring system the equation of motion may be expressed as

$$m_b \ddot{x} + F_T = R_T \tag{52}$$

in which m_b is the mass of the lower plate, and F_T is the total force acting on the lower plate. F_T may be obtained by vectorially adding the individual force acting on each ring as

$$F_T = \sum_{j=1}^{n} F_j \tag{53}$$

in which j = 1,2,...,n, and n is the total number of the ring. The force on each ring can be expressed as

$$F_j = \bar{F}_j \cdot e^{i(\omega t + \phi_{F_j - x})} \tag{54}$$

$$= \bar{F}_j \cos(\omega t + \phi_{F_j - x}) + i\, \bar{F}_j \sin(\omega t + \phi_{F_j - x}) \tag{54'}$$

in which $\bar{F}_j$ is the amplitude of vibration (force), and $\phi_{F_j\text{-}X}$ is the phase shift between the force on the ring and the displacement.

The reaction at the base of each ring may then be expressed by

$$R_j = m_j \ddot{x}_j + F_j \tag{55}$$

or

$$R_j = m_j \ddot{x} + F_j \tag{55'}$$

since for a rigid body, $\ddot{x}_j = \ddot{x}$.

The equation of motion for the total reaction under the footing is then

$$R_T = \sum_{j=1}^{n} R_j = \sum_{j=1}^{n} (m_j \ddot{x} + F_j) \tag{56}$$

Thus, the original equation for the total reaction under the footing [Eq. (17)] is replaced either by Eq. (52) or Eq. (56) in the corresponding ring system.

In Eqs. (17) and (52) are given

$$m_o \ddot{x} + Q = R_T \tag{17}$$

$$m_b \ddot{x} + F_T = R_T \tag{52}$$

Multiplying Eq. (52) by m_o/m_b to obtain

$$m_o \ddot{x} + \frac{m_o}{m_b} F_T = \frac{m_o}{m_b} R_T$$

Subtracting Eq. (17) from the above equation to yield

$$\left(\frac{m_o}{m_b} - 1\right) R_T = \left(\frac{m_o}{m_b}\right) F_T - Q \qquad (57)$$

Equation (57) shows how the three forces are related in terms of a mass ratio between the lower plate and the entire footing. This equation also allows one to compute the total reaction under the footing without measuring the inertia force of the footing.

The inter-relations among forces, reactions and phase angles, as expressed in Eqs. (17), (52)-(56), are graphically illustrated in Figs. 21 and 22. The vector diagram shown as Fig. 21(a) illustrates the relations defined by Eq. (54'). For convenience, the displacement axis is taken as the reference line. Each ring force is plotted for its magnitude with its phase shift from the displacement axis. The total force F_T, which is obtained by Eq. (53) or by graphically as shown in Fig. 21(b), is plotted in reference to the displacement axis. The exciting force Q is also shown. The reaction under each ring, Eq. (55), is illustrated in Fig. 21(c), and the total reaction under the footing, Eq. (52), is shown in Fig. 21(d). In the same manner, the vector diagrams for Eqs. (56) and (17) are drawn in Fig. 22(a), (b), and (c) respectively.

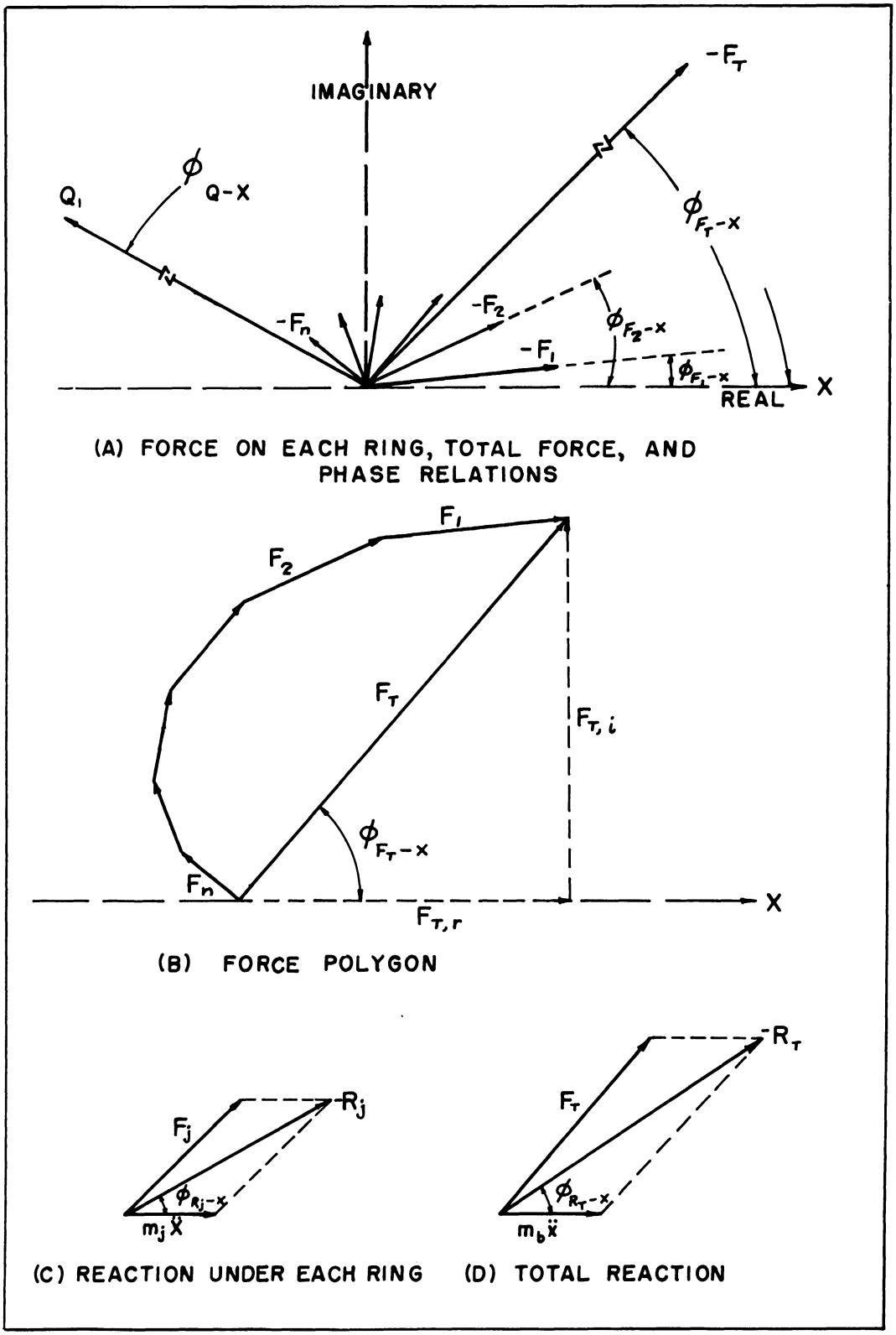

Fig. 21. Vector diagrams for ring force, total force, and phase shifts.

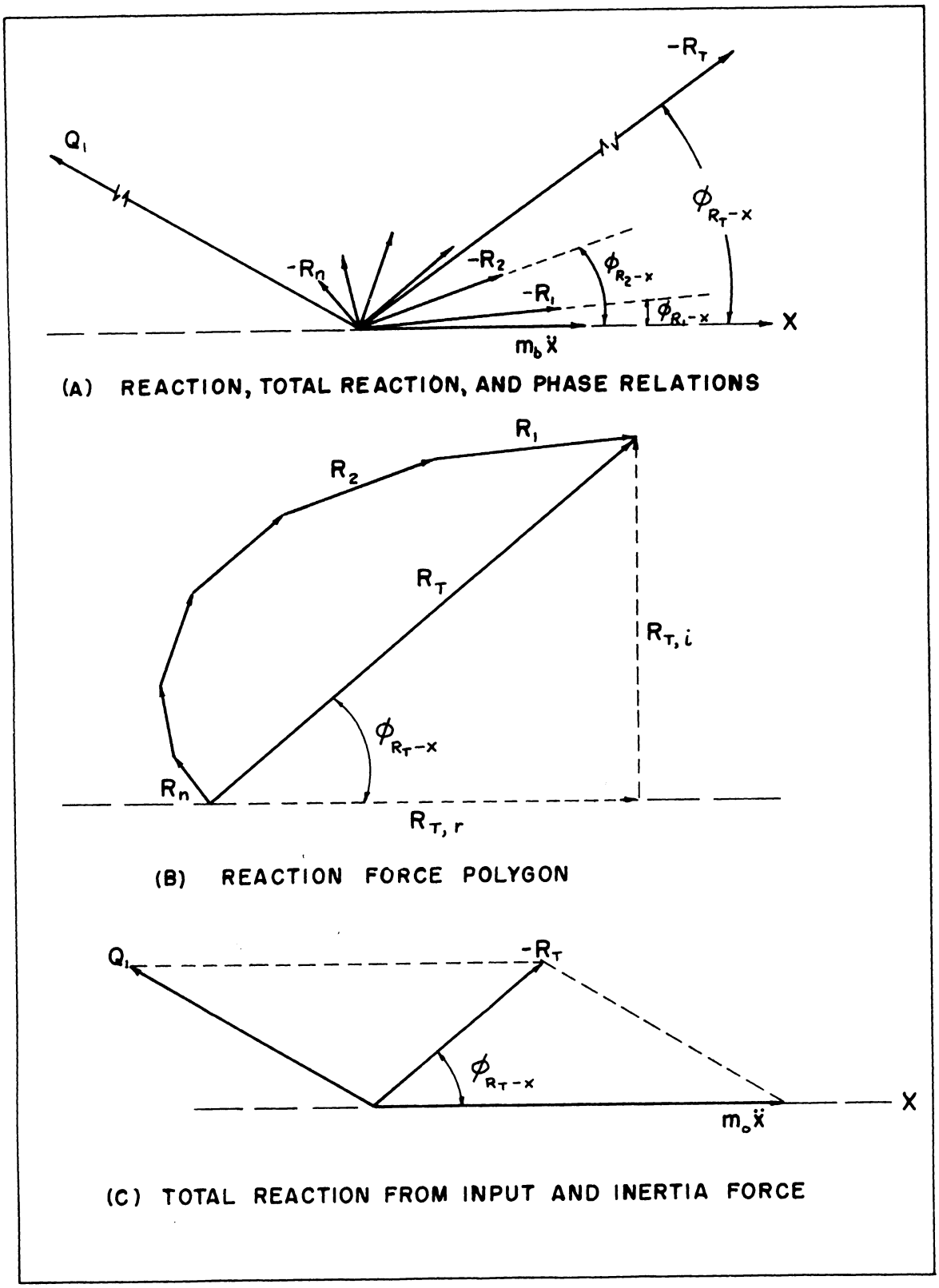

Fig. 22. Vector diagrams for reaction under ring, total reaction, and phase shifts.

COMPUTER ANALYSIS OF DISPLACEMENTS, FORCES, REACTIONS, AND PHASE SHIFTS

The above method for the calculation of displacement, forces, reactions and their phase relations has been programmed for an IBM 7090 computer analysis. The flow diagram for this program is shown in Fig. 23. It may be noted in the diagram that the input data for acceleration (MVA), ring forces (MVF), are fed in millivolts and phase angles (MSAQ, MSA6, MSN6) are fed in units of milliseconds.

DETERMINATION OF THE DISPLACEMENT FUNCTION FROM EXPERIMENTAL DATA THROUGH A COMPUTER PROGRAM

It has been stated previously that the displacement, reaction, and their phase relations may be computed if the displacement function f can be determined, and that the function f is dependent only upon the two variables. Therefore, the function can be determined by solving simultaneously any two of the equations given in Chapter II [Eqs. (28)-(34)].

It has been decided for the present research to use the following two equations for the solution of the functions f_1 and f_2.

$$\chi = \frac{Q_1}{G r_o} \sqrt{\frac{f_1^2 + f_2^2}{(1 + b a_o^2 f_1)^2 + (b a_o^2 f_2)^2}} \tag{30}$$

$$\phi_{Q-x} = \tan^{-1} \frac{-f_2}{f_1 + b a_o^2 (f_1^2 + f_2^2)} \tag{33}$$

The solution of these two equations for f_1 and f_2, as shown in the Appendix, has been reduced, through algebraic manipulation, to the solution of a quadratic equation in the form of

FLOW DIAGRAM (F_T, R_T, Φ)

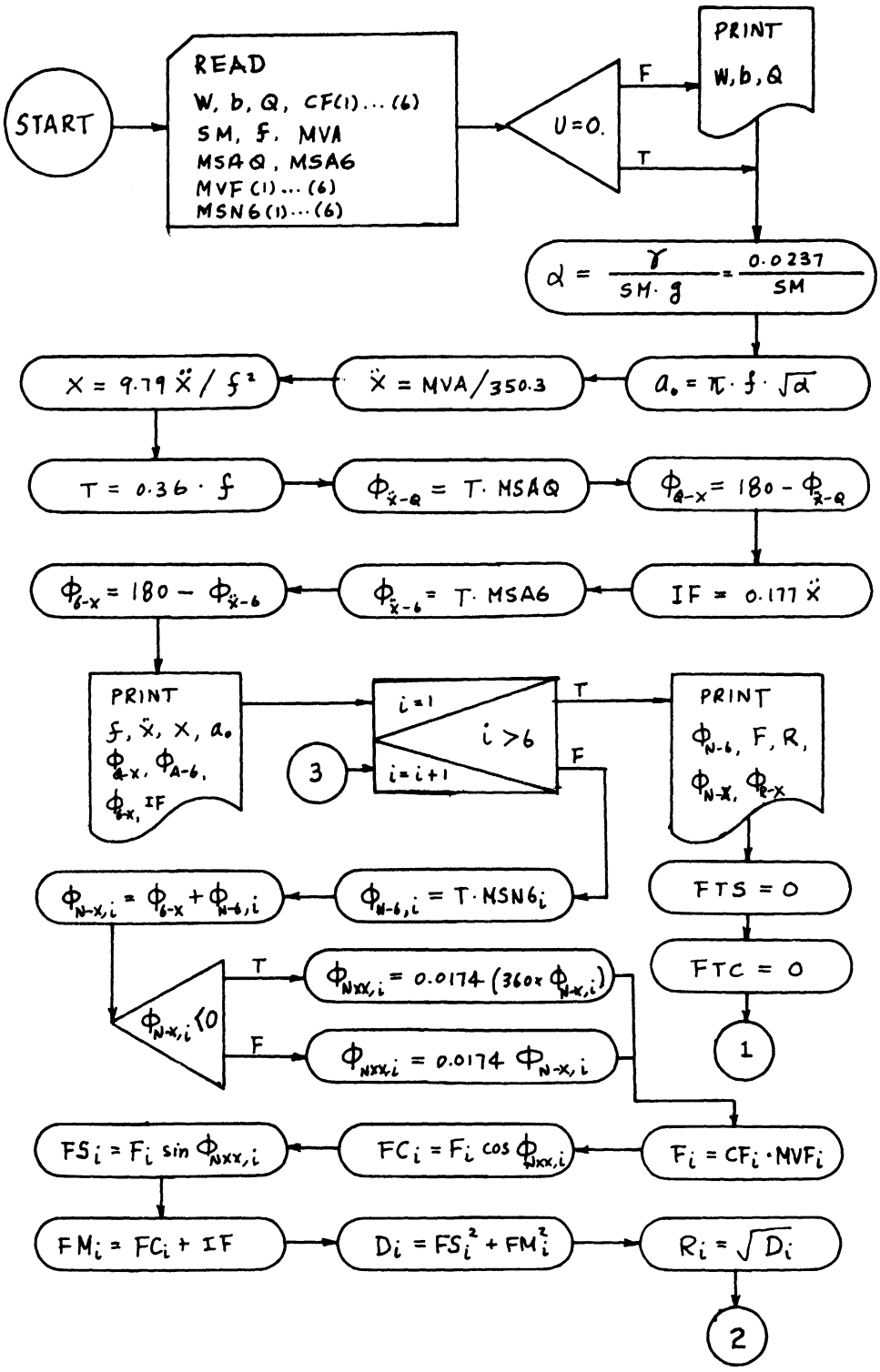

Fig. 23. Flow diagram for computer analysis of force, reactions, and phase shifts.

FLOW DIAGRAM (Continued)

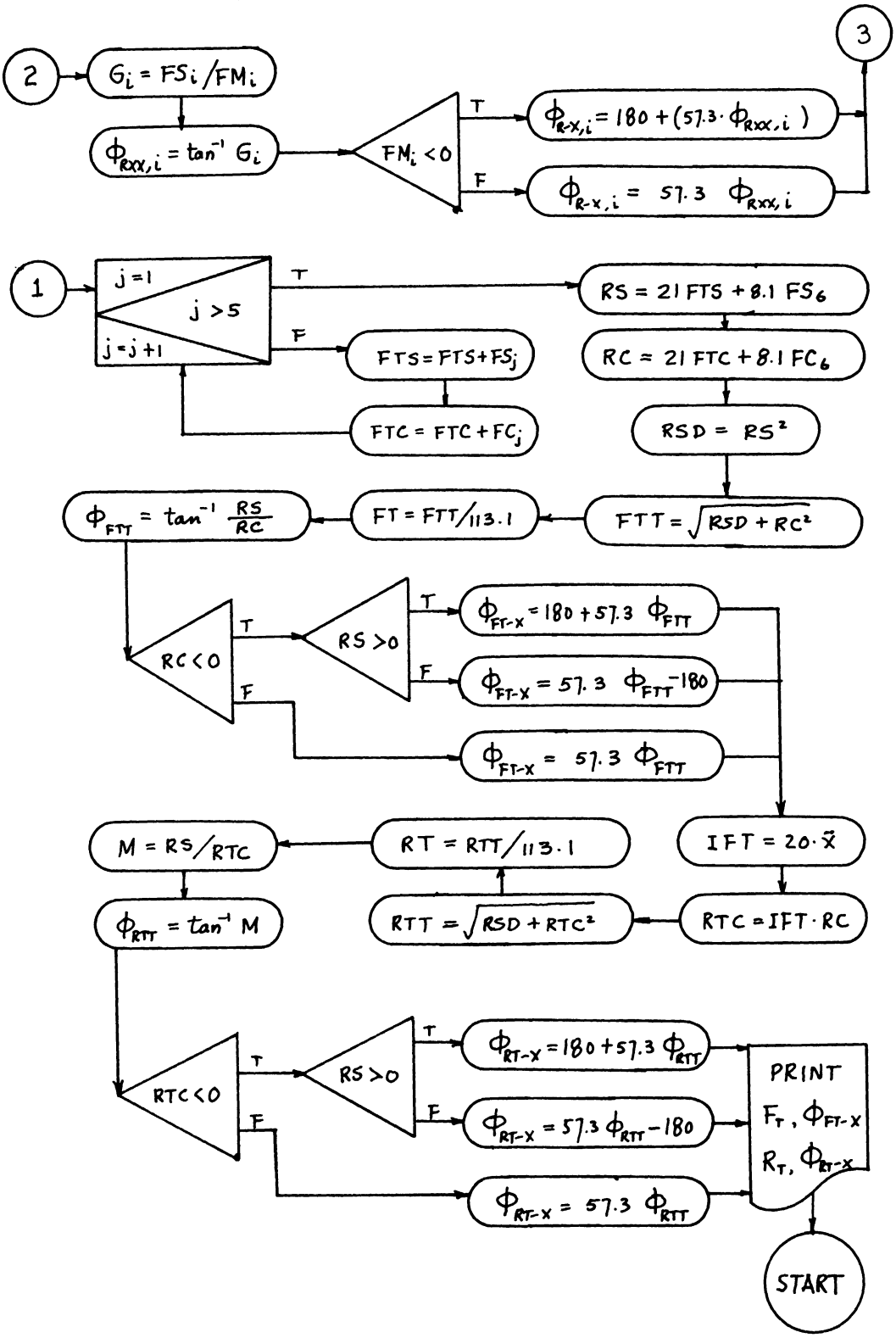

Fig. 23. (Concluded).

$$T f_1^2 + Y f_1 + Q = 0 \tag{58}$$

$$K f_1 + S - f_2 = 0 \tag{59}$$

where Y, T, Q, K, and S are the known quantities as defined below:

$$Y = 2 b a_o^2 \left(\frac{X G r_o}{Q_1}\right)^2 \left\{1 + \left[b^2 a_o^4 \left(\frac{X G r_o}{Q_1}\right)^2 + 1\right] \tan^2 \phi_{Q-X}\right\}$$

$$T = b^2 a_o^4 \left(\frac{X G r_o}{Q_1}\right)^2 \left\{1 + \left[b^2 a_o^4 \left(\frac{X G r_o}{Q_1}\right)^2 + 3\right] \tan^2 \phi_{Q-X}\right\} - 1$$

$$Q = \frac{b^2 a_o^4 \left(\frac{X G r_o}{Q_1}\right)^4 \tan^2 \phi_{Q-X}}{b^2 a_o^4 \left(\frac{X G r_o}{Q_1}\right)^2 - 1} + \left(\frac{X G r_o}{Q_1}\right)^2$$

$$K = \frac{2 b^2 a_o^4 \left(\frac{X G r_o}{Q_1}\right)^2 \tan \phi_{Q-X}}{b^2 a_o^4 \left(\frac{X G r_o}{Q_1}\right)^2 - 1} - \tan \phi_{Q-X}$$

$$S = \frac{b a_o^2 \left(\frac{X G r_o}{Q_1}\right)^2 \tan \phi_{Q-X}}{b^2 a_o^4 \left(\frac{X G r_o}{Q_1}\right)^2 - 1}$$

It may be noted from Eqs. (58) and (59) that both f_1 and f_2 have more than one root, but the theory demands f_1 to be negative and f_2 positive for any frequency factor values.

The solution for the displacement function has been programmed for the IBM 7090 computer analysis, and the flow diagram for the program is

shown in Fig. 24. It may be noted that the program can be used for both types of steady state vibration, that is, constant force and rotating mass type.

The displacement function so determined from the experimental data may then be used for comparisons with the theoretical values, such as shown in Fig. 8.

Theoretical Values for Resonant Frequency and Maximum Amplitude of the Test Systems

As stated previously, the resonant frequency and the maximum amplitude of oscillation of an oscillator-soil system depend on the mass ratio, the elastic constants of the subsoil, and the type of pressure distribution. In the absence of knowledge as to the type of pressure distribution for the test systems employed in the present research, the following theoretical determination of the dynamic characteristics of the test systems are based on the assumption of a rigid base type pressure distribution and Poisson's ratio of 0.25. It should also be pointed out that although the term "theoretical" is employed, the shear wave velocities used are based on experimental data.

THEORETICAL RESONANT FREQUENCY OF TEST SYSTEMS

The theoretical resonant frequencies for the seven test systems have been computed by using the theoretical curves in Fig. 11(a) and Eq. (19)

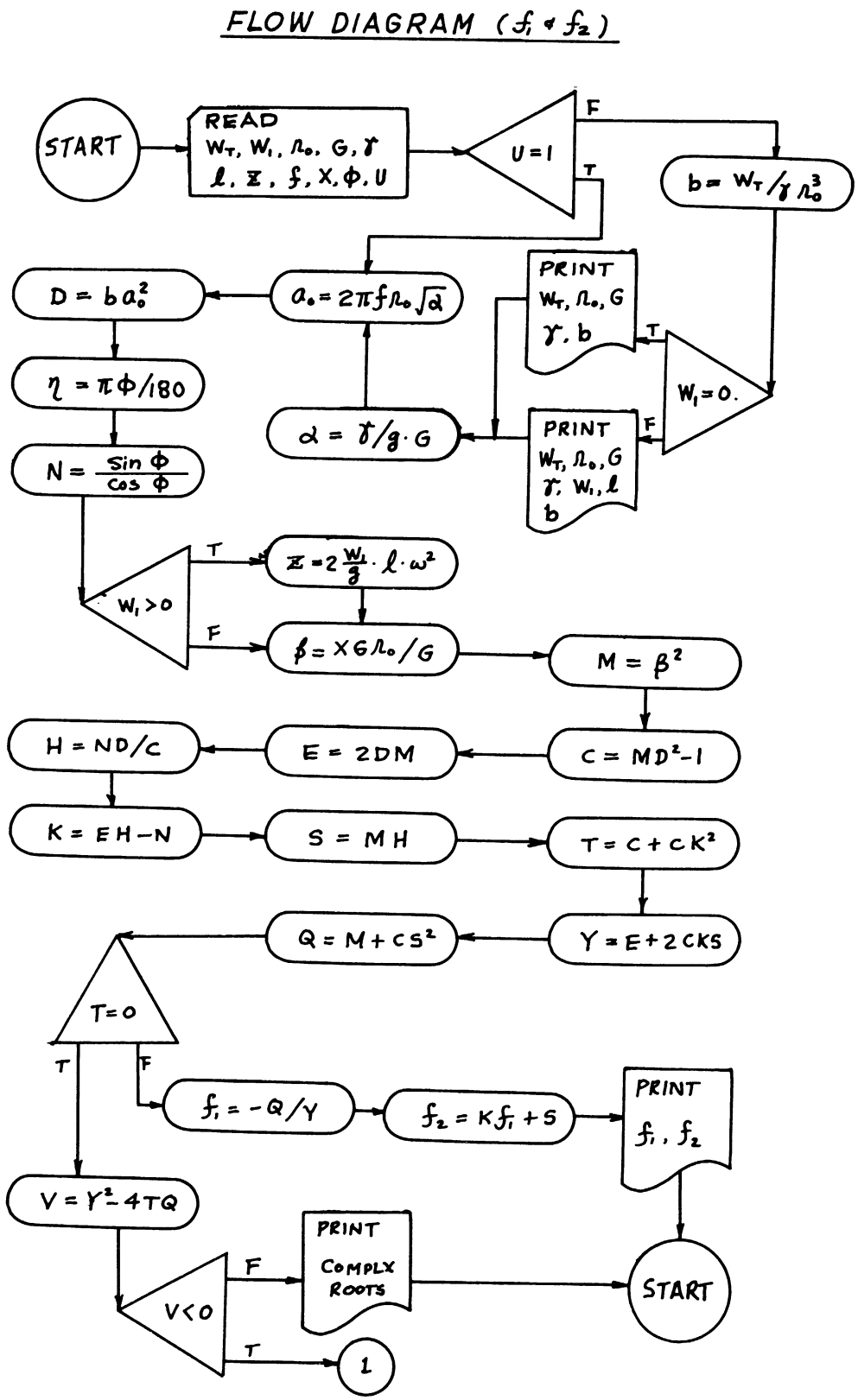

Fig. 24. Flow diagram for computer analysis of displacement functions.

FLOW DIAGRAM (Continued)

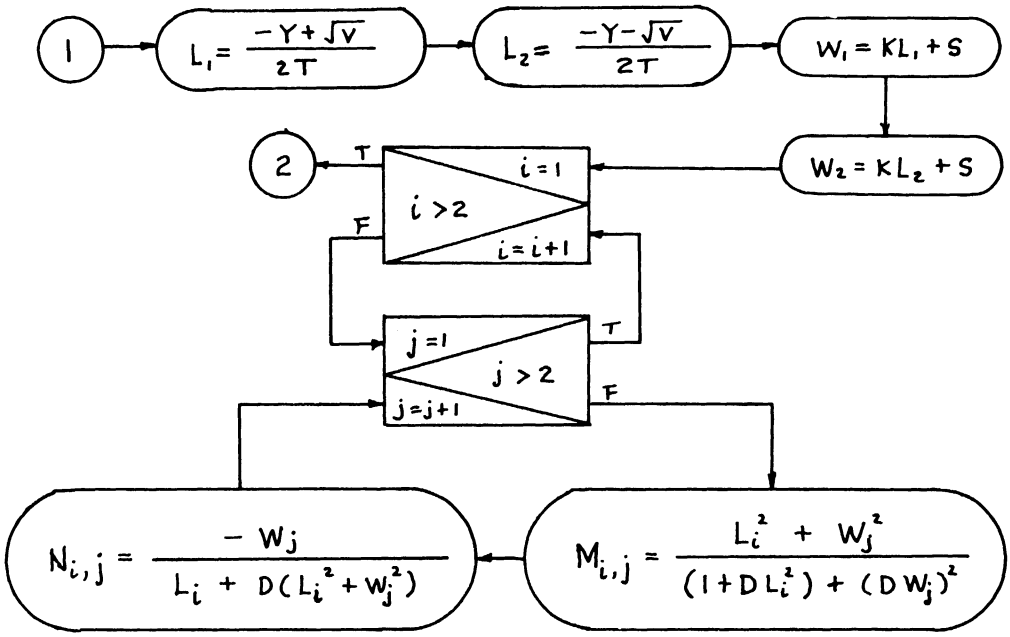

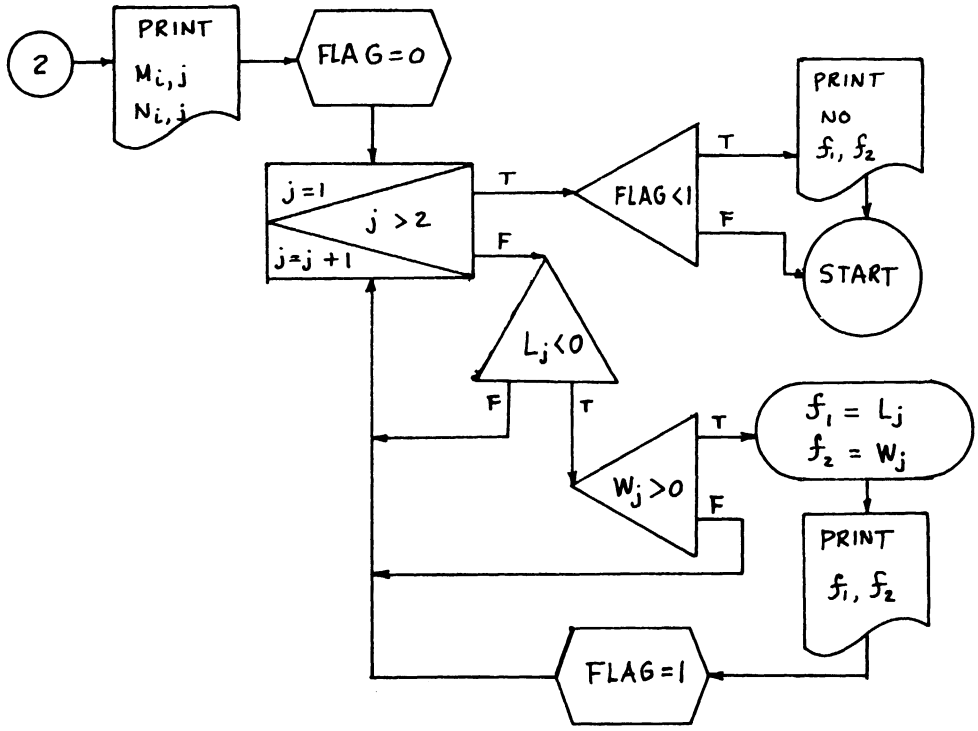

Fig. 24. (Concluded).

$$f_0 = \frac{a_0}{2\pi r_0}\sqrt{\frac{G}{\rho}} \qquad (19')$$

In the use of this equation, however, the shear wave velocity $\sqrt{G/\rho}$ is not a constant value, but varies with confining pressure as indicated by Hardin and Richart (8). In Fig. 25 is drawn a curve showing the relationship between the shear wave velocity and confining pressure for a soil having a void ratio of 0.51. This curve has been obtained by extrapolating a curve, given by Hardin and Richart for a similar soil (Fig. 10, Ref. 8), to include the low confining pressure region. The confining pressure for each system was computed by dividing the static weight of the footing by contact area.

The results of computations are shown in Table VII and are plotted in Fig. 26. It may be observed that the natural frequency is inversely proportional to the mass ratio of the system. It should be noted, however, that the variation of frequency is rather small (12 cps) although the mass ratio is changed from about 6 to 25.

THEORETICAL MAXIMUM AMPLITUDE OF OSCILLATION

The theoretical maximum amplitude of oscillation for each test system has been computed by using the theoretical curves given in Fig. 11(b), and a relation given by

$$A_{max} = A'^{(2)}_{max} \cdot Q_1 \qquad (60)$$

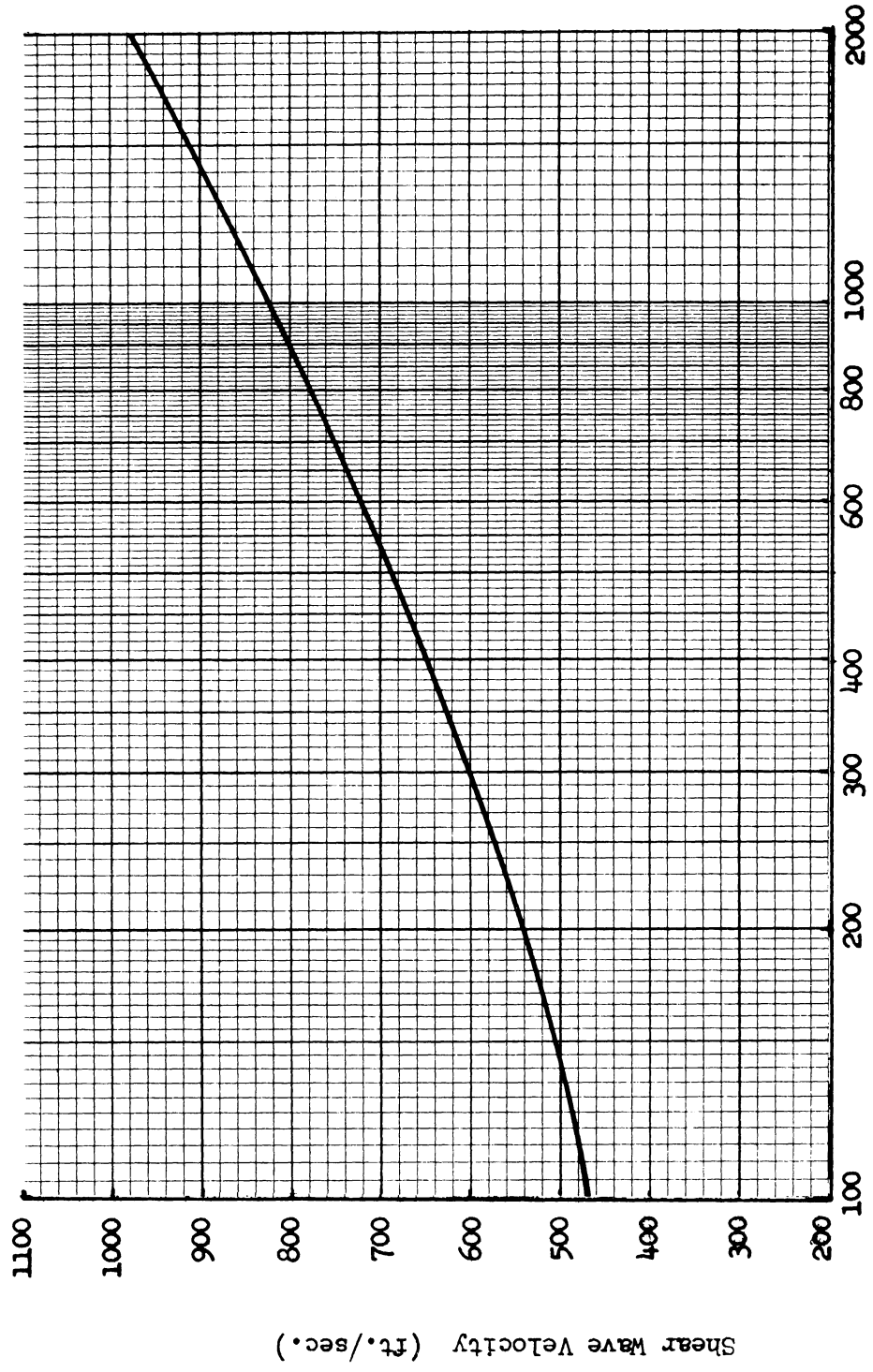

Fig. 25. Shear wave velocity vs. confining pressure for void ratio of 0.51.

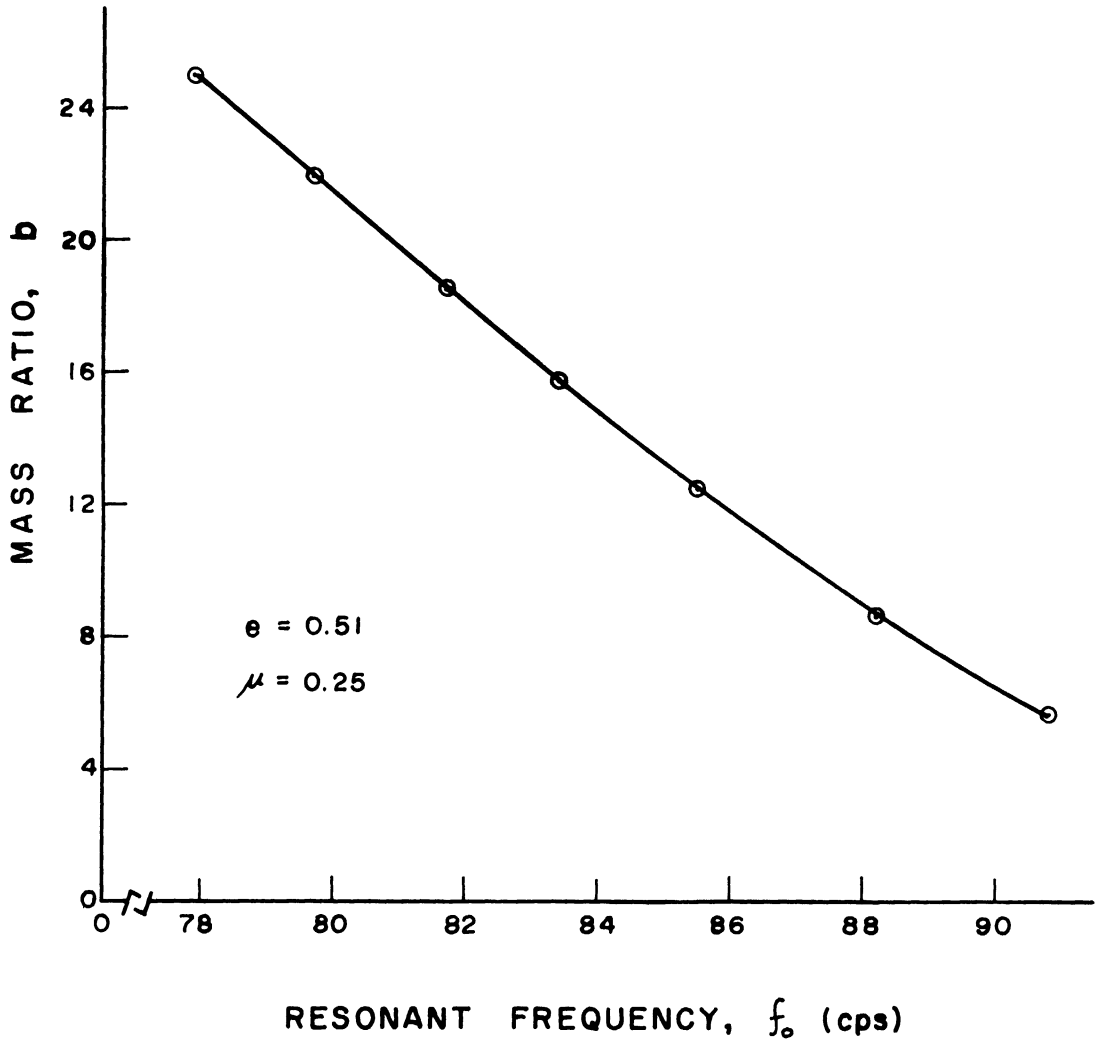

Fig. 26. Theoretical resonant frequencies for various mass ratios.

TABLE VII

THEORETICAL WAVE VELOCITY, AND RESONANT FREQUENCY VS. MASS RATIO

Test System No.	Weight of Footing W (lbs)	Mass Ratio b	Frequency Factor a_o	Confining Pressure W_o/A (psf)	Wave Velocity $\sqrt{\frac{G}{\rho}}$ (ft/sec)	Shear Modulus G (psi)	Resonant Frequency f_o (cps)
1	80.0	5.83	0.770	102	370	3,245	90.8
2	120.0	8.74	0.675	153	410	3,984	88.2
3	171.1	12.47	0.590	218	455	4,906	85.5
4	217.6	15.85	0.535	277	490	5,690	83.4
5	257.1	18.73	0.495	328	518	6,360	81.7
6	302.3	22.02	0.460	386	544	6,965	79.7
7	342.3	24.94	0.435	436	563	7,513	77.9

where

$$A'^{(2)}_{max} = \frac{A^{(2)}_{max}}{G r_o}$$

$A'^{(2)}_{max}$ is an amplitude factor (it has a unit of in./lb) modifying the dimensionless amplitude factor $A^{(2)}_{max}$ to apply for a particular footing-soil system. Thus, $A'^{(2)}_{max}$ may be termed "unit amplitude factor."

The results of computations are summarized in Table VIII and are plotted in Fig. 27. It may be stated that the maximum amplitude is also inversely proportional to the mass ratio of the test systems employed, although the dimensionless amplitude factor is directly proportional to the mass ratio. This is due to the change in shear modulus, which shows a greater rate of increase with increasing mass ratio. It may be of interest also to note that the rate of increase in the maximum amplitude becomes greater as the mass ratio gets smaller. As was the case with the natural frequency, the maximum amplitude varies very little with the change in mass ratio of the system.

TABLE VIII

THEORETICAL SHEAR MODULUS AND MAXIMUM AMPLITUDE FACTOR VS. MASS RATIO

Test System No.	Mass Ratio b	$A_{max}^{(2)}$	Wave Velocity $\sqrt{\frac{G}{\rho}}$ (ft/sec)	Shear Modulus G (psi)	$A_{max}^{\prime\,(2)}$ (in/lbx10)
1	5.83	0.298	370	3,245	1.530
2	8.74	0.345	410	3,984	1.443
3	12.47	0.399	455	4,906	1.356
4	15.85	0.438	490	5,690	1.283
5	18.73	0.474	518	6,360	1.242
6	22.02	0.510	544	6,965	1.220
7	24.94	0.541	563	7,513	1.200

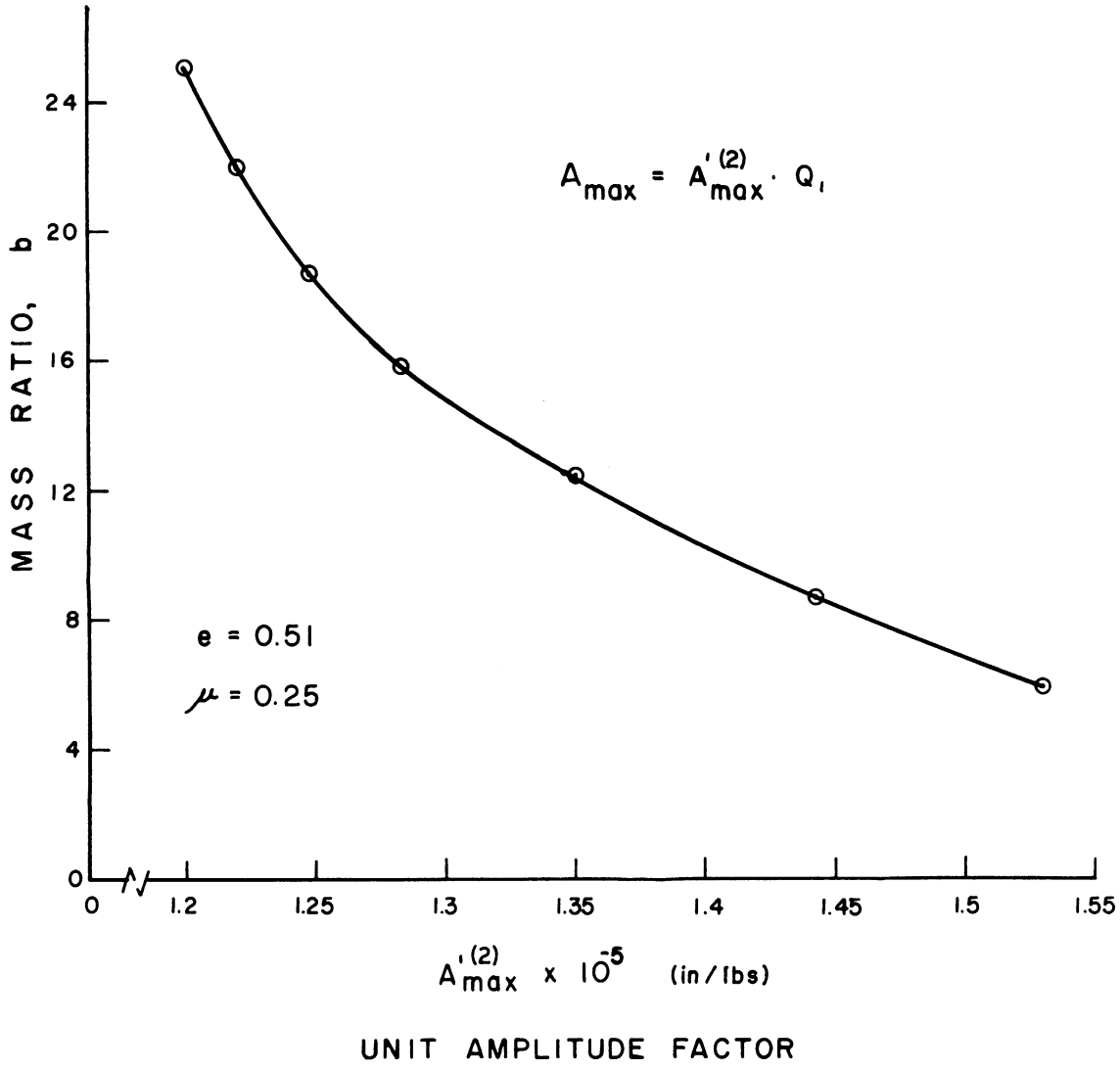

Fig. 27. Theoretical maximum amplitudes for various mass ratios.

CHAPTER IV

DESIGN, CONSTRUCTION, AND CALIBRATION OF TESTING EQUIPMENT, AND TEST PROCEDURE

Design and Construction of Testing Equipment

Structural Equipment

SAND BIN

A sand bin was built with 8 in. three-cell concrete blocks and has the inside dimensions of 4.75 ft by 4.75 ft and 4.0 ft in height. The holes in the blocks were filled with mortar. The wall was reinforced vertically with 3/8 in. diameter, 4 ft long rods, which were placed 8 in. apart. The rods were threaded 2 in. at one end and extended above the wall top to be used for anchoring the loading frame and other apparatus. The horizontal reinforcement of the wall was done with the standard "Dur-O-Wal" reinforcement trusses of type 6-S (manufactured by the Dur-O-Wal Co., Cedar Rapids, Iowa). These reinforcement trusses were used in every course and were spliced 6 in. at the joints. The use of these trusses with "Type M" special mortar (ASTM Standard C-270-59T) gives a transverse strength of about 1.8 times that of unreinforced blocks (allowable working stress of 6 psi). This strength was found to be adequate to resist the lateral earth pressure and the lateral component of the force from the loading frame.

The inside of the wall was first coated with Peerless cement paint to fill the pores on the concrete blocks, and was then coated with regular roofing tar to make it completely waterproof. In order to provide a means for absorbing wave energy, 1/2 in. thick Celotex board was installed on the inside of the wall and the bottom floor of the bin. These Celotex boards were covered with a sheet of Vis-queen to make them waterproof. After the installation of these interior materials the net inside volume of the sand bin was measured to be 83.9 cubic feet.

The sand used was Ottawa Silica Sand. As shown in Fig. 28, 85% of the sand is retained between the nos. 30 and 50 sieves. Its natural moisture content was 0.04%. The maximum void ratio of the sand is 0.80, and the minimum void ratio is 0.51.

The sand was compacted in the bin by a Jackson Vibratory Plate Compactor (manufactured by the Electric Tamper and Equipment Co., Ludington, Michigan). The sand was compacted in 6 layers; the bottom layer was 10 in. thick after compaction and the top layer was 5 in. The four middle layers were about 8 in. each in thickness. This layer thickness of 8 in. was adapted from the trial compaction runs accompanied by density tests. The tests were run by burying a mold (pie pan) of known volume under the sand at different depths. After a specified compaction the mold was dug out and its surface was made even with the top of the mold. Then the sand in the mold was weighed to compute the density. It also indicated that 6 passes of the compactor on each layer gave the maximum density. Figures 29 and 30 show the compactor used for compaction of the sand in the bin,

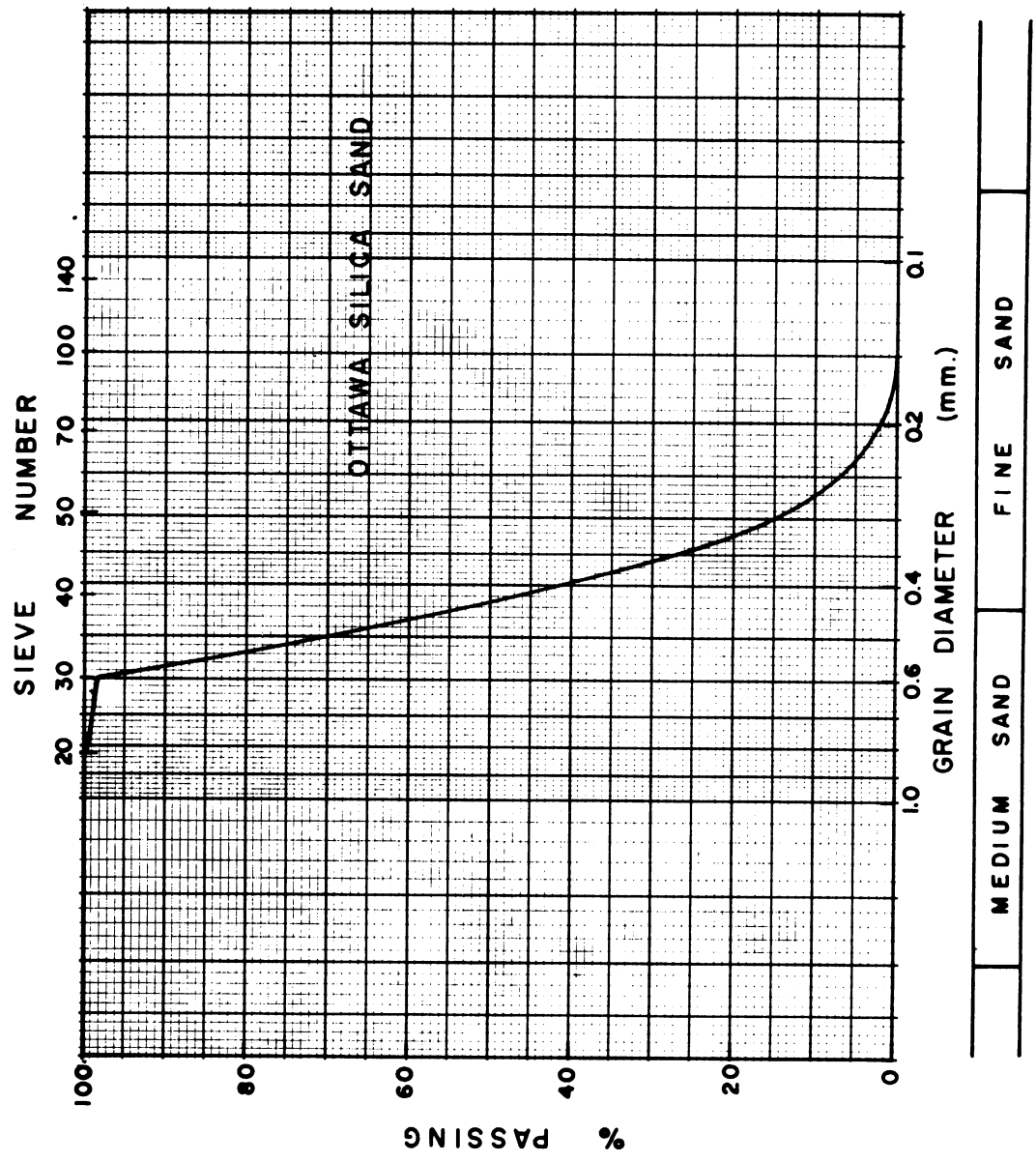

fig. 28. Grain size distribution—Ottawa Silica Sand.

Fig. 29. A vibratory plate compactor used for compaction of sand.

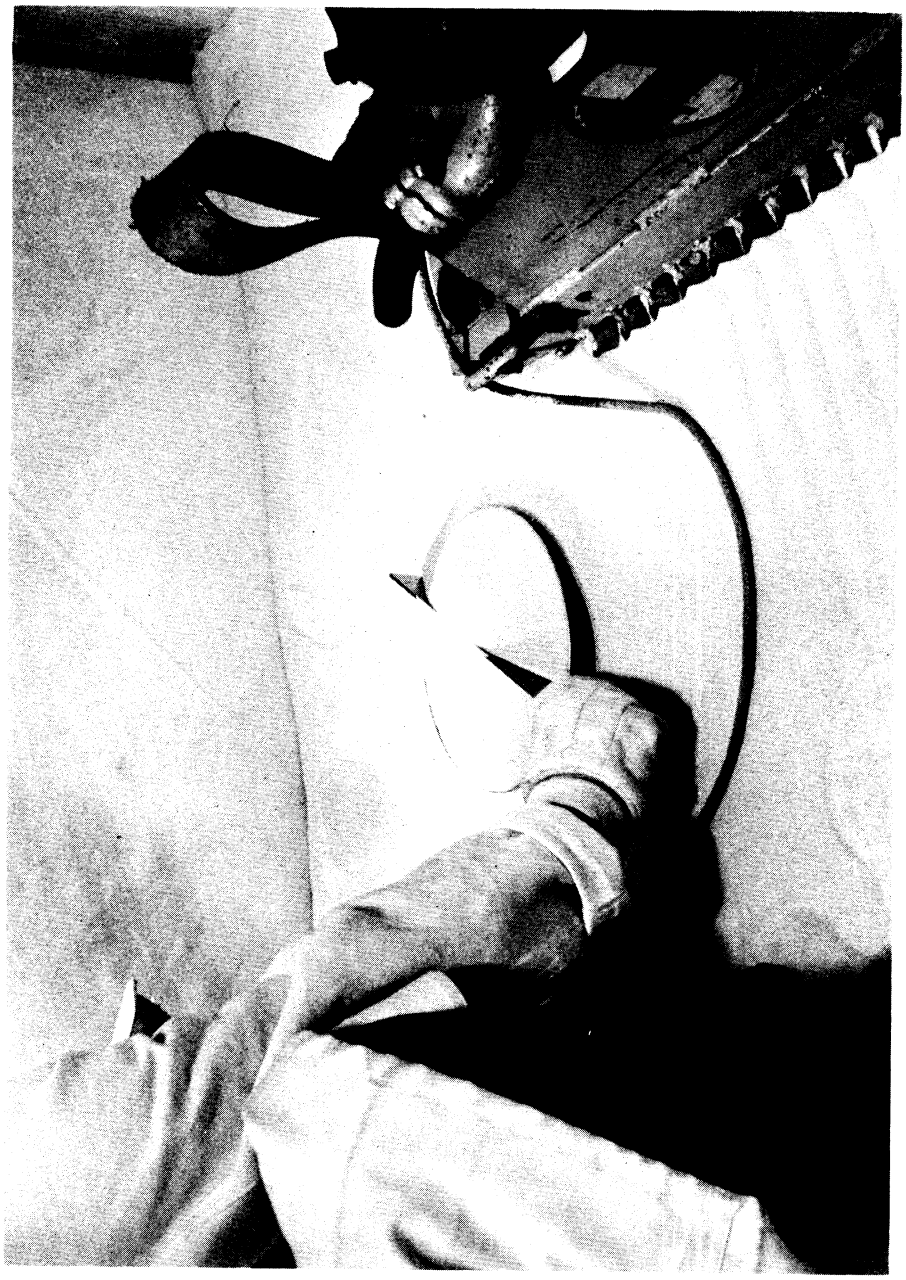

Fig. 30. Measurement of density of sand in the bin.

and the means of measuring the density of sand in the bin.

The total weight of the sand in the bin was 9,135.0 lb, occupying a volume of 83.2 cubic feet. From these, density of the compacted sand in the bin was calculated to be 109.8 lb/cu ft, and a void ratio of 0.51, which was the same as the laboratory test results as previously mentioned. This implies that the method of compaction employed was very effective in obtaining the maximum density.

LOADING FRAME

In designing a loading frame there were two major items to consider: first, to avoid a frame having natural frequency ranges within the range of the test frequencies; second, to make the entire structure as rigid as possible to minimize the amplitude of vibration. Theoretical solutions, as shown in Chapter III, predicted that the test frequencies would be in the range from 78 to 91 cps. After trials of numerous sections to meet the aforementioned requirements, it was found that the frequency requirement could not be met. The section shown in Fig. 31 calculated to be most satisfactory. The structure has a laterally enlarged A shape: two vertical members are connected to a horizontal member at the top, which are supported by the sand bin wall through diagonal members and braces. Another identical section is erected 7 in. apart and these two sections are transversely braced together. The base plates, 7 by 24 in. in size, are bolted rigidly to the wall. The oscillator is bolted to the 8 in. WF beam, which is adjustable in height as necessary by means of

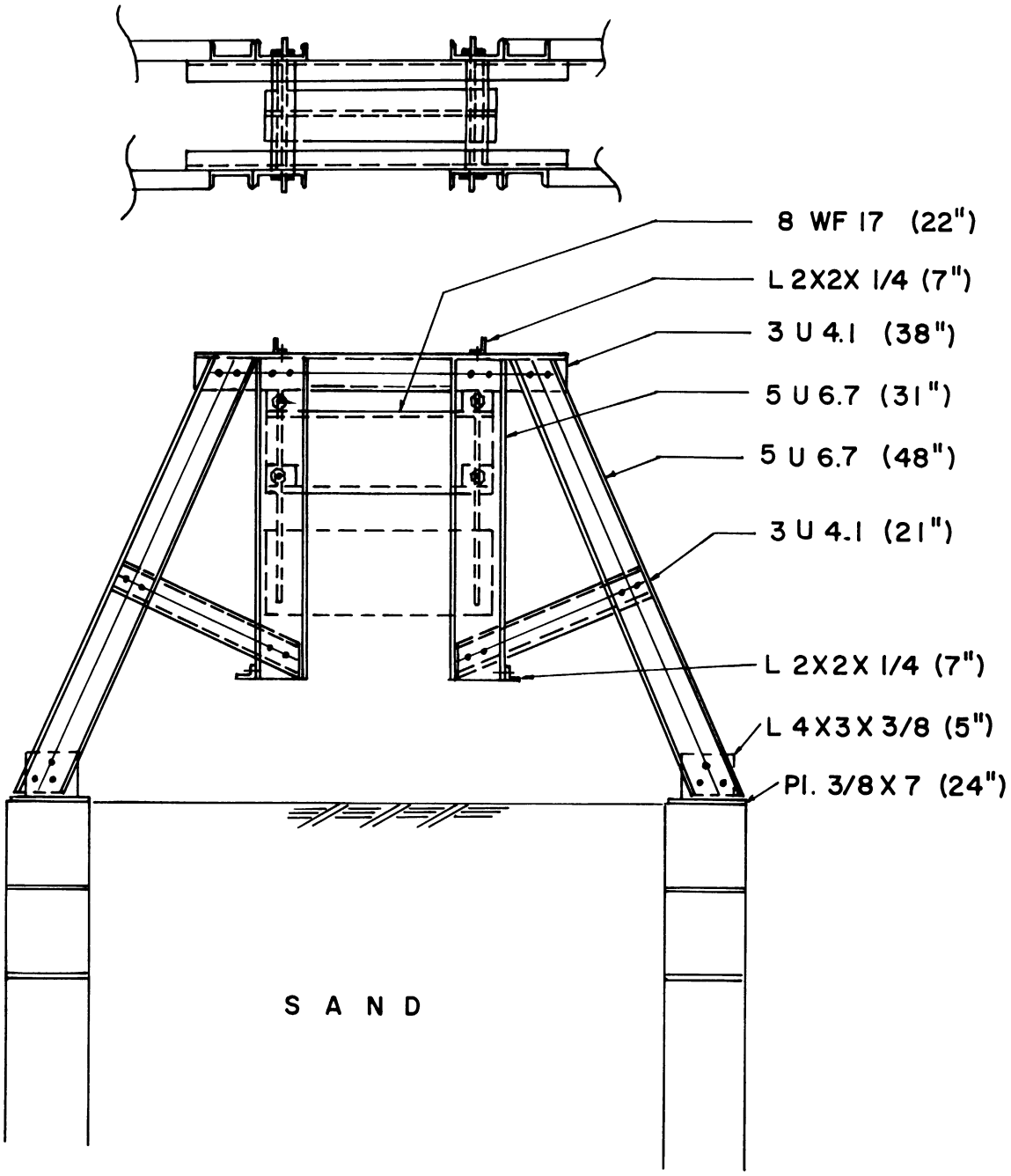

Fig. 31. Loading frame details.

slots in the vertical frames. Figure 32 shows the loading frame and the sand bin setup for the test.

The total weight of the loading frame is about 340 lb and the oscillator weighs about 75 lb. The natural frequency of the loading frame structure was theoretically computed to be about 250 cps.

FOOTING AND LOAD CELLS

The footing employed in the tests is illustrated in Figs. 33 and 34. It consists of two steel plates of 12 in. diameter. The lower plate is formed by six concentric rings so dimensioned that the area of each ring, except the center one, is equal to 21 sq in. Each ring is separated by approximately 1.5 to 3 thousandths of an inch. The upper plate is of one solid piece and receives the test load at its center. The total weight of the footing is 66 lb and it has a total area of 113.1 sq in.

Each of the six rings at the lower plate is connected to the upper plate by means of four load cells on which strain measurements are to be performed. Each load cell is made of a 2 in. long aluminum tube 1/2 in. inside diameter and 0.015 in. thickness. On each load cell is mounted an SR-4 (type C-5-1) strain gage with a resistance of 350 ohm and a gage factor of 3.34. On the upper plate are installed two sets of four strain gages mounted on aluminum tubes to be used as dummy gages. All four gages, both in the upper and lower plate, are connected in series, thus giving a total resistance of 1,400± ohm each.

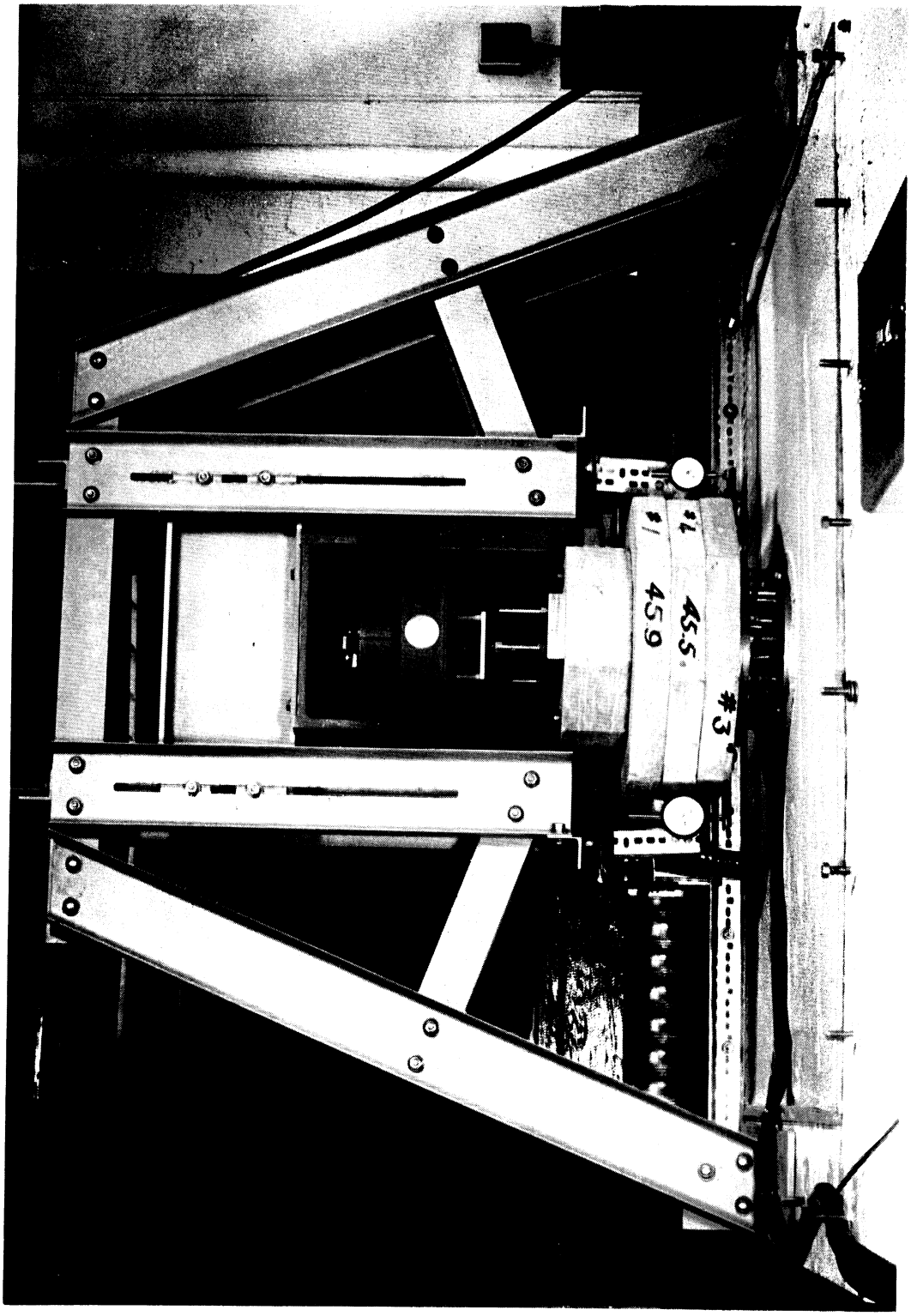

Fig. 32. Test bin and loading frame setup.

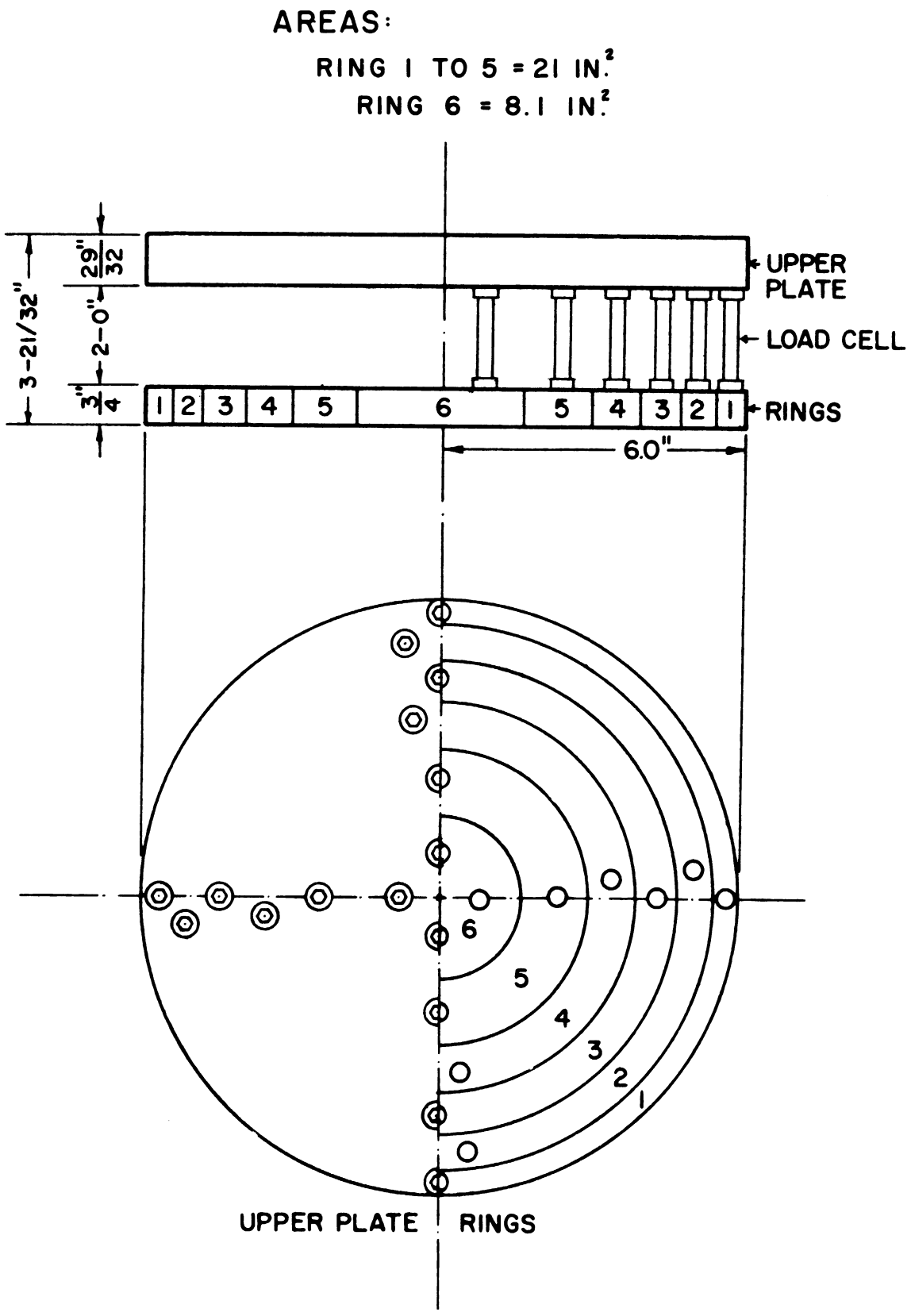

Fig. 33. Details of special footing.

Fig. 34. Footing showing load cells attached to each ring.

STATIC WEIGHTS

For the purpose of varying the weight of the footing, dead weights were made of reinforced concrete blocks. The blocks are of an octagonal shape, vary in thickness from 2 to 4 in., and weigh about 46 lb each. The blocks were reinforced with 5/8 to 7/8 in. diameter steel bars. Extreme care was taken to make the surface of the block as smooth and level as possible to make them rigid when bolted together to the footing. In addition to these concrete blocks a 13 in. diameter, 1 in. thick steel plate was also used as dead weight.

With the use of these weights the footing can be varied from about 80 to 344 lb, giving the mass ratio of the system in the range of 5.8 to 24.9.

APPARATUS FOR MEASURING SETTLEMENT

In order to measure the settlement of the footing under static and dynamic loads, an apparatus was built of Lyon slotted angles as shown in Fig. 32. The frame is firmly bolted to the sand bin wall. At the end of the horizontal member is attached a dial gage, through which settlement can be measured to one thousandth of an inch. This apparatus is erected on both sides of the footing to measure any differential settlement.

Electric and Electronic Equipment

STRAIN GAGE SYSTEM

Design

The basic strain gage measuring circuit is a Potentiometric Circuit, which consists of a direct current supply connected across two series resistors, one of which is an electric resistance strain gage. This circuit is adequate mainly for strain measurements under static loads. For the measurement of strains under dynamic loads, the Wheatstone Bridge is more satisfactory and was used in this investigation.

The Wheatstone Bridge consists of four resistances, any number of which may be strain gages, arranged as shown in Fig. 35.

A supply voltage, V is applied at diagonally opposite corners of the bridge, and the output of the circuit is taken across the other diagonally opposite corners. The output voltage, V' is the difference between V_{bd} and V_{bc} by definition, so that

$$V' = V \frac{R_1 R_3 - R_2 R_4}{(R_2 + R_3)(R_1 + R_4)} \tag{61}$$

where R_1 through R_4 are the gage resistance measured at each arm. When the bridge is balanced, that is, steady output voltage (V') is zero,

$$R_1 R_3 = R_2 R_4 \tag{62}$$

Thus, by the use of appropriate resistances the steady component of the output voltage can be eliminated so as to measure only $\Delta V'$, which is a

function of the strains in the gages which make up the bridge. Accordingly, it is most important to design the circuit to produce a maximum output sensitivity.

Since the active and dummy gages of 1,400 ohm each are installed in the footing, these form the two arms in a proposed bridge. Thus, a basic circuit for solution may be represented as in Fig. 36.

To solve this basic circuit for an optimum output sensitivity requires the appropriate selection of V, R_3, and R_4, and probably the type of a D.C. amplifier, if needed.

The maximum strain gage sensitivity ($S_{s,max}$), which is independent of the circuit type or of any actual values of the circuit components, is a function only of three properties inherent in the gage as:

$$S_{s,\,max} = I_{max} \cdot R_g \cdot K \tag{63}$$

where

I_{max} = maximum current capacity = 0.03 amp

R_g = gage resistance = 1,400 ohm

K = gage factor = 3.34

therefore

$S_{s,max}$ = 0.03 x 1,400 x 3.34 = 140 volt/in./in.-strain

= 140 μv/μin./in.-strain.

The strain gage sensitivity, S_s is expressed as:

$$S_s = S_r \cdot K \tag{64}$$

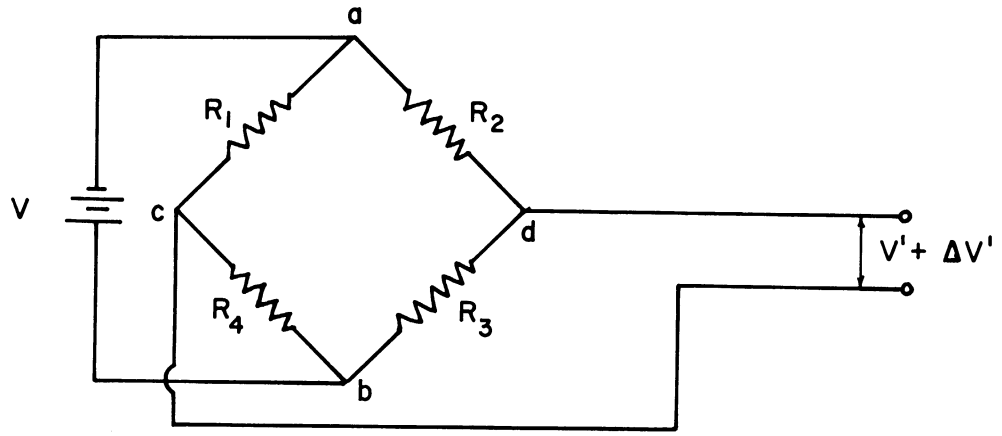

Fig. 35. Basic Wheatstone Bridge circuit.

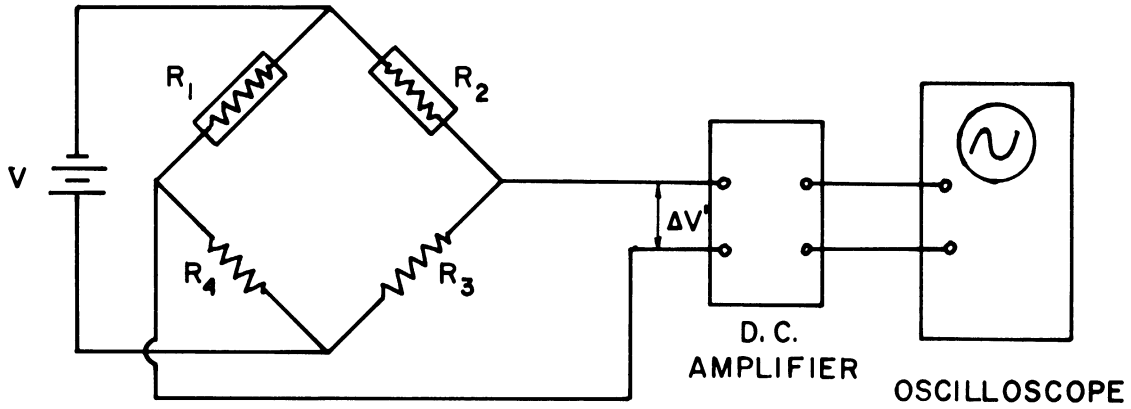

R_1 = ACTIVE GAGE = 1400± ohms

R_2 = DUMMY GAGE = 1400± "

MAX. SENSITIVITY OF OSCILLOSCOPE = 0.2 mv/cm

Fig. 36. A basic circuit for solution.

where

S_r = resistive sensitivity = $V \frac{a}{(1+a)^2}$

$a = R_3/R_1$

and

$$V = I \cdot R_g (1 + a) \tag{65}$$

$$a = \frac{V}{I \cdot R_g} - 1 \tag{66}$$

which shows that it is current-carrying capacity of strain gage that limits the supply voltage, V.

After trails of several circuits it was found that V = 200 volts was most adequate for the purpose (actually batteries of 180 volts are being used for the tests). For a supply voltage of 180 volts computations show that:

Gage ratio	a	= 3.3
therefore,	R_3	= R_4 = 4,620 ohm
Resistive sensitivity	S_r	= 32 μv/μ-ohm/ohm
Strain gage sensitivity	S_s	= 107 μv/μ-in./in.
Circuit efficiency	e_f	= $S_s/S_{s,max}$ = 77%

Of the six sets of strain gages to be instrumented, the center ring and the other five outer rings were made into two separate systems. This was to compare the pressure under each of the outer rings with that under the center one. Figure 37 shows the final circuit designed for the outer rings.

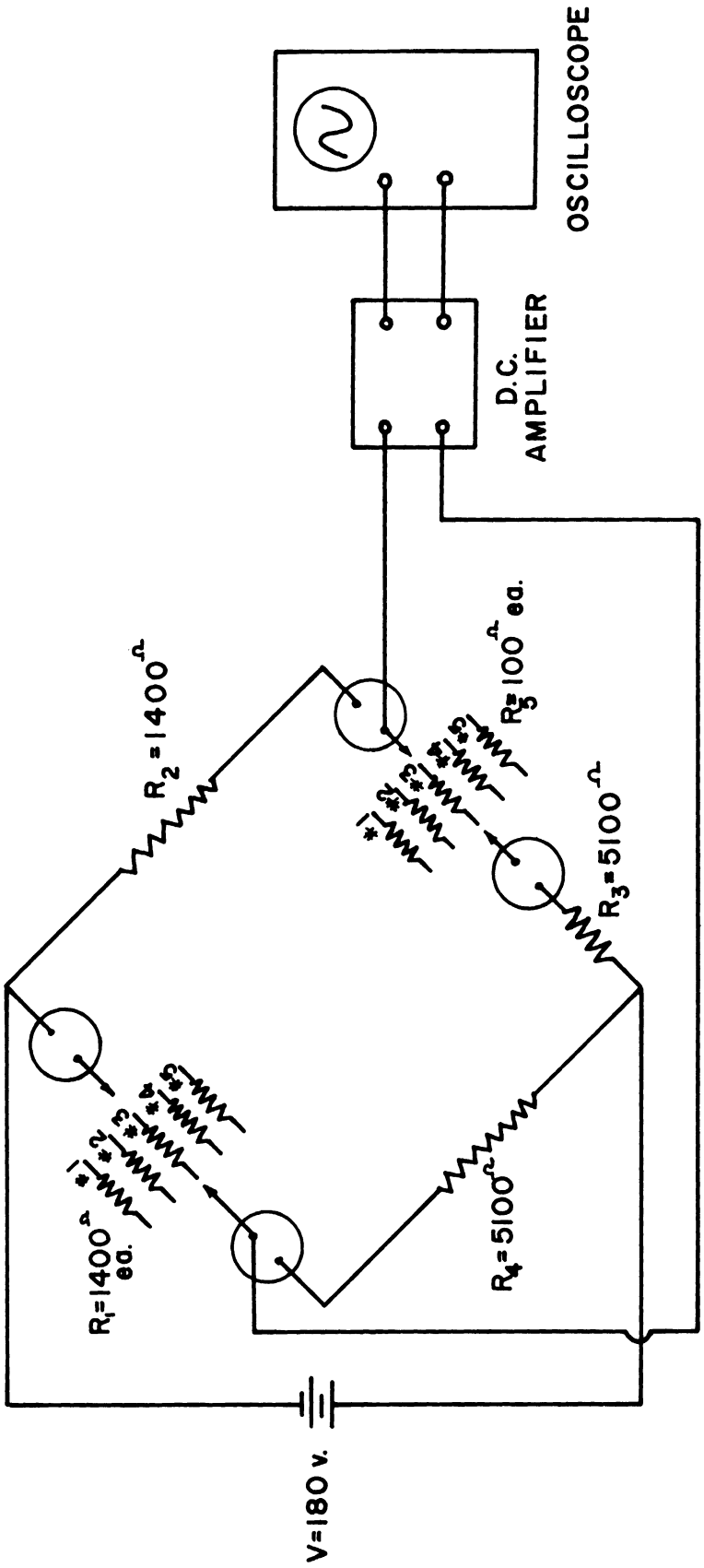

Fig. 37. Final bridge circuit.

Construction of the Bridge and Instrumentation

Two bridges were built for the system: one for the center ring and the other for the five outer rings. The detailed wiring diagrams for these two bridges are shown in Figs. 38 and 39, and Fig. 40 shows the actual bridge as built. For R_3 and R_4, resistors of 5,100 ohm are used. These are wirewound power resistors, having a tolerance of 1% and 10 watt capacity. Since the resistors carried a high resistance, such a small tolerance and a high power capacity were desired, as the maximum power in the resistors was computed to be 4.6 watts. These resistors also have high dielectric strength and heat capabilities.

Since the resistors and the strain gages used did not have the exact resistance specified, R_3 was made variable with potentiometers, which are designated as R_5 in the diagram, to meet such tolerances in the gages and resistors. Balancing of the circuits, based on the actual resistance measured precisely with a Wheatstone Bridge, showed that an additional resistor of 240 ohm was needed for R_4 for the outer ring circuit. It also indicated that a potentiometer of 100 ohm would be sufficient to meet the tolerance in balancing. The potentiometers used are of wirewound, 2 watt capacity, having a tolerance of 5%.

It is noted in the diagram that two capacitors are used in the circuit: one across the oscilloscope and the other across the battery. The capacitor across the oscilloscope (C_2) is to couple the bridge with the oscilloscope. It is of 75 wvdc and 0.1 μfd. To suppress all but desired components of voltage to the bridge, a capacitor (C_1) is con-

CENTER RING (NO. 6)

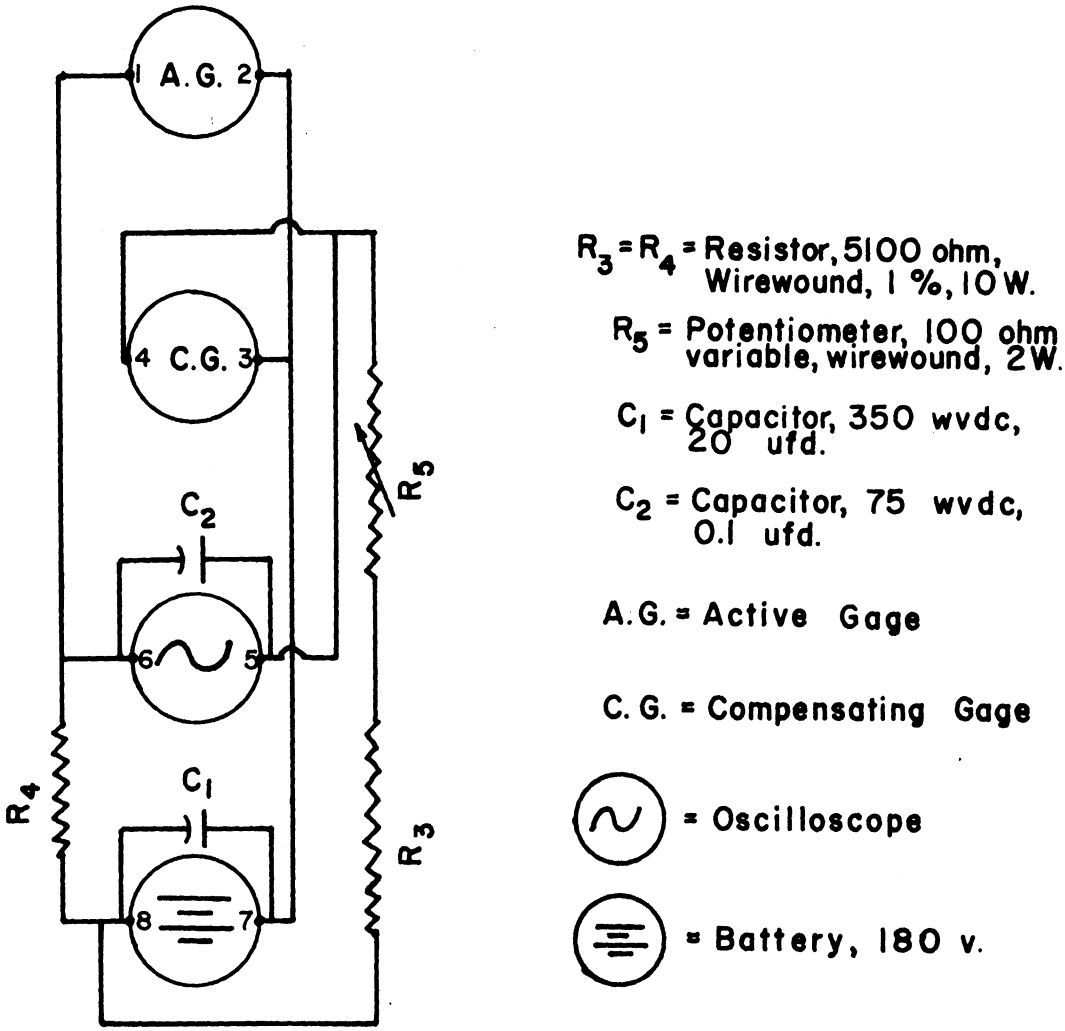

Fig. 38. Bridge wiring diagram for center ring.

OUTER RINGS

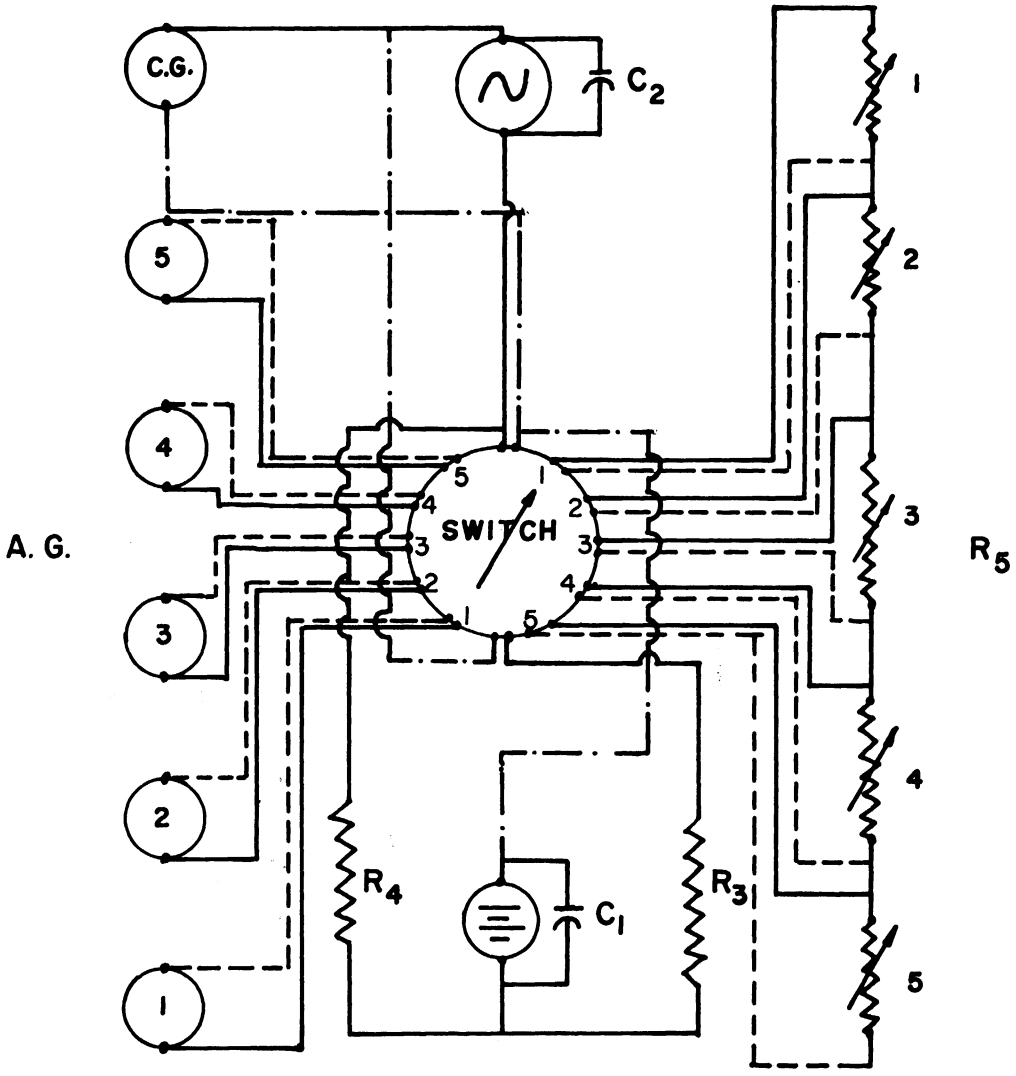

Fig. 39. Bridge wiring diagram for outer rings.

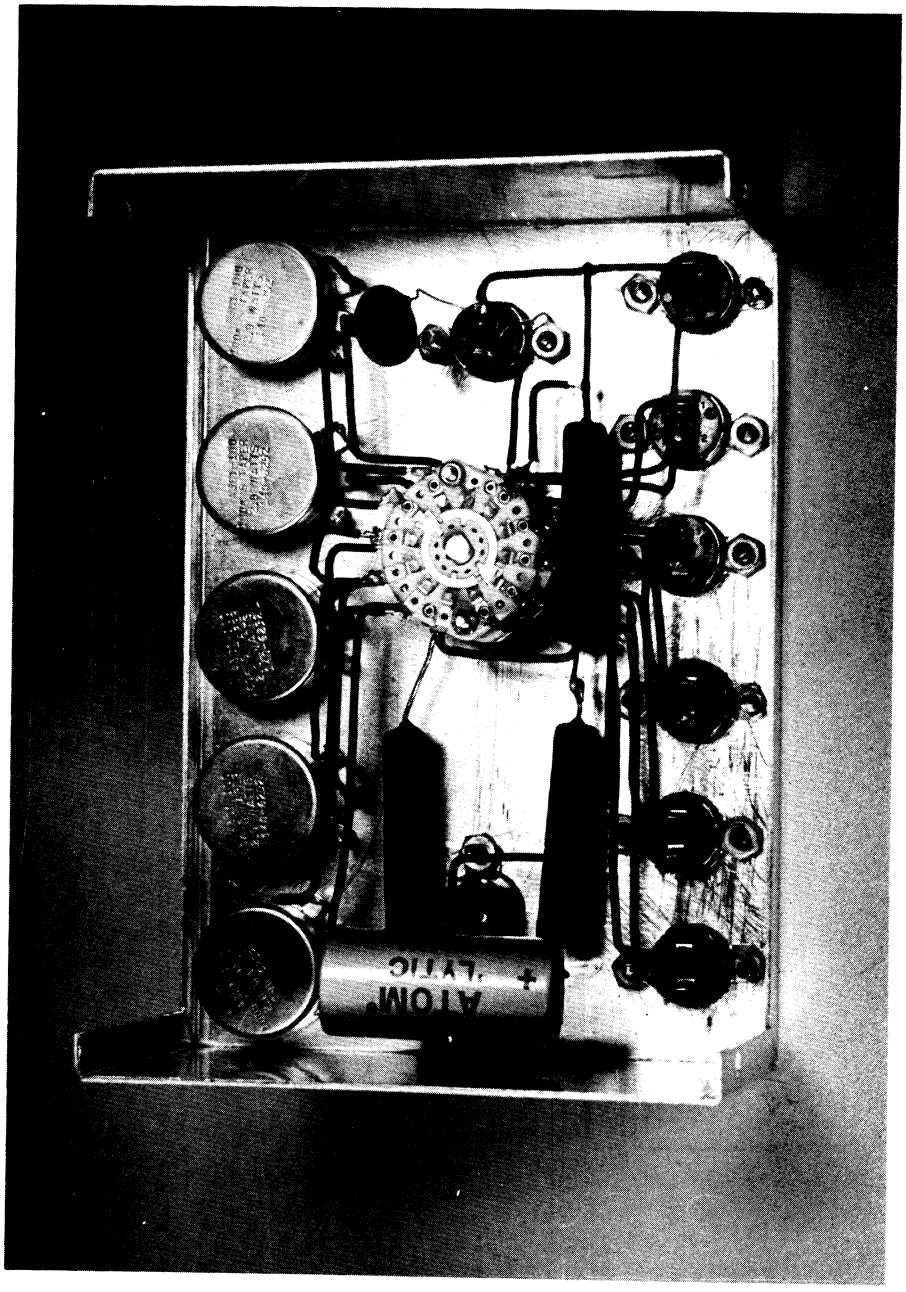

Fig. 40. Wheatstone Bridge as built (outer rings).

nected across the battery. It is of 350 vdc and 20 μfd to be used with the 180 volt battery.

Since there are five outer rings, each of which forms an independent system, switching of the system from one ring to the other is necessary. This is accomplished through a six-channel central switch as shown in the diagram. The switch has two sections, four poles and six pole positions of shorting type. Each bridge is housed in a minibox, with plugs and sockets used for inlets and outlets.

The major difficulties encountered during the instrumentation were high noise level in the system and interference of signal from the outside sources. Originally, the bridges were constructed with the carbon resistors and potentiometers of 2 watt power capacity, and a capacitor across the oscilloscope. The use of these components without filters seemed to give very high noise so that the balancing of the bridge was impossible at high sensitivity ranges. Besides the noise from these components, the connection of a high voltage battery directly to the bridge was detected to be causing additional noise. To correct such noise problems it was decided to change the resistance components to those of wire-wound type, and to raise the power rating to 10 watts so that the noise caused by heat could be minimized. It was also decided to couple the bridge with the battery by connecting it with a capacitor of a high capacitance to suppress the noise from the battery. In addition to these, the bridge circuit was shielded and so were the cables used for various connections.

These remedies taken are believed to have overcome the noise problem; the present noise level in the system is about the same as that of a Tektronix 502 oscilloscope being used.

It may also be noted that a D.C. amplifier is not utilized in the final system as originally planned. It was found that the use of a commercially available amplifier (such as BAM 1, Ellis) was not helpful in increasing the output sensitivity as the noise from the amplifiers compensated for whatever amplification they gave. Consequently, the use of an amplifier was abandoned.

OVERALL EXPERIMENTAL SETUP

Figure 41 is a schematic diagram showing the instrumentation sequence in the overall test setup under steady state vibration. In Fig. 42 is shown the setup in the laboratory. Tests for impact loads may be carried out under the same setup with the exception of the power supply and the exciter. In this section a brief description of the apparatus, which are commercially available, is given.

Power Amplifier and Calibrator-Exciter (MB Electronics Model T132534)

In this experiment the exciter is primarily used as a force generator. The exciter is connected to the A.C. and D C. power sources in the Power-Amplifier. The field coil in the exciter is supplied D.C. to produce a fixed magnetic field. The driver coil is suspended in this field and supplied a variable frequency alternating current. Motion of the driver coil is controlled (amplitude and force) by varying the driver

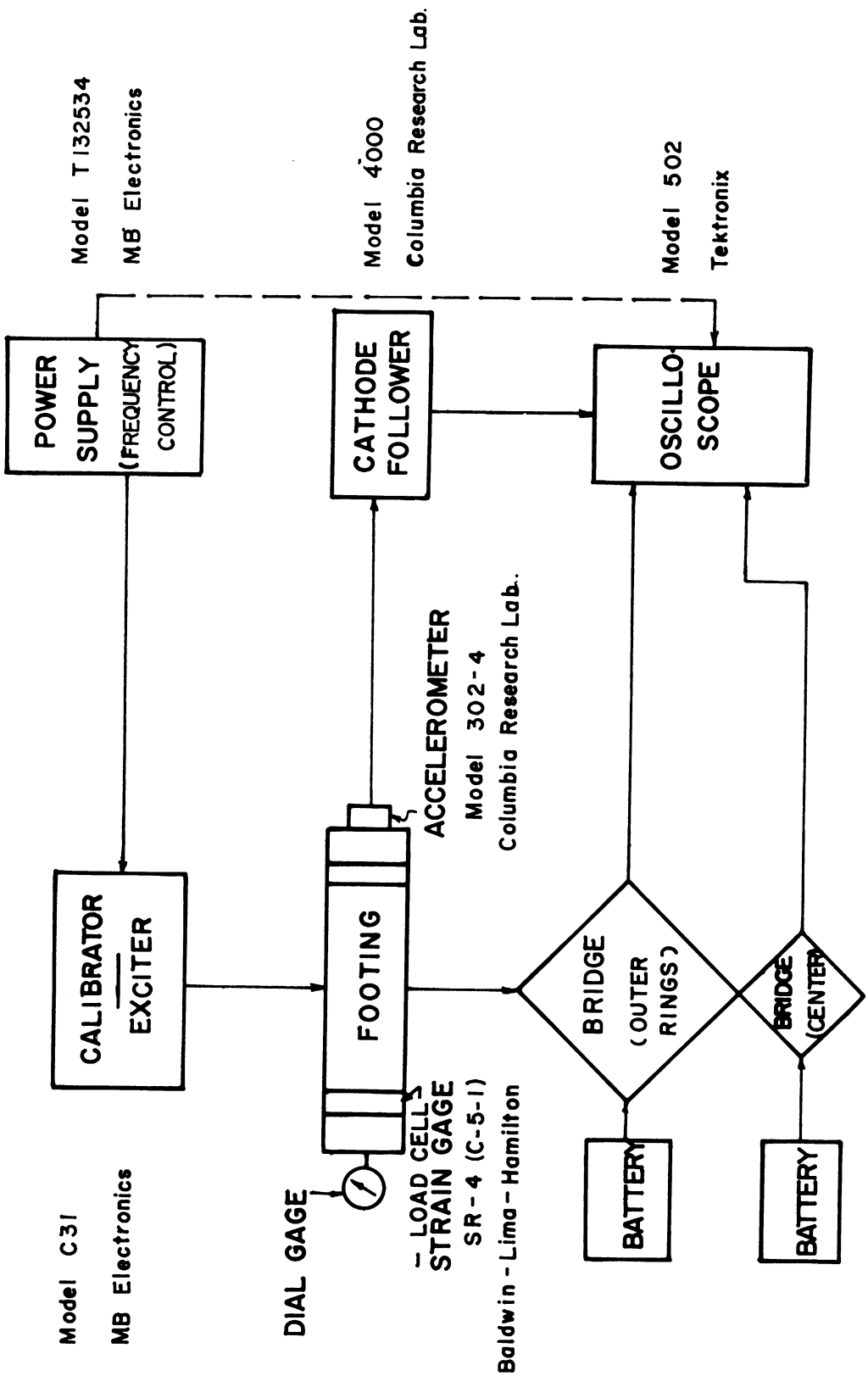

Fig. 41. Schematic diagram showing instrumentation sequence.

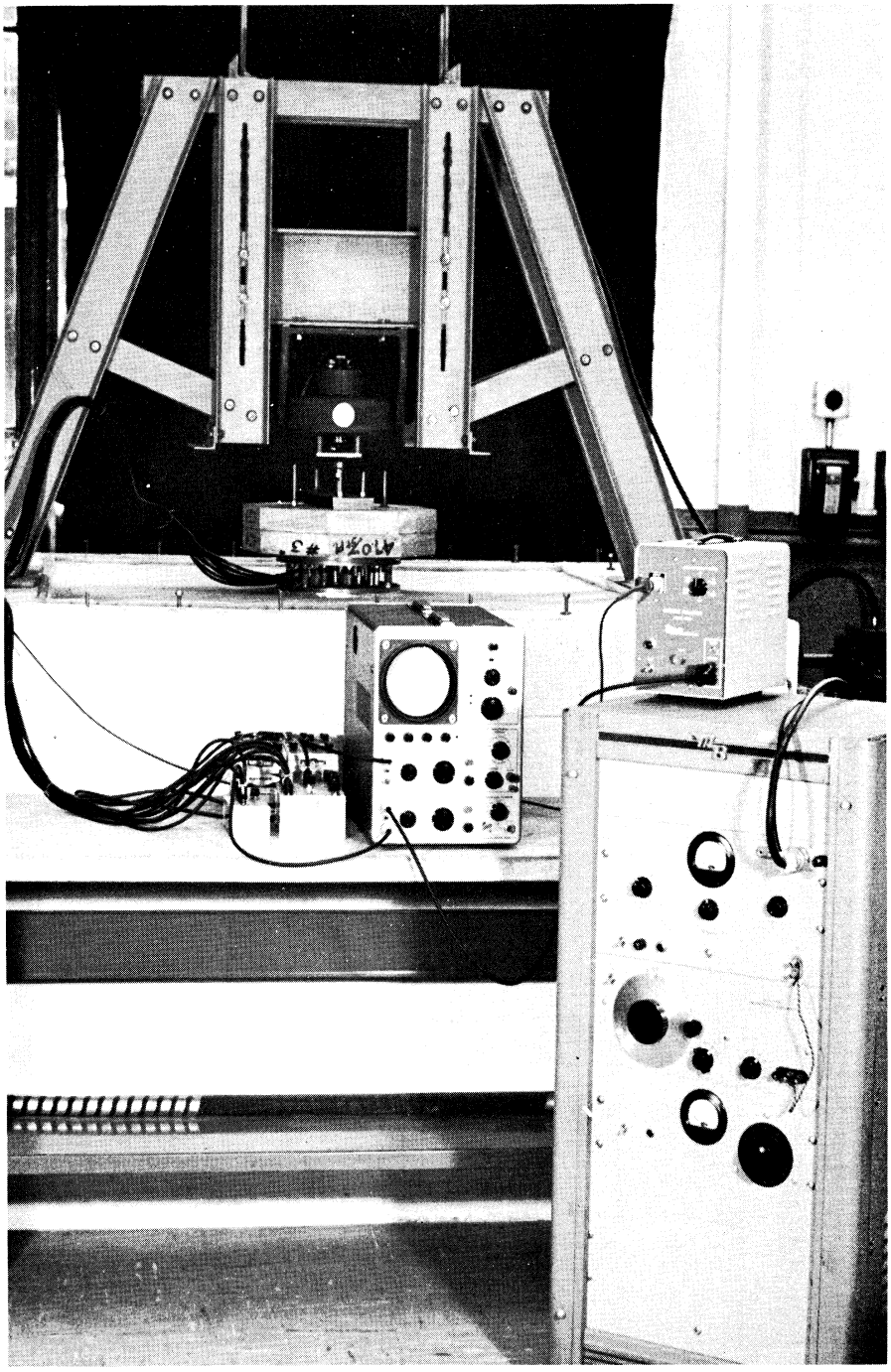

Fig. 42. Overall test setup in the laboratory.

coil current at the desired frequency.

The approximate force rating of the exciter with 0.70 ampere in the field coil is 9 lb vector force for each 1.0 ampere (rms) of A.C. applied to the driver coil. The maximum continuous current is 3.0 ampere in the frequency range of 6 to 500 cps.

Accelerometer and Cathode Follower

The cathode follower(Columbia Research Laboratory Model 4000) is an instrument to provide a means for coupling a signal source, which has a high impedance, to a measuring instrument which has a relatively low impedance.

The accelerometer (Columbia Research Laboratory Model 302-4) has an acceleration range of 0.001 to 1,000 g at a frequency range of 0.4 to 2,000 cps. It has a natural frequency of 10 kilocycles.

Oscilloscope (Tektronix Model 502)

The oscilloscope provides linear dual-beam displays with a wide range of sweep rates combined with high input sensitivity. The horizontal sweep rates range from 1 μ-sec/cm to 5 sec/cm. The maximum sensitivity for vertical deflection is 200 μv/cm.

Calibration of Testing Equipment

PRESSURE-SENSITIVE RINGS

Since the output of the bridge is an electrical signal whose mag-

nitude depends on the strain to which the gage is subjected, the strain must be converted to load in order to calculate the pressure on each ring.

Each ring was calibrated statically through the use of a Tinius-Olson Electomatic Testing Machine. The ring was subjected to a load of 120 lb in five increments and the electrical output signal corresponding to each load was read. The same procedure was followed in the unloading process. From these calibrations it was possible to convert the bridge output signal in millivolts directly to pressure on the ring in psi.

The calibration of load cells on each ring is shown in Fig. 43. In this chart the calibration factor in psi/mv is plotted for each ring against the supply voltage from the battery. It may be noted that the calibration factor varies linearly with the supply voltage. The calibration of load cells for different voltages was necessary because the voltage in the bridge circuit supplied by the battery did not stay constant, but decreased with time. It may also be noted that the calibration factor for ring 6 (center ring) is much higher than that for the outer rings. This is due to the smaller area of the center ring.

ACCELEROMETER

The accelerometer was calibrated by the Columbia Research Laboratory and its sensitivity is:

S = 383.6 pk-mv/pk-g at 0.97 gain of Cathode Follower

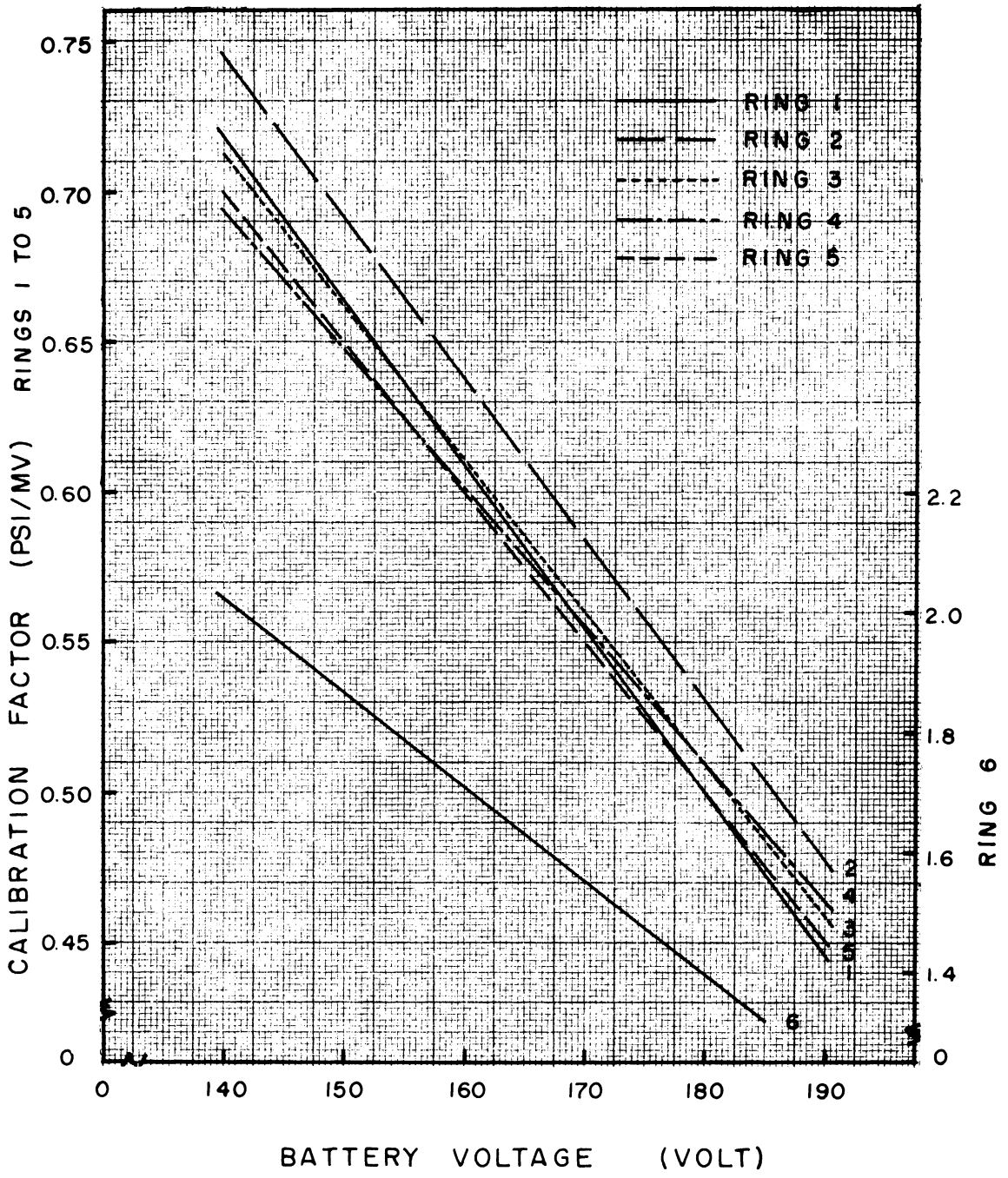

Fig. 43. Calibration of load cells at different supply voltage.

S = 350.3 pk-mv/pk-g at 0.97 gain of Cathode Follower with a 25 ft extension cord.

RESPONSE OF LOADING FRAME IN OSCILLATION

It is desirable that the dynamic response of the loading frame should not, if possible, interfere in any way with that of the oscillator-soil system in vibration. For this reason a check was made on the amplitude response of the loading frame. The amplitude was measured in three directions (vertical, two in horizontal) at a number of different locations in the frame.

In Fig. 44 is shown an experimental curve of frequency vs. amplitude for constant force excitation of the frame. The amplitude refers to a point at the top of the 8 in. WF beam. The first peak occurs at about 75 cps and is due to resonance in the transverse direction. The major peak occurs at about 135 cps and represents the fundamental mode for vertical oscillation. Two small peaks appear at frequencies of about 105 and 175 cps and are found to coincide with resonant frequencies of the frame members.

CHECK ON DISPLACEMENT AND PHASE DIFFERENCE BETWEEN UPPER AND LOWER PLATE

Since the footing employed in this investigation consisted of several separate plates connected together by load cells, it was thought essential to check whether displacement at the upper plate was the same as the lower plate during vibration at different frequencies. Two accelerometers were attached to the footing: One to the upper and the

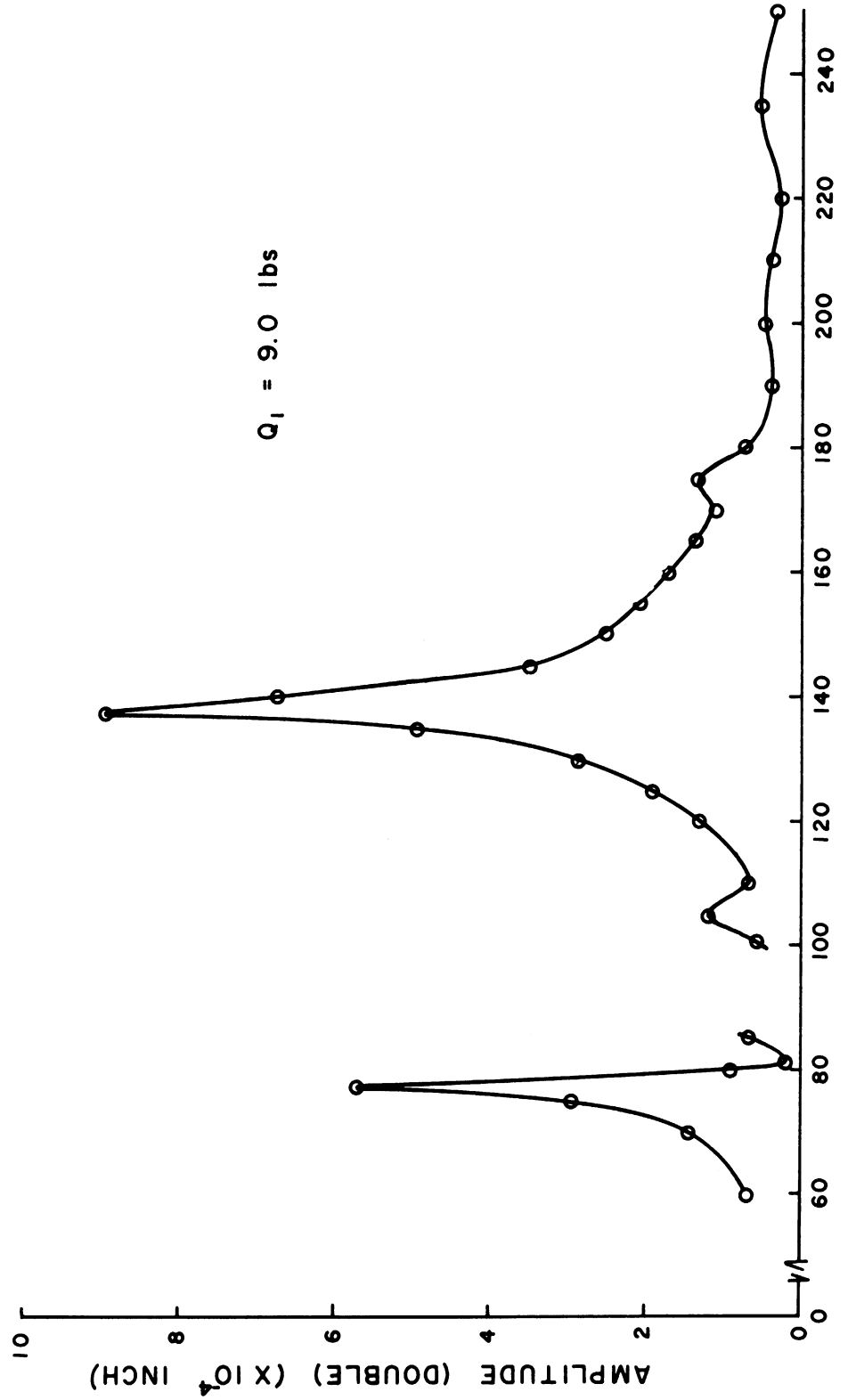

Fig. 44. Frequency vs. amplitude (loading frame).

other to the lower plate, and the displacement was measured at different frequencies. The results of this test showed that the displacement was different between the two plates due to the strains in the load cells. The deflection of the footing was generally 10 times that of the load cells. It was also observed that they were oscillating in phase.

Test Procedure

COMPACTION OF THE SURFACE LAYER OF SOIL

It is important that the density of the sand is uniform and should not be varied from one test to the next due to the effects of a prior run. It is also essential that the surface, especially where the footing is to be placed, is as level and smooth as possible.

Before each test run the surface layer of the sand is thoroughly compacted by means of a vibratory compactor and a square, level board. A wooden board of about 3 ft long, 2 ft wide and 1/4 in. thick, is placed on the surface and several uniform passes of the vibratory compactor are given. To avoid any uneven compaction under the corners of the board the outer portion of the bin is first compacted and then working toward the center portion. It is often desirable that the center portion of the bin where the footing is to be placed be checked by a carpenter's level to insure it is absolutely level.

PREPARATION AND PLACING OF FOOTING

After the footing is assembled it is necessary to make sure that

the lower and upper plates are bolted rigidly together, and the bottom of the footing is level, which can be checked by placing a steel straight edge against it. After the assembly a check is also made for clearance between the rings by a feeler gage to prevent any interference of rings during the tests. Then the bottom of the footing is covered with very thin aluminum foil to prevent sand grains from getting into the gaps between the rings.

To place the footing on the surface of the soil needs a great deal of care and caution, since the center of gravity of the footing has to be lined up with that of the exciter attached to the loading frame, and the footing must be placed squarely down on the soil without disturbing the uniform surface. A rail, made of two aluminum angles braced transversely together, is first placed across the bin to rest on the wall top so that it rests clear of the soil surface. Then the footing is placed on the rail at about the center portion of the bin and beneath the exciter. Alignment of the footing to the oscillator can be made by moving the rail, and when the two are exactly aligned they are connected by a thin, short rod. The oscillator and the footing is then raised by turning four threaded rods to a certain height so that the rail can be slid out of the bin wall. Now the footing is lowered gradually to the soil again by turning the four threaded rods. As the footing approaches nearer the surface care should be taken to see that the footing is lowered evenly so that it can be placed squarely down on the soil. This may be achieved by turning alternately each of the four threaded rods a few

turns at a time. If more than one man is available these rods can be turned simultaneously for a better control.

When the mass of the footing is to be changed the oscillator is disconnected from the footing and is raised to a desired height depending upon the amount of weight to be placed. The dead weights can rigidly be bolted to the footing with six threaded rods. In the case of static tests settlement of the soil due to these dead weights is measured by means of a dial gage as previously described.

RECORDING OF DATA

All the equipment is connected as shown in Figs. 41 and 42. The field coil in the exciter is fed 0.70 ampere and must be kept constant throughout the tests. Then the driver coil is supplied a variable frequency A.C. at a desired amplitude, depending upon the desired magnitude of the input force. With 0.70 ampere in the field coil the force rating of the exciter is 9 lb vector force for each 1.0 ampere of A.C. applied to the driver coil. The current in the driver coil is kept constant at any test frequency so that the amplitude of force remains constant regardless of the test frequency. Under the constant amplitude of force oscillation the force generated by the motion of the driver coil is exerted on the footing through the short connecting rod.

It is desirable that the equipment be warmed for at least 20 min before recording the measurements for various quantities as there is considerable drift as the equipment warms up.

Strain changes in the load cells caused by the oscillating load appear, through the bridge circuit, as a series of waves on the oscilloscope. The amplitude of force is read in millivolts, and then converted to pressure in lb/sq in. through the calibration factors. Since the oscilloscope has a dual channel, the output signals for any two quantities can be simultaneously displaced on the oscilloscope, and the phase shift between two such quantities may be measured in the unit of milliseconds.

In order to compute the displacement and the pressure distribution under the footing, there are 15 quantities to measure at a particular frequency under a constant force input as listed below:

1. Amplitude of acceleration ($\ddot{X}$)
2. Amplitude of force acting on the center ring ($\overline{F}_6$)
3. Amplitude of force acting on each of the five outer rings ($\overline{F}_{1 \text{ to } 5}$)
4. Phase shift between the input force and acceleration ($\phi_{Q\text{-}\ddot{X}}$)
5. Phase shift between the acceleration and the force acting on the center ring ($\phi_{\ddot{X}\text{-}F_6}$)
6. Phase shift between the force acting on the center ring and that on each of the five outer rings ($\phi_{F_6\text{-}F_{1\sim5}}$)
7. Phase shift between the input force and the force on center ring ($\phi_{Q\text{-}F_6}$)—this is to check the readings of $\phi_{Q\text{-}\ddot{X}}$ and $\phi_{\ddot{X}\text{-}F_6}$ by the relation, $\phi_{Q\text{-}\ddot{X}}+\phi_{Q\text{-}F_6} = \phi_{\ddot{X}\text{-}F_6}$.

With the use of only one oscilloscope the above quantities cannot, of course, be read simultaneously. In the course of conducting the tests it is essential that the voltage supplied by the batteries be checked

frequently, at least once before and after the test with each ring system. It has been observed that the voltage decreases with time, and thus the proper calibration factor corresponding to the measured voltage must be used.

The measurement of amplitudes and phase shifts, especially the latter, can best be made from the photographs of curves taken by a Polaroid camera. A set of typical curves are shown in Figs. 45 and 46. Amplitudes can be read in centimeters and then converted to millivolts through the vertical scale factor. Phase shifts read in centimeter are converted to milliseconds through the horizontal scale factor. In taking the data for phase shifts an average value of several readings taken at both upper and lower peaks is usually used. The same process is followed when reading phase shifts directly on the oscilloscope.

In this manner all the 15 quantities are measured at various frequencies. For the measurements of pressures under the footing the frequency was varied up to 250 cps with an interval of 10 cps. Beyond 250 cps the amplitude of forces in the load cells become too small to read for some of the rings. For the measurements of acceleration the frequency was varied up to 1,000 cps.

In Table IX is shown a typical data sheet for the measurements of various amplitudes and phase shifts listed previously.

ANALYSIS OF DATA

From the acceleration measured the displacement of the footing is

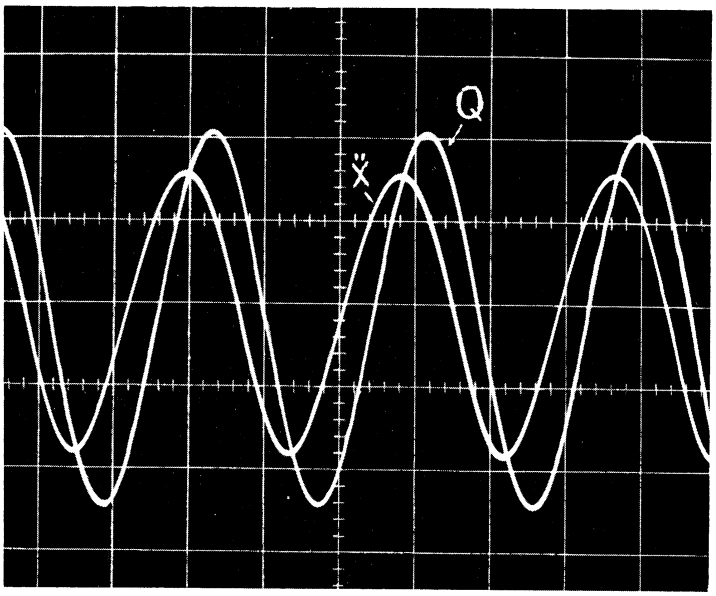

(a) Input Force vs. Acceleration
Vertical Scale: Q: 100 mv/cm; Ẍ: 50 mv/cm
Horizontal Scale: 5 msec/cm

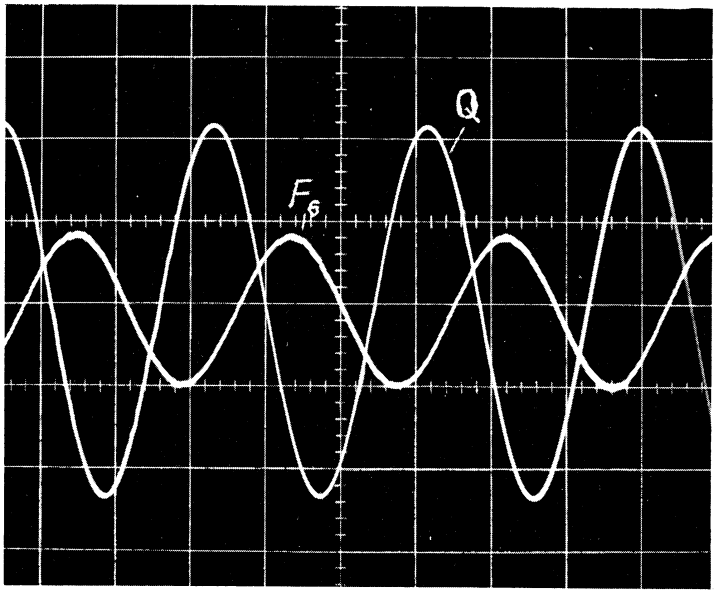

(b) Input Force vs. Force at Center Ring
Vertical Scale: Q: 100 mv/cm; F_s: 1 mv/cm
Horizontal Scale: 5 msec/cm

Fig. 45. Photographs of typical curves showing amplitudes and phase shifts.

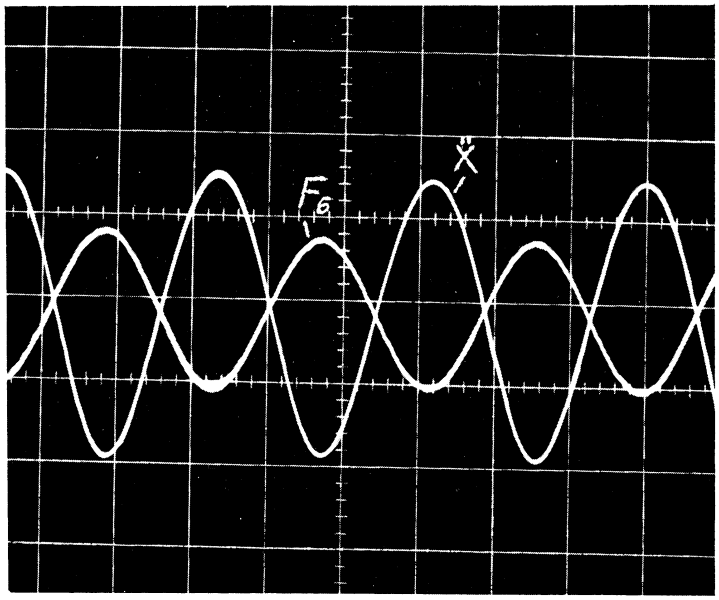

(a) Acceleration vs. Force at Center Ring
Vertical Scale: $\ddot{X}$: 50 mv/cm; F_6: 1 mv/cm
Horizontal Scale: 5 msec/cm

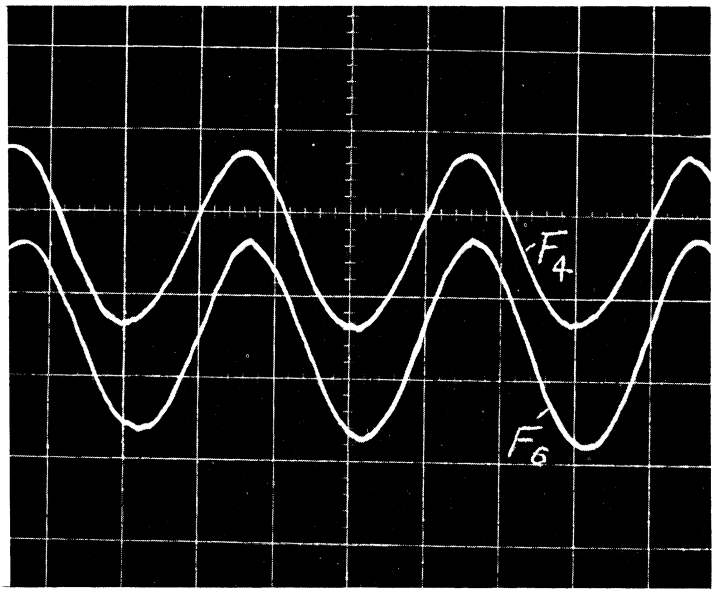

(b) Force at Center and One of the Outer Rings
Vertical Scale: 0.5 mv/cm
Horizontal Scale: 5 msec/cm

Fig. 46. Photographs of typical curves showing amplitudes and phase shifts.

TABLE IX

TYPICAL DATA FOR ACCELERATION, FORCES AND PHASE SHIFTS

Weight of Footing W_0 = 171.1 lbs. Mass Ratio b = 12.5

(a) Frequency - Acceleration - Phase

Amplitude of Input Force Q_1 = 9.0 lbs.

Frequency	Sensitivity	Amplitude		Sensitivity	Phase ($\phi_{\ddot{x}-Q}$)		Remark
(cps)	(mv/cm)	(cm)	(mv)	(msec/cm)	(cm)	(msec)	
50	10	1.8	18	5	1.875	9.375	
60		3.0	30		1.50	7.5	
70	20	5.2	104		1.20	6.0	
73.5		9.7	194	2	2.0	4.0	
80		5.0	100		2.0	4.0	
.		.	.		.	.	
.		.	.		.	.	
.		.	.		.	.	

(b) Frequency - Force - Phase

Ring No. 1

Amplitude of Input Force Q_1 = 18.0 lbs.

Battery Voltage { Before = 163 v, After = 163 v } Calibration Factor = 0.592

Frequency	Sensitivity	Amplitude		Sensitivity	Phase ($\phi_{F_A-F_2}$)		Remark
(cps)	(mv/cm)	(cm)	(mv)	(msec/cm)	(cm)	(msec)	
50	0.2	1.2	0.24	5	0.5	2.5	
60		1.4	0.28		0.56	2.8	
70		3.4	0.68		0.65	3.25	
73		4.0	0.80		0.69	3.45	
80		1.8	0.36		0.66	3.3	
.		.	.		.	.	
.		.	.		.	.	
.		.	.		.	.	

computed for each frequency; the relation between frequency and displacement is then drawn to show the resonant frequency and the maximum amplitude. The phase shift between the input force and displacement is also computed for each testing frequency, and the phase shift is usually drawn against the frequency ratio, that is, the ratio of exciting frequency to the resonant frequency.

The pressure at the base of each ring is a vectorial sum of the force measured in the load cell and the inertia force of the ring. From the results so obtained the pressure distribution at the base of the footing may be drawn at different frequencies or at different input forces. Computations of the total reaction under the footing and its phase shift with respect to displacement requires the summation of all forces acting in the system as described in Chapter III. The computation was manually done at first, but this proved to be very time consuming and laborious (about 2 to 3 hours were needed to compute for just one system at a particular frequency). It was decided, therefore, to use an IBM computer. The flow diagram for this program has been shown in Fig. 23. A sample print-out of the computer results is shown in Table X.

The method of computation of the displacement function through a computer program has been described in Chapter III. Table XI shows a sample print-out of the computer results for the displacement functions f_1 and f_2.

TABLE X

A SAMPLE PRINT-OUT OF COMPUTER RESULTS FOR REACTIONS, FORCES AND PHASE SHIFTS

WEIGHT OF FOOTING(LBS) = 302.3 MASS RATIO = 22.0 AMPL OF INPUT FORCE(LBS) = 18.0

FREQ(CPS)	ACCL(G)	DISPL(IN)	PHI(Q-X)	INER FORCE(PSI)	PHI(A-6)	PHI(6-X)	FREQ FACTOR
50	.0457	.0001789	13.5	.0081	180.0	.0	.27

	RING 1	RING 2	RING 3	RING 4	RING 5	RING 6
PHI(N-6)	37.1	15.0	10.0	4.9	1.8	.0
FORCE(PSI)	.2544	.3059	.6220	.7512	.9883	1.8382
PHI(N-X)	37.1	15.0	10.0	5.0	1.8	.0
REACTION(PSI)	.2609	.3137	.6300	.7593	.9964	1.8463
PHI(R-X)	36.0	14.6	9.9	4.9	1.8	.0

TOTAL FORCE(PSI) = .6653 PHI(FT-X) = 7.0 TOTAL REACTION(PSI) = .6733 PHI(RT-X) = 6.9

FREQ(CPS)	ACCL(G)	DISPL(IN)	PHI(Q-X)	INER FORCE(PSI)	PHI(A-6)	PHI(6-X)	FREQ FACTOR
60	.1142	.0003105	18.0	.0202	179.9	.1	.33

	RING 1	RING 2	RING 3	RING 4	RING 5	RING 6
PHI(N-6)	60.0	28.9	14.0	5.9	.0	.0
FORCE(PSI)	.4452	.5320	1.0574	1.3222	1.8269	3.0960
PHI(N-X)	60.1	29.0	14.1	6.0	.1	.1
REACTION(PSI)	.4556	.5498	1.0770	1.3423	1.8472	3.1162
PHI(R-X)	57.9	28.0	13.8	5.9	.1	.1

TOTAL FORCE(PSI) = 1.1397 PHI(FT-X) = 9.8 TOTAL REACTION(PSI) = 1.1596 PHI(RT-X) = 9.6

TABLE XI

A SAMPLE PRINT-OUT OF COMPUTER RESULTS FOR DISPLACEMENT FUNCTIONS

FOOTING- SOIL SYSTEM DATA

WEIGHT(LBS) = 257.1 RADIUS OF FOOTING(FT) = .500 SHEAR MODULUS(PSI) = 7150.0 UNIT WT OF SOIL(PCF) = 109.8

MASS RATIO = 18.732

DISPLACEMENT FUNCTIONS

FREQ(CPS)	FORCE(LBS)	AMPL(IN)	PHASE(DEG)	FREQ FACTOR	F1	F2
50.0	9.0	.0000950	14.0	.286	-.2665	.0387
60.0	9.0	.0001300	18.0	.343	-.2626	.0350
65.0	9.0	.0002220	28.0	.372	-.2873	.0372
70.0	9.0	.0004520	88.0	.400	-.3236	.0497
80.0	9.0	.0002150	106.0	.458	-.2568	.0659
90.0	9.0	.0001240	115.0	.515	-.2082	.0751
100.0	9.0	.0000780	130.0	.572	-.1864	.0873
110.0	9.0	.0000630	140.0	.629	-.1722	.0758
120.0	9.0	.0000470	145.0	.686	-.1553	.0769
130.0	9.0	.0000330	150.0	.744	-.1442	.0945
140.0	9.0	.0000270	154.0	.801	-.1363	.0923
150.0	9.0	.0000220	157.0	.858	-.1285	.0955
160.0	9.0	.0000185	160.0	.915	-.1247	.0961
170.0	9.0	.0000158	161.0	.972	-.1139	.0955
180.0	9.0	.0000130	162.0	1.030	-.0998	.1103
190.0	9.0	.0000113	162.0	1.087	-.0845	.1085
200.0	9.0	.0000100	163.0	1.144	-.0775	.1068
210.0	9.0	.0000090	163.0	1.201	-.0688	.0989
220.0	9.0	.0000081	164.0	1.258	-.0647	.0969
230.0	9.0	.0000074	164.0	1.316	-.0589	.0890
240.0	9.0	.0000066	165.0	1.373	-.0518	.0926
250.0	9.0	.0000062	165.0	1.430	-.0519	.0809
360.0	9.0	.0000031	165.0	2.059	-.0279	.0347
460.0	9.0	.0000020	166.0	2.631	-.0196	.0178
550.0	9.0	.0000013	166.0	3.146	-.0122	.0166
600.0	9.0	.0000010	166.0	3.432	-.0060	.0177
700.0	9.0	.0000008	166.0	4.004	-.0075	.0104
750.0	9.0	.0000007	166.0	4.290	-.0066	.0089

CHAPTER V

PRESENTATION AND DISCUSSION OF TEST RESULTS

The purpose of the experiment program was to obtain information on the effects of various parameters on the pressure distribution under the footing, and to provide data on the dynamic characteristics of the foundation-soil systems to evaluate the displacement functions. The parameters considered in the evaluation of pressure distribution were the mass ratio, the magnitude of input force, and the frequency of oscillation. For the determination of displacement functions f_1 and f_2, the displacement and the phase shift between the input force and displacement were used.

Dynamic Characteristics of Footing-Soil Systems

RESPONSE OF A FOOTING-SOIL SYSTEM TO CONSTANT FORCE OSCILLATION

The variation of amplitude with excitation frequency was investigated for different mass ratios and the magnitude of input force. The excitation frequency was varied up to 1,000 cps, and the magnitudes of constant input force chosen for the tests were 9.0, 13.5, 18.0 and 22.5 lb. These input forces corresponded to the current of 1.0, 1.5, 2.0 and 2.5 amperes respectively in the driver coil. All the tests were run under constant soil conditions.

Figure 47 is a typical curve showing the variation of amplitude with

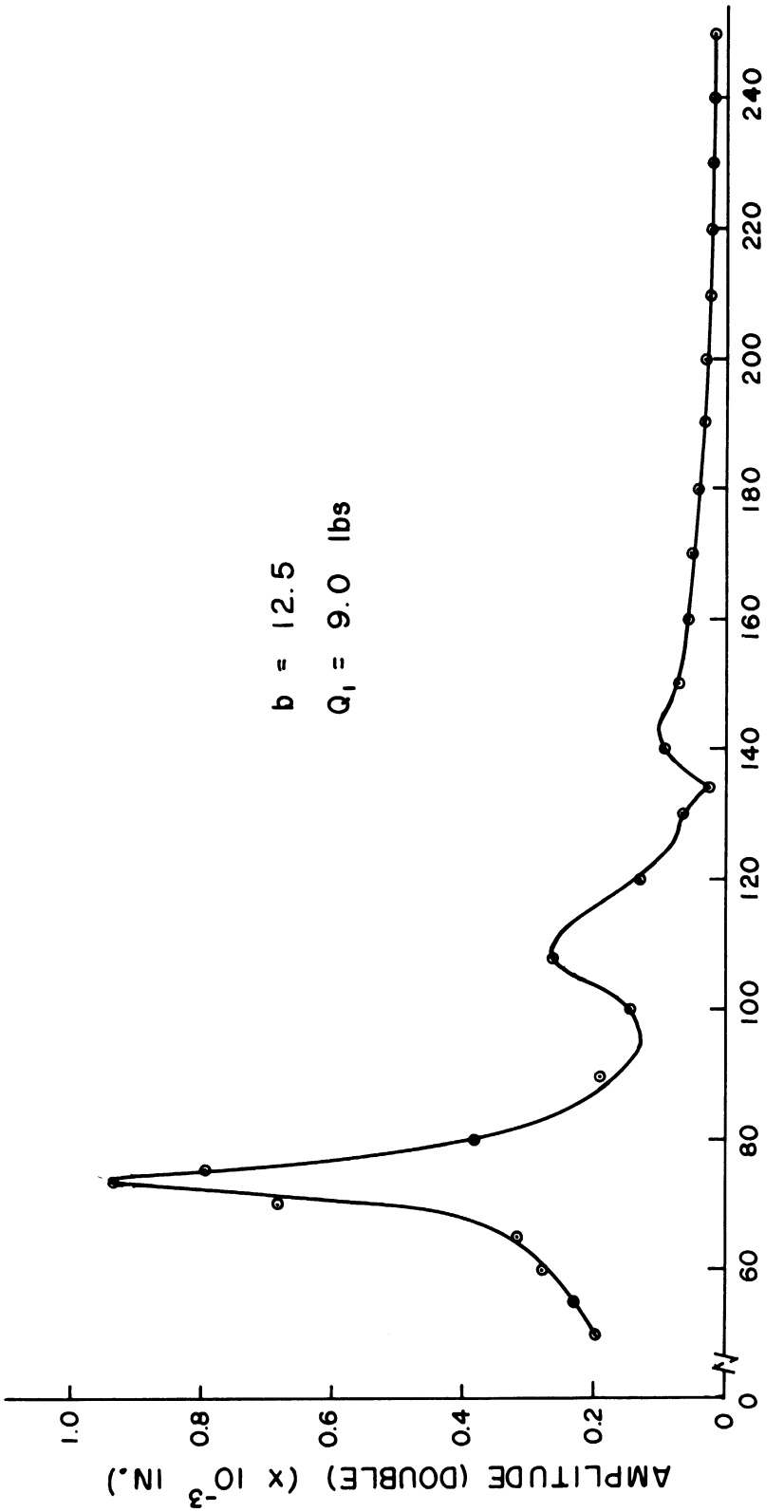

Fig. 47. Typical curve showing amplitude as a function of frequency.

excitation frequency for the system having a mass ratio of 12.5 and for a constant force amplitude of 9.0 lb. Curves similar in character to Fig. 47 were obtained with the other systems having different mass ratios or the magnitude of input force. It may be noted in Fig. 47 that the amplitude was plotted against the frequency of up to 250 cps although the frequency was varied up to 800 cps in the actual test. The amplitudes beyond the frequency of 250 cps were much smaller in magnitude than those shown in Fig. 47.

It may be observed in this figure that the first and major peak occurs at a frequency of about 74 cps, representing the fundamental mode for vertical oscillation. Two small peaks occur at frequencies of about 108 and 142 cps; the former of which was found to be coinciding with the resonant frequency of a frame member as shown in Fig. 44. The peak at the frequency of 142 cps might also be due to the same cause, although no peak was shown to exist at that frequency in Fig. 44. This indicates that the dynamic response of the loading frame and somewhat interfered with that of the footing-soil systems. If it were possible to build a loading frame having the natural frequency ranges outside of the range of the test frequency, these two peaks could have been avoided. Beyond the frequency range of these two peaks the amplitude decreased as the frequency was further increased.

The maximum peak to peak amplitude was measured to be 9.4×10^{-4} in. for this particular system. The resonant frequency was 73.5 cps. It may be pointed out here that the resonant frequency so determined was very

close to the frequency for maximum amplitude. This was true with all other test systems employed in the research. This is typical of an oscillator-foundation system having a small damping factor as illustrated in Fig. 4.

A typical relation between the phase shift of input force with respect to displacement and the excitation frequency is shown in Fig. 48. The curve shown in this figure is for the same system as for Fig. 47 (b = 12.5 and Q_1 = 9.0 lb), and represents one of many similar curves obtained for various test systems. It can be seen that the phase shift was small at low frequencies but increased radically at the region of resonant frequency, approaching 180 degrees as the frequency was further increased. The behavior of this test system in regard to phase shifts resembles those of single-degree-of-freedom forced vibration with viscous damping shown in Fig. 5. Comparing these two figures one may note that the damping factor in the test system was rather small, as stated previously in connection with the amplitude-frequency curve. The frequency at the point of the steepest slope of this curve is observed to be 72.5 cps, and the frequency corresponding to the phase shift of 90 degrees is 76 cps. These frequencies may be compared to the resonant frequency (73.5 cps). The results of the phase shift measurements, such as shown in Fig. 48, are believed to be good, considering the difficulties encountered in measuring the phase angles. The difficulties involved in measuring phase shifts will be discussed later in detail.

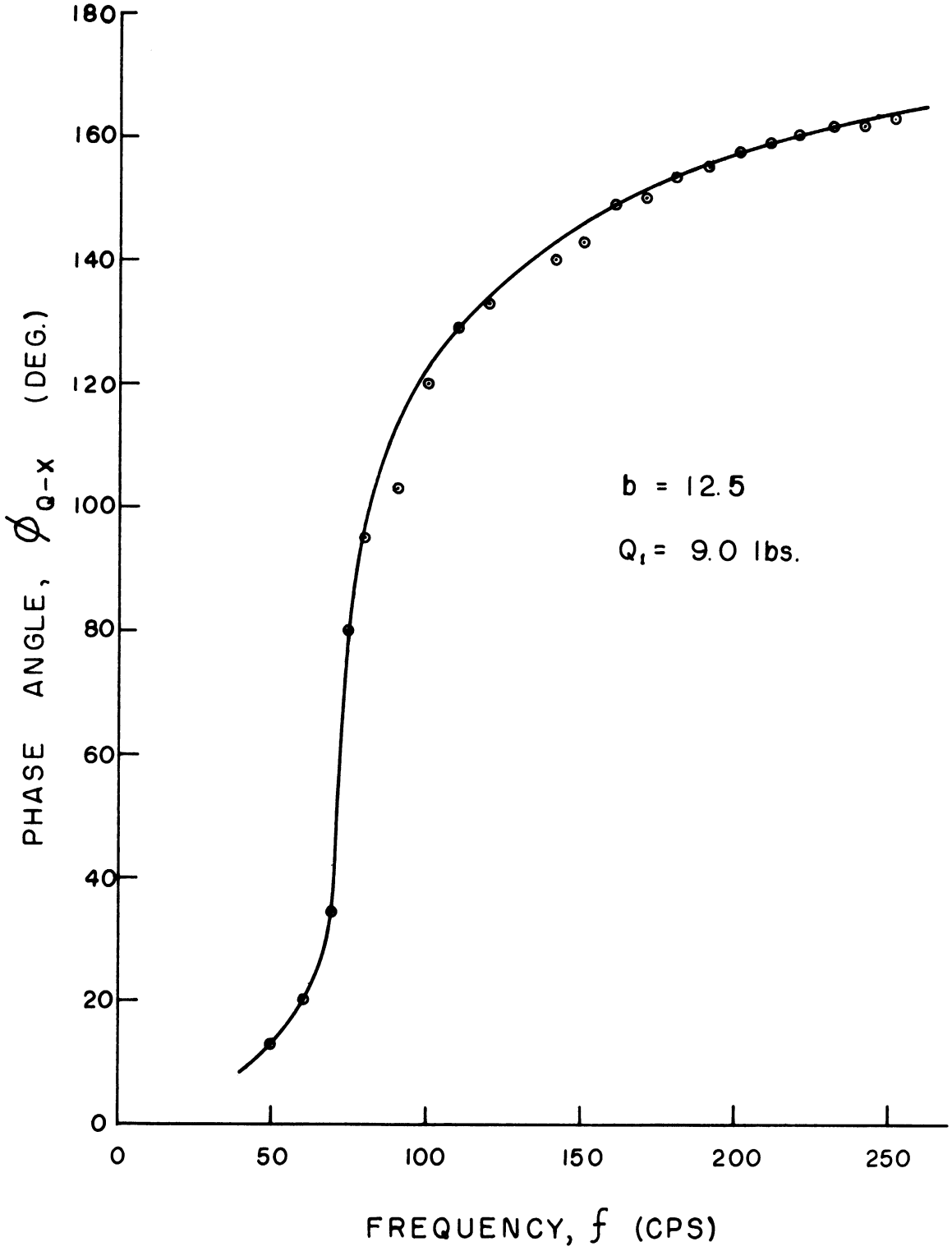

Fig. 48. Typical curve showing phase shift between input force and displacement as a function of frequency.

EFFECT OF MASS RATIO AND INPUT FORCE ON THE RESONANT FREQUENCY AND MAXIMUM AMPLITUDE

In investigating the dynamic characteristics of footing-soil systems, one is primarily concerned with the resonant frequency and the maximum amplitude occurring in the system, which are generally considered to be dependent upon the following parameters: the static weight of the oscillator; the radius of the footing; the mass density, shear modulus, and Poisson's ratio of the foundation; the magnitude of oscillating force, and the pressure distribution. Of these, the first three can be combined into a mass ratio of the system as defined previously, and the mass density and Poisson's ratio of the supporting soil are constant for the present research.

From the results of the seven test systems Fig. 49 has been drawn to show the effects of mass ratio and the magnitude of input force on the resonant frequency of the oscillator-foundation system. It can be seen that the resonant frequency increased from 64 to 80 cps as the mass ratio was decreased from 24.9 to 5.8 for a constant force input of 9 lb, and for the force of 18 lb the increase was from 62 to 79 cps. This shows that the resonant frequency is affected by the variation not only of mass ratio but also of applied force for any given oscillator-foundation system. The same results were observed by Jones (11) as shown in Fig. 16, and in the Waterways Experiment Station tests as analyzed by the writer in Chapter II (note a rotating-mass type oscillator was used in the WES tests). This increase of resonant frequency with smaller mass ratio was

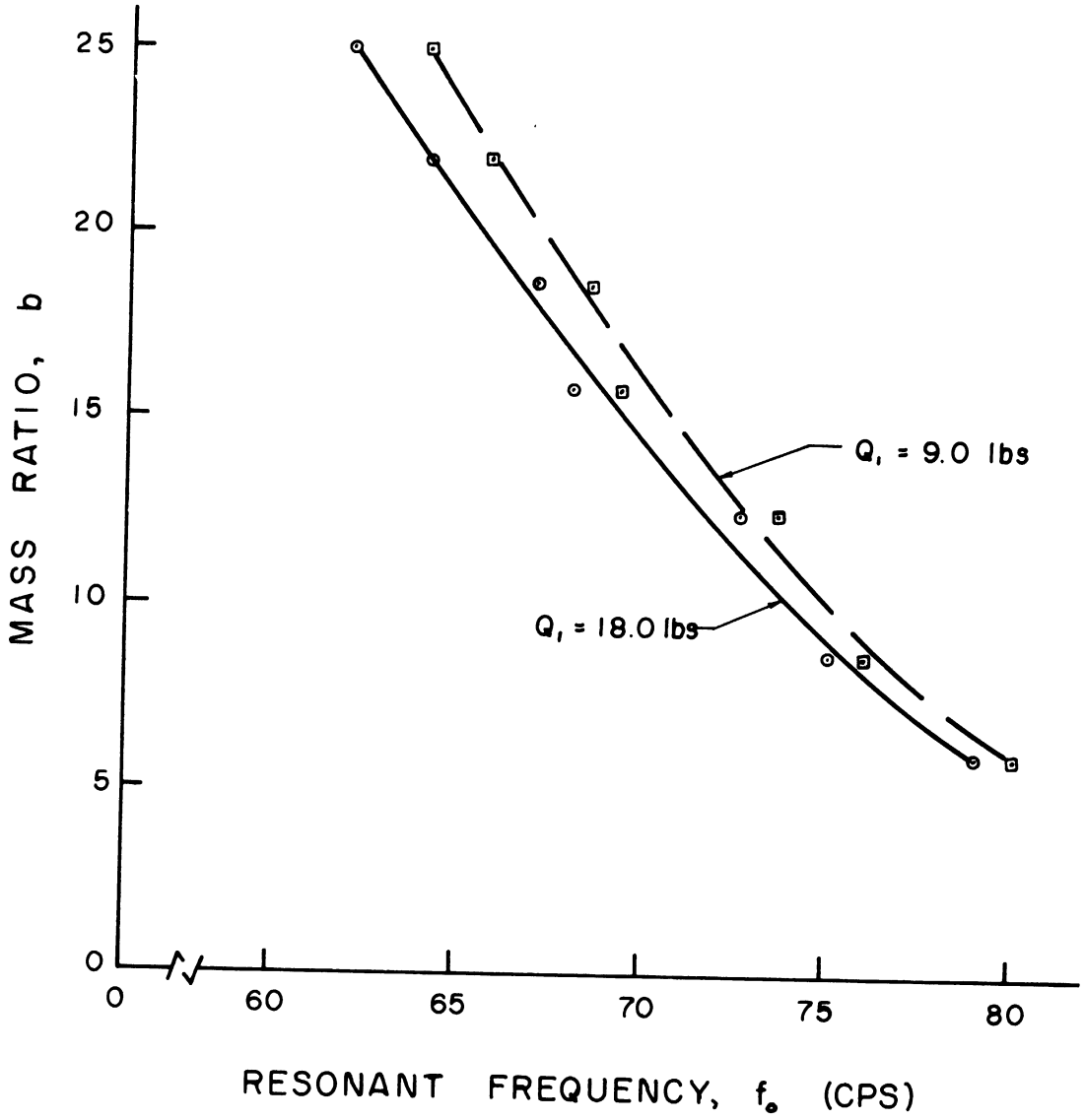

Fig. 49. Variation of resonant frequency with mass ratio and input force.

predicted by the theory of vibrations based on a semi-infinite elastic body as shown in Fig. 26. However, the variation of resonant frequency with the magnitude of input force was not indicated in the original theory developed by Reissner (16). In the past this effect was attributed to a change in the stiffness of soil by some or to a nonlinear elastic behavior of actual soils by others. This effect may be explained, however, by the fact that a change in the magnitude of input force causes a change in the pressure distribution under the footing, and the resonant frequency is in turn dependent upon the pressure distribution. This point was elaborated by Richart (18) in connection with his concept of an "effective radius" to be used as a tool for the transformation of pressure distribution. He pointed out that the decrease of resonant frequency caused by an increase in applied force was consistent with concept of an effective radius, as the pressure tended to become more intense near the center of the footing as the dynamic force was increased.

The theoretical resonant frequency for the test systems (Fig. 26) based on the assumption of rigid type pressure distribution and Poisson's ratio of 1/4 was in the range of 78 to 91 cps. The discrepancy between the theoretical and experimental results is within 20%, showing reasonably good agreement between the two. The discrepancy may be attributed to the assumptions made in theoretical analysis as to the type of pressure distribution, confining pressure, and the shear wave velocity. It is known that the dimensionless frequency factor a_o at maximum amplitude under parabolic loading is smaller than that of a rigid base type dis-

tribution. Consequently, agreement between the theoretical and experimental results could have been better if the parabolic loading was used for comparison.

Table XII shows the results of experimental determination of the shear moduli, the shear wave velocities, and the confining pressures computed from the data obtained for resonant frequencies of the seven test systems. This was done by reversing the process used in computing the theoretical resonant frequencies of the test systems shown in Table VII. The shear wave velocity based on the experimental value of resonant frequency was computed from the relation $f_o = a_o V_s / 2\pi r_o$. The shear modulus was then computed from the determined wave velocity. The confining pressure was then obtained from the wave velocity through the use of Fig. 25. Table XII shows that the confining pressure values used in the theoretical computation were roughly twice the values found experimentally; consequently, the experimental values of the shear modulus and shear wave velocity were lower than originally estimated.

It may be of interest to note in Fig. 49 that the resonant frequency varied only by 30% despite the mass ratio was changed by almost five times.

Figure 50 shows the effect of mass ratio on the maximum amplitude of a system. Under a constant force oscillation of 18.0 lb the maximum amplitude (peak to peak) decreased from 2.08×10^{-3}—1.77×10^{-3} in. as the mass ratio was increased from 5.8 to 24.9. It may be noted from Fig. 11(b) that theoretically the maximum amplitude for constant force oscillation is

TABLE XII

WAVE VELOCITY, SHEAR MODULUS AND CONFINING PRESSURE COMPUTED FROM EXPERIMENTAL DATA ON RESONANT FREQUENCY

Test System No.	Resonant Frequency f_o (cps)	Wave Velocity $\sqrt{\frac{G}{\rho}}$ (ft/sec)	Conf. Pressure (psf)	% of Assumed Pressure	Shear Modulus G (psi)
1	79.0	322	57	56 %	2,457
2	75.0	349	86	56	3,034
3	72.5	386	117	54	3,437
4	68.0	400	140	51	3,792
5	67.0	425	175	53	4,281
6	64.0	437	195	51	4,526
7	62.0	447	212	49	4,735

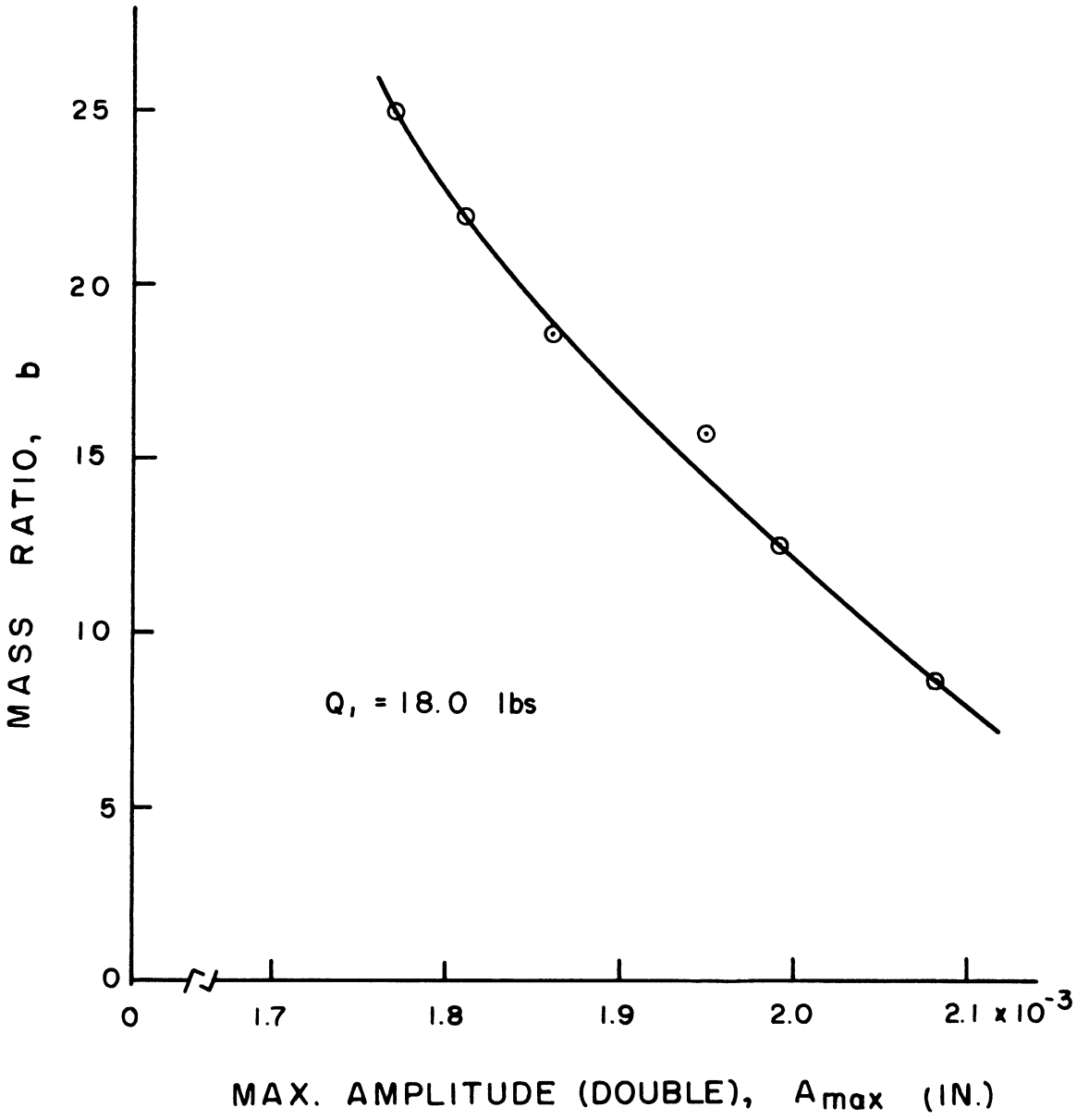

Fig. 50. Variation of maximum amplitude with mass ratio.

directly proportional to the mass ratio, if the shear modulus G remains constant. However, the shear modulus is also dependent upon the mass ratio, and the rate of increase of shear modulus with mass ratio is greater than that of the amplitude factor $A_{max}^{(2)}$ [compare the variation of shear modulus with mass ratio as shown in Table VIII with the variation of $A_{max}^{(2)}$ with mass ratio as shown in Fig. 11(b)]. Consequently, it was theoretically predicted that the maximum amplitude would decrease with increasing mass ratio (Fig. 27), and this was proved by the experiment. Comparing the experimental results with Fig. 27, however, one may note the experimental values are much greater than those predicted by theory. The discrepancy between the theory and experimental results may be explained by the fact that the type of pressure distribution assumed in theory was that of rigid base, which yields smaller amplitude values than the other types of pressure distribution. As was the case with the resonant frequency, if a parabolic type pressure distribution were assumed for comparison, agreement between the two would become much closer. Another attribution is made to the shear modulus value used in the theory, which was computed from an empirical curve based on the assumed values of confining pressure.

It may be of interest to note again that the maximum amplitude varied only by 20% as the mass ratio was changed by almost five times. Note also that the change in maximum amplitude was more pronounced as the mass ratio became smaller (note the same in the theoretical curve).

From the test results and analyses thereof it may be summarized that (1) a change in pressure distribution (input force) or loading area (mass ratio) causes a change in resonant frequency for a given foundation-soil system: under a constant force oscillation the resonant frequency increases with decreasing mass ratio or reduced input force, and the maximum amplitude also increases with decreasing mass ratio within the test systems employed; (2) if the proper assumptions are made as to the type of pressure distribution and confining pressure, the theory of vibration based on a semi-infinite elastic medium gives reasonably accurate predictions on the resonant frequency and the maximum amplitude occurring in the system.

Static Pressure Distribution

Figure 51 shows a typical load vs. settlement curve obtained under static loads. In this particular case the mass ratio of the system was 18.7. The mass of the footing was increased by adding four concrete blocks, and attempts were made to record the settlements due to these dead weights. However, the results were not reliable because of the difficulty in placing the concrete blocks on the footing. The curve shown in Fig. 51 was obtained under static loading (by jacking) of the footing. Since the pressure under each ring could not be recorded simultaneously, the readings were taken in five steps. The footing was first jacked up to a static load of 1,953 lb with an increment of about 100 lb, and the

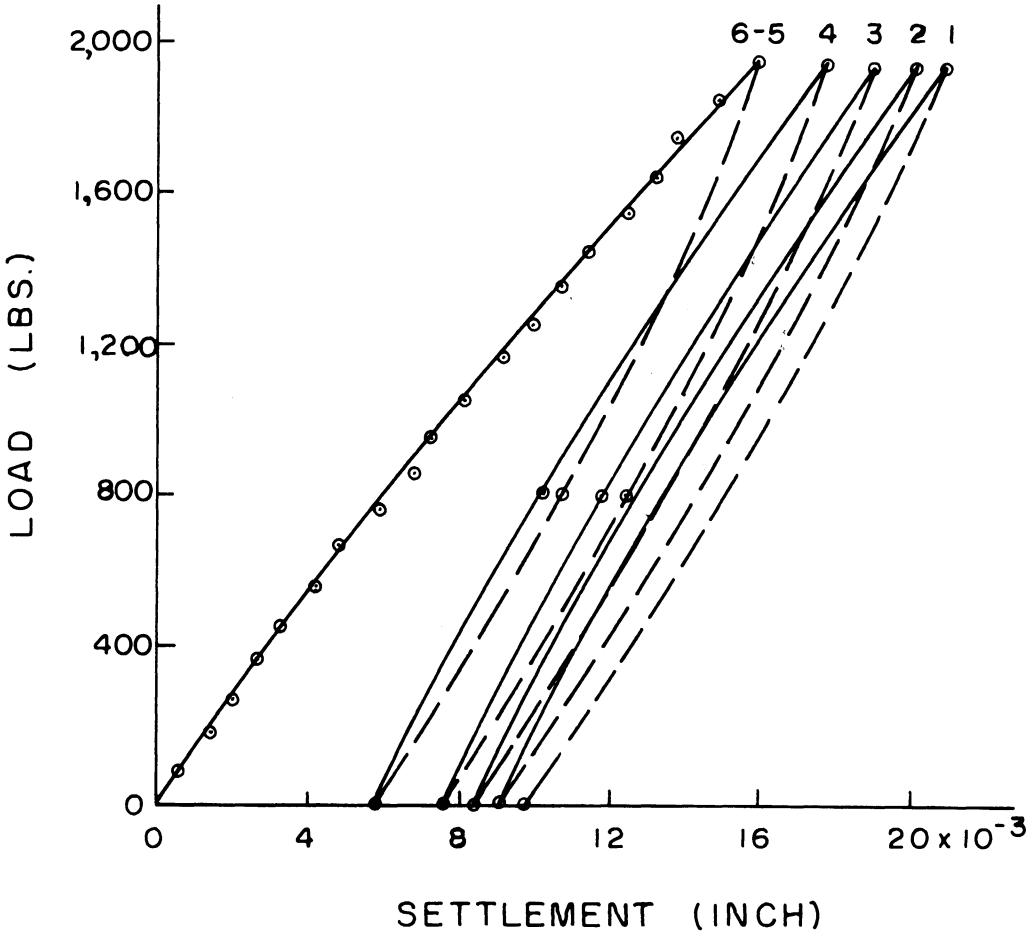

Fig. 51. Typical static load vs. settlement curve.

settlement corresponding to each load was recorded. Under this load (point 6-5 in the chart) pressure readings beneath the center ring and ring 5 were taken. Then the load was completely released and settlement in this unloaded condition was recorded. The footing was then reloaded to the same level as before to read the pressure under ring 4 and the settlement of the footing (point 4 in the chart). The same procedure was repeated until the readings for ring 1 were taken. Since the pressure readings were not taken simultaneously, the readings for rings 1, 2, 3, and 4 should have been affected somewhat by prior loadings.

The pressure at the base of each ring was then plotted to show the static pressure distribution under the footing as illustrated in Figs. 52 and 53. Note the pressure shown under each ring is an average pressure recorded beneath the ring. In Fig. 52 is presented the static pressure distribution at a small stress level (0.4 psi) whereas Fig. 53 shows the curves at high stress levels (9.56 and 17.5 psi).

The results shown in these figures check favorably with those obtained by Faber (5) under comparable test conditions. It may be noted that the pressure at the center is approximately equal to 2.0 to 2.6 times the average unit load applied over the entire footing. This ratio of the maximum pressure at the center to the average applied load appears to be proportional to the magnitude of the applied load. This implies that the pressure becomes more concentrated near the center as the applied load is increased.

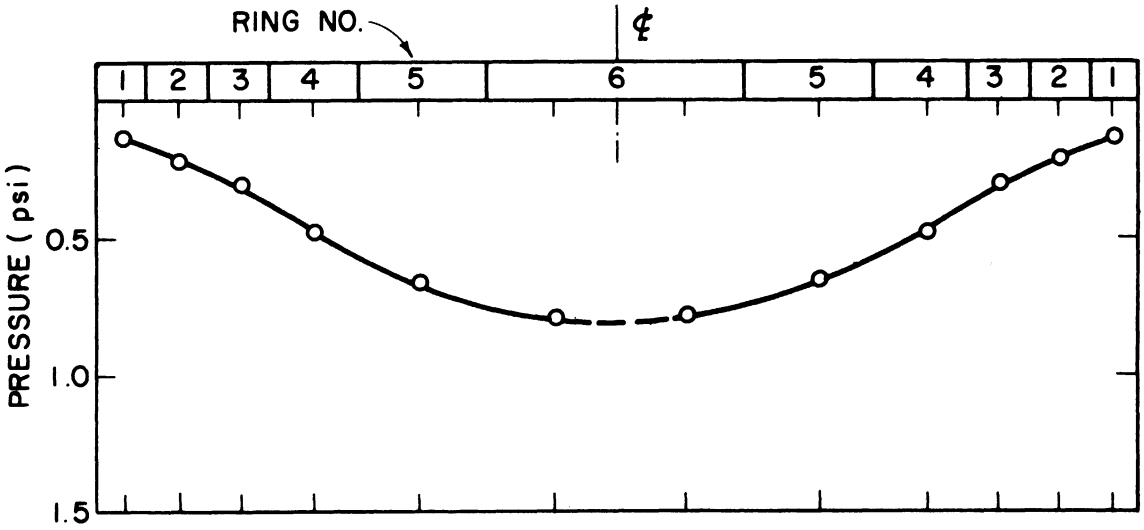

Fig. 52. Static pressure distribution beneath footing (low stress level).

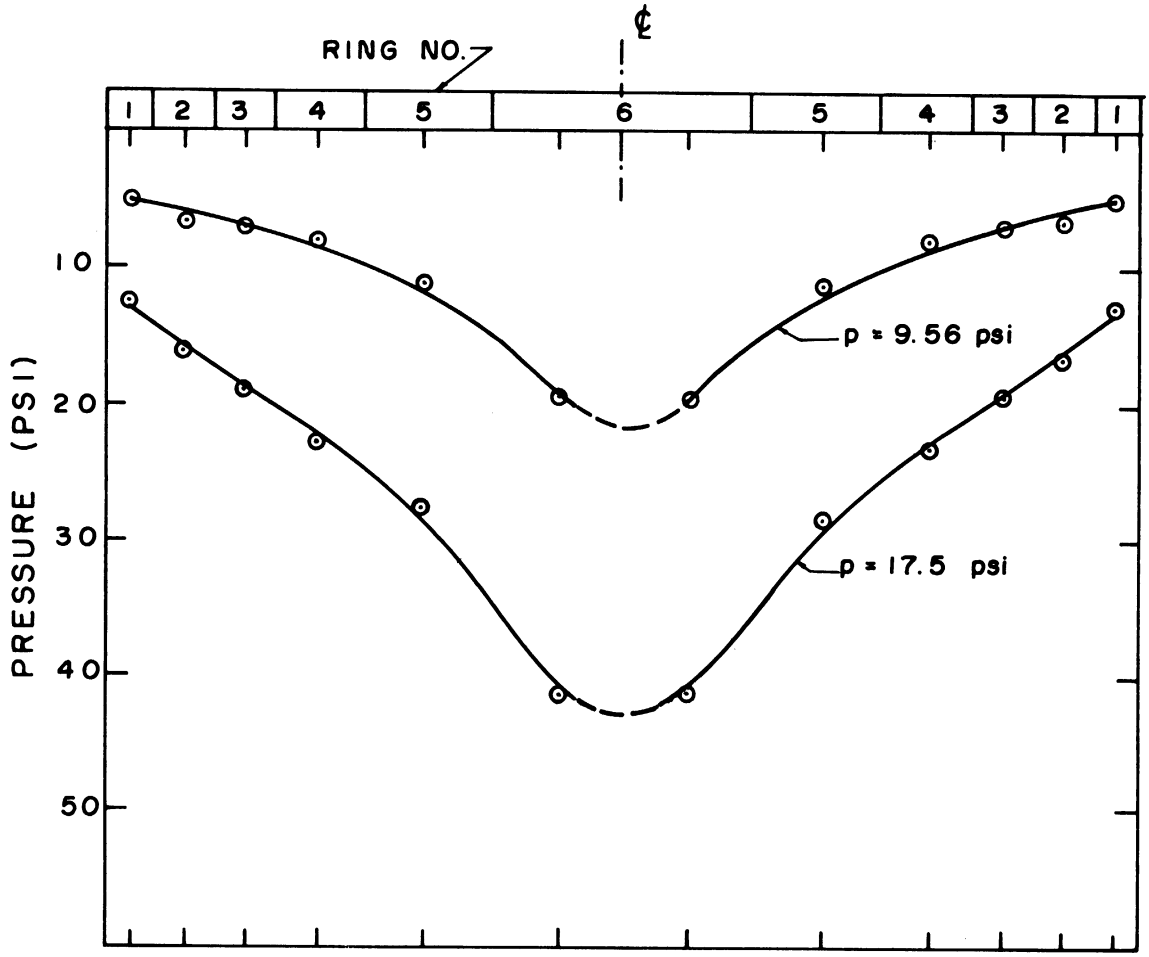

Fig. 53. Static pressure distribution beneath footing (high stress level).

It should be noted that the static pressure distribution, such as Figs. 52 and 53, due to the dead weight of the footing and any applied static load exists before any dynamic loads are superposed. The total pressure beneath the footing, therefore, is composed of the static pressure plus the time-dependent dynamic pressure.

Dynamic Pressure Distribution

MAGNITUDES AND PHASE RELATIONS BETWEEN FORCES AND REACTIONS

It was shown theoretically in Chapter III that the pressure under a rigid footing varied not only in magnitude but also in phase with reference to the center, and these phase relations were illustrated in the form of vector diagrams. Figures 54 and 55 are such vector diagrams drawn from the experimental data obtained. Figure 54 shows the phase relations among the input force, force measured on each ring, inertia force (of upper plate) and the total force acting on the footing. The magnitude of force is indicated by the length of each vector. In this diagram the displacement axis is taken, for convenience, as a reference line. Figure 55 is a vector diagram showing the phase relations among the input force, the soil reaction force under each ring, inertia force of the footing, and the total soil reaction under the footing. It may be noted in these diagrams that the vectors representing forces on, or reactions under the center and outer most rings are about 160 degrees out of phase, with the other vectors having intermediate values of phase lag.

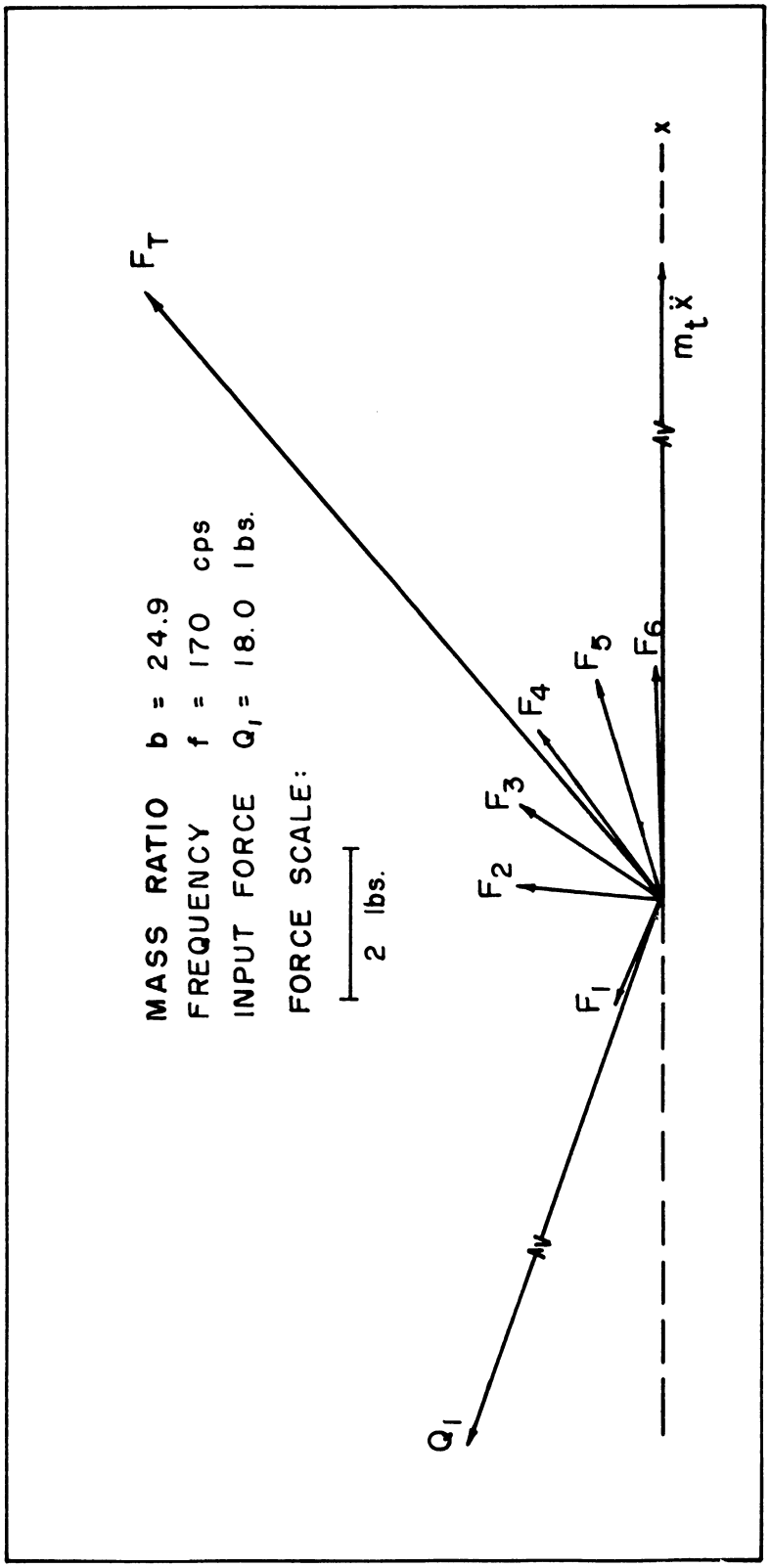

Fig. 54. Vector diagram for phase relations among the force on each ring, input force, inertia force, and displacement.

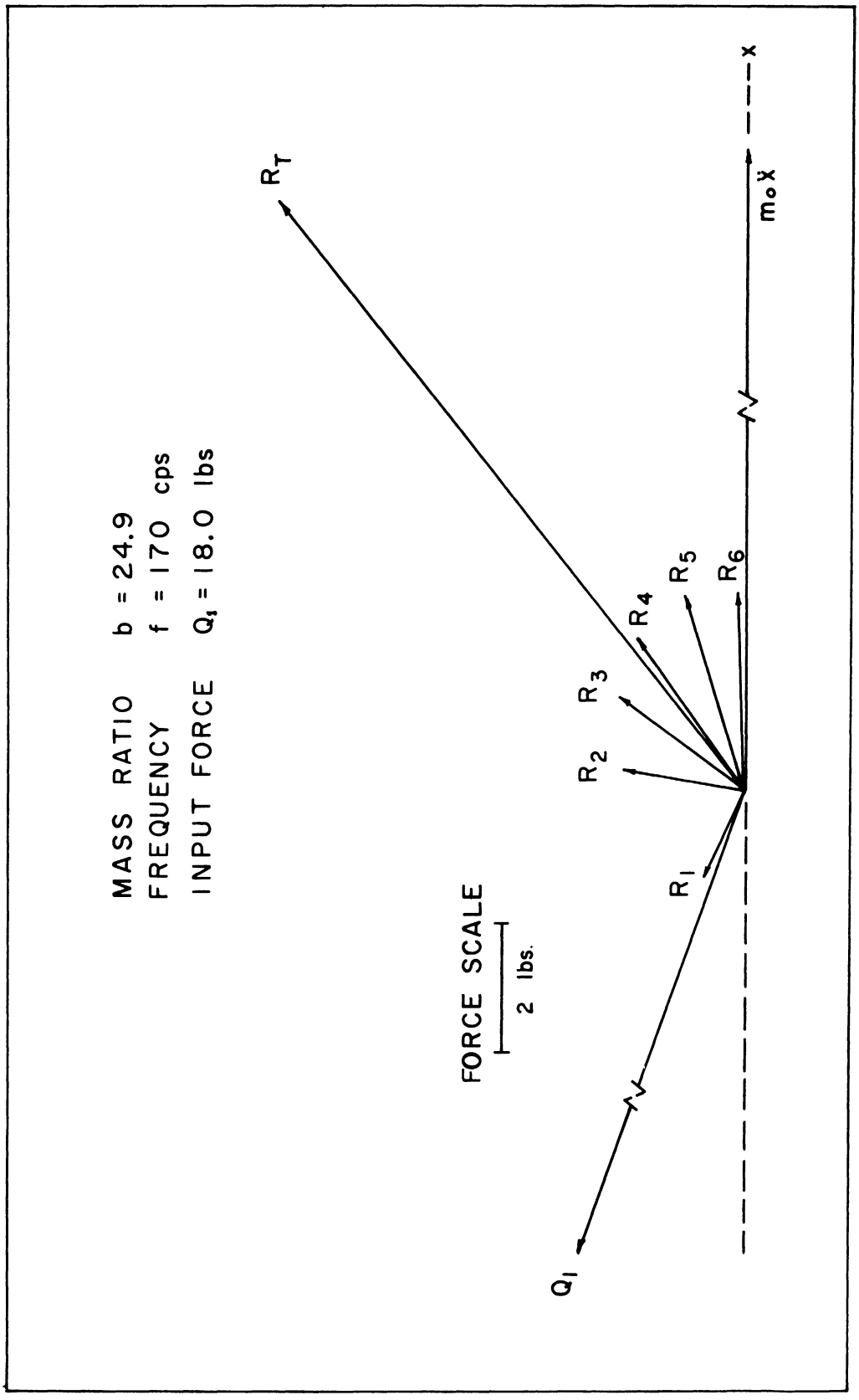

Fig. 55. Vector diagram for phase relations among the soil reaction forces, input force, inertia force, total soil reaction, and displacement

Figures 54 and 55 represent only two sets of many vector diagrams that may be drawn from the test results, as the phase relations change with such variables as excitation frequency and mass ratio. Such variations of the phase relations with frequency and mass ratio are illustrated in Figs. 56 through 59. In Fig. 56 is shown the variation of the phase shifts between the soil reaction forces and displacement with the change of excitation frequency for one chosen value of mass ratio (b = 12.5). It may be observed that the phase angle between the soil reaction force under each ring and displacement increases with excitation frequency, and that the rate of increase is greatest with the outer most ring. Note also that the phase angle between the forces on two adjacent rings becomes greater towards the outer rings at a given frequency, except in the high frequency range where the trend is reversed.

Figure 57, which represents the test system having a mass ratio of 5.8, is drawn to show how the phase relations are affected by varying the mass ratio of the system. Note that the phase angle between the reaction force on center ring and displacement ($\phi_{R_6\text{-}X}$) is greater at any frequency than that for the system having a mass ratio of 12.5 (Fig. 56). It may also be noted that the total phase shift between the force on center and outermost ring ($\phi_{R_6\text{-}R_1}$) is smaller at any given frequency than that for the system having a mass ratio of 12.5. The effect of mass ratio on phase relations is shown in another form in Fig. 58. In this figure the phase shift between the force acting on the center ring and

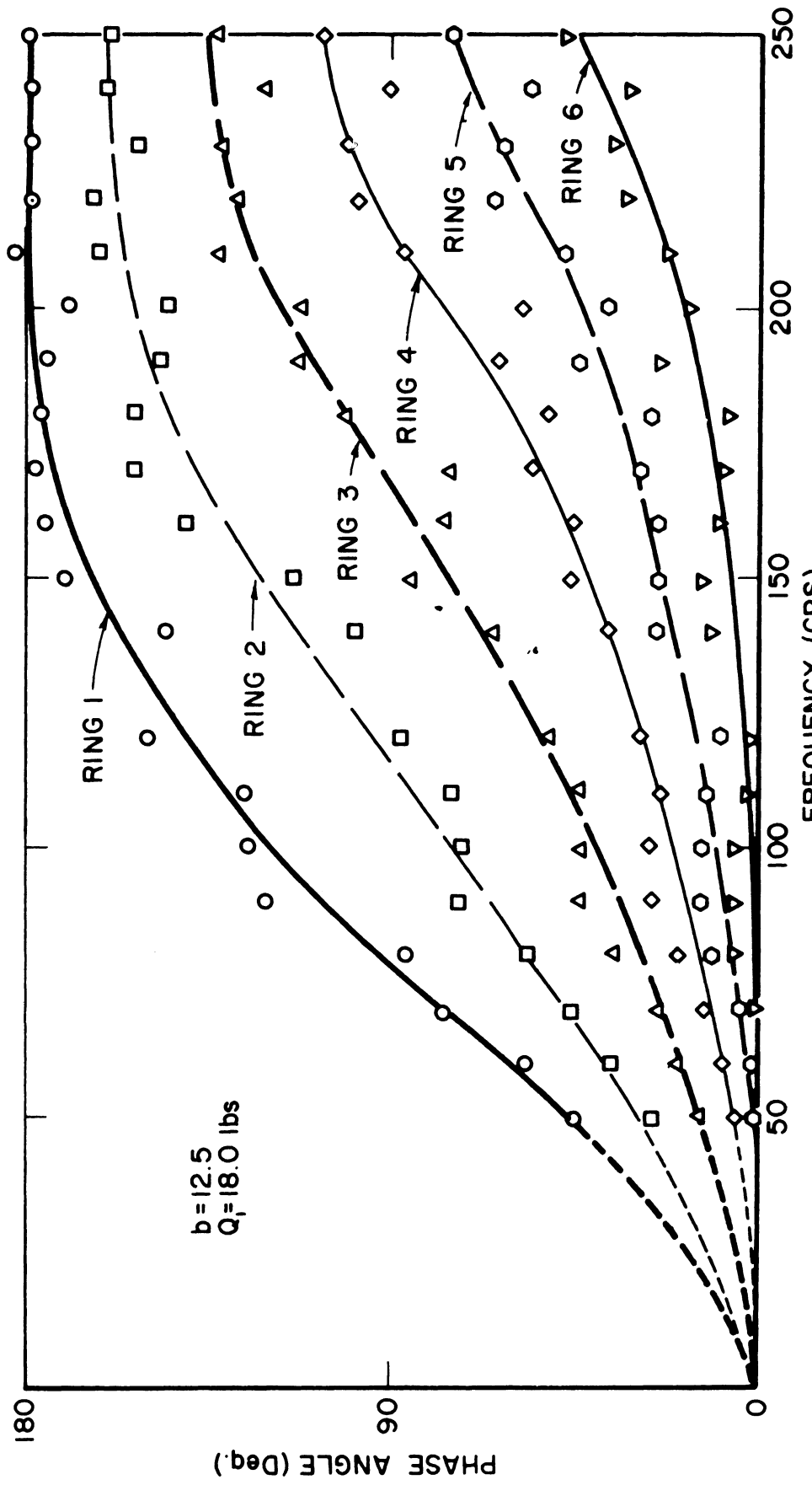

Fig. 56. Phase relations between the soil reaction force on each ring and displacement as a function of frequency (b = 12.5).

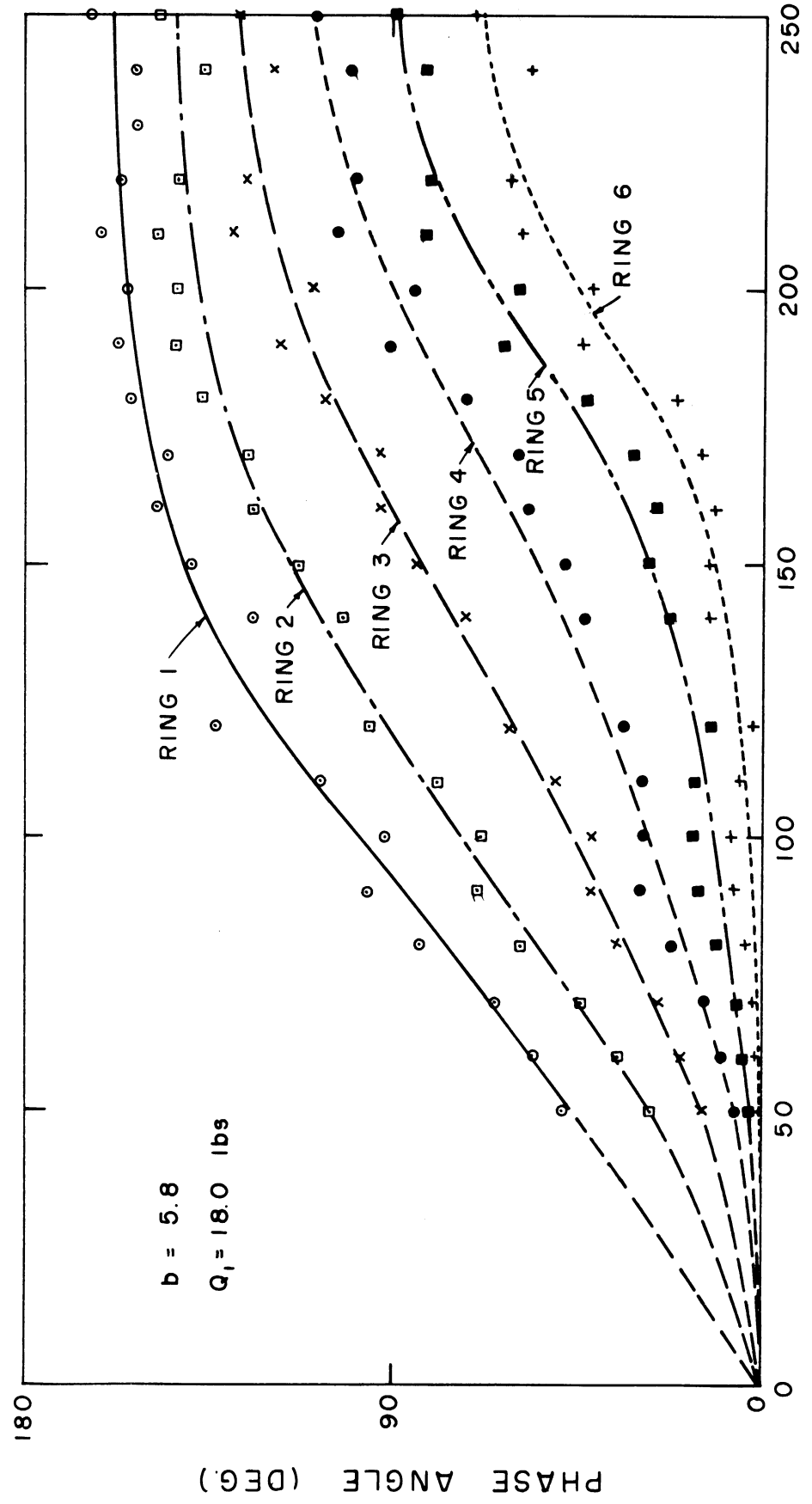

Fig. 57. Phase relations between the soil reaction force on each ring and displacement as a function of frequency (b = 8.7).

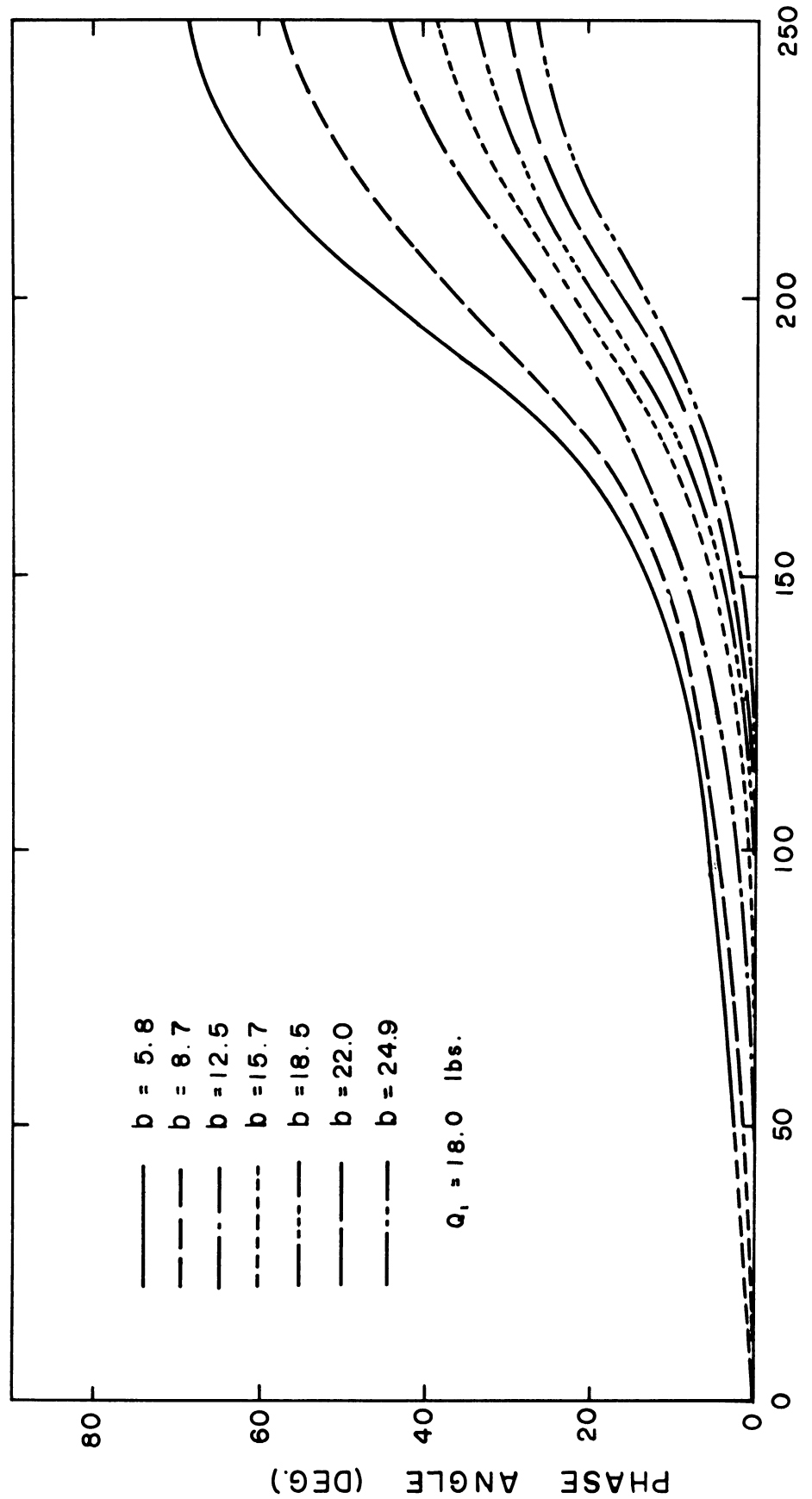

Fig. 58. Phase shift between the force on center ring and displacement for various mass ratios.

the displacement is plotted as a function of frequency for the seven test systems employed. Note that the phase shift becomes greater as the mass ratio of the system is decreased.

The experimental results of phase angle measurements show a scatter of points in the figures. It must be realized that the experimental determination of the phase angle was very difficult with the apparatus available and was lacking in accuracy. This was particularly true with the measurements at high frequency ranges. An error of 0.1 msec in the recording of the phase angle would cause an error of 3.6 degrees at the frequency of 100 cps, and 18.0 degrees at 500 cps in the computation of phase shifts. It was felt that special instrumentation should be used in order to improve the accuracy in recording the phase shift measurements.

It has been shown in Chapter IV that the accuracy in measuring the phase shift between two quantities can be improved by measuring another phase shift involving a third quantity. As illustrated in the figure below, measurement of the phase shift, for instance, between the input force and acceleration ($\phi_{Q-\ddot{X}}$), and that between the acceleration and the force on the center ring ($\phi_{\ddot{X}-F_6}$) can be checked by the measurement of

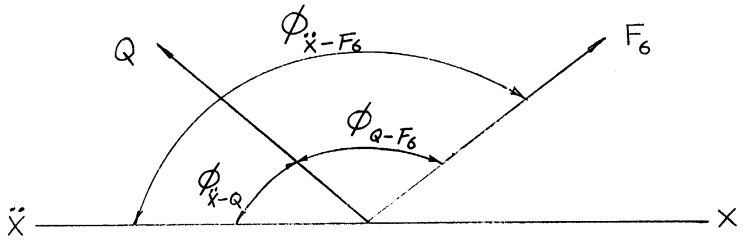

Fig. 59. Vector diagram for phase relations among acceleration, input force and force on center ring.

phase shift between the input force and the force on the center ring ($\phi_{Q\text{-}F_6}$) through a relation $\phi_{Q\text{-}\ddot{X}} + \phi_{Q\text{-}F_6} = \phi_{\ddot{X}\text{-}F_6}$. The measurements of these three phase differences for a specific test system are plotted as a function of frequency as shown in Fig. 60. This chart has no other purpose than to show the results of the three phase angle measurements for a specific mass ratio and how their measurements can be checked against each other.

It may be stated in conclusion that the phase relations between the soil reaction forces are dependent upon the mass ratio of an oscillator-foundation system and the frequency of oscillation. The phase angle increases with an increase in frequency, and such an increase is more pronounced with greater mass ratio. It should be noted that theoretical solution for the variation of phase shift between the soil reaction forces has not been found.

PRESSURE DISTRIBUTION UNDER THE FOOTING

It has been explained previously that the soil reaction force at the base of each ring is computed from the force measured in the load cell above the ring, and the inertia force of the ring. These reaction forces are acting out of phase with respect to each other as described in a previous section, and also are time-dependent as expressed by

$$R_j = \bar{R}_j \sin(\omega t + \phi_{R_6\text{-}R_j})$$

and (67)

$$R_6 = \bar{R}_6 \sin \omega t$$

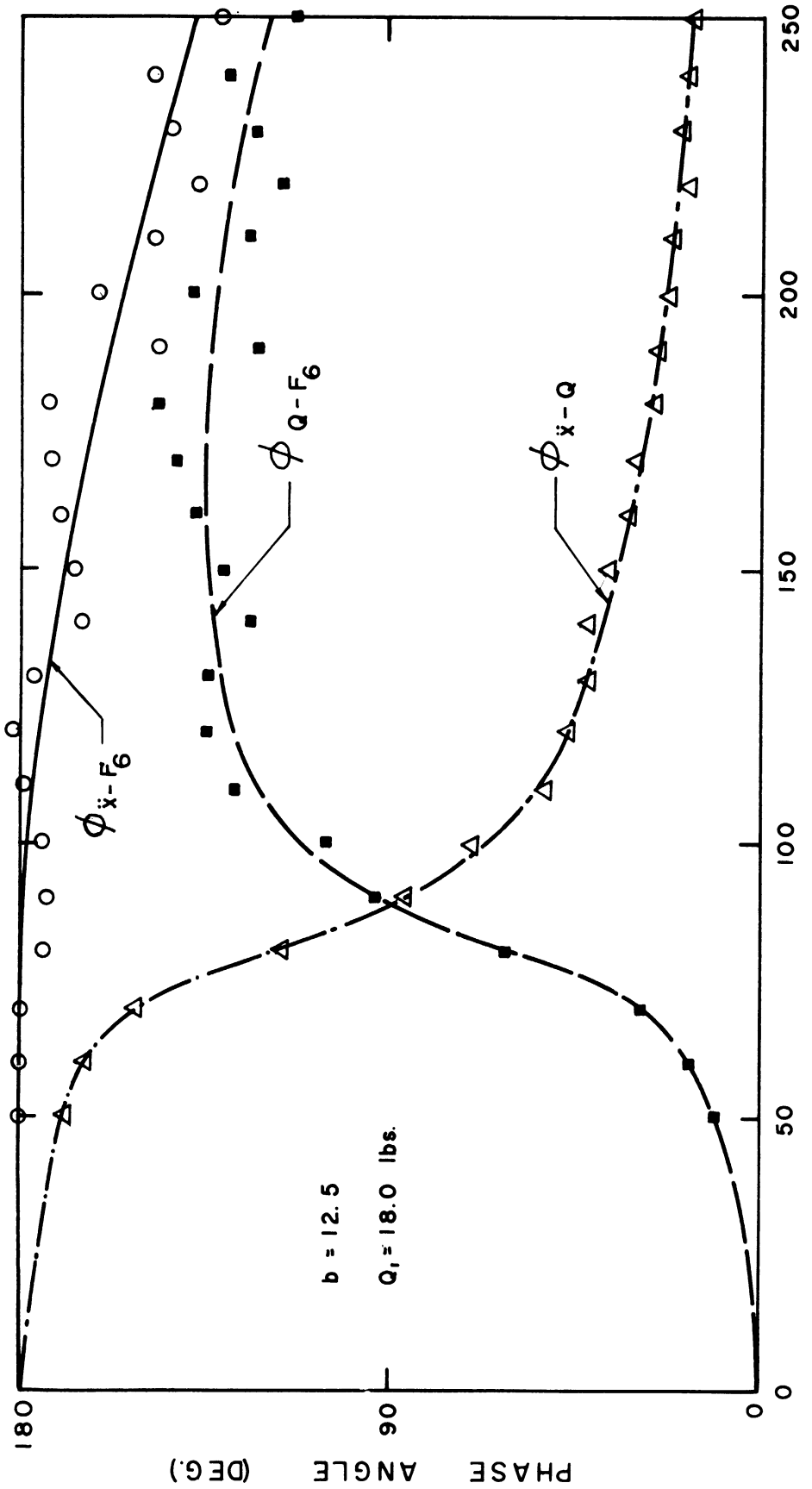

Fig. 60. Phase relations among acceleration, input force, and the force on center ring as a function of frequency.

in which R_6 is the reaction force on the center ring having the amplitude of $\overline{R}_6$, R_j is the force on each of the five outer rings having the amplitude of $\overline{R}_j$ and $\phi_{R_6-R_j}$ is the phase shift between R_6 and R_j. The variation of these reaction forces with time is illustrated in Fig. 61. The curves shown are based on the test results for the system having a mass ratio of 12.5. Figure 61(a) shows the variation of reaction forces at a low frequency, and Fig. 61(b) is for a higher frequency. It should be reminded that these curves are not what one observes on the oscilloscope, but are the combination of forces recorded on the oscilloscope and the inertia force of the ring. Note in the figure that the curve for the center ring is taken, for convenience, as a reference line ($R_6 = 0$, when $\omega t = 0$) to plot the curves for the outer rings. It can be seen clearly from this figure that the distribution of dynamic pressure beneath the footing varies not only with frequency of oscillation but also with time at a specified frequency.

VARIATION OF PRESSURE DISTRIBUTION WITH TIME AND FREQUENCY

The variation of dynamic pressure distribution with time is shown in Figs. 62 and 63. The curves in these figures were obtained from Fig. 61 by plotting the reaction force magnitude of each ring (ordinate) at a specific time (actually ωt, which is the angle of rotation in radians). The variation of pressure is shown for a complete cycle of alternation at an interval of $\pi/4$ radians. Also shown are the envelope of maximum pressures at the base of each ring. It should be noted here that the

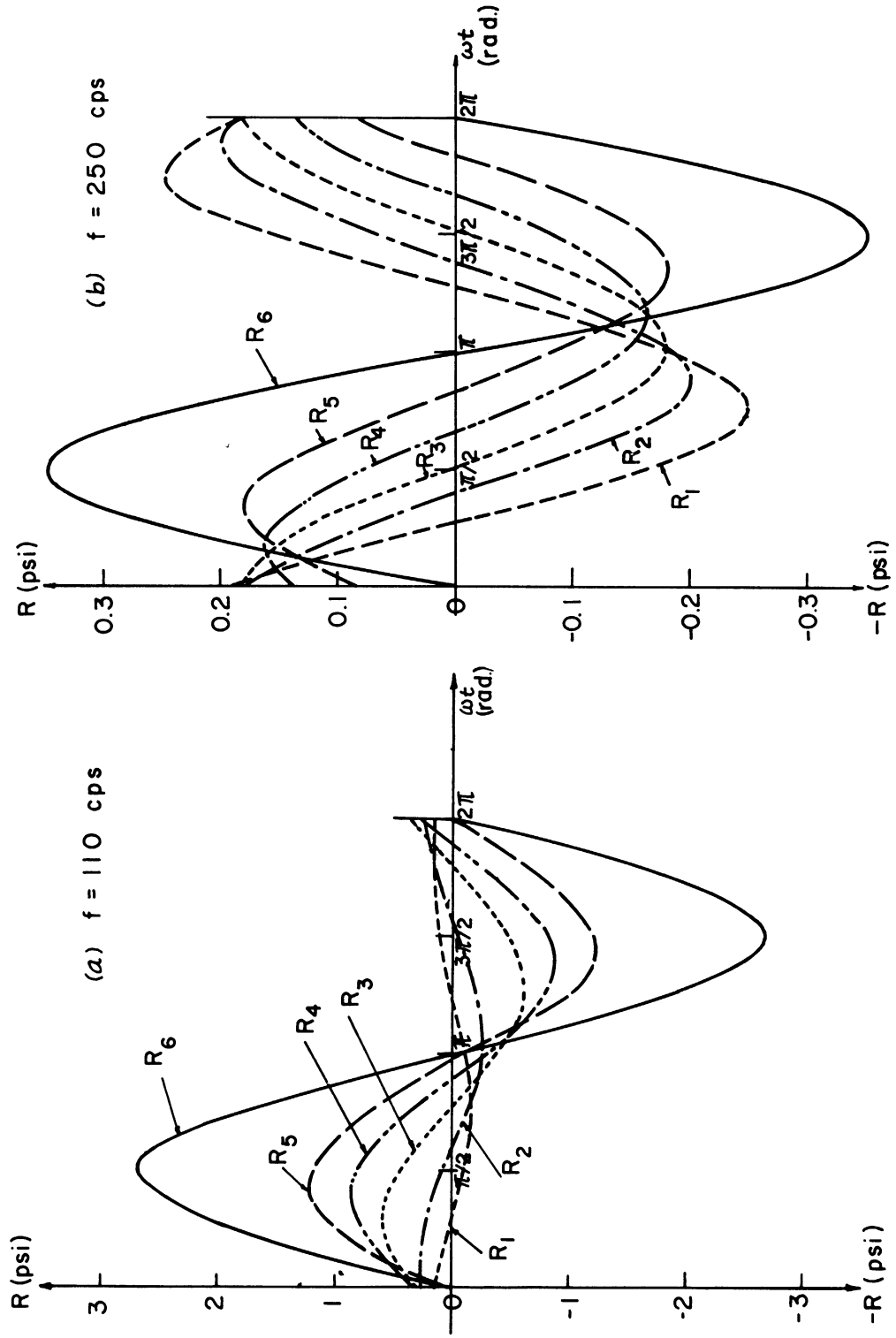

Fig. 61. Variation of soil reaction force on each ring with time.

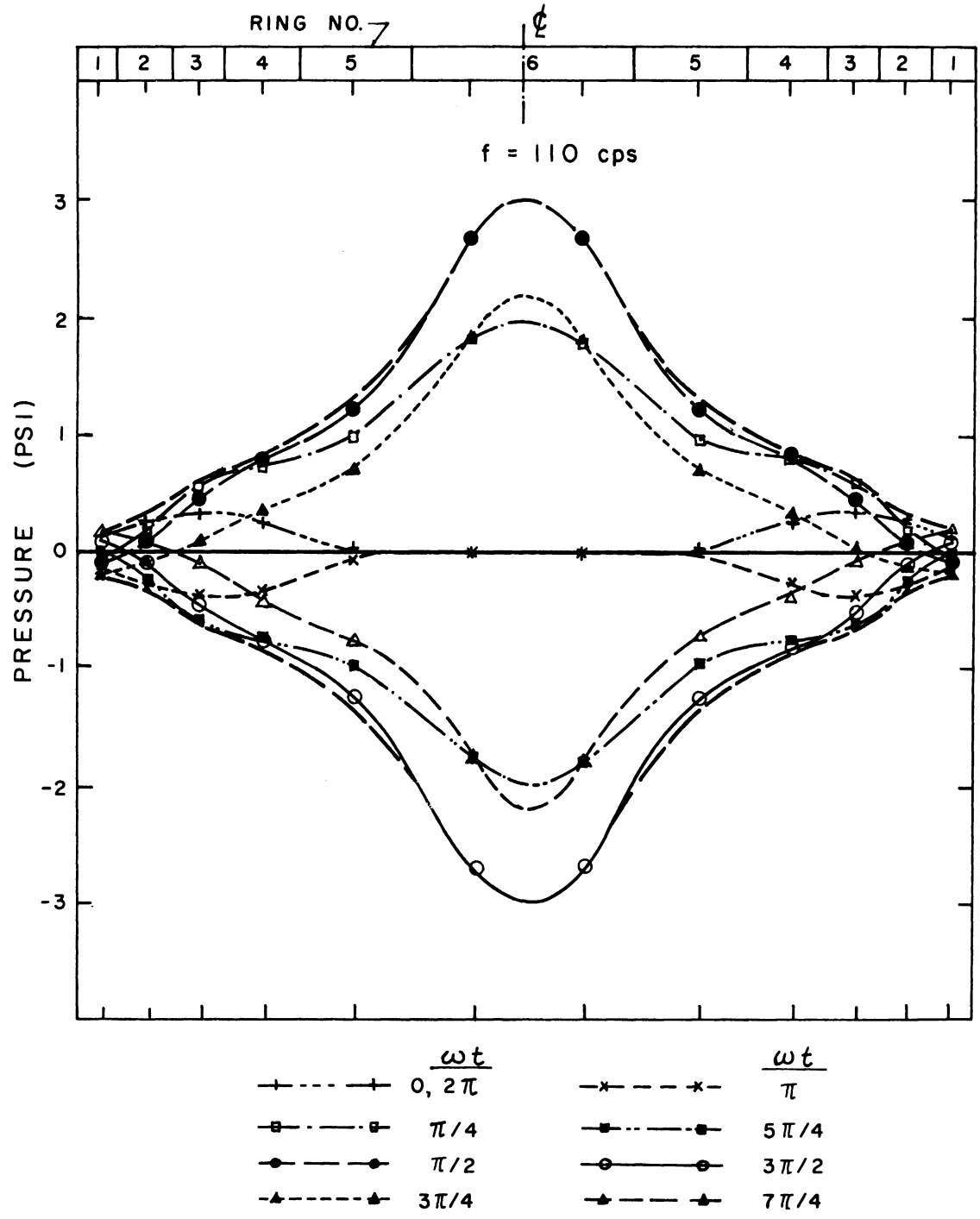

Fig. 62. Variation of dynamic pressure distribution with time (f = 110 cps).

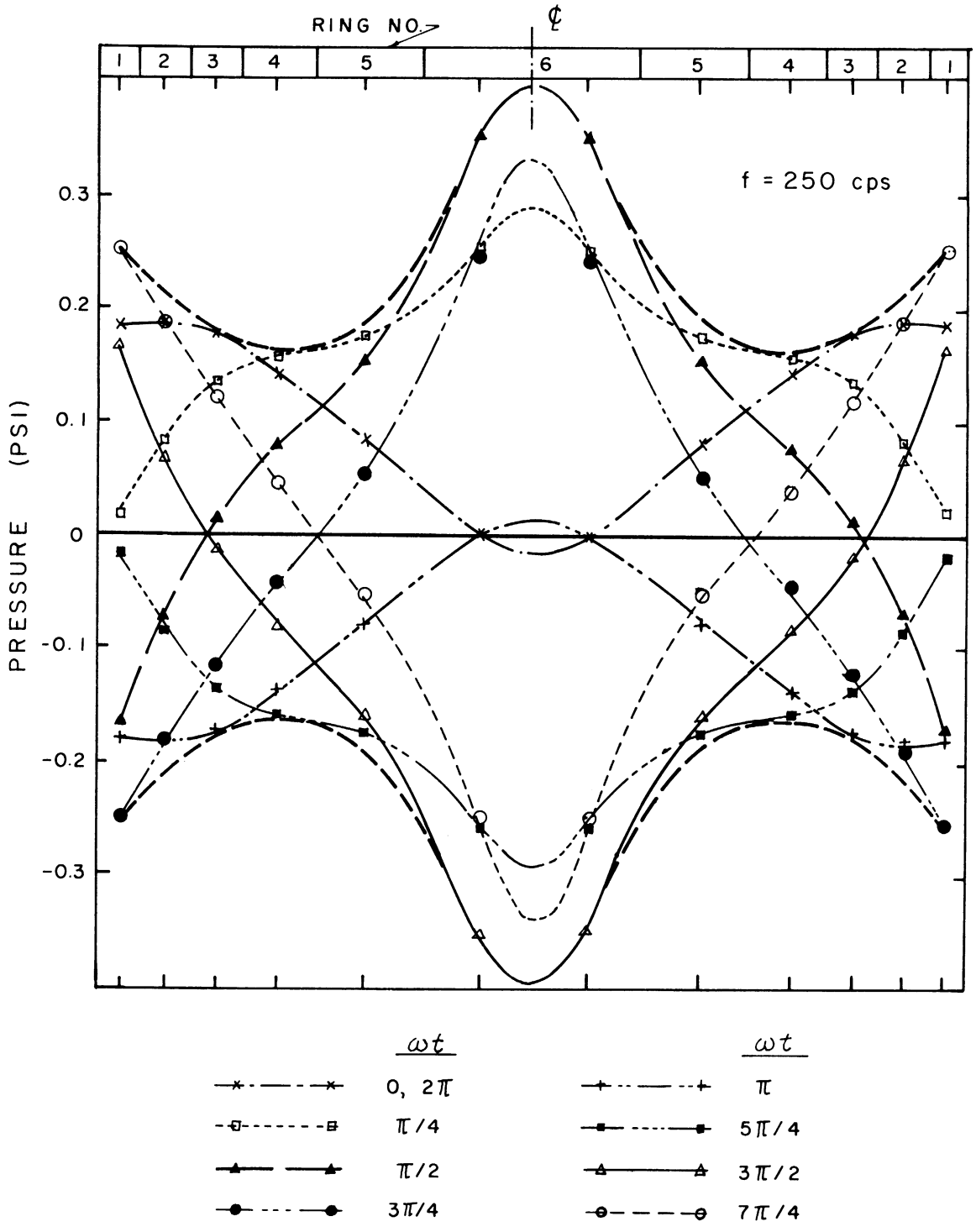

Fig. 63. Variation of dynamic pressure distribution with time (f = 250 cps).

envelope does not indicate the maximum pressure of each ring at a specific time, but is the maximum pressure that occurs at a specific frequency. One is primarily concerned with the dynamic pressure amplitudes because these are the maximum values expected to act against any point in the footing at any time under a given frequency.

It is observed that at the frequency of 110 cps the pressure distribution maintains a parabolic shape throughout the cycle, except for a very short period when the pressure at the center portion becomes zero. The pressure at the edge portion of the footing does not vary much with time, but the variation becomes greater towards the center. It may also be noted that points on the footing, except at the edges, are subjected to the reaction force of the same sign at a specific time.

The pressure distribution at a higher frequency presents quite a different picture, however. As shown in Fig. 63 the shape of the pressure distribution curves varies between that of parabolic to that produced by a rigid base. It is also of interest to note that points on the footing are subjected to the reaction forces of opposite signs at a given time in contrast to what was observed with the frequency of 110 cps. This is due to the fact that as the frequency is increased the length of the elastic wave in the soil becomes shorter [Eq. (21)], resulting in greater changes in phase angles. A change in the direction of acting force is brought upon when the radius of the footing exceeds the wavelength that travels beneath the footing. It may also be noted in this figure that the pressure amplitude curve (envelope connecting the

points of maximum pressure) has a distinctly different shape from that of Fig. 62, that is to say, that the distribution of maximum pressure is changed from parabolic type to a uniform or nearly a rigid base type as the oscillation frequency is increased.

EFFECT OF THE FREQUENCY OF OSCILLATION

Figures 64-68 show the results for the distribution of dynamic pressure amplitude calculated by the IBM computer program, using experimental data on the seven test systems. In these figures the variation of pressure amplitude with excitation frequency, magnitude of input force, and mass ratio is shown. It should be noted again that the pressures shown in these charts are the maximum pressures under each ring computed from the measured force amplitudes, and thus do not necessarily represent the actual pressure distribution at any particular instant because the force vectors on each ring are not acting in phase, and are time-dependent.

Figure 64 shows the variation of dynamic pressure amplitude under the footing as a function of excitation frequency. The results shown in this figure are for the system with a mass ratio of 12.5, and subjected to a constant input force of 18.0 lb. Curves similar in character to Fig. 64 were obtained with other systems having different mass ratios. In these tests the excitation frequency was varied up to 250 cps with an increment of 10 cps, except at the region of resonant frequency where the pressure measurements were taken at a smaller interval. In this chart are shown, however, only those pressure distributions obtained at

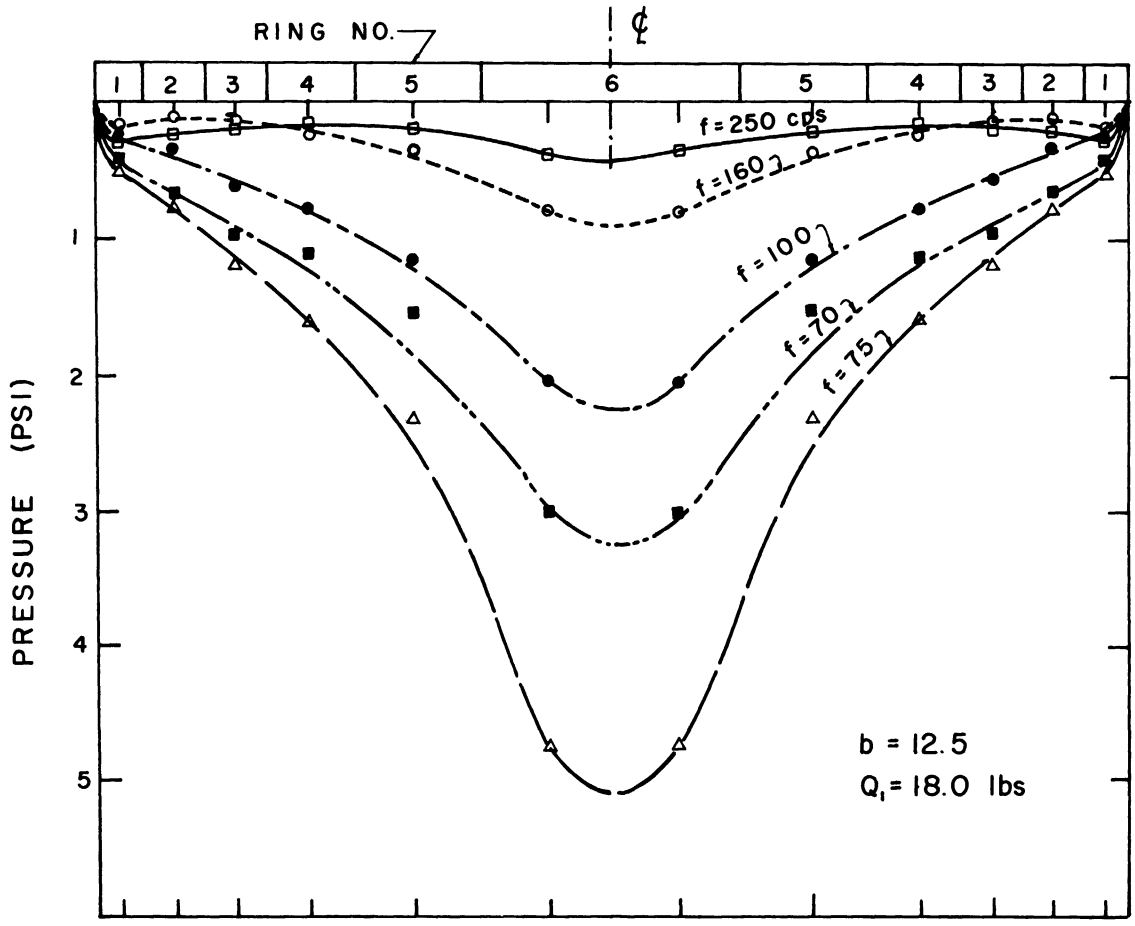

Fig. 64. Variation of dynamic pressure amplitude with frequency (constant input force).

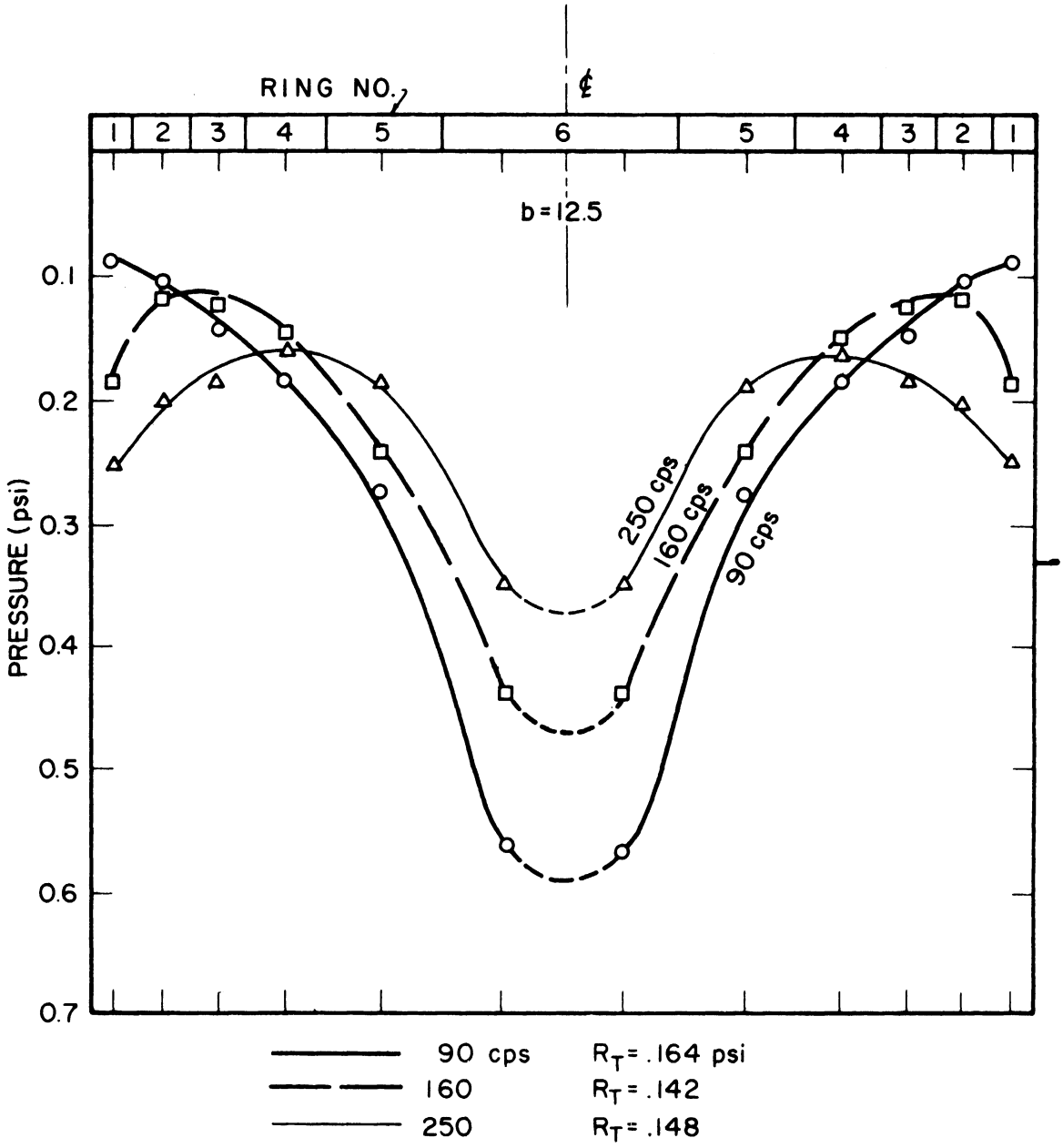

Fig. 65. Variation of dynamic pressure amplitude with frequency (constant total soil reaction).

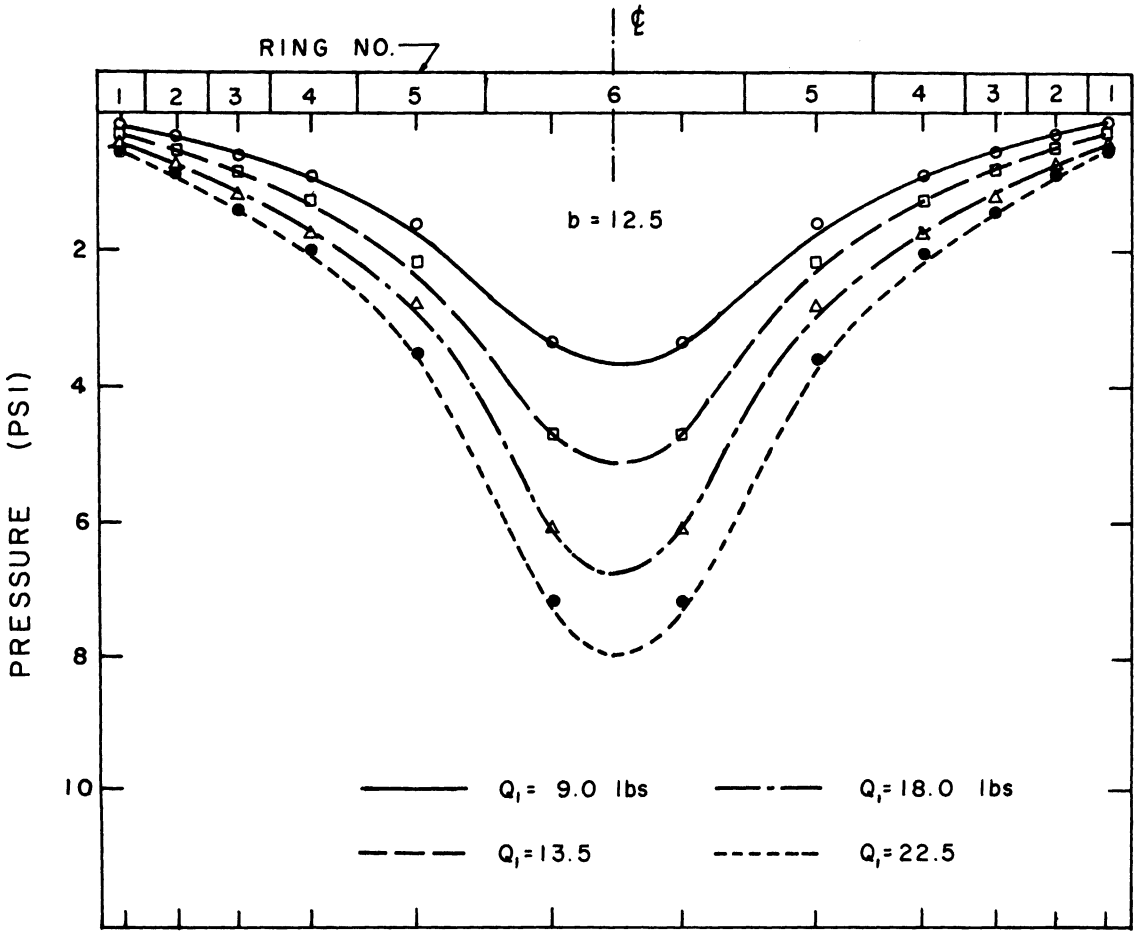

Fig. 66. Variation of dynamic pressure amplitude with input force.

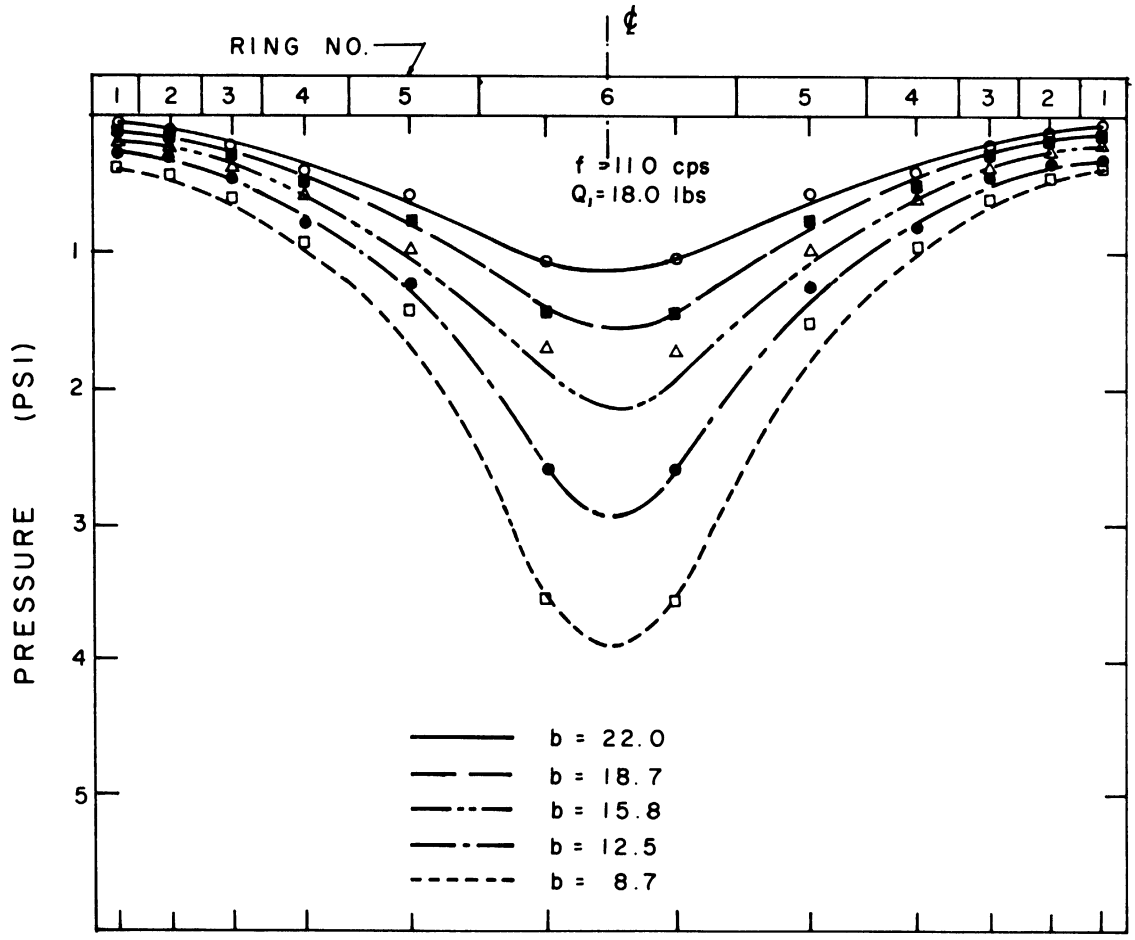

Fig. 67. Variation of dynamic pressure amplitude with mass ratio (f = 110 cps).

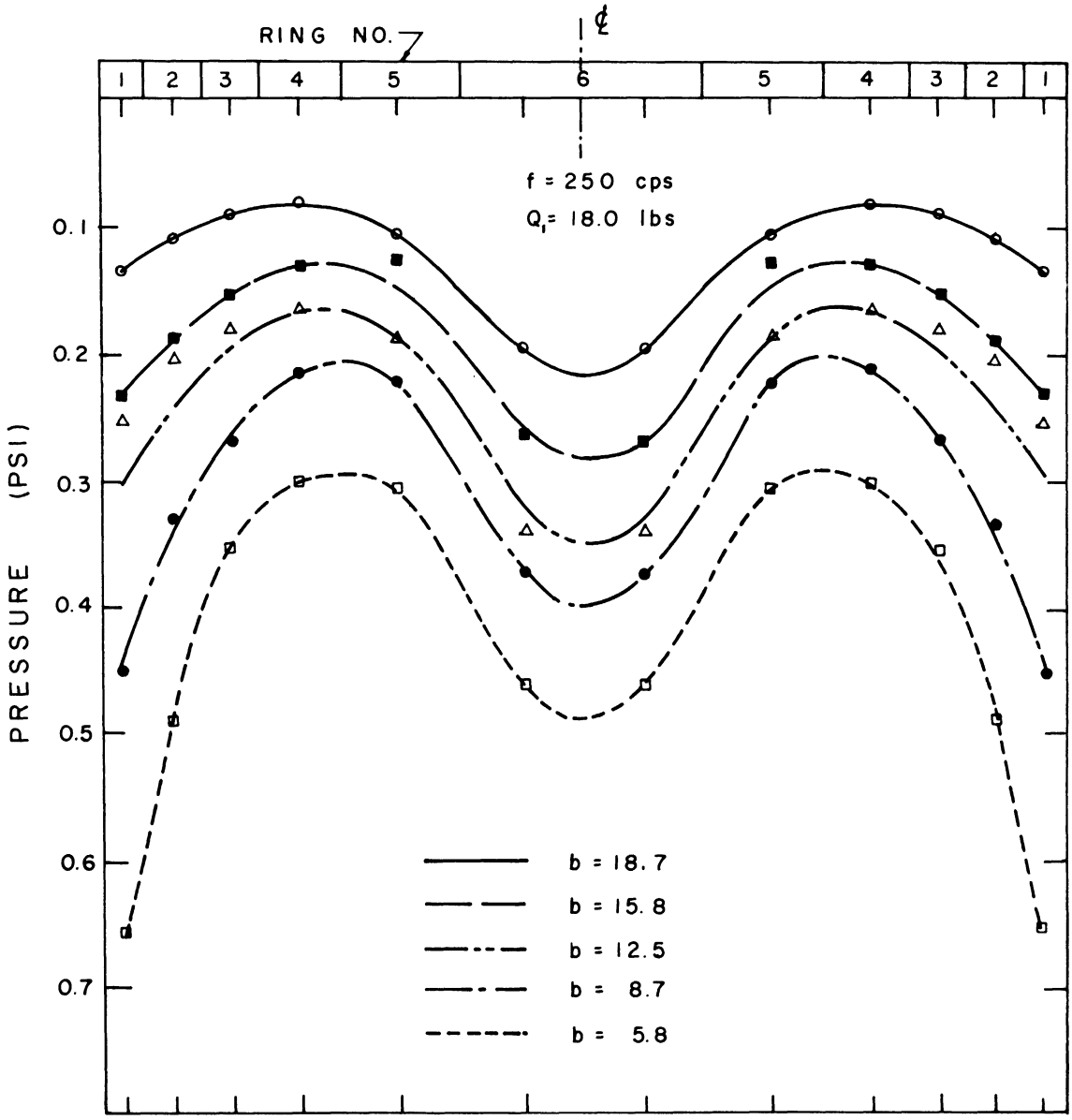

Fig. 68. Variation of dynamic pressure amplitude with mass ratio (f = 250 cps).

several frequencies chosen for the purpose of presentation.

Whereas the curves in Fig. 64 show the variation at a constant input force, those in Fig. 65 demonstrate the variation of pressure amplitudes at a constant total soil reaction. Tests were run under several combinations of input force and frequency to produce a constant total soil reaction, and the distribution of maximum pressure at this constant force was obtained as shown in Fig. 65. It can be seen again that the dynamic pressure amplitudes are dependent upon the frequency of oscillation: as the frequency is increased the pressure appears to shift towards the edge, changing the shape of the pressure curve from a parabolic type to uniform, then to that corresponding to rigid base.

The significant effects of excitation frequency on the dynamic pressure distribution has been clearly demonstrated in the test results shown and the analyses thereof. The variation of dynamic pressure due to a change in frequency is a consequence of the change in amplitude and phase relations between the reaction pressures on each ring, caused by a change in the wave velocity travelling in the soil. Thus the dynamic soil pressure against the footing is a function of the velocity of the footing moving into the soil (rate of loading) and the velocity of the eleastic waves in the soil which dissipate this input energy.

EFFECT OF THE MAGNITUDE OF INPUT FORCE

In Fig. 66 are presented a set of test results on the same system (b = 12.5) to show how the pressure amplitude is affected by varying the

magnitude of constant input force. The input forces used for the tests were 9.0, 13.5, 18.0 and 22.5 lb. The pressure amplitudes shown in this figure were the greatest pressure magnitudes obtained within the range of test frequency under each input force. It may be noted that the ratio of the maximum pressure at the center to the average pressure over the entire footing becomes greater with increasing magnitude of the input force. This implies that the pressure tends to become more concentrated towards the center as the intensity of applied pressure is increased. The pressure curves shown in Fig. 66 represent those observed at the low frequency range where the distribution characteristics are definitely of parabolic, and within the range of input force tested there was no shifting of pressure towards the edge with decreasing magnitude of input force.

The effect of applied pressure on the pressure distribution may be studied by varying the total soil reaction at a constant frequency. From the curves shown for the frequency of 160 cps in Figs. 64 and 65, one can observe that the pressure is shifted towards the center as the total soil reaction is increased from 0.142 to 0.228. It is presumed that should the total soil reaction be decreased further, the pressure distribution shown in Fig. 65 would assume a near uniform type of pressure distribution.

It may be stated in conclusion that the effect of an increased intensity of the applied pressure is to shift the reaction pressure towards the center portion of the footing, and depending upon the intensity and

excitation frequency, the shift of pressure causes a change in the pressure distribution curve between that of parabolic and rigid base type. This conclusion is restricted to the case for footings resting on the surface of a sand bed.

EFFECT OF MASS RATIO

In order to compare the pressure amplitudes obtained for various mass ratios at a given excitation frequency, Figs. 67 and 68 have been prepared. Figure 67 shows how the distribution of pressure amplitudes is changed with varying mass ratio at the frequency of 110 cps under a constant force input. Another set of results to show the same effect at a higher frequency (f = 250 cps) is presented in Fig. 68. It may be noted in these charts that the shape of pressure distribution curves are quite different from each other. These two charts, therefore, also demonstrate again the variation of pressure amplitudes with the excitation frequency.

It is observed that the soil pressure amplitude under each ring increases as the mass ratio is decreased at a given test frequency and input force. This is true regardless of the type of pressure distribution. It is of interest to note, however, that with parabolic pressure distribution the variation of pressure amplitude becomes greater towards the center, whereas with rigid type pressure distribution greater changes take place in the edge portion of the footing. The inverse proportionality between the soil reaction and the mass ratio may be explained by

the fact that with smaller mass ratio the phase difference between the applied force on each ring and displacement becomes smaller (Figs. 56 and 57), while the force of acceleration becomes greater (Fig. 10). It should be noted, however, this inverse proportionality between the mass ratio and soil reaction exists at frequencies beyond the range of resonant frequencies for the systems tested.

TOTAL SOIL REACTION BENEATH THE FOOTING

As described in Chapter III the total soil reaction (R_T) acting on the footing is the vectorial sum of the reaction force (R_j) acting on each ring [Eq. (56)]. Figure 69 presents the results of computations for the soil reaction at the base of each ring at various test frequencies for a chosen value of mass ratio. The total soil reaction beneath the footing also varies with both frequency and mass ratio, and the effects of the two factors are shown in Fig. 70. This figure presents the test results of all the seven test systems employed. Note that in this figure the total soil reaction is plotted as a function of excitation frequency for each of the seven different mass ratios.

It may be observed that the maximum pressure amplitudes and the total soil reaction occur approximately at the frequency for maximum amplitude (displacement). Two small peaks are shown to appear at frequencies of 105 and 145 cps. A possible explanation for these peaks is that modes of vibration of the loading frame members have interfered with the footing-soil system as previously explained with the amplitude-

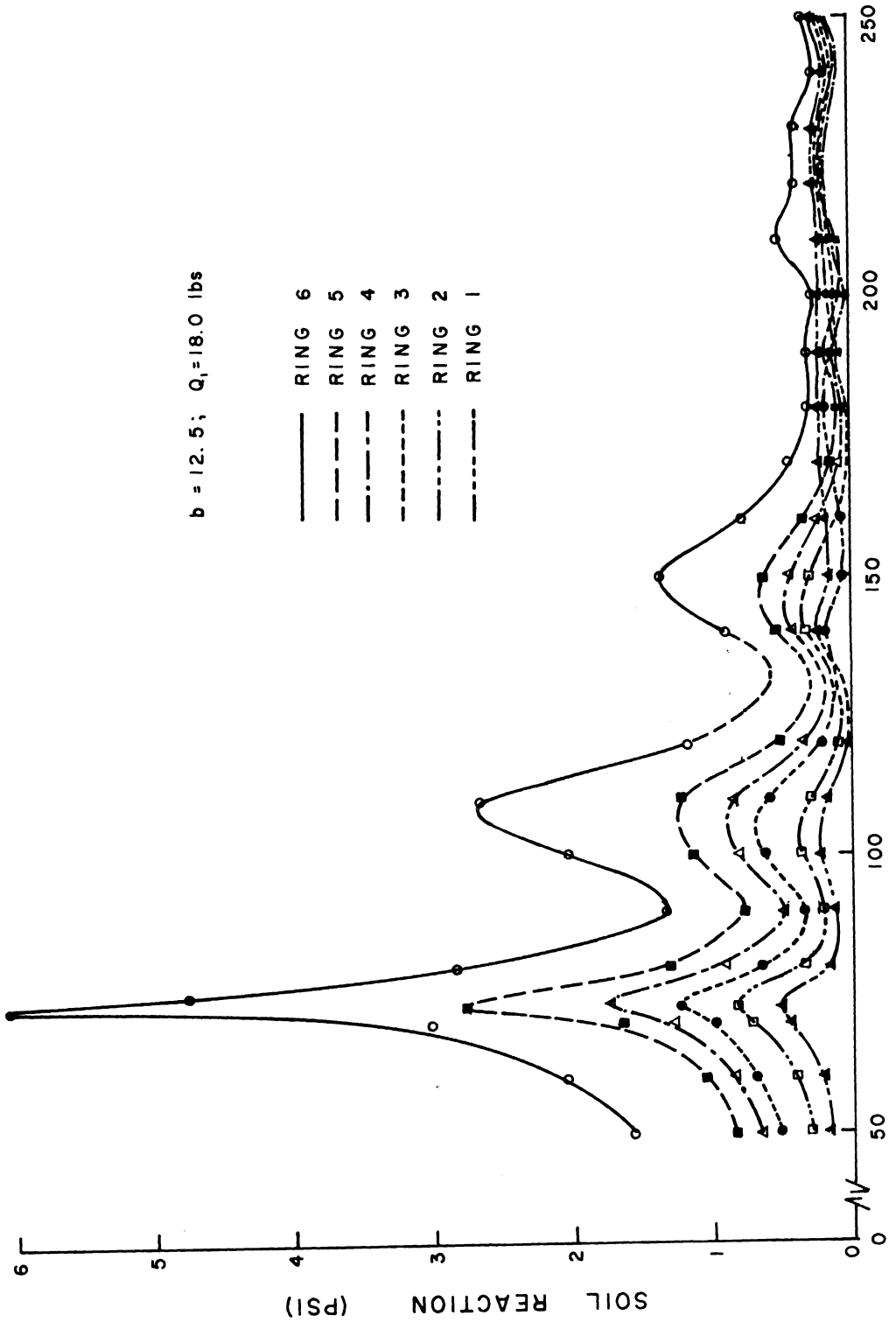

Fig. 69. Variation of soil reaction force under each ring with frequency.

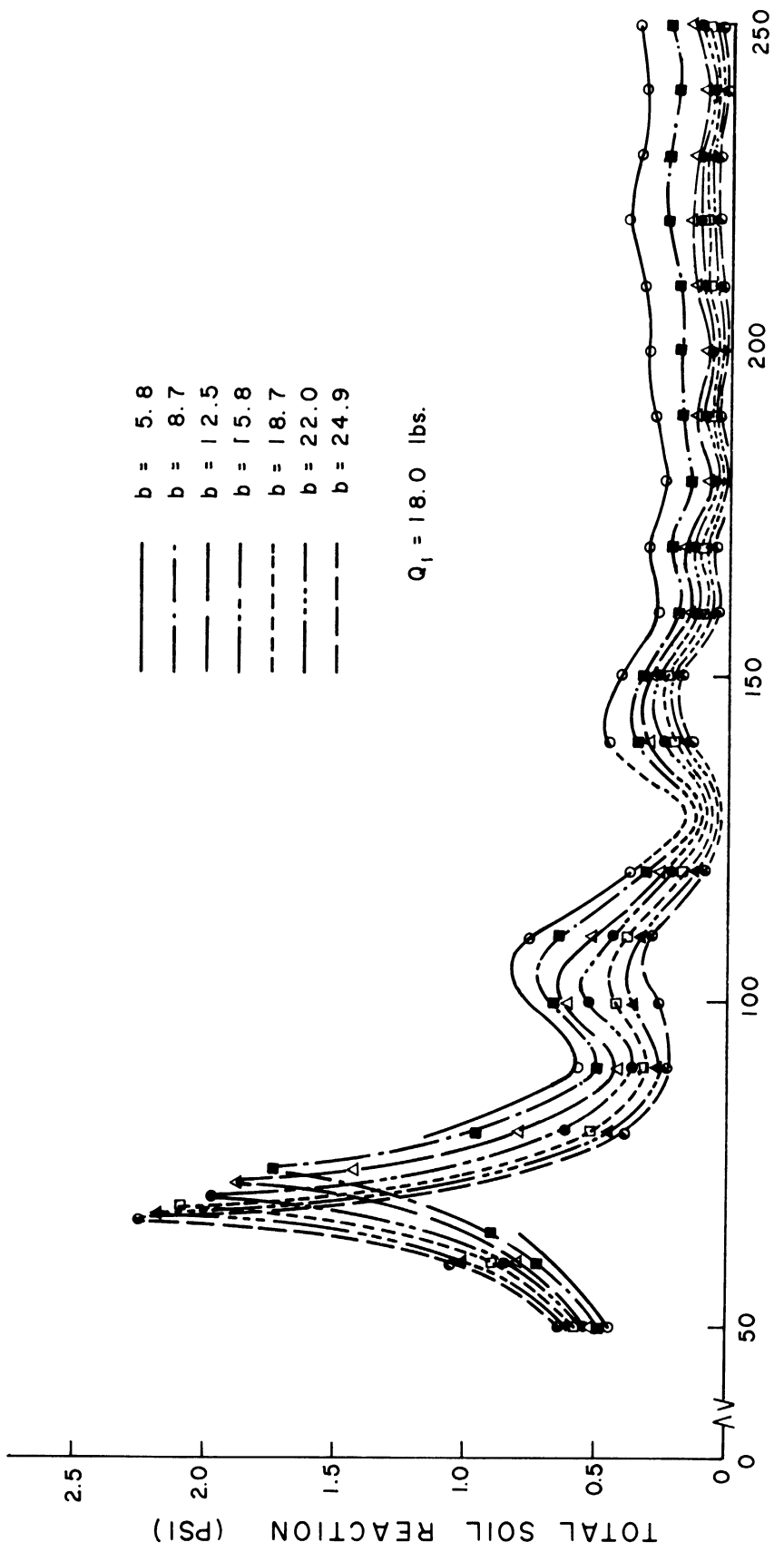

Fig. 70. Variation of total soil reaction under footing with frequency for various mass ratio.

frequency curve in Fig. 47. The two peaks shown in Fig. 70 are comparable to those of Fig. 47 as far as the frequencies are concerned. A check was made to see whether this was possibly due to the reflection of elastic waves by the sand bin, but no such evidence was found to exist.

Figure 69 also shows how the pressure distribution is affected by the frequency of oscillation. It may be noted that the distribution of pressure amplitude is of parabolic type up to the frequency of about 130 cps. As the frequency is increased further the pressure is shifted towards the edge, forming uniform or approximately rigid base type pressure distribution.

Comparing the curves of Fig. 70 with those of Fig. 47, one may note that the curves for the total soil reaction have the same pattern as those of the amplitude-frequency obtained under constant amplitude of force oscillations. It may be stated, therefore, that the total soil reaction acting under the footing is directly proportional to the acceleration. This was theoretically indicated in Eq. (17). It can be seen from this equation that if the mass of the footing m_o and the input force Q are held constant, the reaction R becomes a direct function of acceleration $\ddot{x}$.

Figure 71 shows the effect of excitation frequency on the phase relations among the total soil reaction, the input force, and the displacement. This represents the results of tests under a specific test

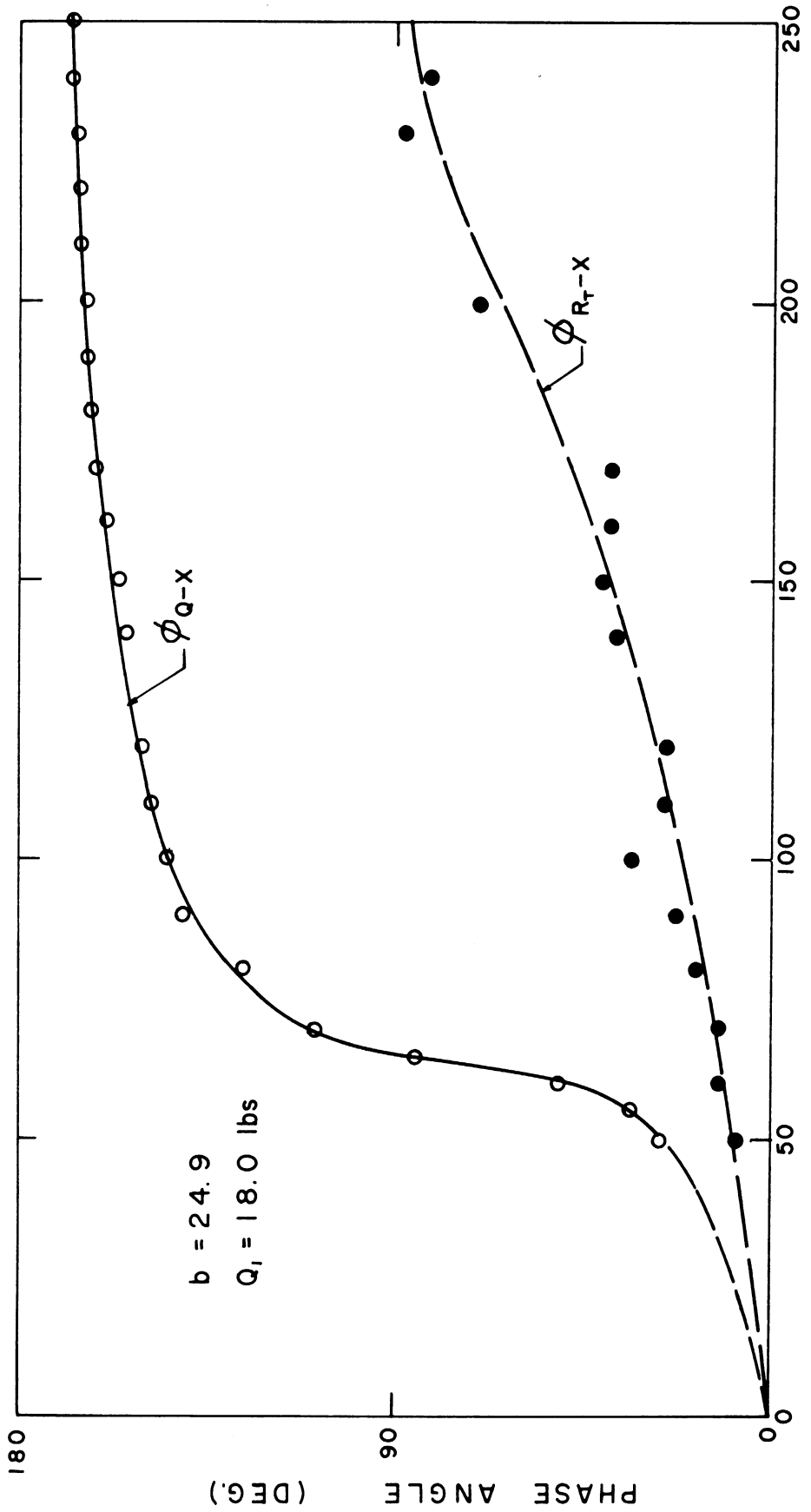

Fig. 71. Phase relations among the total soil reaction, input force, and displacement (b = 24.9).

condition. The variation of phase angle between the total soil reaction and displacement ($\phi_{R_T\text{-}X}$) with frequency is shown in another form in Fig. 72. Since $\phi_{R_T\text{-}X}$ is independent of mass ratio and depends only on the frequency factor, all the results from the seven test systems are plotted on the same chart. The theoretical curves shown in this figure for the three types of pressure distribution are based on the displacement function values determined by Sung.

It is interesting to note in Fig. 71 that while the phase shift between the input force and displacement ($\phi_{Q\text{-}X}$) increases radically at the resonant frequency, and approaches 180 degrees as the frequency is further increased, the phase shift between the total soil reaction and the displacement increases gradually to approach 90 degrees as the frequency is increased.

The purpose of presenting Fig. 72 is not merely to compare the experimental results for the phase shift $\phi_{R_T\text{-}X}$ with the theoretical values for any particular type of pressure distribution. Its purpose is, rather, to demonstrate the effect of excitation frequency and the type of pressure distribution on the phase shift $\phi_{R_T\text{-}X}$. It can be observed that the phase angle $\phi_{R_T\text{-}X}$ increases with increasing frequency; in the region of low frequency ($a_o < 0.4$) the experimental values indicate the pressure distribution to be that of parabolic, but as the frequency is increased ($0.4 < a_o < 0.7$) the theoretical curve for uniform pressure distribution appears to fit the experimental data points. In the region

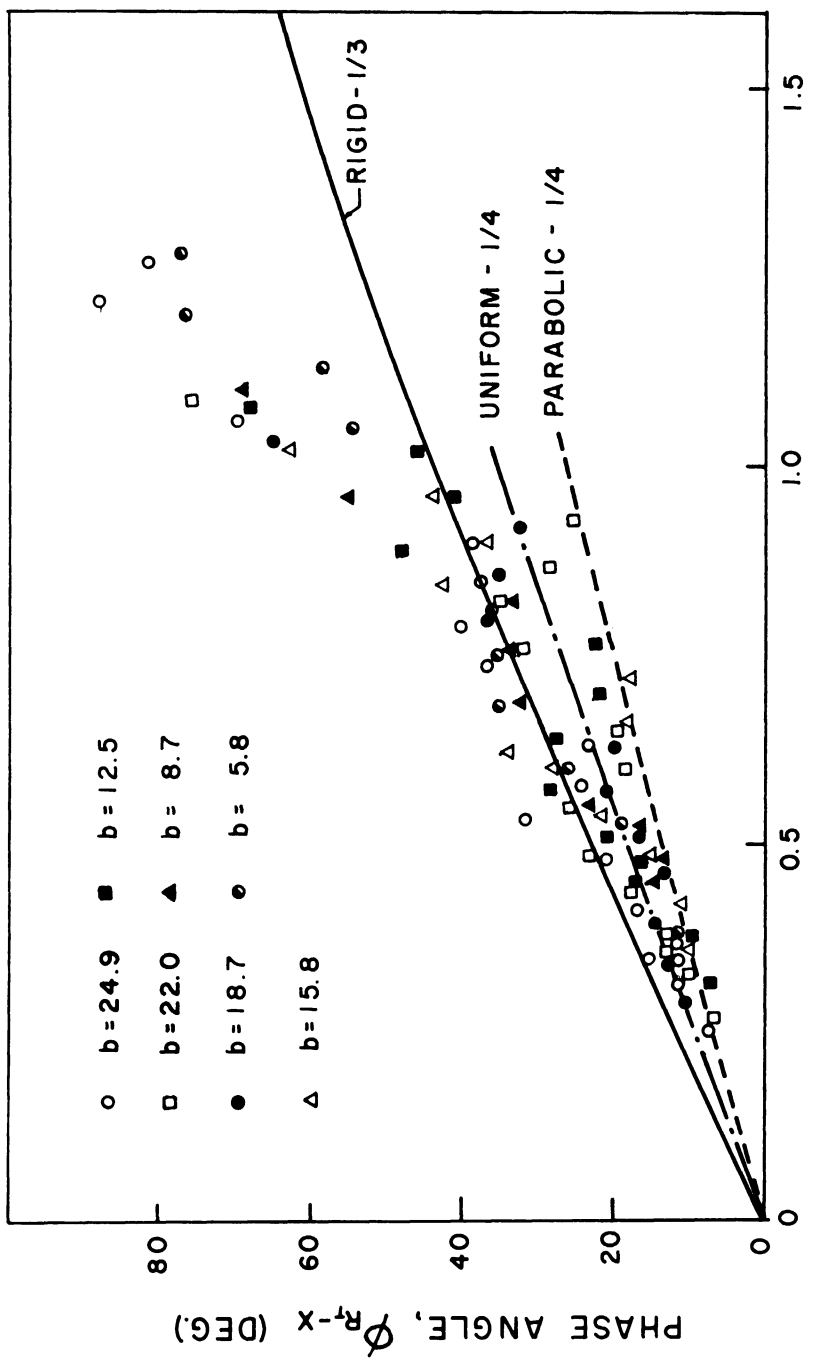

Fig. 72. Variation of phase shift between the total soil reaction and displacement with frequency factor.

of high frequency ($a_o > 0.7$) the data indicate the pressure distribution to be that of rigid base type. This confirms the findings made previously in conjunction with the experimental determination of pressure distribution at various frequencies.

One may note that there is quite a scatter of experimental data points, and beyond the region of the frequency factor greater than 1.1 the experimental points do not seem to agree with the theoretical curves. Factors responsible for this discrepancy are mainly the difficulties in measuring the phase angles, especially in the high frequency range. Furthermore, the phase shift $\phi_{R_T\text{-}X}$ is not the quantity that can be measured directly: it is a computed product of 13 measured quantities involving the measurements of six different amplitudes and seven phase angles.

A BRIEF DISCUSSION OF EXPERIMENTAL ERRORS

It may be appropriate here to discuss, as a whole, some of the reasons for inconsistency in the test results and the discrepancy between the theory and the experiment.

1. Accuracy in phase angle measurements—the experimental determination of phase angles was very difficult with the equipment used. As previously discussed on page 149 a slight error in recording the phase angle causes a great error in the final computation of the phase shift, especially in high frequency range. The use of special instrumentation is desirable for the improvement of accuracy in recording

the phase angle measurements.

2. Gradual change in the battery voltage—it was shown on page 110 that the voltage in the bridge circuit varied with time. Although carefully and often checked, there could be undetected changes in voltage, which might affect the proper calibration factor to be used. The use of a D.C. generator should eliminate this problem.

3. Interference of loading frame with the dynamic response of the footing-soil system as previously discussed in detail on page 112.

4. Uniform test condition of the soil surface—efforts were made to maintain uniform test condition of the soil surface for every test series; uniformity was not checked from test to test within a series, however.

5. Shear wave velocity values used for theoretical curves—although the word "theoretical" was used, the shear wave velocity values used to determine the shear modulus and frequency factor were based on an empirical curve (Fig. 25) obtained in a previous research.

6. The material used (sand) is not an ideally elastic, homogeneous, isotropic semi-infinite medium, on which the theoretical analysis is based.

Displacement Functions

The test results obtained for the displacements, and the phase shifts between the input force and the displacement were used in determining the

experimental values of the displacement functions. Figures 73-79 show the results for the displacement functions calculated through the computer program for the seven test systems employed. Since the displacement functions are dependent only upon the frequency of excitation for a particular footing-soil system, the function f_1 and f_2 are plotted as a function of frequency factor. Also shown in these charts are the theoretical curves computed on the assumption of rigid base pressure distribution and Poisson's ratio of one third.

The displacement function for the case of $a_o = 0$, which corresponds to static loading, can be determined if the static displacement is known. Since the function f_1 is zero when $a_o = 0$, the expression for displacement X defined in Eq. (30) becomes

$$X = \frac{Q_1}{G r_o} f_1 \quad for \quad a_o = 0 \tag{68}$$

and by this equation the function f_1 for the case of static loading can easily be computed. This also provides a good means of checking the theoretical computation. The vertical displacement of a footing resting on an elastic half-space and subjected to three types of loading may be expressed (from the theory of elasticity) as:

$$X = \begin{cases} -\frac{(1-\mu)}{4} \frac{Q_1}{G r_o} & \text{for rigid base} \\ -\frac{(1-\mu)}{\pi} \frac{Q_1}{G r_o} & \text{for uniform loading} \\ -\frac{4(1-\mu)}{3\pi} \frac{Q_1}{G r_o} & \text{for parabolic loading} \end{cases} \tag{69}$$

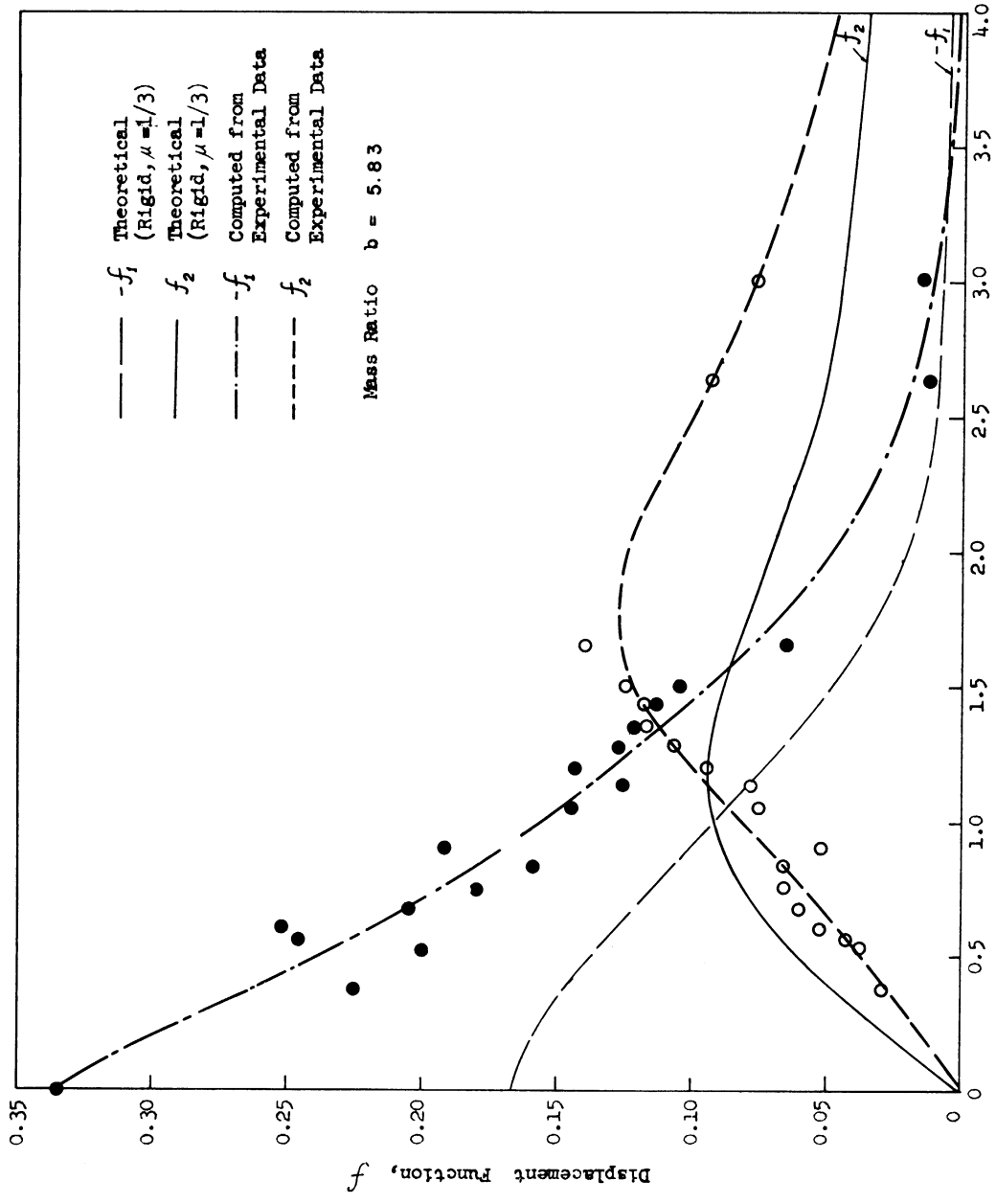

Fig. 73. Displacement functions computed from experimental data for mass ratio of 5.83.

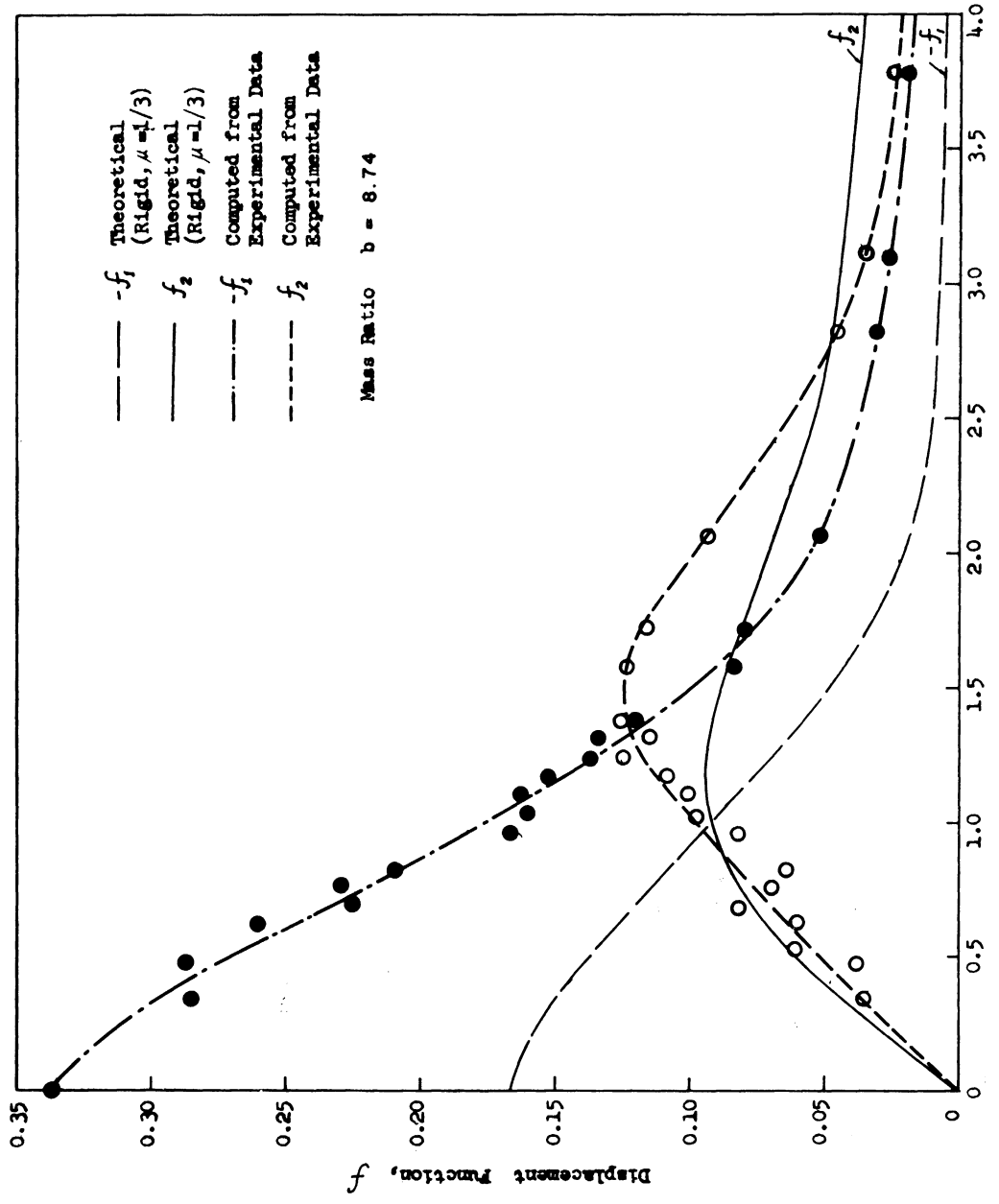

Fig. 74. Displacement functions computed from experimental data for mass ratio of 8.74.

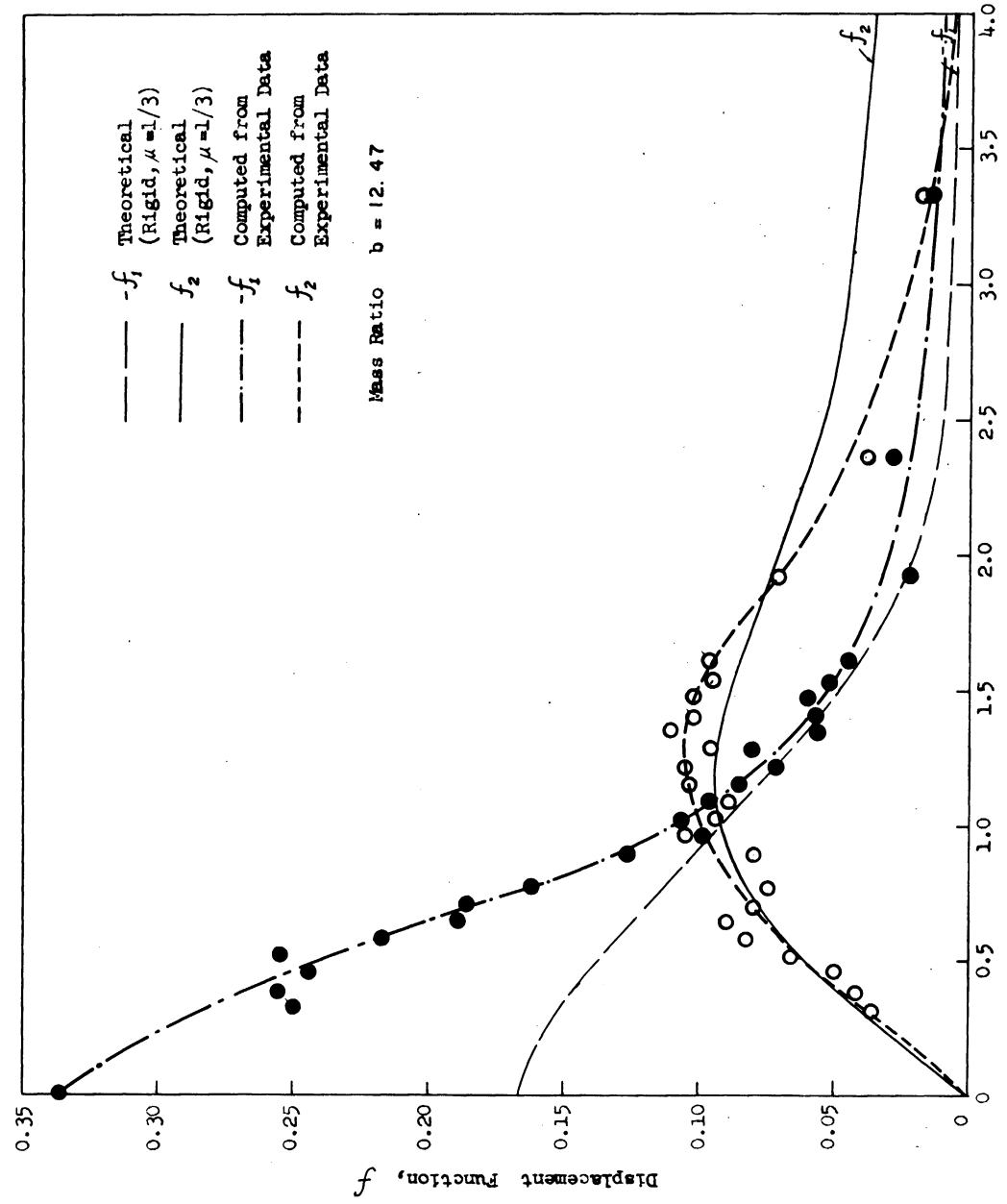

Fig. 75. Displacement functions computed from experimental data for mass ratio of 12.47.

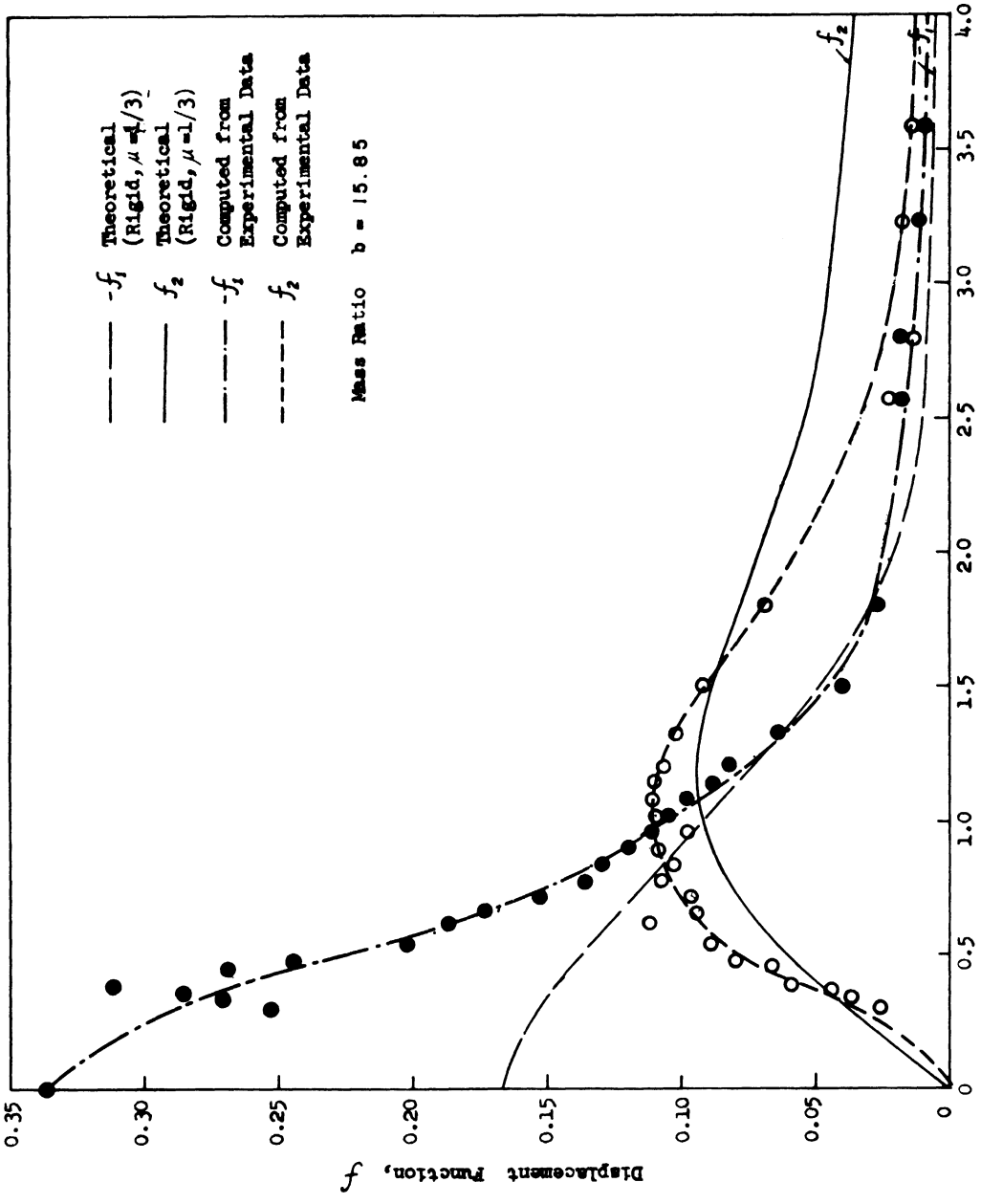

Fig. 76. Displacement functions computed from experimental data for mass ratio of 15.85.

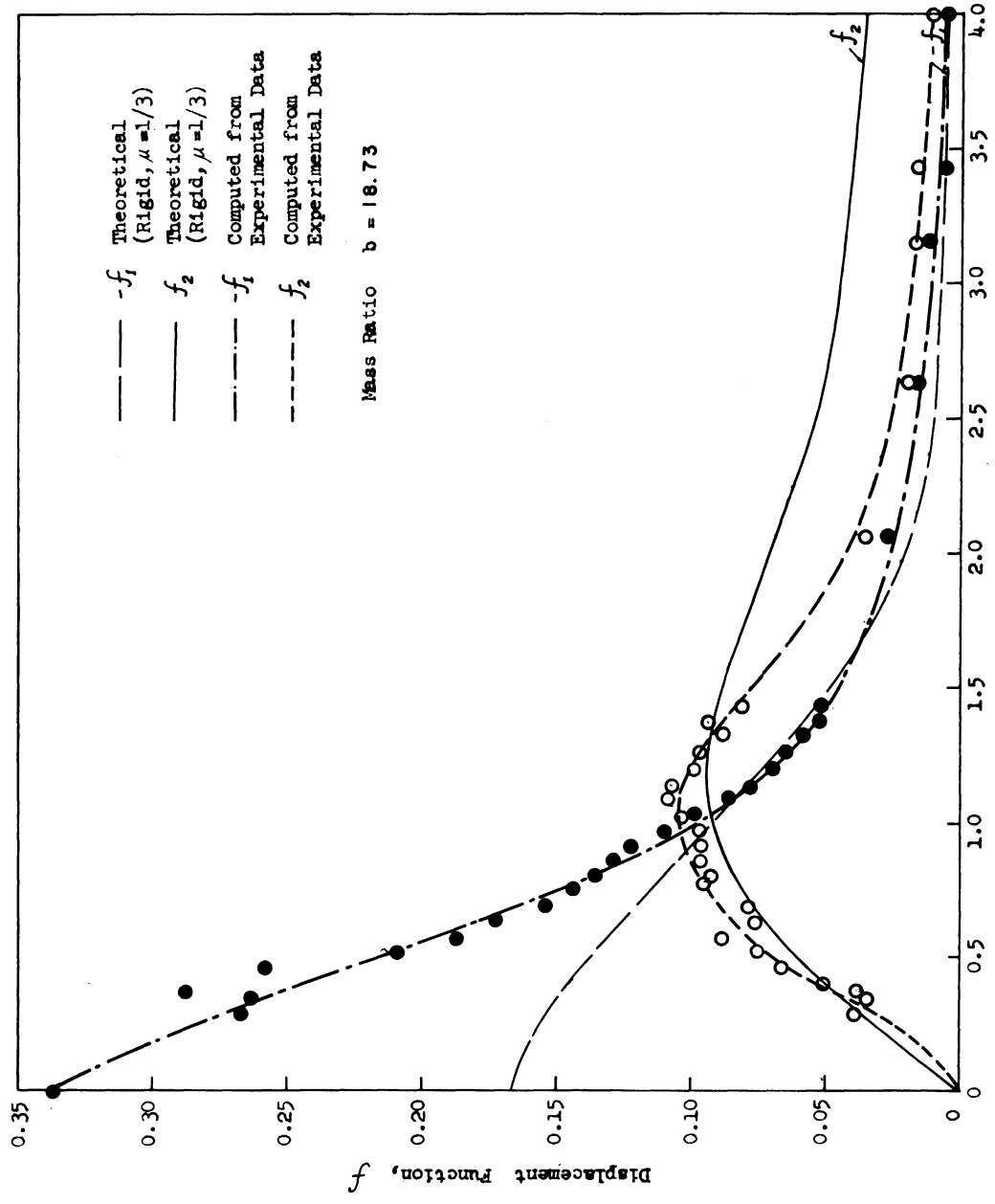

Fig. 77. Displacement functions computed from experimental data for mass ratio of 18.73.

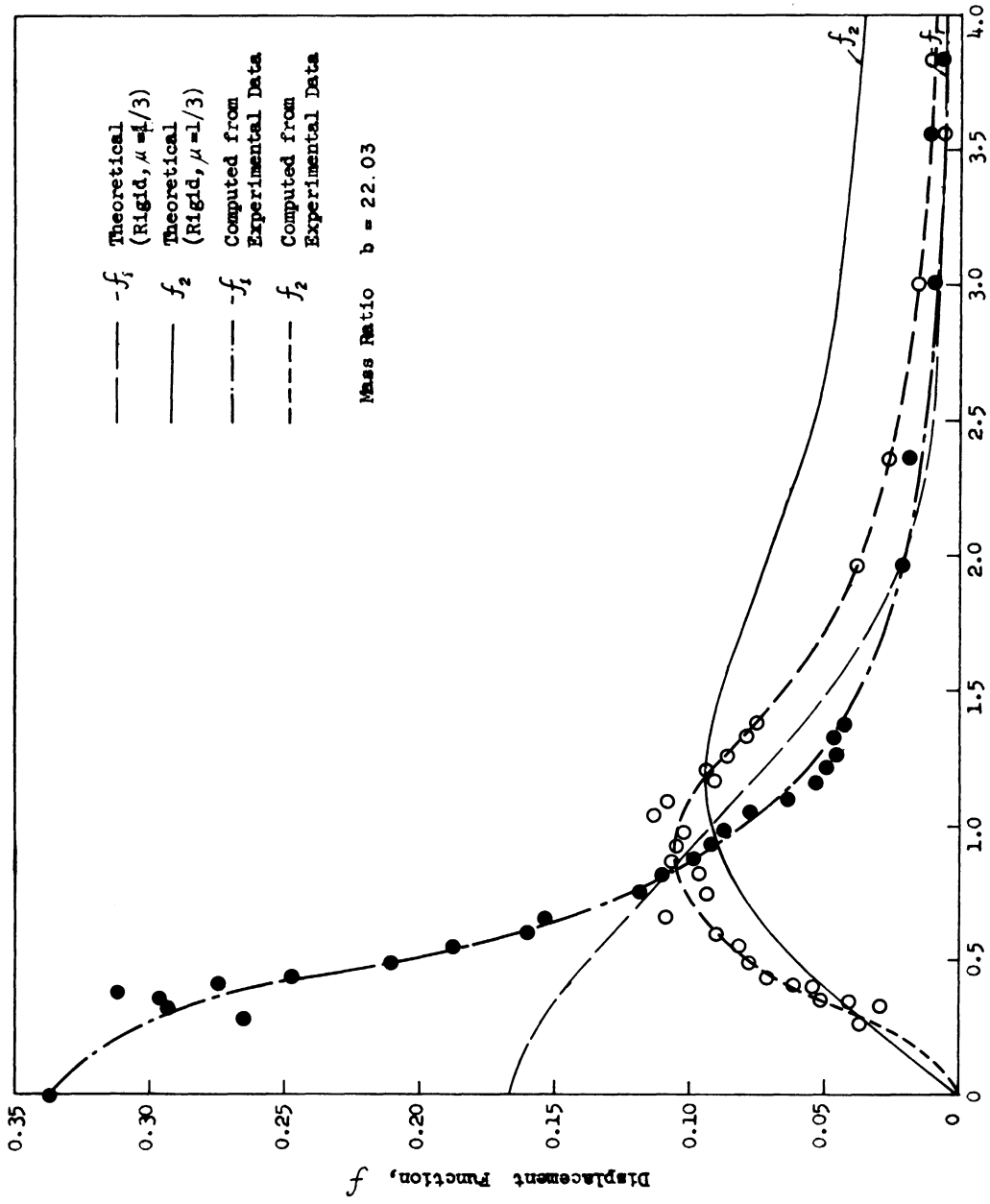

Fig. 78. Displacement functions computed from experimental data for mass ratio of 22.03.

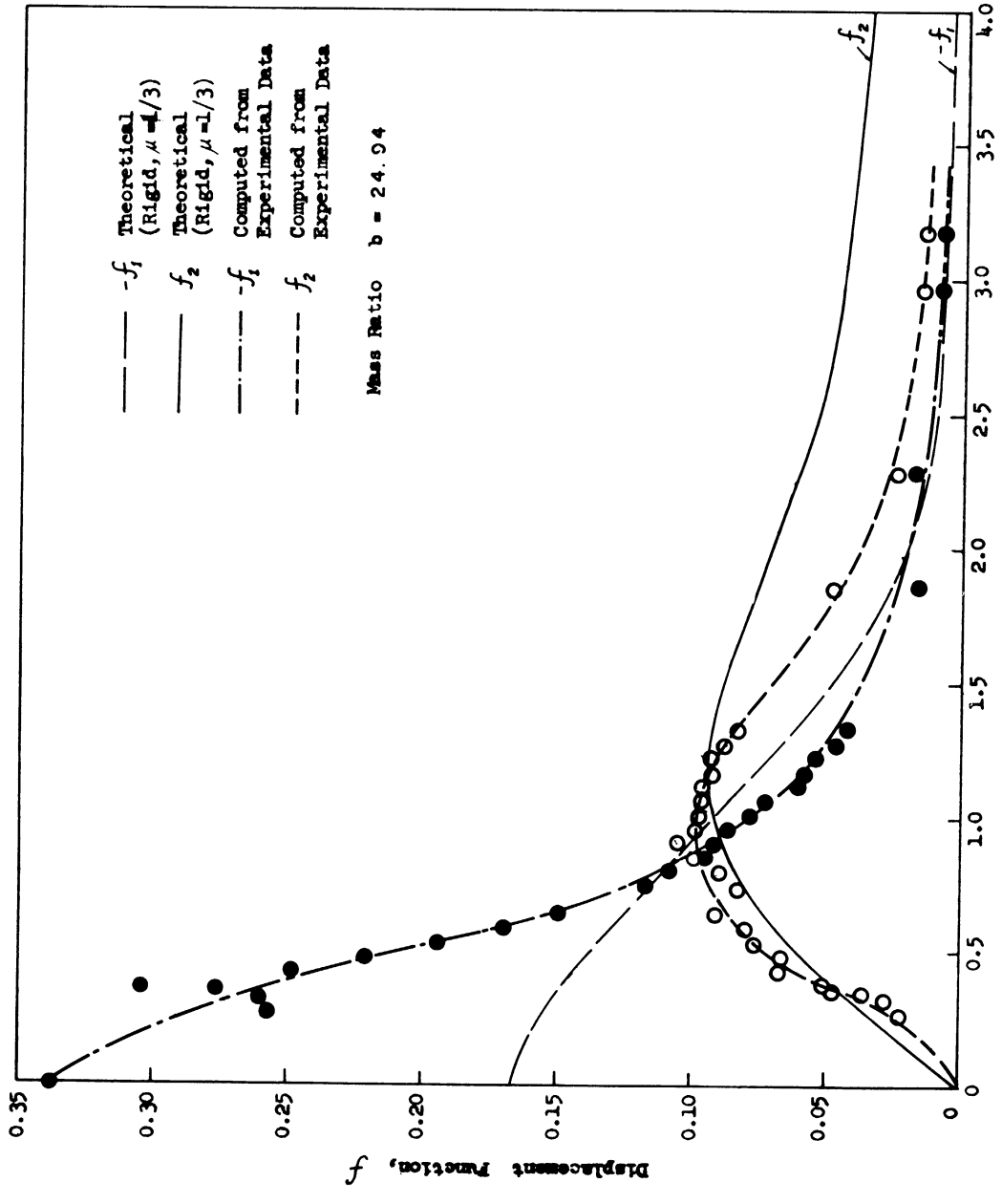

Fig. 79. Displacement functions computed from experimental data for mass ratio of 24.94.

By correlating Eq. (69) with Eq. (68) the theoretical values of the function f_1 can be determined only if Poisson's ratio is known. For $\mu = 0.25$, the f_1 values become

$$f_1 = \begin{cases} -0.1875 & \text{for rigid base} \\ -0.2387 & \text{for uniform loading} \\ -0.3183 & \text{for parabolic loading} \end{cases}$$

The static loading tests were conducted to obtain data on the static displacement of the footing. From these measurements the function f_1 was computed by Eq. (68), and the results were plotted in Figs. 73-79. The experimental results show close agreement with the theoretical value for parabolic pressure distribution, and the discrepancy between the two is within the range of 13%.

Since the displacement functions are independent of the mass ratio of foundation-soil systems, the curves shown in Figs. 73-79 could be redrawn in Figs. 80 and 81 as the composite diagrams to show the real part f_1 and imaginary part f_2 of the displacement function. Note in these charts that the curves for three of the seven different mass ratio values (5.8, 12.5, and 24.9) are shown. These curves are taken as representatives of the seven curves, and show the range of test results obtained. Also shown are the theoretical curves obtained by Sung based on the assumptions of two types of pressure distribution and Poisson's ratio of 1/4.

It can be seen in these diagrams that the displacement function

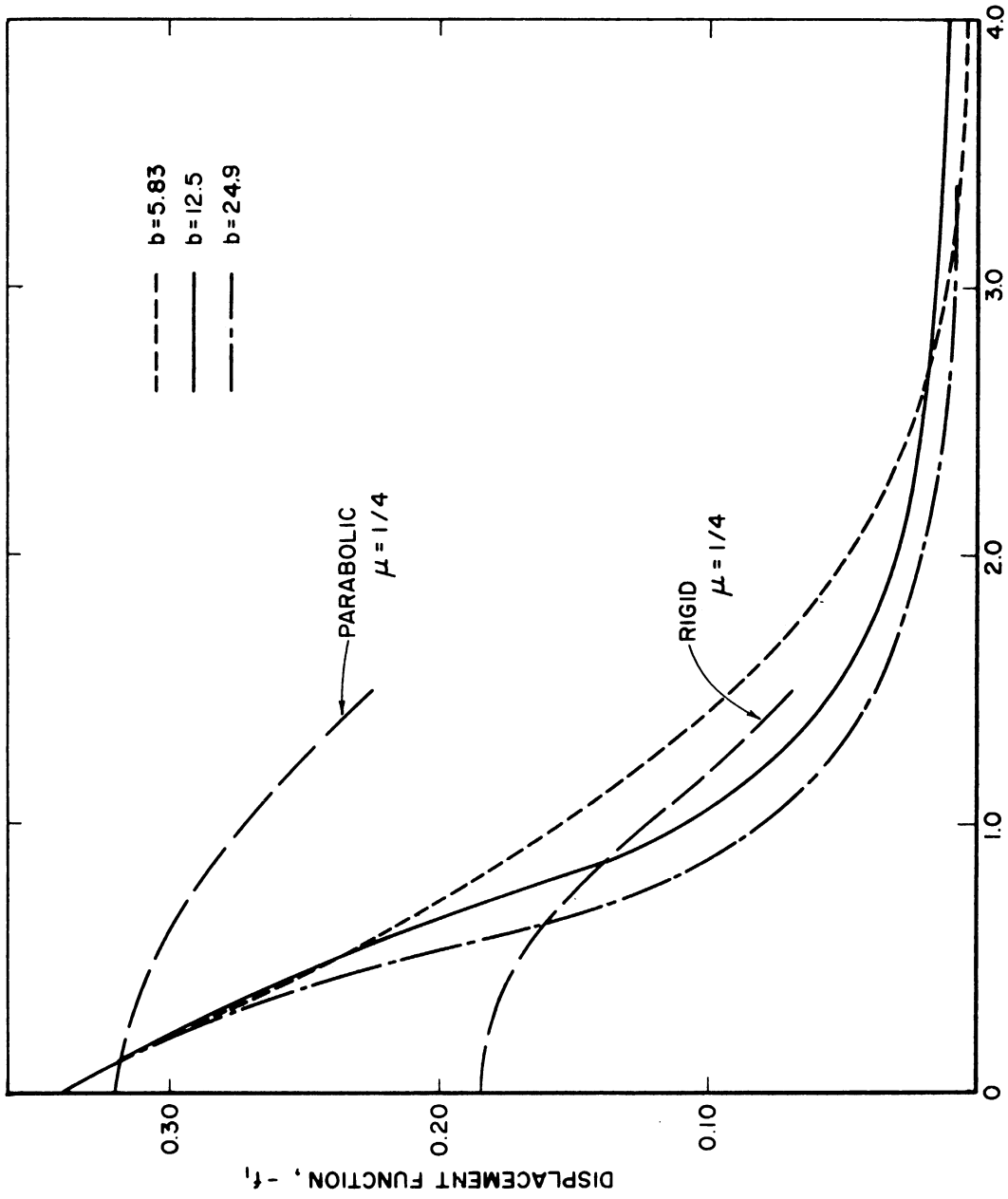

Fig. 80. Real part of displacement function computed from experimental data.

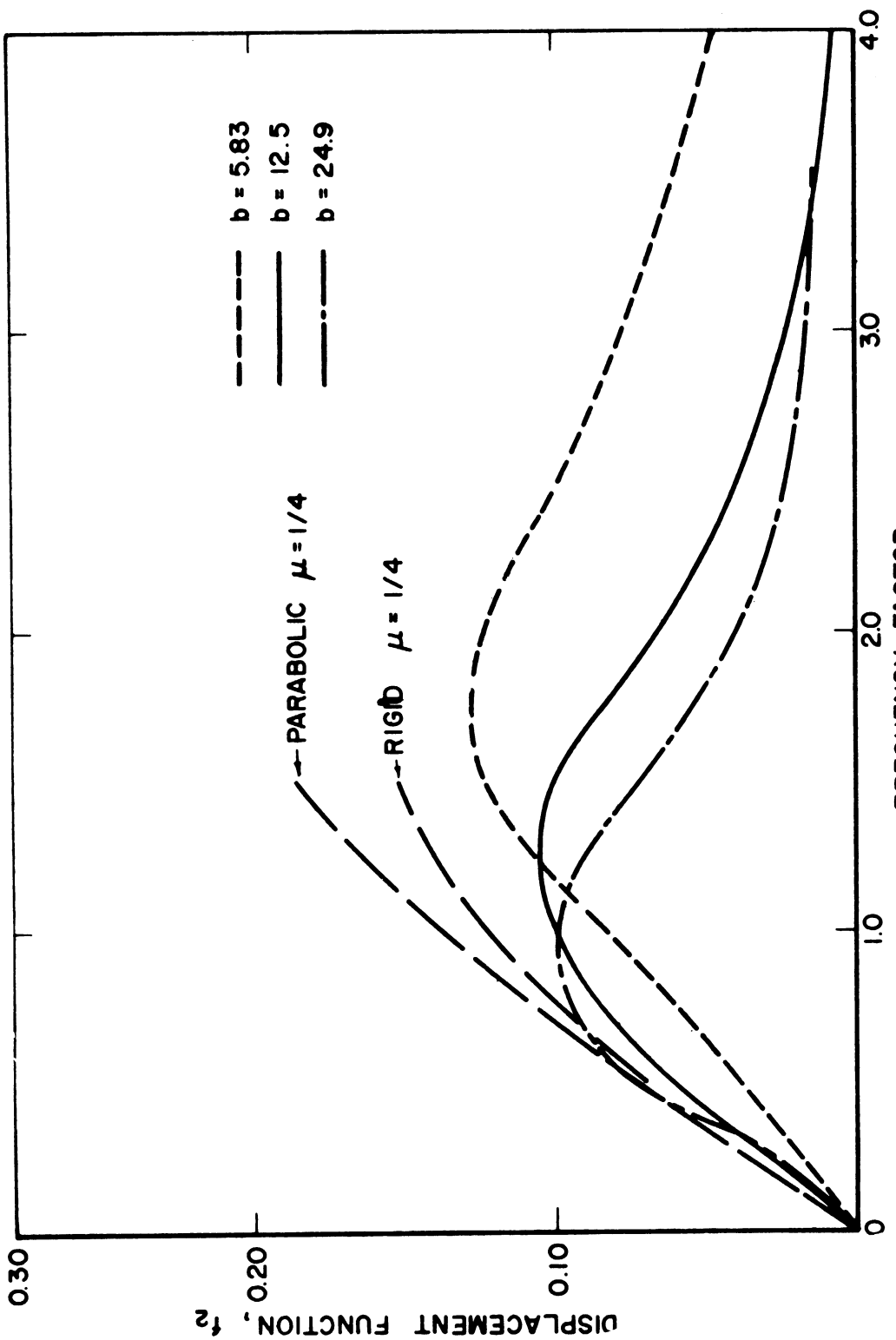

Fig. 81. Imaginary part of displacement function computed from experimental data.

values are dependent upon the excitation frequency, and the change in frequency causes a change in the type of pressure distribution. When the frequency factor is zero ($a_o = 0$), which corresponds to static loading, the shape of pressure distribution is definitely parabolic, and stays so until the frequency is increased up to about $a_o = 0.3$. In the region of $0.3 < a_o < 0.6$ the experimental function values indicate the type of pressure distribution to be uniform, and beyond this region rigid base type pressure distribution curve appears to represent the experimental data. This is in complete agreement with the observation made in connection with the pressure distribution curves and phase relations as described previously.

Recalling that the experimental values of displacement functions are based on measured values for the displacement and the phase shift between the input force and displacement, it should be noted that three different approaches used to find the effect of excitation frequency on the pressure distribution have yielded the same empirical conclusion that the pressure at the base of the footing does not maintain the same shape of distribution curve, but changes with the frequency of oscillation. This also verifies the validity of the displacement functions to use for the determination of dynamic characteristics of an oscillator-soil system. This is to say that the displacement, soil reactions and their phase relations can be defined by the dimensionless displacement functions.

CHAPTER VI

CONCLUSIONS

Conclusions are based on model tests for a footing resting at the surface of a sand bed. Therefore, for comparable conditions the following may be expected.

1. A change in input force and mass ratio causes a change in resonant frequency of oscillator-soil systems. Under a constant amplitude of force oscillation, the resonant frequency increases with decreasing mass ratio or with reduced magnitude of input force. For the test systems employed the maximum amplitude also decreases with increasing mass ratio. The increase of resonant frequency and maximum amplitude is small (20 to 30%), however, despite a change of mass ratio by almost five times.

2. If the proper assumptions are made as to the type of pressure distribution and the confining pressure, the theory of vibration based on a semi-infinite elastic body gives reasonably accurate predictions on the resonant frequency and the maximum amplitude occurring in the oscillator-soil system.

3. Under static loading the pressure at the base of a footing assumes a parabolic type of distribution. The ratio of the maximum pressure at the center to the average applied load over the entire footing appears to be proportional to the magnitude of the applied load: the

pressure becomes more concentrated near the center as the applied load is increased.

4. The pressure under a rigid footing varies, both in magnitude and phase, with reference to the center. The phase shift between the soil reaction force on each ring and displacement increases with the frequency of oscillation, and the rate of increase is greater with the outer rings. At a given frequency the phase shifts between the reaction forces become greater as the mass ratio of the system is increased.

5. The dynamic pressure distribution is a function of time. In the low frequency range the pressure distribution maintains a parabolic shape throughout the nearly entire period of vibration. The pressure at the edges does not vary much with time, and the reaction forces are acting in the same direction. In the high frequency range, however, the shape of the pressure distribution curves varies with time between that of parabolic to that produced by a rigid base. The variation of pressure under the outer rings is more significant as compared to that observed in the low frequency range. Points on the footing are subjected to the reaction forces of opposite signs at a given time of vibration.

6. Under a constant force input to the footing or constant total contact pressure between the footing and the soil, the pressure distribution is affected by the frequency of oscillation: as the frequency is increased the pressure appears to shift towards the edge, changing the shape of distribution from a parabolic type to uniform, then to that corresponding to a rigid base.

7. Under a given frequency, the effect of an increased intensity of the applied load is to shift the reaction pressure towards the center portion of the footing. The same effect is observed with the static pressure distribution.

8. The soil pressure amplitude under each ring increases with decreasing mass ratio at a given frequency and input force, regardless of the type of pressure distribution. However, with parabolic pressure distribution (low frequency) the variation of pressure amplitude with mass ratio becomes greater towards the center, whereas with rigid type distribution greater changes take place in the edge portion of the footing.

9. The total soil reaction under the footing varies with frequency, input force and the mass of the footing. As indicated by theory, the dynamic soil reaction is directly proportional to the acceleration, if the mass of the footing and the input force are held constant.

10. The phase shift between the total soil reaction and displacement ($\phi_{R_T\text{-}X}$) is a function of frequency and the type of pressure distribution. Experimental results for the phase shift $\phi_{R_T\text{-}X}$ indicate that the pressure distribution changes from a parabolic type at low frequencies to that of rigid base at high frequencies.

11. Empirical displacement functions obtained indicate that the dynamic pressure distribution is a function of frequency. The dynamic pressure at the base of the footing does not maintain the same shape of distribution curve, but changes with the frequency of oscillation. For

the test systems employed the pressure distribution is parabolic in the region of low frequency, but changes to that of uniform and rigid base type as the frequency is further increased.

12. It has been established experimentally that the displacement, soil reactions and their phase relations can be defined by the dimensionless displacement functions f_1 and f_2.

REFERENCES

1. Arnold, R. N., Bycroft, G. N., Warburton, G. B: Forced Vibration of a Body on an Infinite Elastic Solid, J. Appl. Mech., Trans., ASME, vol. 77, 1955, pp. 391-400.

2. Barkan, D. D.: Dynamics of Bases and Foundations, McGraw-Hill, 1962.

3. Crockett, S.H.A. and Hammond, R.E.R.: The Natural Oscillation of Ground and Industrial Foundations, Proc. 2nd Int. Conf. Soil Mech. and Found. Eng., vol. 3, 1948, pp. 88-93.

4. Eastwood, W.: Vibrations in Foundations, Structural Engineer, vol. 31, 1953, pp. 82-98.

5. Faber, O.: Pressure Distribution Under Bases and Stability of Foundations, Structural Engineer, vol. 11 (New Series), no. 3, March, 1933, pp. 116-125.

6. Hall, J. R., Jr.: Effect of Amplitude on Damping and Wave Propagation in Granular Materials, Ph.D. Dissertation, University of Florida, August, 1962.

7. Hall, J. R., Jr. and Richart, F. E., Jr.: Dissipation of Elastic Wave Energy in Granular Soils, J. of Soil Mech. and Found. Div., ASCE, Nov., 1963, pp. 27-56.

8. Hardin, B. O. and Richart, F. E., Jr.: Elastic Wave Velocities in Granular Soils, J. of Soil Mech. and Found. Div., ASCE, Feb., 1963, pp. 33-65.

9. Hertwig, A., Früh, G., and Lorenz, H.: Die Ermittlung der für das Bauwesen wichtigsten Eigenschaften des Bodens durch erzwungene Schwingungen, DEGEBO, no. 1, J. Springer, Berlin, 1933.

10. Hsieh, T. K.: Foundation Vibrations, Proc., Inst. Civil Engr. (London), vol. 22, 1962, pp. 211-226.

11. Jones, R.: In-Situ Measurement of the Dynamic Properties of Soil by Vibration Methods, Geotechnique, vol. 8, no. 1, March, 1958, pp. 1-21.

12. Lamb, H.: On the Propagation of Tremors over the Surface of an Elastic Solid, Philosophical Trans., Roy. Soc. of London, A, vol. 203, 1904, pp. 1-42.

13. Lysmer, J. and Richart, F. E., Jr.: A Theoretical Study of the Response of Rigid Footings Subject to Vertical Pulses, Preliminary Report to Waterways Experiment Station, U.S. Army, Corps of Engineers, 1963.

14. Pauw, A.: A Dynamic Analogy for Foundation-Soil System, Symp. Dynamic Testing Soils, ASTM Spec. Tech. Pub. no. 156, 1953, pp. 90-112.

15. Quinlan, P. M.: The Elastic Theory of Soil Dynamics, Symp. Dynamic Testing Soils, ASTM Spec. Tech. Pub. no. 156, 1953, pp. 3-34.

16. Reissner, E.: Stationäre, axialsymmetrische, durch eine schüttelnde Masse erregte Schwingungen eines homogenen elastischen Halbraumes, Ingenieur-Archiv, vol. 7, Dec., 1936, pp. 381-396.

17. Richart, F. E., Jr.: Foundation Vibrations, J. Soil Mech. and Found. Eng. Div., ASCE, Aug., 1960, pp. 1-34.

18. Richart, F. E., Jr.: Discussion of Sung's Paper (20), 1953, pp. 64-68.

19. Richart, F. E., Jr., Hall, J. R., Jr., and Lysmer, J.: Study of the Propagation and Dissipation of "Elastic" Wave Energy in Granular Soils, Report to Waterways Experiment Station U.S. Army, Corps of Engineers, Sept., 1962.

20. Sung, T. Y.: Vibrations in Semi-Infinite Solids due to Periodic Surface Loading, Symp. Dynamic Testing Soils, ASTM Spec. Tech. Pub., no. 156, 1953, pp. 35-63.

21. Tschebotarioff, G. P.: Performance Records of Engine Foundations, Symp. on Dynamic Testing of Soils, ASTM Spec. Tech. Pub., no. 156, 1953, pp. 163-168.

22. Warburton, G. M.: Forced Vibration of a Body on an Elastic Stratum, J. of Appl. Mech., ASME, vol. 79, 1957, pp. 55-58.

23. Waterways Experiment Station, Corps of Engineers, U.S. Army: Development and Evaluation of Soil Bearing Capacity, Presentation of Data (Draft), Report no. 1, March, 1963 (unpublished).

APPENDIX

DETERMINATION OF THE DISPLACEMENT FUNCTIONS f_1 AND f_2 FROM DISPLACEMENT X AND PHASE SHIFT $\phi_{Q\text{-}X}$

Equation (24)

$$X = \frac{Q_1}{G r_o} \sqrt{\frac{f_1^2 + f_2^2}{(1 + b a_o^2 f_1)^2 + (b a_o^2 f_2)^2}} \tag{A-1}$$

Equation (27)

$$\tan \phi_{Q\text{-}X} = \frac{-f_2}{f_1 + b a_o^2 (f_1^2 + f_2^2)} \tag{A-2}$$

$(1)^2$

$$\left(\frac{X G r_o}{Q_1}\right)^2 = \frac{f_1^2 + f_2^2}{(1 + b a_o^2 f_1)^2 + (b a_o^2 f_2)^2}$$

Let

$$b a_o^2 = D, \quad \left(\frac{X G r_o}{Q_1}\right)^2 = M, \quad \text{and} \quad \tan \phi_{Q\text{-}X} = N$$

then Eqs. (A-1) and (A-2) may be expressed as:

$$\frac{f_1^2 + f_2^2}{(1 + D f_1)^2 + (D f_2)^2} = M \tag{A-3}$$

$$\frac{-f_2}{f_1 + D(f_1^2 + f_2^2)} = N \tag{A-4}$$

From Eq. (A-3)

$$f_1^2 + f_2^2 = M(1 + Df_1)^2 + MD^2 f_2^2$$

$$= M + 2MDf_1 + MD^2 f_1^2 + MD^2 f_2^2$$

$$= M + 2MDf_1 + MD^2(f_1^2 + f_2^2)$$

and from Eq. (A-4)

$$-f_2 = Nf_1 + ND(f_1^2 + f_2^2)$$

$$MD^2(f_1^2 + f_2^2) - (f_1^2 + f_2^2) + 2DMf_1 + M = 0$$

$$(MD^2 - 1)(f_1^2 + f_2^2) + 2DMf_1 + M = 0 \qquad \text{(A-5)}$$

$$ND(f_1^2 + f_2^2) + Nf_1 + f_2 = 0 \qquad \text{(A-6)}$$

Let

$$MD^2 - 1 = C, \qquad 2DM = E$$

$$C(f_1^2 + f_2^2) + Ef_1 + M = 0 \qquad \text{(A-7)}$$

$$ND(f_1^2 + f_2^2) + Nf_1 + f_2 = 0 \qquad \text{(A-8)}$$

(A-7) x $\frac{ND}{C}$

$$ND(f_1^2 + f_2^2) + \frac{END}{C} f_1 + \frac{MND}{C} = 0 \qquad \text{(A-9)}$$

(A-9)-(A-8)

$$\left(\frac{END}{C} - N\right) f_1 - f_2 + \frac{MND}{C} = 0 \qquad \text{(A-10)}$$

$$\therefore \quad f_2 = \left(\frac{END}{C} - N\right) f_1 + \frac{MND}{C}$$

Let

$$\frac{ND}{C} = H, \quad \text{then} \quad \frac{END}{C} = EH, \quad \frac{MND}{C} = MH$$

$$EH - N = K, \quad \text{and} \quad MH = S$$

$$\therefore \quad f_2 = K f_1 + S \qquad \text{(A-11)}$$

Substituting Eq. (A-11) to (A-7)

$$C\left[f_1^2 + (Kf_1 + S)^2\right] + Ef_1 + M = 0$$

$$C\left[f_1^2 + K^2 f_1^2 + 2KSf_1 + S^2\right] + Ef_1 + M = 0$$

$$Cf_1^2 + CK^2 f_1^2 + 2CKSf_1 + CS^2 + Ef_1 + M = 0$$

$$(C + CK^2) f_1^2 + (E + 2CKS) f_1 + CS^2 + M = 0$$

Let

$$C + CK^2 = T, \quad E + 2CKS = Y, \quad CS^2 + M = Q$$

then

$$Tf_1^2 + Yf_1 + Q = 0$$

$$\therefore \quad f_1 = \frac{-Y \pm \sqrt{Y^2 - 4TQ}}{2T} \qquad \text{(A-12)}$$

$$f_2 = Kf_1 + S \qquad \text{(A-11)}$$

where,

$$Y = 2ba_o^2\left(\frac{XGr_o}{Q_1}\right)^2\left\{1+\left[b^2a_o^4\left(\frac{XGr_o}{Q_1}\right)^2+1\right]\tan^2\phi_{Q-x}\right\}$$

$$T = b^2a_o^4\left(\frac{XGr_o}{Q_1}\right)^2\left\{1+\left[b^2a_o^4\left(\frac{XGr_o}{Q_1}\right)^2+3\right]\tan^2\phi_{Q-x}\right\}-1$$

$$Q = \frac{b^2a_o^4\left(\frac{XGr_o}{Q_1}\right)^4\tan^2\phi_{Q-x}}{b^2a_o^4\left(\frac{XGr_o}{Q_1}\right)^2-1}+\left(\frac{XGr_o}{Q_1}\right)^2$$

$$K = \frac{2b^2a_o^4\left(\frac{XGr_o}{Q_1}\right)^2\tan\phi_{Q-x}}{b^2a_o^4\left(\frac{XGr_o}{Q_1}\right)^2-1}-\tan\phi_{Q-x}$$

$$S = \frac{ba_o^2\left(\frac{XGr_o}{Q_1}\right)^2\tan\phi_{Q-x}}{b^2a_o^4\left(\frac{XGr_o}{Q_1}\right)^2-1}$$

DISTRIBUTION LIST

(One copy unless otherwise noted)

BRL, Terminal Ballistics Lab.
Aberdeen Proving Ground
Aberdeen, Maryland
Attn: Mr. W. J. Taylor
Attn: Mr. A. A. Thompson

Bureau of Mines
Washington, D.C.
Attn: J. E. Crawford

Chief, Bureau of Yards & Docks
Department of the Navy
Washington, D.C. 20370
Attn: Code D-440

Chief, Defense Atomic Support Agency
Department of Defense 5
Washington, D.C. 20301
Attn: Document Library

Chief of Engineers
Department of the Army
Washington, D.C. 20315
Attn: ENGTE-E
Attn: ENGMC-E 2

Chief of Naval Operations
Department of the Navy
Washington, D.C. 20350
Attn: OP-75

Chief of Research & Development
Department of the Army
Washington, D.C. 20310
Attn: Atomic Division

Air Force Ballistics Missile Division
P. O. Box 262
Inglewood 49, California
Attn: WDGN

Defense Documentation Center 20
Cameron Station
Alexandria, Virginia 22314
Attn: TISIA-21

Air Force Weapons Laboratory 4
Kirtland AFB, New Mexico 87117

Aeronautical Research Laboratory
Wright-Patterson AFB,
Ohio 45433

Commanding General 3
U.S. Army Materiel Command
Washington, D.C. 20310
Attn: AMCRD-DE-N

Commanding Officer and Director 2
U.S. Naval Civil Engineering Lab.
Port Hueneme, California

Director, Weapons Systems Evaluation Group, OSD
Room 1E880
The Pentagon
Washington, D.C. 20301

Director
U.S. Army Engineer Waterways 25
Experiment Station
P.O. Box 631
Vicksburg, Mississippi 39181

Director of Civil Engineering, Hq.
U.S. Air Force
Washington, D.C. 20330
Attn: AFOCE

U.S. Coast & Geodetic Survey
Washington, D.C.
Attn: D. S. Gardner

DISTRIBUTION LIST (Continued)

Director of Defense Research and
Engineering
Washington, D.C. 20330
Attn: Technical Library

Division Engineers 10
U.S. Army Engineer Divisions
Continental United States
(one copy to each)

Headquarters 2
U.S. Air Force
Washington, D.C. 20330
Attn: AFTAC, C. F. Romney

U.S. Coast & Geodetic Survey
San Francisco, California
Attn: W. K. Cloud,

U.S. Geological Survey
Department of the Interior
Washington, D.C.
Attn: J. R. Balsley

California Institute of Technology
Pasadena, California
Attn: F. Press
Attn: R. Benioff

Columbia University
New York, New York
Attn: J. E. Oliver

Iowa State University
Ames, Iowa
Attn: Prof. M. G. Spangler

Pennsylvania State College
Atomic Defense Engineering Dept.
State College, Pennsylvania
Attn: Prof. Albright

Barry Wright Corp.
700 Pleasant St.
Watertown 72, Massachusetts
Attn: Mr. Cavanaugh

General American Transportation Corp.
7501 North Natchez Avenue
Niles 28, Illinois

Holmes and Narver, Inc.
AEC Facilities Division
849 S. Broadway
Los Angeles 14, California
Attn: Mr. Frank Galbreth

IIT Research Institute 2
10 West 35th Street
Chicago 16, Illinois
Attn: Library

Lawrence Radiation Laboratory
P. O. Box 808
Livermore, California

Space Technology Laboratories
Inglewood, California
Attn: B. Sussholz

Stanford Research Institute 2
Physical Sciences Division
Menlo Park, California
Attn: Dr. R. B. Vaille, Jr.

United Research Services
1811 Trousdale Drive
Burlingame, California
Attn: Mr. Harold G. Mason

RAND Corporation
Dr. Harold Brode
1700 Main Street
Santa Monica, California

Prof. W. J. Hall
Department of Civil Engineering
University of Illinois
111 Talbot Laboratory
Urbana, Illinois 61803

DISTRIBUTION LIST (Concluded)

Prof. B. O. Hardin
Department of Civil Engineering
University of Kentucky
Lexington, Kentucky

Prof. H. O. Ireland
Department of Civil Engineering
Talbot Laboratory
University of Illinois
Urbana, Illinois

Dr. Robert L. Kondner
The Technologic Institute
Northwestern University
Evanston, Illinois

Prof. Gerald A. Leonards
School of Civil Engineering
Purdue University
Lafayette, Indiana

Prof. N. M. Newmark
Civil Engineering Hall
University of Illinois
Urbana, Illinois

Prof. H. Bolton Seed
Department of Civil Engineering
University of California
Berkeley, California

Prof. L. J. Thompson
Department of Civil Engineering
University of New Mexico
Albuquerque, New Mexico

Mr. Stanley D. Wilson
Shannon and Wilson
1105 North 38th Street
Seattle 3, Washington

Mr. C. J. Nuttall
Wilson, Nuttall, Raimond Engineers, Inc.
Chestertown, Maryland

Prof. R. B. Peck
Talbot Laboratory
University of Illinois
Urbana, Illinois

Mr. W. R. Perret
5112 Sandia Corporation
Sandia Base
Albuquerque, New Mexico

Dr. Grover L. Rogers
RECON, Inc.
Box 3622 MSS
Tallahassee, Florida

Mr. Fred Sauer
Physics Department
Stanford Research Institute
Menlo Park, California

Prof. H. Neils Thompson
Civil Engineering Department
University of Texas
Austin 12, Texas

Prof. R. V. Whitman
Department of Civil and Sanitary Engineering
Massachusetts Institute of Tech.
Cambridge 39, Massachusetts

Dr. Ralph E. Fadum
Box 5628
North Carolina State College of Agriculture and Engineering
Raleigh, North Carolina